DFT Studies on quantification of substituent effects and ligand modifications to tune the reactivity of transition metal complexes

Thesis Submitted to AcSIR for the Award of the Degree of
DOCTOR OF PHILOSOPHY
in Chemical Sciences

By

Remya G S

Registration No: **10CC17A39015**

Under the Guidance of

Dr. C. H. Suresh

Chemical Sciences and Technology Division
CSIR-National Institute for Interdisciplinary Science and Technology
Thiruvananthapuram-695019, Kerala, India

August 2020

DECLARATION

I hereby declare that the Ph. D. thesis entitled "**DFT Studies on quantification of substituent effects and ligand modifications to tune the reactivity of transition metal complexes**" is an original work carried out by me at Chemical Sciences and Technology Division(CSTD), CSIR-National Institute for Interdisciplinary Science and Technology (CSIR-NIIST), Thiruvananthapuram, under the supervision of Dr. C. H. Suresh, Senior Principal Scientist, CSTD, CSIR-NIIST, and it has not been submitted somewhere else for any other degree, diploma or title.

CSIR-NIIST

07/08/2020

Remya

Remya G S

Council of Scientific & Industrial Research
National Institute for Interdisciplinary Science and Technology
Thiruvananthapuram-695019, Kerala, India

Dr. C. H. Suresh
Senior Principal Scientist
Chemical Sciences & Technology Division
Tel: +91- 4712515472
E-mail: sureshch@gmail.com
sureshch@niist.res.in

7th august 2020

CERTIFICATE

This is to certify that the work incorporated in this Ph. D. thesis entitled "**DFT Studies on quantification of substituent effects and ligand modifications to tune the reactivity of transition metal complexes**" submitted by Ms. Remya G S to Academy of Scientific and Innovative Research (AcSIR) in fulfillment of the requirements for the award of the Degree of Doctor of Philosophy, embodies original research work done under my supervision. I further certify that this work has not been submitted to any other University or Institution in part or full for the award of any degree or diploma. Research material obtained from other sources has been duly acknowledged in the thesis. Any text, illustration, table, etc. used in the thesis from other sources, have been duly cited and acknowledged.

Remya. G. S
(Student)

Dr. C. H. Suresh
(Thesis Supervisor)

Acknowledgments

I would like to extend my heartfelt gratitude and appreciation to all the people who have contributed directly or indirectly for the successful conclusion of my Ph. D thesis.

First and foremost, I would like to express my sincere gratefulness towards my research advisor, Dr. C. H. Suresh for suggesting me an excellent research topic and providing fruitful guidance throughout my Ph. D. work. I admire his knowledge in the subject I greatly motivated by his eagerness in scientific activities. His timely initiatives and support as the AcSIR coordinator for the successful conduct of my academic procedures is also acknowledged.

I would like to record my gratitude to Dr. A. Ajayaghosh, Director, CSIR-NIIST, and former directors, Dr. Suresh Das and Dr. Gangan Pratap for extending all the required institutional facilities for carrying out my research in this prestigious institute.

I would like to extend my thankfulness to Dr. P. Sujatha Devi, Head, Chemical Sciences and Technology Division. I am thankful to Dr. R. Luxmi Varma, former Head and AcSIR coordinator for her endless support, insightful comments and encouragement. I am also grateful to former HOD Dr. K. R. Gopidas for the support and supervision.

I am grateful to my Doctoral Advisory Committee members, Dr. Sunil Varughese*, Dr.* B. S. Sasidhar*, and Dr. Bhoje Gowd for their helpful suggestions and guidance throughout my AcSIR coursework and Ph. D programme. I would like to thank Dr V. Karunakaran, who has been nominated to coordinate my* PhD thesis submission for his timely support and guidance.

I would like to extend my heartfelt gratitude to all the former members of our research group, Dr. Sandhya, Dr. Neetha, Dr. Prabha, Dr. Remya K, Dr. Remya P. R., Dr. Della, Dr. Rakhi, Dr. Anjali B and Dr. Renjith, for their friendship, well-timed suggestions and support. I am thankful to all the present members of our group Bijina, Divya, Anila, Anjali, Krishnapriya and Haritha for all their help, affection and friendship.

I am grateful to all my friends, scientific and non-scientific staff at CSIR-NIIST. I will definitely miss the green and peaceful campus of NIIST. Special thanks to the AcSIR faculty who have taken the coursework classes.

I deeply acknowledge Council of Scientific and Industrial Research (CSIR), and Department of Science and Technology (DST) for the financial support.

I acknowledge high-performance computational facilities at CSIR-NCL, Pune, and CSIR-4PI, Bangalore.

I express my deep sense of gratitude to all my dearly loved teachers in the past for teaching me the fundamentals of science. I would like to thank all my friends and well-wishers for extending the support and care.

I am really indebted to my entire family for their love, care, and concern. Special thanks to my parents, my husband and my little daughter for all their support and sacrifice. I would not have been able to procure my ventures, without their help right through my life.

Above all, I thank the Almighty for giving me health, mental power, knowledge, an opening to carry out this research study and allowing me to complete this endeavour successfully.

Thank you all....

Remya

CONTENTS

Part B: Computational Chemistry Methods

Chapter 2

Quantification and classification of substituent effects in organic chemistry

Chapter 3

Part A: Assessment of Electron Donor Properties of Substituted Phenanthroline Ligands in Molybdenum Carbonyl Complexes using MESP

Part B: Substituent Effect Parameters: Extending the Applications to Organometallic Chemistry

Chapter 4

Part A: Pincer Ligand-Modifications to Tune the Activation Barrier for H_2 Elimination in Water Splitting Milstein Catalyst

Part B. Hydrogen Elimination Reactivity of Ruthenium Pincer Hydride Complexes

List of Figures

List of Tables

List of Schemes

List of Abbreviations

AIMD : *ab initio* Molecular Dynamics
AMBER : Assisted Model Building with Energy Refinement
AO : Atomic Orbitals
AM1 : Austin model 1
ASE : Aromatic stabilization energy
BO : Born Oppenheimer
CASSCF : Complete Active Space Self Consistent Field
CBS : Complete Basis Set

CC : Coupled Cluster
CEP : Computed Electronic Parameter
CFF : Consistent Force Field
CFT : Crystal Field Theory
CG : Contracted Gaussian
CGTO : Contracted Gaussian-Type Orbitals
CHARMM : Chemistry at Harvard Macromolecular Mechanics
CI : Configuration Interaction
CMD : Classical Molecular Dynamics
CNDO : Complete Neglect of Differential Overlap
CP : Critical Point
CPMD : Car Parrinello Molecular Dynamics
DAM : Deformed Atoms in Molecules
DCD : Dewar-Chatt-Duncanson
DFT : Density Functional Theory
DZ : Double-Zeta
ECEPP : Empirical Conformational Energy Program for Peptides
ECP : Effective Core Potential
EFF : Empirical Force Field
GGA : Generalized Gradient Approximation
GROMACS : Groningen Machine for Chemical Simulations
GROMOS : Groningen Molecular Simulation
GTO : Gaussian Type Orbital
HEP : Huynh Electronic Parameter
HER : Hydrogen Evolution Reaction
HF : Hartree-Fock
HOMA : Harmonic Oscillator Model of Aromaticity
INDO : Intermediate Neglect of Differential Overlap
LANL : Los Alamos National Laboratory
LDA : Local Density Approximation

LEP : Ligand Electronic Parameter/Lever Electronic Parameter

LFT :Ligand Field Theory

LSDA : Local Spin Density Approximation

LTEP : Local Tolman electronic parameter

MCSCF : Multi Configurational Self Consistent Field

MD : Molecular Dynamics

MESP : Molecular Electrostatic Potential

MINDO : Modified Intermediate Neglect of Differential Overlap

MLEP : Metal Ligand Electronic Parameter

MM : Molecular Mechanics

ModEP : Modified Electronic Parameter

MNDO : Modified Neglect of Differential Overlap

MO : Molecular Orbital

MP : Moller-Plesset Perturbation

MRCI : Multiconfiguration-Reference Configuration Interaction

NDO :Neglect of Differential Overlap

NDDO : Neglect of Diatomic Differential Overlap

NHC : N-Heterocyclic Carbene

NICS : Nucleus Independent Chemical Shift

ONIOM : Our own N-layered integrated molecular orbital and molecular mechanics

PCM : Polarizable Continuum Model

PDI : Para Delocalization Index

PES : Potential Energy Surface

PM3 : Parametric Method 3

QALE : Quantitative Analysis of Ligand Effect

QM : Quantum Mechanics

QSAR : Quantitative Structure Activity Relationship

QZ : Quadruple-Zeta

RHF : Restricted Hartree-Fock

SCF : Self Consistent Field

SCRF	: Self Consistent Reaction Field
SESE	: Substituent Effect Stabilization Energy
STO	: Slater-Type Orbital
SMD	: Solvation Model Density
TDDFT	: Time Dependent Density Functional Theory
TEP	: Tolman Electronic Parameter
TZ	: Triple-Zeta
VNW	: Vosko, Wilk and Nusair local functionals
ZDO	: Zero Differential Overlap

PREFACE

The design and modification of ligand environment is noteworthy in tuning the reactivity patterns of transition metal complexes. Thus, the ligand electronic parameters have paramount importance in organometallic chemistry. There are both experimental and computational quantifiers are known in this regard. The experimental parameters include Hammett constants(σ_m, σ_p), Tolman Electronic Parameter (TEP), Lever Electronic Parameter (LEP), NMR chemical Shifts, and quantitative analysis of ligand effects (QALE), whereas the computationally derived parameters include computed electronic parameter (CEP), average local ionization energy and molecular electrostatic potential (MESP). Computational assessment imparts enormous importance for the consistent prediction and understanding of ligand substituent effects and metal ligand interactions. The major objective of the thesis is the computational prediction and fine tuning of activation barriers and interaction energies of different transition metal complexes and revealing their one to one relationship with the ligand electronic parameters using density functional theory. The MESP based parameters associated with the electron rich centers of the ligands as well as the metal complexes are found to be prevailing descriptors of the stereoelectronic effects caused by the ligands. Since CO ligand is present in all the metal complexes discussed herein, Tolman parameters also have significant roles wherever appropriate. The thesis is systematically divided into four chapters.

In **Chapter 1**, **Part A** presents a concise description of ligand electronic parameters including a general idea of the literature in MESP and **Part B** of **Chapter 1** gives an overview of assorted computational methodologies.

Chapter 2 discusses the applicability of MESP parameters to address the electron donating/ withdrawing effect of different substituents in organic chemistry. The MESP quantities associated with the reference monosubstituted benzene systems (ΔV_C) are proposed to use instead of the popular Hammett constants. A total of 381 substituents are broadly classified as electron withdrawing and electron donating substituents on the basis of positive and negative ΔV_C values respectively. On the basis

of the magnitude of ΔV_C values, the classification is further extended as very strong/strong/medium/weak electron donating/withdrawing categories. The MESP based assessment is accounted to be transferable and additive for representative set of conjugated molecules.

Chapter 3 presents the transferability of ΔV_C based quantification of substituent effect achieved for monosubstituted benzenes to predict the interaction energies of a succession of transition metal carbonyls. The chapter is divided into two parts. **Part A** deals with the prediction of binding energies of substituted 1, 10-phenanthroline based molybdenum complexes. The study is based on experimentally and theoretically characterized thirteen complexes reported by Brenna *et al.* The ΔV_C and MESP minimum values associated with the ligands ($\Delta V_{N,}$ ΔV_{min}) and corresponding metal complexes ($V_{min\text{-}CO}$) are used as the quantifiers. The correlation of these parameters with the interaction energies with significant r values opened up the possibility of extending the prediction to 50 selected substituents in mono, di and tetra combinations along with 5000 randomly generated ligands. Since metal carbonyl complexes are advantageous for the initial verification of the substituent effect data, the studies are broadened further in **Part B** for metal carbonyls with variety of ligands such as pyridine, NHC and η^6 coordinated ligands. Representative third, second and first row transition metals (W, Mo, and Ni) are selected for better clarity of the concept. The transferability property also holds good like previous in evaluating the binding between ligand part and metal fragment and also the decarbonylation reaction. Thus, the MESP based innovation provide a priori prediction of ligand effects without any theoretical or experimental verification and the most easily available strategies for the estimation of electron donating power of aromatic N-heterocyclic and η^6 coordinated ligands.

Chapter 4 is divided into two parts. **Part A** deals with the pincer ligand modifications to address the activation barrier for H_2 elimination in water splitting Milstein catalyst. Milstein catalyst is a ruthenium pincer complex with tridentate PNN ligand ((2-(di-tert-butylphosphinomethyl)-6-diethylaminomethyl)pyridine) proposed by Milstein *et al*. in 2009 to address the consecutive water reduction under thermal condition and water oxidation under light driven condition. The catalyst has attained

significant interest over the years, and is attributed to the miscellaneous catalytic activity in synthesizing variety of organic compounds such as esters, alcohols, amides, and aldehydes. The Milstein catalyst is modified by introducing different substituents at the para position of the pyridyl group of **PNN** ligand and different alkyl substituents at the P- and N-arms of pincer ligand. In total, there are 48 new catalysts arranged in four categories, *viz*. **1-X, 2-X, 3-X** and **4-X.** All the proposed catalysts are tested with the hydride ligand-assisted outer sphere mechanism of hydrogen elimination from water. It is observed that reducing the steric bulkiness over the P and N arms of the **PNN** pincer complex is beneficial for improving the efficiency of the catalyst. The modifications over the pyridyl unit of the pincer ligand cause only a minor effect in reducing the energy barriers. MESP V_{min} at the hydride ligand and Tolman parameters are proposed to quantify the hydricity of the ligand and activation barriers for the H_2 elimination reaction. In **part B**, 20 different pincer complexes are designed by using the feasible permutations of the donor atoms, P, N, S and O. The energetics of hydrogen elimination is noted as per the same outer sphere mechanism for both the pyridine based (**XNY**) and benzene based (**XCY**) pincer catalysts. The more electron rich **XCY** pincer catalysts are reported as more efficient water reduction catalysts with significantly lower activation barriers. Here, the MESP at the metal centre is used as a guage to interpret the activation barriers.

Chapter 1

Part A

An Overview of Ligand Electronic Parameters

Part B

Computational Chemistry Methods

Part A: An Overview of Ligand Electronic Parameters

1.1 Ligand Electronic Parameters

Transition metal centered chemical reactions are well explored in the field of organic synthesis and catalysis.[1, 2] The metal-ligand bonding and interactions are getting wide attention nowadays.[3] The popular model used to describe the bonding in transition metal complexes is the ligand field theory (LFT).[4, 5] This theory can be considered as a simple brand of MO theory that considers the frontier orbitals of the ligands and the valence d orbitals of the transition metal. LFT can also be meditated as a more refined form of crystal field theory (CFT) that studies electrostatic interactions between the metal and the ligands. One of the popular MO-theoretical models used along with LFT is Dewar-Chatt-Duncanson (DCD) model which considers the metal-ligand interactions in terms of ligand to metal donation and metal to ligand back-donation. The model was put forward by Dewar[6] and by Chatt and Duncanson[7] to describe the transition metal-olefin interactions in ethene complexes (Figure 1.1).

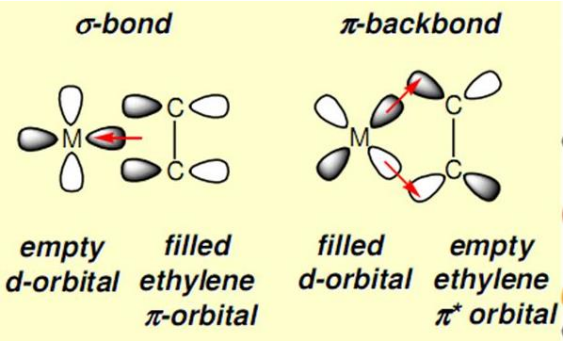

Figure 1.1 Orbital interactions in a metal-ethylene complex.

The most intriguing part of the transition metal chemistry is the introduction and modification of new ligands.[8-13] On the basis of electron donation, ligands encountering in organometallics are classified as σ-donor, σ-donor-π-acceptor and σ-donor-π-donor ligands.[14] A representative image for the electron donation scheme of ligands is depicted

in Figure 1.2. The tuning of ligand environment of the metal has attracted paramount importance in deducing the reactivity of organo-transition metal complexes.[15-18] A small modification of the coordinated ligand can often change the entire reactivity of the transition metal complexes, which leads to variety of estimated applications.[19-21] The ligands with anticipated donor properties can be proposed by knowing the electronic and steric contributions.[22-24] The parameters describing perturbations caused by the steric and electronic effects of complexes enable us the prediction of ligand effects before further experimentation.[25, 26] Numerous research groups have established the prediction of the stereoelectronic properties of ligands, for eg; Tolman,[27, 28] Giering,[29, 30] Crabtree,[23, 31] Fey,[10, 32] Gusev,[33, 34] and Cremer[35, 36] and the ligand effects were summed up on the basis of their kinetics, thermodynamics, spectroscopic and structural behaviors. Various experimental as well as computational approaches have been used to evaluate the electron-donating ability of different types of ligands.[37, 38]

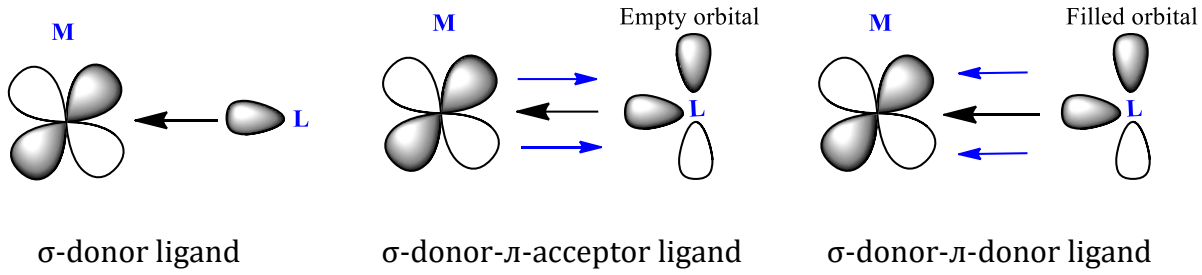

σ-donor ligand σ-donor-л-acceptor ligand σ-donor-л-donor ligand

Figure 1.2 Various types of ligands.

1.1.1 Experimental Ligand Electronic Parameters

1.1.1.1 Hammett Constants

Hammett introduced a linear free energy relationship connecting reaction rates and equilibrium constants for reactions involving quite a few *meta*- and *para*-substituted benzoic acids using a substituent constant and a reaction constant.[39-41]

$$log \frac{k}{k^0} = \rho\sigma \qquad \text{(Eq. 1.1)}$$

k = rate constant for meta or para substituted aromatic compound

k° = the rate constant for the unsubstituted aromatic compound

ρ = a constant for the specific reaction and taken as unity for the ionization of benzoic acids

σ = a constant for a given substituent

= (log K_X — log K_H) where K_X is the ionization constant for a substituted benzoic acid in water at 25°C and K_H is the ionization constant for benzoic acid itself.

Hammett constant, σ has been accepted as one of the most commonly employed substituent descriptor.[42] The electron withdrawing groups can increase the equilibrium constant by stabilizing the carboxylate anion, whereas the electron donating ones can decrease the equilibrium constant (Figure 1.3).[43] Consequently, σ values are positive for the electron withdrawing and negative for the electron donating categories.[44] A comprehensive study in 1991 by Hansch, Leo and Taft portrayed Hammett constants of around 500 various substituents along with the possible inductive and resonance effect parameters.[45] Hammett constants have been popularized to deduce linear free energy relationships towards the reactivity of substrates in several organic reactions.[46-48]

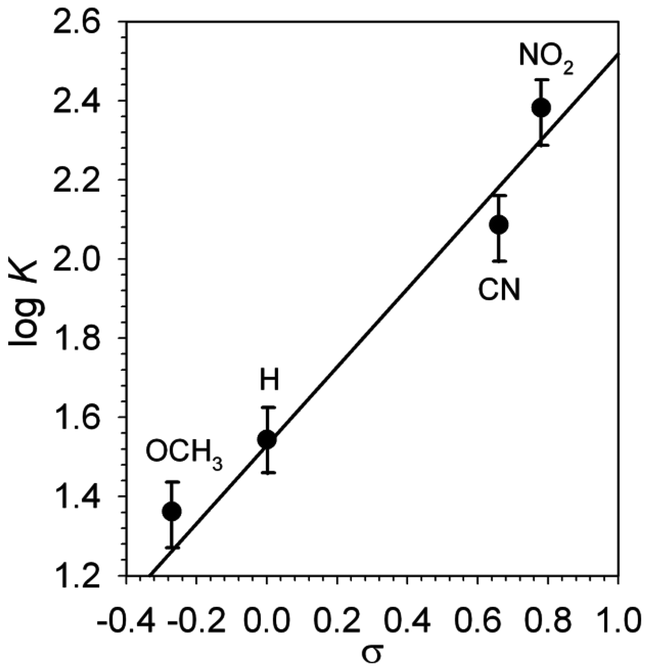

Figure 1.3 A representative Hammett plot for the equilibrium constants of transimination reactions.[43]

It was confirmed that Hammett constants are in accordance with the other reactivity parameters such as electrophilicity index,[49, 50] NMR chemical shift,[51] *etc*. Structure–reactivity relationships are critical in tuning the reactivity of different organometallic complexes (Figure 1.3).[52] Recently, Hammett constants are used to interpret the resonance or inductive effect from the phosphazane ligand in the electrochemical CO_2 reduction profile for rhenium phosphazane complexes.[53] Hammett constants are trending in visualizing the effect of a range of ligands in a series of manganese based catalysts used for the electrochemical reduction of CO_2.[54] The tunability of substituent control over the $Co^{III/II}$ redox potential is recognized by introducing Hammett constants for bis(dipyridylpyrrolide)cobalt complexes.[55]

1.1.1.2 Tolman Electronic Parameter (TEP)

The pioneering works of Tolman paved the foundations for the quantitative analysis of ligand effects in organometallic chemistry.[27, 28] The experimental studies involving the use of CO stretching frequency as a quantitative descriptor for the metal-ligand bonding were pioneered by Tolman in 1970's . Tolman suggested the IR frequency of the totally symmetric carbonyl stretching mode, ν_{CO} of $(PR_3)Ni(CO)_3$ complexes as a parameter to interpret the electronic properties of a range of phosphine ligands[27] and was named after the developer as Tolman Electronic Parameter, TEP. TEP only accounts for the donating ability of ligands and were not affected by the steric bulkiness over the $Ni(CO)_3$ fragment by the substituents on phosphorus. For that purpose, the ligand cone angle, θ was introduced as a steric parameter,[28, 56] which is defined as the apex angle of a cylindrical cone, centered 2.28 Å from the center of the P atom, which just touches the van der Waals radii of the outermost atoms of the model (Figure 1.4).

The lowest CO stretching frequency corresponds to the most electron rich ligand and the highest CO stretching frequency for the most electron deficient ligand. Carbonyl ligand is chosen as it is small and so steric factors do not complicate the analysis. Besides, the ligand is more sensitive to the electronic structure at the metal center. Another advantage is that the CO stretching frequency is very much separable from other frequencies in the IR spectrum and it can be calculated both experimentally and

computationally. The more electron-donating the ligand, the lower will be the CO stretching frequency, due to the π-back-donation from the filled metal d orbitals into the low-lying antibonding π^*CO orbital.[57] Thus, Tolman's concept for the phosphine ligand relies on the use of CO as an "electronic probe" for estimating the donating properties of the CO ligand. The changes noted in TEP by varying the ligand environment can directly account for the metal-ligand bond strength. Various possible modifications for the concept were computationally reported later in the form of calculated descriptors and those will be discussed in the computational ligand electronic parameters section (1.1.2).

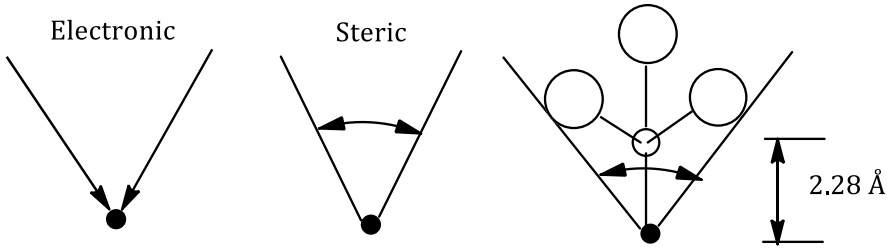

Figure 1.4 A schematic definition of (a) electronic and steric effects and (b) the cone angle.[28]

1.1.1.3 Lever Electronic Parameter (LEP)

An alternative attempt made by Lever and co-workers was based on the estimation of electrochemical redox potential, E_0 for a redox couple ($Ru^{II/III}$) in a series of complexes bearing the NHCs of interest.[58-60] The data was abbreviated as Lever electronic parameter (LEP) for a choice of ligands. LEP can be defined as one-sixth that of the $Ru^{(III)}/Ru^{(II)}$ potential for species RuL_6 in acetonitrile. The prediction of M(n)/M(n-1) redox potentials was achieved by assuming that all ligand contributions are additive. So it can be asserted that LEP performs in a mode similar to that of the Dq parameter that defines the crystal field electronic spectrum of a metal complex in electronic spectroscopy. LEP is found to be more beneficial than the Tolman parameter as it could envelop an expansive series of ligands, comprising anionic and O- and N-donor ligands. Technically, LEP measurement is found to be more tedious since it needs an electrochemical arrangement. Moreover, the computation of LEP is not clear-cut because of the solvent effects and for the reason that Ru(III) is an open shell system.

1.1.1.4 NMR Chemical Shift

NMR has been shown to be an appropriate technique for comparing the ligand donor ability in metal complexes. The carbonyl chemical shift statistics has been accounted as a measure for the electronic effect of ligands in 116 $LNi(CO)_3$ complexes of phosphorus, arsenic, and antimony and for $LCr(CO)_5$, $LMo(CO)_5$, and $(\eta^6\text{-}C_6H_6)Cr(CO)_2L$ derivatives in the 1980's.[61] The use of ^{13}C chemical shift values of the CO groups in $LNi(CO)_3$ complexes were reported in literature instead of TEP for the phosphorus and arsenic ligands.[62] In 2009, Huynh group introduced an electronic parameter called Huynh electronic parameter (HEP)[63] using ^{13}C NMR spectroscopy on trans-$PdBr_2$(iPr-bimy)(L) complexes (Figure 1.5) which is more convenient than IR data to interpret the donor abilities of both Werner-type and organometallic ligands. Subsequently, HEP is further applied by the same research group for 15 different bidentate ligands, such as aromatic diimines, diazabutadienes, and di-NHCs in $[PdBr(iPr_2\text{-bimy})(L_2)]PF_6$ complexes,[64] and for NHC ligands in Au(I) hetero-NHC complexes.[65]

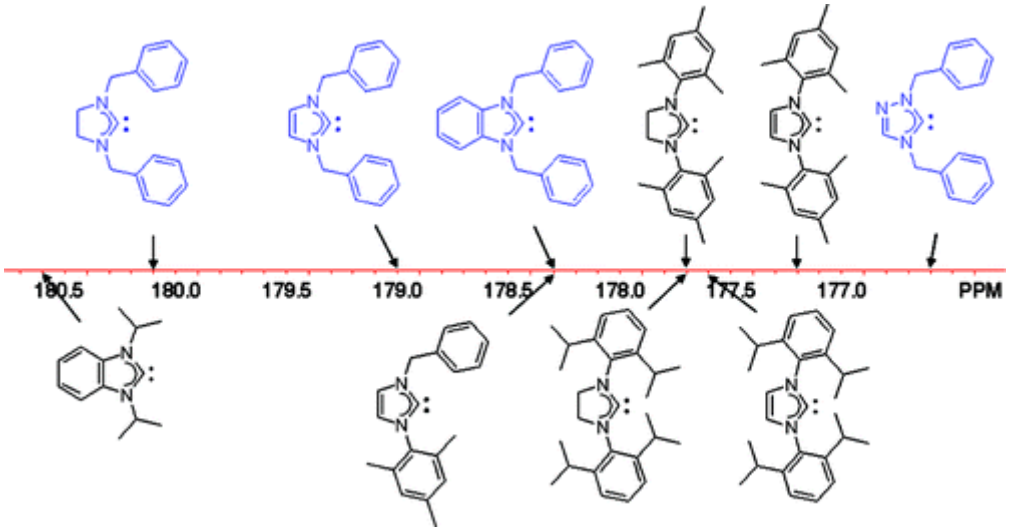

Figure 1.5 Donor abilities of common NHCs on the ^{13}C NMR scale.[63]

Very recently, the concept of HEP is extended to HEP2 for neutral, symmetrical cis-chelating ligands and unsymmetrical chelators.[66] The elucidation of stereoelectronic participation of diphosphine ligands on $[Rh(COD)(diphosphine)]^+$ complexes has been achieved by the DFT studies on the ^{103}Rh NMR measurements.[67] Excellent correlations

were reported between ^{57}Fe NMR and the TEP and steric factor (θ) in the case of [Fe(η^5-Cp)($SnPh_3$)(CO)(PR_3)] complexes.[68] The π-accepting properties of NHCs[69] has been experimentally verified by the ^{31}P NMR chemical shifts in carbene–phosphinidene adducts[70] and ^{77}Se chemical shifts in selenium carbene adducts.[71]

1.1.1.5 Quantitative Analysis of Ligand Effect (QALE)

The concept of QALE[31] was initially put forward by Giering *et al.*[30, 72-78] and interpreted by other research groups[79-83] and applied to experimental data. The QALE representation is based on a linear relationship connecting the experimentally measured properties and a set of stereoelectronic descriptors of the common form:

$$\text{Property} = a\,\chi_d + b\,(\theta - \theta_{st})\lambda + c\,E_{ar} + d\,\pi_p + e\,i + f \qquad \text{(Eq. 1.2)}$$

where χ_d[84] describes σ-electron donor capacity, θ is the Tolman cone angle,[28] θ_{st} is a steric threshold, λ is a switching function for the steric term, E_{ar} is a secondary electronic effect,[85] originally described as aryl effect, π_p describes the π-acidity,[86] and i describes the number of hydrogens in PZ_3-iHi. The coefficients a-f in the QALE equation were found out from a blend of graphical as well as regression analyses for different types of ligands coming across. The stereoelectronic parameters χ_d, θ, E_{ar} and π_p are available for around 300 ligands.[87]

1.1.2 Computational Ligand Electronic Parameters

1.1.2.1 Computed Electronic Parameter (CEP)

Computational chemistry has been extensively applied to unravel the geometry and reactivity of transition metal complexes.[88-91] Computationally derived parameters can play a vital role in assessing the electronic effect of ligands in various metal complexes.[92, 93] Crabtree *et al.* used quantum chemical techniques to forecast the CO stretching vibration of $LNi(CO)_3$ complexes for a broad range of 68 ligands (Figure 1.6).[31] The resultant parameter is termed as Computed Electronic Parameter (CEP) and is well correlated with the experimental terms such as Tolman parameter (TEP), Lever Electronic Parameter (LEP) and Hammett substituent constants (σ_m). Thus the parameter, CEP offers a simple and proper way to fairly accurate the electronic effects

for any ligand L. Assorted studies are reported in the literature subsequently, connecting the computational CEPs and experimental TEPs for different transition metal complexes with the help of suitable DFT methods.[33, 34, 94-96] Gusev used the IR data of $Ni(CO)_3(NHC)$ complexes to classify 76 NHC ligands according to the electron donor power[33] and compiled the CEPs of several complexes like $IrCl(CO)_2L$, $IrCp(CO)L$, $IrCp(CH_2{=}CH_2)L$ and $Ni(CO)_3L$.[34] In a similar way, Tonner and Frenking evaluated the CEPs of several $LNi(CO)_3$ and $L\text{-}RhCl(CO)_2$ complexes and estimated the donor strength of divalent carbon(0) compounds compared to common carbon(II) ligands.[94] The semiempirical calculations are also employed in this regard for $Mo(CO)_5L$, $W(CO)_5L$, and $CpRh(CO)(L)$ complexes[97] and for trans-$Rh(PR_3)_2(CO)X$ complexes[98] to derive semiempirical electronic parameter (SEP).

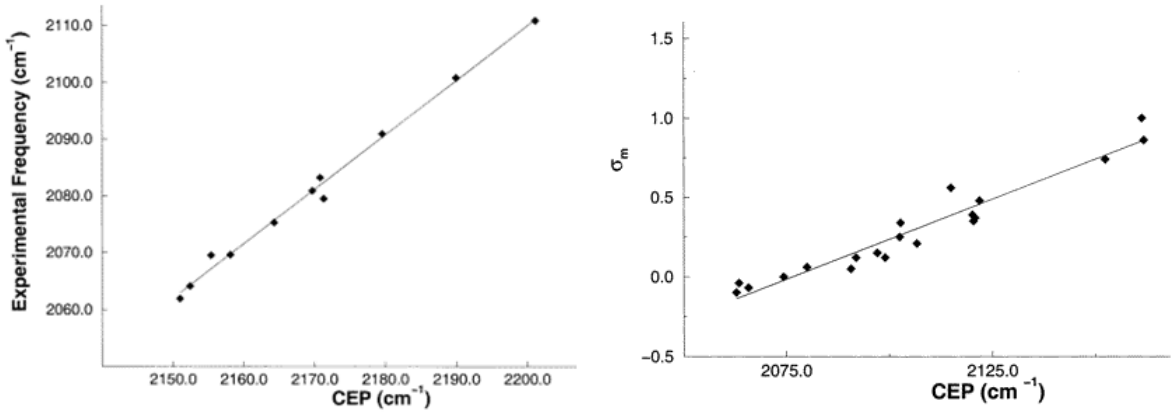

Figure 1.6 Correlation between CEP and experimental parameters for a wide range of 68 ligands.[31]

Computational ligand electronic parameters are developed by various research groups to quantify the effect of a variety of ligand groups. Mitsopoulou *et al*. reported the use of a Modified Electronic Parameter (ModEP) for the diimine ligands to obtain their contribution to the reduction potential of the M(diimine)(dithiolato) complexes where M = Pt, Pd, or Ni.[99] By analogy to the Tolman electronic parameter, a ligand electronic parameter, referred to as L_2EP, is introduced here for estimating the donating ability of chelating ligands.[100] The descriptor is based on the average of the computed stretching frequencies of CO in a series of isostructural $LL'Rh(CO)_2$ complexes. Recent reports by

Cremer *et al*. proposed the use of local CO stretching force constants instead of normal mode frequencies and arrived at local Tolman electronic parameter (LTEP) and were tested to verify the electronic properties of L ligands for a set of 42 $LNi(CO)_3$ complexes.[35] In fact, this method offered a straight understanding of the CO bond strength with no mode coupling. Soon after, another parameter called Metal Ligand Electronic Parameter (MLEP) is introduced by the same group using the local Ni-L stretching force constant to quantitatively judge the stereoelectronic factors of ligands like phosphines, and its main-group analogues for 181 $LNi(CO)_3$ complexes.[36] Very recently, the MLEP parameter is comprehensively employed to foretell the catalytic ability of transition metal complexes by evaluating the M–L bond strengths.[101]

1.1.2.2 Average Local Ionization Energy

The average local ionization energy, $I(r)$[102-103, 104] based studies established by Politzer *et al.* have been listed as another important calculated quantifier for the electronic effects caused by the ligands. The $I(r)$ function has been interpreted as the average energy needed to remove an electron at any particular point in the space of the molecule.[105] The $I(r)$ parameter is found to be more consistent with the ligands like phosphines and phosphites as they are soft bases.[106, 107] The smallest $I(r)$ value on the surface of a molecule, I_{min} can be regarded as a useful index to represent the electron donating and accepting power of substituents on the benzene ring. This has been verified by Politzer's group by deducing strong linear correlation between I_{min} values with Hammett constants.[105]

1.1.2.3 Molecular Electrostatic Potential (MESP)

The molecular electrostatic potential (MESP) at a given point p(x,y,z) in the neighborhood of a molecule is the force acting on a positive test charge located at p through the electrical charge cloud generated through the molecules, electrons and nuclei. The electrostatic potential of a molecule is considered as a high-quality steer in assessing the molecule's reactivity although the molecular charge distribution remains unperturbed through the external test charge. MESP is a real physical property and can be determined experimentally by x-ray diffraction studies[108, 109] as well as

theoretically.[110] The concept has been particularly useful as an indicator of the regions of electrophilic attack. The roots of the concept come from Coulomb's law, which is an experimental law that gives the amount of force between two stationary, electrically charged particles. According to this law, the force of attraction or repulsion between two point charges is directly proportional to the product of the charges and inversely proportional to the square of the distance between the charges:

$$F = \frac{q_1 q_2 \hat{\mathbf{r}}}{4\pi\varepsilon_0 \mathbf{r}^2} \qquad \text{(Eq. 1.3)}$$

where q_1 and q_2 are point charges separated by a distance $\mathbf{r}$, and a unit vector $\hat{\mathbf{r}}$ joins the position vectors of q_1 and q_2. $4\pi\varepsilon_0$ is the proportionality constant, where ε_0 is the vacuum electric permittivity. The magnitude of the electric field, E created by a single source point charge, q at a certain distance from it $\mathbf{r}$ in vacuum is given by:

$$|E| = \frac{1}{4\pi\varepsilon_0}\frac{|q|}{\mathbf{r}^2} \qquad \text{(Eq. 1.4)}$$

The familiar form of the Coulomb potential is given by,

$$V(\mathbf{r}) = \frac{-1}{4\pi\varepsilon_0}\frac{q_1 q_2}{\mathbf{r}^2} \qquad \text{(Eq. 1.5)}$$

The electrostatic potential, at a point $\mathbf{r}$ in the vicinity of a molecular system, having an electronic density function $\rho(\mathbf{r}')$ is given in Hartree units, as [111, 112]

$$V(\mathbf{r}) = \sum_A^N \frac{Z_A}{|\mathbf{R}_A - \mathbf{r}|} - \int \frac{\rho(\mathbf{r}')}{|\mathbf{r}' - \mathbf{r}|}\mathrm{d}\mathrm{r}' \qquad \text{(Eq. 1.6)}$$

where N is the total number of nuclei, Z_A is the nuclear charge of nucleus A, located at $\mathbf{R}_A$. The two terms in Eq. 1.6 stand for the nuclear and electronic contributions respectively. As seen in the expression itself, the two terms have opposite signs and opposite effects. Generally**,** the topological features of a function of many variables are expressed in terms of its gradient field.[113] Here, the gradient of V has the physical meaning, E=-∇V, which is the electric field generated by the nuclear and electronic charge distribution. The MESP at the nucleus, N is given by,

$$V_{\mathrm{N}} = \sum_{\mathrm{B}\neq\mathrm{A}} \frac{Z_{\mathrm{B}}}{|\mathbf{R}_{\mathrm{B}} - \mathbf{R}_{\mathrm{A}}|} - \int \frac{\rho(\mathbf{r}')}{|\mathbf{r} - \mathbf{r}'|} d^3\mathbf{r}' \qquad \text{(Eq. 1.7)}$$

The conception of electrostatic potential is very much related to electron density and it can do an important role in density functional theories. It was given by Poisson's equation that

$$\nabla^2 V(\mathbf{r}) = 4\pi\rho(\mathbf{r}) \qquad \text{(Eq. 1.8)}$$

The topological analysis of $\nabla V(\mathbf{r})$ is based on the identification and location of the critical points (CPs),[114] the points at which $\nabla V(\mathbf{r}) = 0$. Rank of the CP is given by the number of nonzero eigenvalues of the Hessian matrix A, the elements of which are defined by

$$A_{ij} = \frac{\partial^2 V(\mathbf{r})}{\partial \boldsymbol{r}_i \partial \boldsymbol{r}_i}, \ \boldsymbol{r} = \boldsymbol{r}_c \qquad \text{(Eq. 1.9)}$$

where $\boldsymbol{r}_c$ is defined as a critical point. The Eq. 1.9 presents a check on the trace of the Hessian matrix. The CP becomes nondegenerate if none of the eigenvalues of the Hessian matrix is zero. A nondegenerate CP is illustrated by two terms, R and σ and is represented as (R, σ). R denotes the rank of matrix A and σ is the signature, which is an algebraic sum of the signs of the eigenvalues. A nondegenerate CP having rank 3 can be of the following four probable types; (3, -3), (3, -1), (3, +1), and (3, +3). The CP corresponding to σ = - 3 refers to a maximum while a CP of σ= + 3 corresponding to a local minimum. A CP observed between a "bonded" pair of nuclei, is a (3, -1) CP and it will be located in the positive MESP region. The topology showing a (3, +1) has been associated with the presence of a ring structure. The (3, +3) CP[115, 116] which is usually found in the negative MESP region may be designated by the existence of either lone-pair electrons or a π-bond. The most negative-valued points in the MESP topography, denoted as V_{min} is a (3, +3) CP, and has been used to estimate the electron richness of a molecule.[117]

1.1.2.3.1 Substituent Effects

Molecular electrostatic potential (MESP) based electron distribution studies were pioneered by Tomasi *et al*.[118] In early 1970's they calculated the electronic charge distribution of unconjugated molecules and small cyclic molecules, but could not deal

with conjugated ones.[119] Afterward, the studies were extended to benzene[120] and found to be valid for assessing large molecules, even with hetero atoms. Politzer *et al.* have pointed out MESP analysis as a fundamental tool for studying the behavior of atoms and molecules.[121] The effectiveness of MESP analysis is unraveled in understanding a substituent's total electron attracting tendency and also used to interpret the electrophilic substitution reactions in monosubstituted benzenes.[122] The effect of substituents is even extended to bridgehead carbons.[123]

The MESP provides a three dimensional visualization of charge distribution and theoretical characterization of molecules.[124-129] The MESP analysis helps to perceive a wide variety of phenomena such as resonance effects, inductive effects, proximity effects, noncovalent interactions and aromaticity. Gadre and coworkers employed MESP and molecular tailoring approach[130-139] for emphasizing the molecular structure, reactivity and interactions. The most negative-valued MESP minima (V_{min})[140] is one of the most frequently used tools for the theoretical characterization of substituent effects. MESP at nucleus, V_n measures MESP at the position of atom A due to the rest of the nuclei and all the electrons.[141] Earlier research from Gadre and Suresh have shown the usefulness of V_{min} based studies conducted on mono substituted benzenes to characterize the circular aromatic π-electron delocalization.[142] The study was further extended to 45 doubly substituted benzenes and certain new parameters were coined such as D_p, D_m, and D_o, to account for the substituent pair-constants and additivity effect.[143] The V_{min} over the aromatic ring and MESP at the nucleus of *para* carbon, V_C are excellent descriptors to gauge substituent effect (Figure 1.7).[144] The V_C showed strong linear correlation with Hammett constants. An activating group, generally electron donating showed V_{min} near the *ortho* and *para* carbons, while the deactivating groups promoted the formation of V_{min} near the *meta* carbons. The phenomenon of aromaticity was well explored by the MESP topography for the π-regions of polycyclic aromatic hydrocarbons.[145-147] An account for the additive effects and steric effects was given with the help of MESP topography in substituted benzoic acids.[148] The deepest MESP point over the aromatic ring, V_{min} was regarded as a gauge for examining the through-bond and through-space substituent effects in substituted arenes for a variety of substituents.[149] The quantification of various

effects such as inductive, resonance, and through-space effects for variety of substituents, X in cation-π interactions was also reported with the help of V_{min} parameters.[150-152]

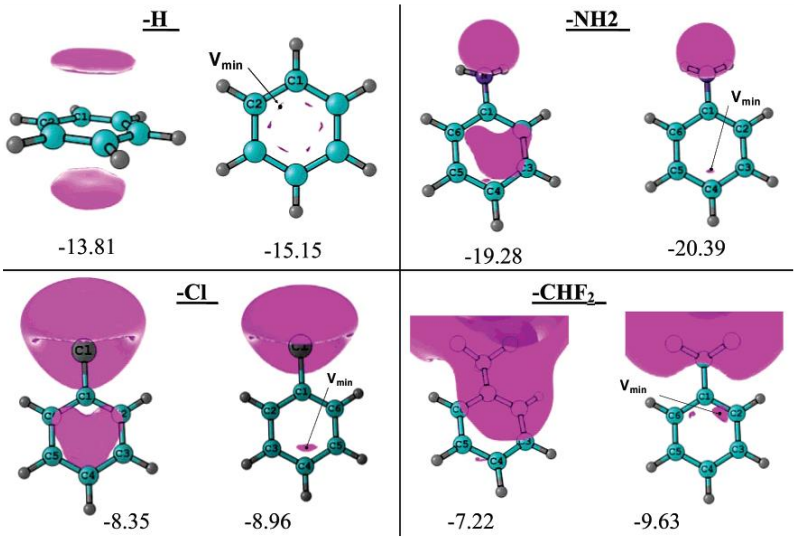

Figure 1.7 MESP isosurface values of benzene and substituted benzenes.[144]

1.1.2.3.2 Non -covalent Interactions

The MESP analysis is very useful in dealing with non-covalent interactions governed by substituents and hetero atoms.[153] Dougherty *et al*.[154, 155] showed that the prediction of cation-π interaction is possible through the analysis of electrostatic potential surface of the corresponding aromatics. Wheeler and Houk used MESP analysis[156-158] to study non-covalent interactions, including anion–π, cation-π and aryl-aryl interactions. The change in electron density due to substitution is reflected on the electrostatic potential, and dominated by the through-space effects.[159, 160] The MESP analysis of benzene dimers unpicks the direct interaction between the unsubstituted ring and the substituent.[161] In the case of ion-π complexes, the substituent effects can be interpreted by the direct interaction between ion and the substituent.[162] In anion- π interactions involving benzene ring, the predicted interaction energies correlate very well with computed MESP above the ring centroid.[163] The MESP approach has been also used for portraying non-covalent interactions in biological systems.[164] The relative magnitude of positive electrostatic potential helps to assess the reactivity of nucleophiles and then to interpret nucleophilic processes. [165, 166]

The positive character of the σ-hole concept is well explained by Politzer *et al*.[167] The σ-hole is a positive electro potential region formed by the non-covalent interaction between the covalently-bonded atoms of Groups IV–VII and a negative site.[168] Halogen bonding, an important class of non-covalent interaction, considered as a subclass of σ-hole interactions[169] could be precisely explained by MESP features. The competitiveness of σ-hole bonding over hydrogen bonding can be verified with the help of electrostatic potentials under comparable chemical environments.[170] Another analogous aspect, π-hole, which is a region of positive electrostatic potential and perpendicular to a portion of a molecular framework has also been proposed[171] for interpreting molecular interactions. Recently, topographical characterization of V_{min} is used by Suresh and coworkers to characterize lone pairs[172, 173] and to explain the lone pair-π interactions and C-C interactions.[174-176] The donor–acceptor (D-A) interactions were explained by the MESP minimum (V_{min}) and MESP at the nuclei (V_n) because of the more negative MESP at A, rather than D.[177, 178] The MESP topography is suggested as a tool to deduce the H_2 binding affinity of polyatomic anions,[179] π-bowls,[180] and endohedral fullerenes[181] and structural motifs of C_{60},[182] C_{50}[183] and lithium-cation-encapsulated C_{60}.[184]

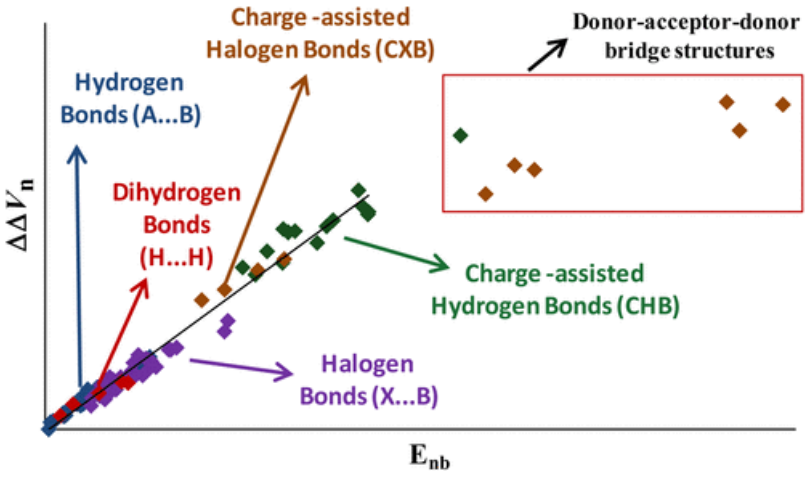

Figure 1.8 MESP Analysis of Hydrogen, Halogen, and Dihydrogen Bonds.[177]

1.1.2.3.3 MESP as a Ligand Electronic Parameter

Molecular electrostatic potential analysis has been regarded as a brilliant tool for the interpretation of stereoelectronic contour of various ligands to fine tune the reactivity

and catalytic activity of transition metal complexes and the earlier reports by Suresh *et al.* meticulously demonstrated the same. An understanding in this regard was achieved by Suresh et.al. in 2000,[185] by taking the substituted arene-$Cr(CO)_3$ complexes[186] as the epitome. The MESP analysis over the selected complexes confirmed the electron richness associated with the carbonyl oxygen compared to the arene moiety. A trigonal prismatic geometry has been suggested for the arene-$Cr(CO)_3$ complexes through a (3, -1) bond CP obtained from the electron density topography. The phosphines (PR_3) constitute a noteworthy class of ligands[187-190] and are very much beneficial for the design of a range of catalytic systems, including Grubbs ruthenium-based metathesis catalysts[191, 192] by appropriate usage of various R groups.

The electron donating power of a substituted phosphine ligand is attributed to the electron rich character of its lone pair. Suresh and Koga[193] used the molecular electrostatic potential minimum, V_{min} values to quantify the electronic effect of a substituted phosphine ligand. Moreover, the binding energies for the reaction $Ni(CO)_3 + PR_3 \longrightarrow Ni(CO)_3PR_3$ and $ScH_3 + PR_3 \longrightarrow ScH_3PR_3$ were found to be correlated with the V_{min} values. The V_{min} gave good linear correlations with pK_a of phosphine ligands and Tolman electronic parameter and it was further concluded that the MESP based parameters are more advantageous than the TEP and pK_a based ligand electronic parameters. Later, Suresh discussed about the usage of MESP steric value calculated from the V_{min} value of two-layer QM-MM geometry of the PR_3 ligands.[194] MESP analysis has been proven as a substitute for the Hammett constants as it can offer a perceptive about the steric effect separately from the electronic effect. Mathew and Suresh used a collective treatment of both the QM and QM/MM methods to facilitate the separation of steric and electronic effects of phosphines (Figure 1.9).[195] The QM derived MESP V_{min} of a PR_3 ligand furnished a straight gauge of the stereoelectronic effect of the ligand as ($E_{eff} + S_{eff}$), whereas the V_{min} of the ONIOM-optimized PR_3 provided the steric effect alone as $S_{eff.}$ The two-layer QM-MM ONIOM method helped to create electronic effect free environment of the substituents for the PR_3 ligands. The expressions derived in the two steps are denoted in equations Eq. 1.10 and Eq. 1.11 and the resulting expression only for the electronic effect, E_{eff} is given in Eq. 1.12. In this regard, the fourty six studied phosphines are classified into four categories, such as ($+E_{eff}$, $+S_{eff}$), ($+E_{eff}$, $-S_{eff}$), ($-E_{eff}$, $+S_{eff}$), and ($-E_{eff}$, $-S_{eff}$), for which plus

sign stands for electron donation and minus sign indicates electron withdrawal characters.

$$E_{eff} + S_{eff} = V_{min}(PH_3) - V_{min}(PR_3) \quad \text{(Eq. 1.10)}$$

$$S_{eff} = V_{min}(PH_3) - V_{min}(ONIOM\_PR_3) \quad \text{(Eq. 1.11)}$$

$$E_{eff} = V_{min}(ONIOM\_PR_3) - V_{min}(PR_3) \quad \text{(Eq. 1.12)}$$

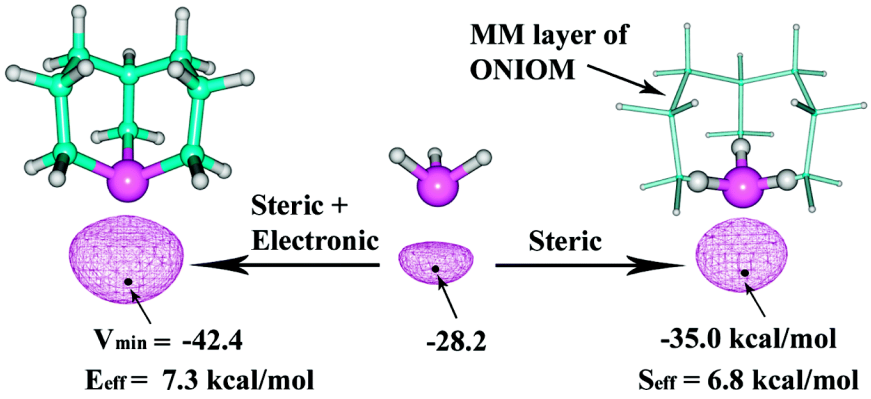

Figure 1.9 Stereoelectronic profile of phosphine ligands.[195]

The MESP at the phosphorous nucleus of the active form and ethylene-coordinated form of the Grubbs first-generation olefin metathesis catalysts are used to evaluate the effect of stereoelectronic features of the PR_3 ligand on the activation energy for the metallacyclobutane formation.[196] For the metathesis reaction, generally low activation barriers are reported with the first-generation Grubbs catalysts, having bulky ligands and so the steric effects dominate. Since electron rich ligands can decrease the activation barriers for a reaction, the electronic effects associated with the transition state for the formation of metallacyclobutane can also come to the picture. Thus it was concluded that for the metathesis reaction, a combined analysis of steric and electronic effects is required for the efficient tuning of the right catalyst, which can be effortlessly done by the quantum mechanically resulting MESP supported descriptors. For the second-generation Grubbs olefin metathesis catalysts,[197] a similar strategy was reported for the stereoelectronic properties of N-heterocyclic carbenes by the same group. Here, the MESP at the carbene carbon of both the NHC ligand and the alkylidene moiety are taken as the suitable quantifiers.[198]

N-heterocyclic carbenes are another important class of ligands normally encountering in organometallic chemistry.[199-201] The electron donating power associated with N-heterocyclic carbenes are assessed with MESP topological features like MESP at the carbene nucleus, V_C and MESP minimum at the carbene lone pair region, V_{min}.[202] The MESP parameters are found to be correlated with Tolman electronic parameters also. An organic model for the formation of NHC-CO_2 adducts was developed by Ajitha and Suresh for the assessment of stereoelectronic properties associated with the NHC ligands (Figure 1.10).[203] The MESP minimum, observed at the carbene lone pair region of NHC and at the carboxylate region of the NHC-CO_2 adducts are used as the possible descriptors. The CO_2 binding mostly depends on the electronic effect, for substitution at the carbon center, and steric effect dominates for the substitution at the N center.

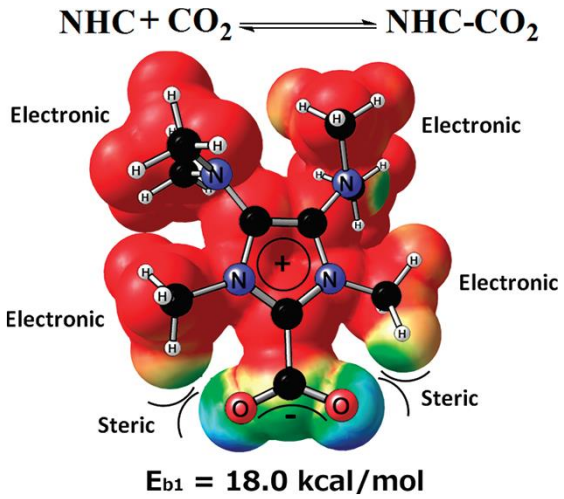

Figure 1.10 Stereoelectronic properties of NHC in terms of MESP.[203]

Another important thermodynamic aspect called trans influence[204, 205] which is very common in both square planar and octahedral transition metal complexes is figured out with the support of MESP analysis. The trans effect is termed as the effect of a ligand over the rate of substitution of another ligand which is present trans to it.[206] In 2011, Sajith and Suresh elucidated the trans influence governed by the ancillary phosphine ligands, L in the reductive elimination mechanism in cis-[$Pd(CH_3)_2L_2$] and cis-[$Pd(CH_3)(Cl)L_2$] square planar complexes with the aid of MESP analysis.[207] The activation barriers for the proposed reactions are influenced by the stereoelectronic effects caused

by the phosphine ligands. The electronic effect of the phosphine ligands is expressed in terms of the V_{min} at the lone pair region of phosphine ligands which showed linear correlation with the thermodynamic trans influence parameter, E_{trans}. Soon after, the topological features of MESP are used to reveal the trans influence of various X ligands in hypervalent iodine (III) CF_3[I(X)Cl] complexes. The MESP V_{min} at the lone pair regions of the chlorine atom is proposed as the suitable descriptors for the trans influence of X in hypervalent iodine complexes. The energy of the isodesmic reaction for the exchange of ligands, E_{XY} is recommended as a trans influence parameter for the CF_3[I(X)Y] complexes, and the same is used to classify the ligands into four sets, *viz*. very strong, strong, medium, and weak trans-influencing ligands.[208] In a similar study, the cis and trans Influences in hypervalent iodine(III) complexes of the type Ph[XI(OH)] are discussed by taking MESP V_{min} at the OH lone pair as the quantifier.[209]

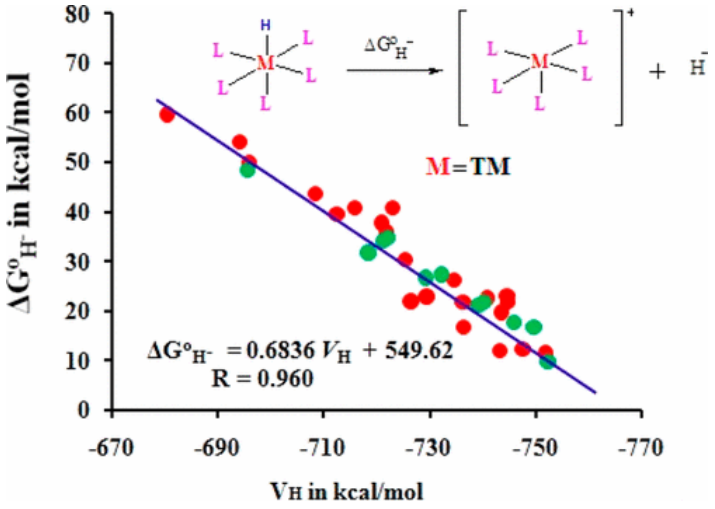

Figure 1.11 Quantification of thermodynamic hydricity using MESP.[210]

The hydridic character of octahedral metal hydride complexes of groups VI, VII and VIII is well explored through the tuning of hydride ligand environment with the help of MESP parameters.[211] Sandhya and Suresh proposed the MESP V_{min} at the hydride ligand and the MESP at the hydride nucleus (V_H) as good quantifiers for the hydride donor ability. The implication of the proposed MESP based hydridic parameter lies in tuning the activity of water splitting catalysts. The hydricity factor, $\Delta G°_{H^-}$ obtained from a thermodynamic cycle that describing hydride abstraction reaction by H_3O^+ ions gave

good correlations with the V_H values.[210] The greater the negative character of V_H, higher will be the hydricity of the complex which implies easy hydride ion elimination.

The ligand environment can also be tuned with the help of the MESP at the metal center and works in this regard are reported by Anjali and Suresh. The MESP at the Co center is used to predict the reduction potential of tetraza macrocyclic cobalt complexes.[212] The MESP at the palladium nucleus serves as an effective electronic parameter for predicting activation barriers of the oxidative addition reactions.[213] Moreover, the change in the reduction potential (ΔE^0) caused by the difference in ligand environments is measurable from the MESP at the chromium center in Fischer carbene complexes (FCCs) of chromium.[214] Thus, MESP based parameters can contribute largely in judging the substituent effects, bonding and molecular interactions in various organic, inorganic and organometallic systems. In the present thesis, the MESP parameters and Tolman parameter are comprehensively employed to gauge the reactivity patterns of organometallic systems.

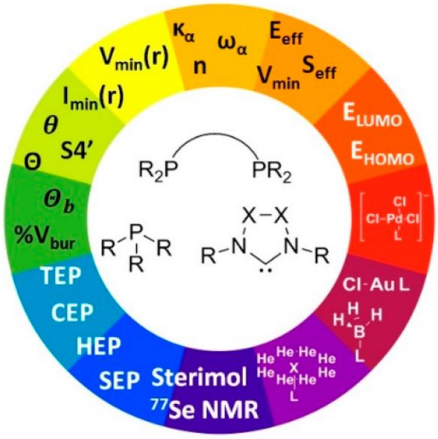

Figure 1.12 Computational ligand descriptors for catalyst design.[93]

In summary, there are numerous experimental as well as computational ligand electronic parameters available for the better tuning the reactivity of transition metal complexes.[25, 32, 92] Very recently, Durand and Fey reviewed the role of computational ligand descriptors to estimate the performance of homogeneous organometallic catalysts.[93] The study mainly focused on the ligand electronic parameters associated with

assorted monodentate phosphorus(III) donor ligands, bidentate P,P-donor ligands, and carbenes ligands. Both the individual descriptors and descriptor databases have been considered for each category of ligand. They have discussed the widespread application of the ligand electronic parameters such as TEP, CEP, HEP, SEP, ^{77}Se NMR, E_{eff}, S_{eff}, I_{min}, and V_{min} together with a few reaction-specific parameters for the known catalysts (Figure 1.12). The grouping of different descriptors for estimating the stereoelectronic contributions of the modified ligands will provide useful perceptions to fine-tune the properties of organometallic complexes.

Part B: Computational Chemistry Methods

1.2 An overview of computational chemistry

Computational chemistry uses the techniques and possibilities of theoretical chemistry and computer simulations to unravel diverse chemical problems. The earlier attempts by theoretical physicists, in 1928, to solve the Schrödinger equation, was the basis for most of the computational chemistry techniques. It was spotted that solutions to the Schrödinger equation are able to reproduce experimentally observed features of simple systems such as helium atom and hydrogen molecule. Later, the approximate solutions for larger systems and exact solutions to simple models inspired chemists and physicists to make qualitative briefing of various chemical aspects. The Schrödinger equation computational chemistry has been built up significantly enough to provide exceptionally accurate and appropriate tools to explore the properties of molecules within the framework of quantum mechanics. Useful insights are offered on the subjects of geometry prediction, molecular properties, spectroscopic observables, reaction mechanisms, catalysis *etc*. Another positive aspect concerning computational chemistry is that it is useful in investigating materials that are too difficult to locate or too expensive to procure.

The important computational methods are *ab initio* quantum chemical methods, density functional theory (DFT) methods, semiempirical methods, molecular mechanics (MM), molecular dynamics (MD), and hybrid quantum mechanics/molecular mechanics (QM/MM) methods. The *ab initio* quantum chemical methods constitute a group of methods where molecular structures are calculated using the Schrödinger equation. The semiempirical methods making use of experimentally derived parameters to provide the input into the mathematical models. In density functional theory, electron density is the key parameter to calculate the ground-state electronic structure of atoms, molecules and solid state materials. Molecular mechanics relies on force-field with embedded empirical parameters to elucidate and interpret the behavior of atoms and molecules. Molecular dynamics calculates the time dependent behavior of a molecular system and provides

comprehensive information regarding the fluctuations and conformational changes of biological molecules.

1.2.1 *Ab initio* Quantum Chemical Methods

The fundamental proposal of nearly all the quantum mechanical methods is to solve the Schrödinger equation for a system having many electrons and nuclei.[215] The term *ab initio* means calculations from first principles, and computational solution of the electronic time-independent Schrödinger equation.[216] The typical form of Schrödinger equation is given as,

$$H\Psi = E\Psi \qquad \text{(Eq.1.13)}$$

where H stands for the Hamiltonian operator for a system with nuclei and electrons explained by position vectors $\mathbf{R}_A$ and $\mathbf{r}_i$, Ψ is the many-electron wave function and E is the energy eigenvalue of the system. The Hamiltonian operator for a many-body system of N electrons and M nuclei can be written in atomic units as,

$$H = -\sum_{i=1}^{N}\frac{1}{2}\nabla_i^2 - \sum_{A=1}^{M}\frac{1}{2M_A}\nabla_A^2 - \sum_{i=1}^{N}\sum_{A=1}^{M}\frac{Z_A}{\mathbf{r}_{iA}} + \sum_{i=1}^{N}\sum_{j>i}^{N}\frac{1}{\mathbf{r}_{ij}} + \sum_{A=1}^{M}\sum_{B>1}^{M}\frac{Z_A Z_B}{\mathbf{R}_{AB}} \qquad \text{(Eq. 1.14)}$$

where M_A is the ratio of the mass of the nucleus A to the mass of an electron, Z_A is the atomic number of nucleus A, $\mathbf{r}_{ij}$ is the distance between the ith and jth electrons and $\mathbf{R}_{AB}$ is the distance between A^{th} and B^{th} nuclei., $\mathbf{r}_{iA}$ is the distance between i^{th} electron and A^{th} nucleus. The exact approach of solving Schrödinger equation is in principle and limited to hydrogen atom. Some simplifying assumptions are generally needed for the accurate calculation in all other systems. The most common assumptions made in this regard are the Born–Oppenheimer approximation and one-electron approximation.[217] In the Born–Oppenheimer approximation,[218] the solution is limited only for the electrons by assuming that the nuclei are fixed since the electrons move much faster than the nuclei. As a consequence, the nuclear kinetic energy term in the above equation turn into zero, and the repulsion term between the nuclei can be regarded as a constant. The remaining electronic Hamiltonian describing the motion of N electrons is given by,

$$H_{\text{elec}} = -\sum_{i=1}^{N}\frac{1}{2}\nabla_i^2 - \sum_{i=1}^{N}\sum_{A=1}^{M}\frac{Z_A}{\mathbf{r}_{iA}} + \sum_{i=1}^{N}\sum_{j>i}^{N}\frac{1}{\mathbf{r}_{ij}} \quad \text{(Eq.1.15)}$$

The Schrödinger equation including the electronic Hamiltonian thus becomes

$$H_{\text{elec}}\Phi_{\text{elec}}(\{\mathbf{r}_i\};\{\mathbf{R}_A\}) = E_{\text{elec}}\Phi_{\text{elec}}(\{\mathbf{r}_i\};\{\mathbf{R}_A\}) \quad \text{(Eq.1.16)}$$

and the solution for the electronic wave function is obtained as,

$$\Phi_{\text{elec}} = \Phi_{\text{elec}}(\{\mathbf{r}_i\};\{\mathbf{R}_A\}) \quad \text{(Eq. 1.17)}$$

The constant nuclear repulsion term should also be included in the calculation of the total energy for fixed nuclei.

$$E_{total} = E_{elec} + \sum_{A=1}^{M}\sum_{B>A}^{M}\frac{Z_A Z_B}{\boldsymbol{R}_{AB}} \quad \text{(Eq. 1.18)}$$

The above mentioned equations (Eq.1.13 to Eq.1.18) correspond to the electronic problem. Afterwards, the same assumptions are used to solve for the motion of nuclei. The nuclear Hamiltonian is thus formulated as,

$$H_{\text{nucl}} = -\sum_{A=1}^{M}\frac{1}{2M_A}\nabla_A^2 + E_{total}\,(\{\mathbf{R}_A\}) \quad \text{(Eq. 1.19)}$$

The total energy term, E_{total} provides an insight about the potential for nuclear motion. The solution to the nuclear Schrödinger equation,

$$H_{\text{nucl}}\Phi_{\text{nucl}} = E\Phi_{\text{nucl}} \quad \text{(Eq. 1.20)}$$

is specified by the expression,

$$\Phi_{\text{nucl}} = \Phi_{\text{nucl}}(\{\mathbf{R}_A\}) \quad \text{(Eq. 1.21)}$$

Here, *E* is the B-O approximation to the total energy which is comprised of the electronic, rotational, vibrational, and translational energy terms. The consequent approximation for the total wave function is deduced as,

$$\Phi(\{\mathbf{r}_i\};\{\mathbf{R}_A\}) = \Phi_{\text{elec}}(\{\mathbf{r}_i\};\{\mathbf{R}_A\})\,\Phi_{\text{nucl}}(\{\mathbf{R}_A\}) \quad \text{(Eq. 1.22)}$$

Thus, B-O approximation furnished the separation of electronic and nuclear Hamiltonians, as well as the electronic wave functions. The electronic wave functions show an explicit dependance over the electronic coordinates and a parametrical dependance over nuclear coordinates.

1.2.1.1 Hartree-Fock Theory

Hartree Fock calculation is the most general type of *ab initio* calculation in which the many-electron Schrödinger equation breaks into many simpler one-electron equations.[219, 220] Each one-electron equation is solved for a single-electron wave function, called an orbital, capable to describe the behavior of an electron in the net field of other electrons. The wave function is formed from linear combinations of atomic orbitals or, more precisely, basis functions and as a consequence, HF calculations provide a computed energy greater than the HF limit. To explain the exact wave function for a fully interacting system, a simple system containing non-interacting electrons can be selected first; having the characteristic Hamiltonian,

$$H = \sum_{i=1}^{N} h(i) \qquad \text{(Eq. 1.23)}$$

Here, $h(i)$ corresponds to the operator describing the kinetic and potential energies of electron *i*. A set of eigenfunctions,represented as spin orbitals, χ_j can be proposed for $h(i)$.

$$h(i)\chi_j(\mathbf{x}_i) = \varepsilon_j \chi_j(\mathbf{x}_i) \qquad \text{(Eq. 1.24)}$$

The corresponding many-electron wave function can be written as the product of individual spin orbital wave functions and is called the *Hartree Product* (HP), given by,

$$\Psi^{\mathrm{HP}}\left(\mathbf{x}_1, \mathbf{x}_2, \ldots, \mathbf{x}_N\right) = \chi_i(\mathbf{x}_1)\chi_j(\mathbf{x}_2) \ldots \ldots \chi_N(\mathbf{x}_N) \qquad \text{(Eq. 1.25)}$$

There are some basic drawbacks associated with the Hartree product. It doesn't justify the indistinguishability of electrons, but managed to distinguish electron-one as occupying spin orbital, χ_i and electron-two as occupying χ_j. The vital requirement associated with the exact wave function apart from satisfying the Schrödinger equation

is that it should obey the antisymmetry principle (a general form of Pauli's principle). *ie*, "a many electron wave function must be antisymmetric, with respect to the interchange of both the spin and space of any two electrons".

$$\Phi(\mathbf{x}_1, \dots, \mathbf{x}_i, \dots, \mathbf{x}_j, \dots, \mathbf{x}_N) = -\Phi((\mathbf{x}_1, \dots, \mathbf{x}_i, \dots, \mathbf{x}_j, \dots, \mathbf{x}_N) \quad \text{(Eq. 1.26)}$$

But the Hartree product fails to satisfy the antisymmetry principle. The antisymmetrized wave function can be accomplished by organizing the one-electron spin-orbital in a determinant form called Slater determinant. The Slater determinant for an N-electron wave function can be written as:

$$\Psi(\mathbf{x}_1, \mathbf{x}_2, \dots, \mathbf{x}_N) = \frac{1}{\sqrt{\mathrm{N!}}} \begin{vmatrix} \chi_i(\mathbf{x}_1) & \chi_j(\mathbf{x}_1) & \dots & \chi_N(\mathbf{x}_1) \\ \chi_i(\mathbf{x}_2) & \chi_j(\mathbf{x}_2) & \dots & \chi_N(\mathbf{x}_2) \\ . & . & & . \\ . & . & & . \\ . & . & & . \\ \chi_i(\mathbf{x}_N) & \chi_j(\mathbf{x}_N) & \dots & \chi_N(\mathbf{x}_N) \end{vmatrix} \quad \text{(Eq. 1.27)}$$

where $\frac{1}{\sqrt{\mathrm{N!}}}$ is called normalization factor. For N electrons, N spin orbitals are there, the rows of the determinant are designated by electrons ($\mathbf{x}_1$, $\mathbf{x}_2$, etc.) and columns by spin orbitals (χ_i, χ_j, etc.). The interchange of the coordinates of two electrons will correspond to the interchange of the two rows of the determinant resulting in the sign change. If the two electrons occupy the same spin orbitals, it will result in two equal columns in the determinant, and consequenlty, determinant will be zero. Thus, the Pauli's exclusion principle and antisymmetry condition are assured. The normalized form of Slater determinant having only the diagonal elements can be further simplified and expressed as,

$$\Psi(\mathbf{x}_1, \mathbf{x}_2, \dots, \mathbf{x}_N) = |\chi_i \chi_{j \dots\dots} \chi_N\rangle \quad \text{(Eq. 1.28)}$$

Thus, the Slater determinant represents the occupied spin orbitals from which it originates. The determinants with orthonormal spin orbitals will be normalized, whereas with different orthonormal spin orbitals will be orthogonal. Another significance concerned with the Slater determinants is that it encompasses exchange correlation with the judgment that, the motion of two electrons with parallel spins is correlated and that

with opposite spins continued as uncorrelated. According to the variation principle, the appropriate wave function of the functional form of Ψ will be the one with the lowest possible energy, given as,

$$E_0 = \langle \Psi_0 | H | \Psi_0 \rangle \qquad \text{(Eq. 1.29)}$$

where H is the full electronic Hamiltonian. The HF equation will be obtained by minimizing E_0, corresponding to the choice of spin orbitals and can be written as an eigenvalue equation of the general form,

$$f(i)\chi(\mathbf{x}_i) = \varepsilon\chi(\mathbf{x}_i) \qquad \text{(Eq. 1.30)}$$

Here, $f(i)$ is the effective one-electron operator, called the Fock operator, having the form,

$$f(i) = -\frac{1}{2}\nabla_i^2 - \sum_{A=1}^{M}\frac{Z_A}{\mathbf{r}_{iA}} + \nu^{\mathrm{HF}}(i) \qquad \text{(Eq. 1.31)}$$

where $\nu^{\mathrm{HF}}(i)$ is the average potential experienced by i^{th} electron due to the effect of other electrons. The HF equation is a non-linear one and the iterative procedure for solving it is called self-consistent-field (SCF) method. For that, an initial guess at the spin orbitals is made to get the average fields to solve the eigenvalue equation for a new set of spin orbitals. The new spin orbitals will give new fields and the procedure is repeated for self-consistency. The solution to Eq. 1.30 provides a set of orthonormal HF spin orbitals χ_k having orbital energies $\mathcal{E}_k$. The Slater determinant formed from occupied spin orbitals will give the HF ground state wave function. The orbitals other than the occupied spin orbitals are termed as virtual or unoccupied orbitals. For the HF equation, there will be infinite number of solutions and virtual spin orbitals and for solving it, a finite set of spatial basis functions are used.

There are two important theorems associated with the HF equations, namely Koopman's theorem and Brillouin's theorem.[219] The Koopman's theorem presents an interpretation of the HF orbital energies as ionization potentials and electron affinities. The theorem states that for an N-electron HF single determinant with occupied and virtual spin orbital energies $\mathcal{E}_a$ and $\mathcal{E}_r$, the ionization potential to produce (N-1) –electron

single determinant obtained by removing an electron from spin orbital, χ_a and the electron affinity to produce (N+1) –electron single determinant obtained by adding an electron to spin orbital, χ_r are respectively -$\mathcal{E}_a$ and -$\mathcal{E}_r$. According to Brillouin's theorem, the matrix element between a HF single determinant and determinants differ by a single excitation is zero. It can also be stated that singly excited determinants, $|\Psi_a^r\rangle$ will not interact directly with a reference HF determinant, $|\Psi_0\rangle$.

$$\langle\Psi_0|H|\Psi_a^r\rangle = 0 \qquad \text{(Eq. 1.32)}$$

The derivation of HF equations regarding closed shell systems are built up separately by Clemens C. J. Roothaan and George G. Hall.[221, 222] The HF equation in Eq. 1.30 can be amended by considering the spin orbitals as linear combinations of basis functions (Φ_μ).

$$\psi_i = \sum_{\mu=1}^{K} C_{\mu i}\Phi_\mu \qquad i = 1, 2, \ldots\ldots, K \qquad \text{(Eq. 1.33)}$$

where $C_{\mu i}$ are the coefficients of Φ_μ, and K is the total number of basis functions. The Roothan-Hall equation for closed shell systems is also known as restricted Hartree-Fock theory (RHF). In a single matrix form, it can be written more compactly as,

$$\mathbf{FC} = \mathbf{SC\varepsilon} \qquad \text{(Eq. 1.34)}$$

where **F** is the Fock matrix, **C** is a matrix of coefficients, **S** is the overlap matrix of the basis functions and **ε** is the matrix of orbital energies. From here onwards, the determination of HF molecular orbitals, ψ_i and orbital energies $\mathcal{E}_i$ means solving Eq.1.34.

1.2.1.2 Post Hartree-Fock Methods

HF method does not consider electron correlation which confines the accuracy of it. Post Hartree-Fock methods are a set of electron correlation methods developed to improve on the SCF or HF method by adding electron correlation more precisely. [223-225] The correlation energy is given by the difference between the exact energy and the energy obtained by the HF method.

$$E_{corr} = \varepsilon_0 - E_{HF} \qquad \text{(Eq. 1.35)}$$

where E_{HF} is the energy in the Hartree-Fock limit and ε_0 is the exact nonrelativistic energy of a system. The famous post HF methods include Møller-Plesset perturbation theory (MPn), configuration interaction (CI), and coupled cluster theory.

1.2.1.2.1 Møller-Plesset Perturbation Theory

Møller-Plesset perturbation (MP) theory [226] was proposed by Møller and Plesset in the early 1930's in order to apply the perturbation theory for calculating correlation energy.[227, 228] The MPn methodology is not variational as the calculated energy may be lower than the true ground state energy. For the second order perturbation (MP2),[229] two electron integrals over those corresponding to the combination of two occupied and two virtual MOs are only desirable, which makes it the most economical method for including electron correlation. MP2 energy can be calculated at a very similar cost that is required for obtaining the HF energy. Higher orders of perturbation are available for the improved convergence.[230] In third order perturbation (MP3), the matrix elements involving doubly excited determinants are only being estimated. Within the MP4 level, integrals involving triply and quadruply excited determinants come into view and this makes it the costliest one. The exact Hamiltonian operator H for the MPn method can be given by,

$$H = H_0 + \lambda V \qquad \text{(Eq. 1.36)}$$

where H_0 is the unperturbed or 'zeroth order' Hamiltonian, V is the perturbation and C is an arbitrary parameter that controls the size of the perturbation. When $\lambda = 0$, then $H = H_0$ and when $\lambda = 1$, then H equals its true value. Here, the zeroth-order wave function is an exact eigenfunction of the Fock operator, which can be refered as the unperturbed operator. For a given λ value, the exact energy of the ground state can be written as an infinite summation of all the perturbation terms.

$$E = \sum_{i=0}^{\infty} \lambda^i E^i \qquad \text{(Eq. 1.37)}$$

1.2.1.2.2 Configuration Interaction (CI)

Configuration Interaction is the oldest and simplest multiple-determinant wave function based on the variational principle.[231] The wave Function is constructed by starting with the HF wave function and making new determinants by promoting electrons from the occupied to unoccupied orbitals and the subscripts S, D, T, *etc*., are used to designate the singly, doubly, triply, etc., excited determinants. Cosequently, CI calculations are categorized on the basis of number of excitations used to make each determinant.[232, 233] Configuration interaction single- excitation (CIS) calculation is achieved by moving one electron for each determinant. Configuration interaction double-excitation (CID) is restricted to double excitations only and single-and double-excitation (CISD) calculations for single- and double-excitations. Triple-excitation (CISDT) and quadruple-excitation (CISDTQ) calculations are compiled exceptionally for high precision results. The configuration interaction calculation with all possible excitations is called a full CI. The general form of CI wavefunction can be written as:

$$|\Phi_0\rangle = c_0|\Psi_0\rangle + \sum_{ar} c_a^r|\Psi_a^r\rangle + \sum_{\substack{a<b \\ r<s}} c_{ab}^{rs}|\Psi_{ab}^{rs}\rangle + \sum_{\substack{a<b<c \\ r<s<t}} c_{abc}^{rst}|\Psi_{abc}^{rst}\rangle + \cdots \qquad \text{(Eq. 1.38)}$$

The first term denotes the Slater determinant corresponding to the HF wave function and all other terms constitute singly, doubly, triply,..., n-tuply excited determinants with appropriate expansion coefficients. The indices *a*, *b*, *c*, etc. represent the occupied orbitals and *r*, *s*, *t*, etc. represent the virtual orbitals involved in the electron excitations. Multi-configurational self-consistent field (MCSCF) methods are based on multiple-determinant wave functions.[234] They can offer the most accurate results with more of the correlation energy with fewer configurations when compare to a CI calculation. The MCSCF calculation for which all combinations of the active space orbitals are included is termed as a complete active space self-consistent field (CASSCF)[235] calculation and is popular for the maximum correlation given in the valence region. Another type of calculations called multi-reference configuration interaction (MRCI)[236] are starting from a reference state with a MCSCF calculation rather than a HF wave function.

1.2.1.2.3 Coupled Cluster (CC) Theory

In Coupled cluster calculations, the wave function is a linear combination of many determinants constructed using the exponential cluster operator to account for electron correlation. The theory was put forward by Čížek in 1966 and the means for selecting the determinants in a CC calculation is more complex than that in CI formalism.[237, 238] The CC method proposes the full CI wave function as,

$$\Psi_{CC} = e^{T}\Psi_{HF} \qquad \text{(Eq. 1.39)}$$

where Ψ_{HF} is a Slater determinant created from HF molecular orbitals and e^{T} is given by Eq. 1.22.

$$e^{T} = 1 + T + \frac{1}{2}T^{2} + \frac{1}{6}T^{3} + \cdots = \sum_{k=0}^{\infty}\frac{1}{k!}T^{k} \qquad \text{(Eq. 1.40)}$$

Here, T is called cluster operator which acts on Ψ_{HF} to produce a linear combination of excited slater determinants and can be given as:

$$T = T_1 + T_2 + T_3 + \ldots. + T_n \qquad \text{(Eq. 1.41)}$$

where n represents the total number of electrons, and various T_i operators generate all possible determinants having i^{th} excitation from the reference.

$$T_2 = \sum_{i<j}^{\text{occ.}}\sum_{a<b}^{\text{vir.}} t_{ij}^{ab}\,\Psi_{ij}^{ab} \qquad \text{(Eq. 1.42)}$$

The amplitude values t are determined by the constraint that (Eq. 1.21) should be satisfied. Considering the double excitation $T = T_2$, the Taylor expansion of the exponential function in (Eq. 1.21) gives:

$$\Psi_{CCD} = \left(1 + T_2 + \frac{1}{2!}T_2^{2} + \frac{1}{3!}T_2^{3} + \cdots\right)\Psi_{HF} \qquad \text{(Eq. 1.43)}$$

where CCD implies coupled cluster with only the double excitation operator. Similar to CI, there are assorted orders of the CC expansion, called CCD, CCSD, CCSD (T), and so on.[239] The mere inclusion of a T_1 operator may not give any improvement over HF, as

matrix elements between the HF and singly excited states are zero. Therefore, the lowest level of approximation available is $T = T_2$, and is denoted as coupled cluster doubles (CCD). Using $T = T_1 + T_2$ gives the CCSD model, and $T = T_1 + T_2 + T_3$,… giving the CCSD (T) model.

1.2.2 Semiempirical Methods

Semiempirical methods are the simplified forms of HF theory using certain parameters from empirical data. [240-242] The methods were useful in the earlier days, when execution of HF calculations without any further approximations was hard to perform with the minimal computational facilities. These are having the same layout for calculation like a HF method, and within the format, some information is either approximated or completely avoided. The parameters to get the neglected values are adopted from experimental data or *ab initio* calculations. The calculations are faster and less reliable compared to the *ab initio* methods. These are generally useful in forecasting molecular geometry including transition state structures, vibrational modes and energetics and are not suitable for van der Waals and dispersion intermolecular interactions, since diffuse basis functions are not available. Semiempirical methods are based on the primary approximations, *viz*. elimination of core electrons from the calculation, minimum required number of basis sets, and the reduction of the number of two-electron integrals. The Hückel method can be considered as the simplest and primitive semiempirical method which meant to forecast orbital coefficients by modeling π valance electrons in a planar conjugated hydrocarbon.[243]

John Pople in 1965 introduced the neglect of differential overlap (NDO) method which involves the approximation of the overlap matrix **S** as unit matrix in the HF equation $\mathbf{FC=SC\varepsilon}$.[244] The overlap matrix is approximated as the unit matrix, $\mathbf{S}=1$ by avoiding all the integrals involving different atomic orbitals in the complete neglect of differential overlap (CNDO) method. The contemporary semiempirical methods are based on the modified neglect of differential overlap (MNDO) approach.[245] Here, chemical properties are interpreted from parameters assigned for different atomic types. The zero differential overlap (ZDO) approximation is another method to reduce the two-

electron integral which neglects all products of basis functions. The primitive semiempirical models are varying in nature with the approximations used to evaluate the one- and two-electron integrals and also the parametrizaton strategies. In this manner, certain other models are also coined, *viz*. intermediate neglect of differential overlap (INDO),[246] in which all one-center two-electron integrals are included with CNDO, and the neglect of diatomic differential overlap (NDDO),[247] where all two-center integrals for repulsion between a charge distribution on one-center and a charge distribution on another center. The INDO method is hardly used nowadays, but the modifiied forms are available such as, MINDO (Modified Intermediate Neglect of Differential Overlap), ZINDO (Zerner's INDO) and SINDO (symmetrically orthogonalized intermediate NDO). The CNDO and INDO are the models pertinent to solve the Roothaan equation by adding approximations for the integrals given in Fock matrix. The commonly used Austin model 1 (AM1)[248] and Parametric Method 3 (PM3)[249] methods are the modifications of MNDO version. The AM1 method making use of a modified form for nuclear-nuclear core repulsion, when compared to MNDO. This makes it advantageous over conventional MNDO, in explaining chemical properties such as heats of formation. The PM3 method is found to be more reliable than AM1, as the parametrization is in such a way to reproduce a series of molecular properties.

1.2.3 Density Functional Theory (DFT)

Density Functional Theory is primarily applicable to the electronic ground state structure of atoms and molecules and it has gained wide interest through these years.[250] The theory is based on electron density distribution ρ (**r**), instead of the many-electron wave function Ψ (r_1, r_2, r_3,...) used in HF theory.[251] Wavefunction of an *N* electron system depends on 3N variables while density is a function of only three variables which makes it convenient to deal with. The first reports on DFT were made by Hohenberg and Kohn in 1964 and subsequently by Kohn and Sham in 1965. The ground rules of the theory were implanted from the Thomas Fermi model proposed in 1927, soonafter the fundamental report of Schrödinger in 1926.[252] The basic idea behind the theory is that there exists a one-to-one relationship between total electron density and total electronic energy. In short, energy *E* is a unique functional of electron density ρ(**r**). A functional

facilitates a function to be mapped onto a number. $\rho(\mathbf{r})$ is a physical observable defined as the number of electrons in the unit volume around a point **r** in space and which on integration over all space, gives the total number of electrons *N*.

$$N = \int \rho(\mathbf{r}) d\mathbf{r} \qquad \text{(Eq. 1.44)}$$

DFT provides a close connection between experiment and theory by enabling the calculation of an ample choice of molecular properties which in turn furnish the vital links regarding the molecular geometry and electronic properties.[253]

1.2.3.1 Thomas-Fermi Model

Thomas-Fermi model [254-256] can be considered as the primitive form of DFT, formulated in 1920's and is used to express the total kinetic energy of the electrons in terms of the spatially varying electron density. The Thomas–Fermi (TF) equations, along with an implicit variational principle, characterized the first attempts to define the DFT formalism and the energy is computed not in relation to a wave function. The kinetic energy of the uniform electron gas, $T_{\mathrm{TF}}[\rho(\mathbf{r})]$ can be written as:

$$T_{\mathrm{TF}}[\rho(\mathbf{r})] = \frac{3}{10}(3\pi^2)^{2/3} \int \rho^{5/3}(\mathbf{r}) d\mathbf{r} \qquad \text{(Eq. 1.45)}$$

The energy functional in TF theory is given as,

$$E_{\mathrm{TF}}[\rho] = T_{\mathrm{TF}}[\rho] + E_{\mathrm{ne}}[\rho] + J[\rho] \qquad \text{(Eq. 1.46)}$$

Here, $T_{\mathrm{TF}}[\rho]$ is the kinetic energy, $E_{\mathrm{ne}}[\rho]$ is the attraction between nucleus and electrons and $J[\rho]$ is the Coulomb part. In 1930, the inclusion of the exchange part $K_{\mathrm{D}}[\rho]$ in Eq. 1.46 constituted a modified version, known as Thomas–Fermi–Dirac model.[257] Although both the models are important as they constitute the basic elements of DFT, the assumptions used within makes it inferior in the current formalism. The assumption of uniform electron gas is satisfactory in the case of valence electrons in certain systems, but is not sufficient for atoms and molecules.

1.2.3.2 Hohenberg-Kohn Theorem

The Hohenberg–Kohn theorem formulated in 1964 established a dependence of the energy on the density can be considered as the foundation aspect of modern DFT techniques.[258] As per the formulation of DFT, electrons interact with one another and with an external potential. The first theorem of Hohenberg and Kohn is an existence theorem and it states that the ground state energy and other properties of a system were uniquely defined by the electron density, $\rho(\mathbf{r})$. Otherwise, it can also be stated that the energy E is a unique functional of $\rho(\mathbf{r})$. The energy functional can be written as,

$$E[\rho(\mathbf{r})] = \int V_{\text{ext}}(\mathbf{r})\rho(\mathbf{r})d\mathbf{r} + F[\rho(\mathbf{r})] \qquad \text{(Eq. 1.47)}$$

Here, the first term corresponding to the interaction of electrons with an external potential $V_{\text{ext}}(\mathbf{r})$, and F $[\rho(\mathbf{r})$ is the sum of kinetic energy of the electrons and the contribution from interelectronic interactions. Acccording to the second Hohenberg–Kohn variational theorem, the density obeys a variational principle in such a way that the density that minimizes the total energy is the exact ground state density. For the minimization of energy, the constraint on the electron density is introduced as a Lagrangian multiplier.

$$\frac{\delta}{\delta\rho(\mathbf{r})}\left[E[\rho(\mathbf{r})] - \mu\int \rho(\mathbf{r})d\mathbf{r}\right] = 0 \qquad \text{(Eq. 1.48)}$$

This can be simplified as,

$$\left(\frac{\delta E[\rho(\mathbf{r})]}{\delta\rho(\mathbf{r})}\right)_{V_{\text{ext}}} = \mu \qquad \text{(Eq. 1.49)}$$

The Eq. 1.49 is the DFT equivalent representation of the Schrödinger equation. The Lagrangian multiplier, μ can be related with the chemical potential of an electron cloud and in turn with the electronegativity, χ as,

$$\left(\frac{\delta E}{\delta N}\right)_{V_{\text{ext}}} = \mu = -\chi \qquad \text{(Eq. 1.50)}$$

1.2.3.3 The Kohn-Sham Equations

Soon after the seminal DFT paper by Hohenberg and Kohn, Kohn and Sham formulated a useful method for carrying-out DFT calculations that maintains the precise character of DFT. [259] The inconvenience with Eq. 1.47 is that the function $F[\rho(\mathbf{r})]$ is unknown. For that, Kohn and Sham suggested that $F[\rho(\mathbf{r})]$ can be represented as the sum of three terms.

$$F[\rho(\mathbf{r})] = E_{\mathrm{KE}}[\rho(\mathbf{r})] + E_{\mathrm{H}}[\rho(\mathbf{r})] + E_{\mathrm{XC}}[\rho(\mathbf{r})] \qquad \text{(Eq. 1.51)}$$

Here, $E_{\mathrm{KE}}[\rho(\mathbf{r})]$ is the kinetic energy of non-interacting electrons, given by,

$$E_{\mathrm{KE}}[\rho(\mathbf{r})] = \sum_{i=1}^{N} \int \Psi_i(\mathbf{r}) \left(-\frac{\nabla^2}{2}\right) \Psi_i(\mathbf{r}) d\mathbf{r} \qquad \text{(Eq. 1.52)}$$

$E_{\mathrm{H}}[\rho(\mathbf{r})]$ is the electron-electron Coulombic energy or Hartree electrostatic energy,

$$E_{\mathrm{H}}[\rho(\mathbf{r})] = \frac{1}{2} \iint \frac{\rho(\mathbf{r}_1)\rho(\mathbf{r}_2)}{|\mathbf{r}_1 - \mathbf{r}_2|} d\mathbf{r}_1 d\mathbf{r}_2 \qquad \text{(Eq. 1.53)}$$

and $E_{\mathrm{XC}}[\rho(\mathbf{r})]$ is the energy contributions from exchange and correlation. The full expression of enery of an N electron system within the structure of Kohn-Sham scheme is obtained by combining the $E_{\mathrm{KE}}[\rho(\mathbf{r})]$ and $E_{\mathrm{H}}[\rho(\mathbf{r})]$ terms with the electron–nuclear interaction.

$$E[\rho(\mathbf{r})] = \sum_{i=1}^{N} \int \Psi_i(\mathbf{r}) \left(-\frac{\nabla^2}{2}\right) \Psi_i(\mathbf{r}) d\mathbf{r} + \frac{1}{2} \iint \frac{\rho(\mathbf{r}_1)\rho(\mathbf{r}_2)}{|\mathbf{r}_1 - \mathbf{r}_2|} d\mathbf{r}_1 d\mathbf{r}_2 + E_{\mathrm{XC}}[\rho(\mathbf{r})] - \sum_{A=1}^{M} \int \frac{Z_A}{\mathbf{r} - \mathbf{R}_A} \rho(\mathbf{r}) d\mathbf{r} \qquad \text{(Eq. 1.54)}$$

The exchange correlation functional, $E_{\mathrm{XC}}[\rho(\mathbf{r})]$ of a system, made up of the elements from the exchange and correlation also depends on the difference between precise kinetic energy and the kinetic energy of non-interacting electrons, $E_{\mathrm{KE}}[\rho(\mathbf{r})]$. Accordingly, Kohn and Sham represented the density of the system as a sum of the square moduli of the one-electron orthonormal orbitals as,

$$\rho(\mathbf{r}) = \sum_{i=1}^{N} |\psi_i(\mathbf{r})|^2 \qquad \text{(Eq. 1.55)}$$

The one-electron Kohn-Sham equation can be formulated by applying the variational condition in Eq. 1.55 and is represented as,

$$\left\{-\frac{\nabla_1^2}{2}-\left(\sum_{A=1}^{M}\frac{Z_A}{\mathbf{r}_{1A}}\right)+\int\frac{\rho(\mathbf{r}_2)}{\mathbf{r}_{12}}d\mathbf{r}_2+V_{\mathrm{XC}}[\mathbf{r}_1]\right\}\psi_i(\mathbf{r}_1)=\varepsilon_i\psi_i(\mathbf{r}_1) \qquad \text{(Eq. 1.56)}$$

where the external potential arises with the interaction with M nuclei, ε_i represents orbital energy and V_{XC} constitutes the exchange – correlation functional. The relation between V_{XC} and E_{XC} is as follows:

$$\mathrm{V_{XC}}[\mathbf{r}]=\frac{\delta E_{\mathrm{XC}}[\rho(\mathbf{r})]}{\delta\rho(\mathbf{r})} \qquad \text{(Eq. 1.57)}$$

Now it is made convenient to calculate total electronic energy via Eq. 1.54. The self-consistent approach is adopted to solve for the Kohn – Sham equations, where the convergence is attained initially by a guess of density in Eq. 1.56 to develop a set of orbitals and better value for density, followed by the second iteration and so on.

1.2.3.4 Exchange-Correlation Functionals

Exchange-correlation functionals, E_{xc} accounts for the difference between the classical and quantum mechanical electron–electron repulsion terms and also describes the difference in kinetic energy between the non-interacting system and the real system. The functional is having two parts, a pure exchange part, E_{x} and a correlation part, E_{c}.

$$E_{\mathrm{xc}}[\rho(\mathbf{r})]=E_{\mathrm{x}}[\rho]+E_{\mathrm{c}}[\rho] \qquad \text{(Eq. 1.58)}$$

The interaction between the electron density and an energy density, $\mathcal{E}_{\mathrm{xc}}$ can be used to express the dependence of E_{xc} on the electron density, $\rho(\mathbf{r})$. $\mathcal{E}_{\mathrm{xc}}$ is taken as a sum of individual exchange and correlation contributions.

$$E_{\mathrm{xc}}[\rho(\mathbf{r})]=\int\rho(\mathbf{r})\,\mathcal{E}_{\mathrm{xc}}[\rho(\mathbf{r})]d\mathbf{r} \qquad \text{(Eq. 1.59)}$$

Here, electron density is a per unit volume density, whereas the energy density is a per particle density and within this outline, the Slater exchange energy density is given by,

$$\mathcal{E}_{\mathrm{x}}[\rho(\mathbf{r})]=-\frac{9\alpha}{8}\left(\frac{3}{\pi}\right)^{\frac{1}{3}}\rho^{\frac{1}{3}}(\mathbf{r}) \qquad \text{(Eq. 1.60)}$$

The total density is the sum of α and β contributions ($\rho = \rho_\alpha + \rho_\beta$) where α and represent spin up and down, respectively. Several approximations such as local density approximation (LDA), generalized gradient approximation (GGA) and meta-GGA have been designed by modifying the exchange-correlation potential for the practical applications of DFT.

1.2.3.4.1 Local Density Approximation

The local density approximation (LDA) method was used to express the density functional theory where the value of $\mathcal{E}_{xc}$ at some position **r** could be computed exclusively from the local value of ρ at that position and the only obligation is that ρ must be single-valued at every position. Practically, the only functionals coming under this description are those derived from analysis of the uniform electron gas and as a result LDA is hardly used. Within the LDA approach, the exchange function is given by:

$$E_{\mathrm{X}}^{\mathrm{LDA}}[\rho(\mathbf{r})] = -\frac{3}{4}\left(\frac{3}{\pi}\right)^{\frac{1}{3}} \int \rho^{\frac{4}{3}}(\mathbf{r}) d\mathbf{r} \qquad \text{(Eq. 1.61)}$$

In the more general case, where the α and β densities are not equal, LDA has been virtually replaced by the local spin density approximation (LSDA) which is given as the sum of the individual densities raised to the 4/3 power. LSDA method is an exact DFT method for the special case of a uniform electron gas. LDA is often used interchangeably with LSDA for closed shell systems. The exchange functional in LSDA approach is given by:

$$E_X^{LDA}[\rho(\mathbf{r})] = -2^{1}/_{3}\left(-\frac{3}{4}\left(\frac{3}{\pi}\right)^{\frac{1}{3}}\right)\int\left(\rho_\alpha{}^{\frac{4}{3}}(\mathbf{r}) + \int \rho_\beta{}^{\frac{4}{3}}(\mathbf{r})\right) d\mathbf{r} \qquad \text{(Eq. 1.62)}$$

The correlation energy of a uniform electron gas is a purely dynamical correlation and has been derived in the high and low density limits. For fitting in intermediate densities, the correlation energy has to be determined to a high accuracy by quantum Monte Carlo methods.[260] In order to use these results in DFT, Vosko, Wilk and Nusair designed local functionals (VWN) of the density fitting to these analytical low and high density limits.[261]

1.2.3.4.2 Generalized Gradient Approximation

Generalized Gradient Approximation (GGA) methods sometimes refered to as non-local methods and the functionals depend only on the density and its derivative ($\nabla\rho(\mathbf{r})$) at a given point, not on a space volume as the Hartree–Fock exchange energy. The first derivative of the density is included as a variable.

$$E_{\mathrm{XC}}\left[\rho_\alpha(\mathbf{r}),\rho_\beta(\mathbf{r})\right] \equiv \int \varepsilon_{\mathrm{xc}}(\rho_\alpha(\mathbf{r}),\rho_\beta(\mathbf{r}),\nabla\rho_\alpha(\mathbf{r})\rho_\beta(\mathbf{r}))d^3\mathbf{r} \qquad \text{(Eq. 1.63)}$$

One of the primitive and most popular GGA exchange functionals was proposed by A. D. Becke (B88) in 1988 as a correction to the LSDA exchange energy.[262] The exchange functional B88 can be combined with any of their correlation counterparts belonging to this family, such as the LYP[263] and P86[264] functionals, to form the global exchange-correlation energy. The frequently used PW91[265] and PBE[266] correlation and exchange functionals also belong to the GGA formalism.

1.2.3.4.3 meta-GGA

Higher order gradient or meta- GGA methods allow the exchange and correlation functionals to depend on higher order derivatives of the electron density, with the Laplacian $\nabla^2\rho(\mathbf{r})$ being the second-order term. The functionals which use orbital information may also cover this category and calculation of the orbital kinetic energy density is numerically more stable than calculation of the Laplacian of the density. The cost of an m- GGA calculation is comparable with a GGA calculation, and the former is usually more exact than the latter for a pure density functional. B95, B98, *etc*. are examples for m-GGA functionals. One of the most successful functional of this kind is TPSS functional, which incorporate the kinetic energy density and has been proven exceptionally fine for systems conaining transition metals.[267]

A noteworthy advancement in the application of DFT to modern chemistry was attained by the entry of hybrid density functional methods[268] in which the exchange-correlation of a GGA or m-GGA method is combined with a fraction of the non-local exchange energy from HF theory. B3LYP, B3P86, B3PW91, B97-1, MPWB1K, and X3LYP are examples of hybrid-GGA methods and B1B95, BB1K, and MPW1B95 are examples for

hybrid m-GGA methods.[269] The most commonly used representation for the exchange-correlation energy is the Becke three parameter Lee-Yang-Parr (B3LYP) functional[270] and it can be considered as the typical option for an average quantum chemistry problem. The mathematical form of B3LYP method can be written as,

$$E_{\mathrm{XC}}^{\mathrm{B3LYP}} = aE_{\mathrm{X}}^{\mathrm{HF}} + (1-a)E_{\mathrm{X}}^{\mathrm{LSD}} + bE_{\mathrm{X}}^{\mathrm{B88}} + E_{\mathrm{C}}^{\mathrm{LSD}} + c(E_{\mathrm{C}}^{\mathrm{LYP}} - E_{\mathrm{C}}^{\mathrm{LSD}}) \qquad \text{(Eq. 1.64)}$$

where the empirical constants a, b, c have the values 0.20, 0.72 and 0.81correspondingly.

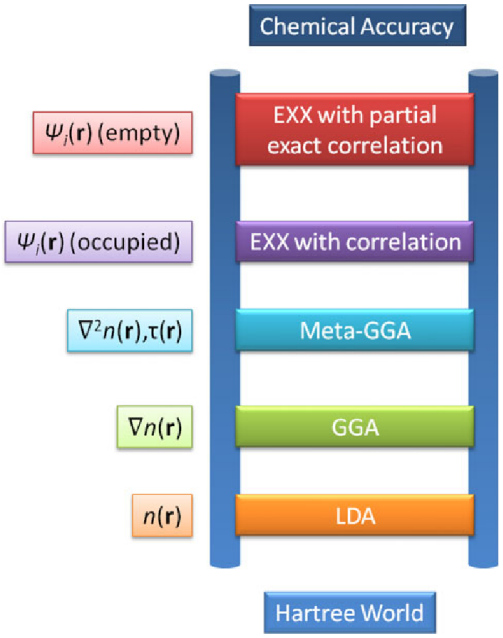

Figure 1.13 Jacob's ladder proposed for DFT.

The famous Minnesota functional such as M05, M06, M06-2X and M06-L developed by Zhao and Truhlar are also based on the m-GGA approximation with different fractions of HF exchange.[271] The most accurate functional available with the current scenario are the double hybrids, which improve the hybrid-GGA ones together with some correlation energy calculated through MP2 scheme based on the Kohn-Sham orbitals. One of the commonly used double hybrid functionals is the B2-PLYP scheme by Grimme *et al*.[272] In 2001, Perdew and Schmidt arranged the density functional approximations as various rungs of a ladder of approximations (Figure1.13) for the exchange-correlation energy (Jacob's ladder) as a functional of the electron density.[273]

The lowest rung is the local spin-density approximation of Kohn and Sham, the second rung is the generalized gradient approximation and the higher rungs are increasingly more complex.[274]

1.2.3.5 Dispersion Corrections

Dispersion interactions can be defined as the attractive part of the van der Waals (vdW) type interaction potential between atoms and molecules that are not directly bonded. The normally encountering GGA including hybrid density functional are unable to give an accurate explanation regarding the long range (London dispersion) interactions.[275] The inclusion of dispersive interactions may enhance the accuracy of theoretical calculations. Some of the approaches developed for explaining the non-covalent interactions include those reported by Grimme,[276] Becke and Johnson,[277] Tkachenko and Scheffler.[278] The Minnesota functional can also be mentioned here as a broad variety of non-covalent interactions can be accounted within its framework.[279] The total energy of the system obtained by adding the dispersion corrections to the KS-DFT functional is represented as,

$$E_{MF-D} = E_{MF} + E_{disp} \qquad \text{(Eq.1.65)}$$

where E_{MF} describes the mean field energy obtained either in HF or DFT and the dispersion energy, E_{disp} can be expressed as:

$$E_{disp} = -S_6 \sum_{i=1}^{N_{at}-1} \sum_{j=i+1}^{N_{at}} \frac{C_6^{ij}}{R_{ij}^6} f_{dmp}(R_{ij}) \qquad \text{(Eq. 1.66)}$$

where N_{at} is the number of atoms in the system, S_6 is a global scaling factor depending on the dispersion function, C_6^{ij} is the dispersion coefficient for atom pair *ij*, R_{ij} is the interatomic distance.[280] f_{dmp} is the damping function used to circumvent the near-singularities for small *R* and is given by,

$$f_{\text{dmp}}(R) = \frac{1}{1 + \mathrm{e}^{-\alpha(R/R_0 - 1)}} \qquad \text{(Eq. 1.67)}$$

where R_0 is the sum of atomic van der Waals radii.

1.2.4 Basis Sets

A basis set is a set of functions which are expanded as a linear combination with coefficients to be resolved in order to generate the molecular orbitals. Although the concept is central for atoms, functions centered in bonds or lone pairs and basis sets composed of sets of plane waves are also used, especially in calculations involving systems with periodic boundary conditions. There are two types of commonly used basis functions or atomic orbitals (AO), Slater Type Orbitals (STO) and Gaussian Type Orbitals (GTO). STOs developed by J. C. Slater[281] constitute a set of basis functions which decay exponentially with the distance from the nuclei and were used in the early days of quantum chemistry due to the similarity with the eigenfunctions of the hydrogen atom. STOs can be mathematically expressed as:

$$\Phi_{abc}^{\mathrm{STO}}(x,y,z) = Nx^a y^b z^c e^{-\zeta r} \qquad \text{(Eq. 1.69)}$$

where N is the normalization constant, a, b, c are the components of angular momentum (L = a+b+c), r is the radius in angstrom and ζ (zeta) is the orbital exponent. However, the STOs do not have any radial nodes in the radial part are introduced by making linear combinations of STOs.[282] STOs are mainly used for atomic and diatomic systems which demand high precision, semiempirical methods where all three- and four-center integrals are neglected and DFT methods that do not include exact exchange. S. F. Boys [283] introduced another type of orbitals known as Gaussian-type orbitals (GTOs) having the exponential dependence, $e^{-\zeta r^2}$. GTOs are mathematically expressed as:

$$\Phi_{abc}^{\mathrm{GTO}}(x,y,z) = Nx^a y^b z^c e^{-\zeta r^2} \qquad \text{(Eq. 1.70)}$$

The r^2 dependence in the exponential makes the GTOs inferior to the STOs in the following respects. At the nucleus a GTO has a zero slope, in contrast to an STO which has a discontinuous derivative and GTOs are poor in representing the accurate character near the nucleus. Also, the GTO falls off too rapidly far from the nucleus when compared with an STO. Both STOs and GTOs can be chosen to form a complete basis, and a linear combination of enough GTOs can be used to characterize an STO. A combination of n Gaussians to take off an STO is often called STO-nG. Basis sets assign a group of basis

functions to each atom within a molecule to approximate its orbitals. These basis functions are composed of a linear combination of Gaussian functions; such basis functions are called contracted functions, and the component Gaussian functions are termed as primitives.

After deciding the type of function, whether is STO/GTO, and the position of nuclei, then comes the selection of number of functions to be used. The primitive one is the *minimum basis set*, in which number of functions is least. The STO-3G basis set is a minimal basis set, where there is only one basis function defined for each type of orbital core through valence. Consequently, for the first row elements in the periodic system two s-functions (1s and 2s) and one set of p-functions are there, whereas for the second row elements, three *s*-functions (1s, 2s and 3s) and two sets of *p*-functions (2p and 3p) are there. The subsequent upgrading of the basis sets is done by doubling of all basis functions, resulting in a Double Zeta (DZ) basis set. Double Zeta making use of two *s*-functions for hydrogen (1s and 1s'), four s-functions (1s, 1s', 2s and 2s') and two sets of *p*-functions (2p and 2p') for first row elements, and six *s*-functions and four sets of *p*-functions for second row elements. A split valence basis is produced by doubling the number of valence orbitals of the DZ type basis. In the next higher basis set Triple Zeta (TZ), there will be three times as many functions as the minimum basis, such that for first row elements six *s*-functions and three *p*-functions will be available. A triple split valence basis set can save some of the core orbitals by only splitting the valence. The addition of more functions may result in higher multiple-zeta basis sets, such as the Quadruple Zeta (QZ) and Pentuple Zeta (PZ). The most commonly used basis sets of these kinds are the cc-pCVDZ and cc-pCVTZ (correlation-consistent polarized Core and Valence Double/Triple Zeta) introduced by Dunning and co-workers.[284]

The popular split valence basis sets proposed by Pople *et al*.[285] include 3-21G, 6-21G, 4-31G, 6-31G, and 6-311G, where the first number indicates the number of primitives used in the contracted core functions, the numbers after the hyphen indicate the numbers of primitives used in the valence functions (if there are two such numbers, it is a valence-double-zeta , and if there are three, valence-triple-zeta). cc-pVDZ, and cc-pVTZ[286] (correlation-consistent polarized Valence Double/Triple zeta) are the two

widely used split-valence basis sets having general contractions. The meaning of the term correlation-consistent is that the exponents and contraction coefficients were variationally optimized for HF calculations and also for calculations together with electron correlation methods.

For the majority of cases, apart from the number of *s*- and *p*-functions for each atom, higher angular momentum functions also play a major part, and these are symbolized as polarization functions.[287] The most useful polarization functions are for first-row atoms are *d* GTOs and that for hydrogen is *p* GTOs. A sample representation by adding polarization functions can be given as 6-31G** or 6-31G (d,p). The standard basis sets are frequently augmented with diffuse functions[288] when a basis set does not have the flexibility necessary to allow a weakly bound electron to localize far from the remaining density. The Pople family of basis sets with diffuse functions are denoted by + or ++, with the first + indicates one set of diffuse *s*- and *p*-functions on heavy atoms, and the second + indicating that a diffuse *s*-function is added to hydrogen. 6-31+G(d) is a split valence basis set with one set of diffuse *sp*-functions on heavy atoms only and a single *d*-type polarization function on heavy atoms. Ahlrichs reported segmented contracted split valence (SV), triple zeta valence (TZV) and quadruple zeta valence (QZV) basis sets scheme for atoms H to Kr.[289] QZVP basis set with added polarization functions are recommended in assessments of HF and DFT based methods preferring chemical accuracy.

For very heavy elements having large numbers of electrons, it is necessary to use a large number of basis functions and since these extra electrons are generally core electrons, a minimal representation will be sufficient. In this regard, in 1935, Hellmann proposed to replace the electrons with analytical functions that would precisely symbolize the combined nuclear–electronic core to the remaining electrons (core electrons are replaced with an approximate pseudopotential) and such functions are termed as effective core potentials (ECPs). The popular pseudopotentials commonly used include those of Hay and Wadt developed by Los Alamos National Laboratory (LANL),[290] those of Stevens *et al*.[291] and the Stuttgart–Dresden pseudopotentials developed by Dolg

and co-workers.[292] Later, Check *et al*. incorporated polarization and diffuse functions in conjunction with the LANL double zeta basis set.[293]

The basis sets utilized for the calculations in the thesis are (a) Pople's split-valence basis sets 6-31G(d,p), 6-311+G(d,p) and 6-311++G(d,p) with *d* polarization functions for non-hydrogen atoms and *p* polarization function for hydrogen atom in addition to diffuse functions for non-hydrogen and hydrogen atom, b) Hay and Wadt double zeta basis set with the overall combination of ECP and valence basis set, LANL2DZ for defining transition metal Ru, and quadruple zeta valence, QZVP for the transition metals ,Cr, Mo and W.

1.2.5 Molecular Mechanics (MM)

The molecular mechanics energy expression consists of an algebraic equation for the energy of a compound without using a wave function or total electron density parameter.[294] A set of equations with their related constants is called a force field and the constants in this equation are obtained either spectroscopic data or *ab initio* calculations.[295] The advantage of molecular mechanics is that it allocates the representation of enormous molecules, such as proteins and segments of DNA, which makes it computational biochemist's primary tool. Molecular mechanics conveys the total force field energy based on conformation as a sum of Taylor series expansions for stretches for every pair of bonded atoms, and adds additional potential energy terms coming from bond bending (E_{bend}), rotation around a bond *ie*., torsional energy (E_{tor}), and also from non-bonded interaction energies such as van der Waals energy (E_{vdw}), and electrostatic energy (E_{elec}).

$$E_{\text{tot}} = E_{\text{str}} + E_{\text{bend}} + E_{\text{tor}} + E_{\text{vdw}} + E_{\text{elec}} \qquad \text{(Eq.1.68)}$$

There are several commonly used molecular mechanics force fields.[296-298] Assisted model building with energy refinement (AMBER) and Chemistry at Harvard macromolecular mechanics (CHARMM) are force fields parameterized specifically for proteins and nucleic acids. AMBER uses only five bonding and nonbonding terms along with a complicated electrostatic treatment and CHARMM uses five valence terms, out of

one is an electrostatic term. The consistent force field (CFF) was proposed to yield consistent accuracy of results for conformations, vibrational spectra, strain energy, and vibrational enthalpy of proteins. Carbohydrate hydroxyls represented by external atoms (CHEAT) is another force field designed specifically for representing carbohydrates and empirical force field (EFF) is designed for modeling hydrocarbons. DREIDING is the force field extensively used for large biomolecular systems. MM1, MM2, MM3, and MM4 are satisfying general purpose for organic force fields.[299-301] MM1 is not popular nowadays and MM3 method can be quoted as one of the most accurate ways of modeling hydrocarbons.

1.2.6 Molecular Dynamics (MD)

Molecular dynamics is a simulation of the time-dependent behavior such as vibrational motion or Brownian motion of atoms and molecules. It can be used to explore the conformational space, and is often the preferential method for large molecules such as proteins and nucleic acids to assess the structure-to-function relationships.[302] They are also used in the determination of structures from x-ray crystallography and from NMR experiments. The first attempt of molecular dynamics simulation over a realistic system (liquid water) was attained by Rahman and Stillinger in 1974[303] and the first protein simulation was done on bovine pancreatic trypsin inhibitor (BPTI) in 1977 by McCammon *et al*.[304] In order to do the simulations, the first step is the design of force field to describe the intermolecular forces and vibrations away from equilibrium. For instance, a force field designed for geometry optimization can be taken if the purpose of the simulation is to search conformation space. Verlet algorithm is the most commonly used algorithm for performing the numerical integration of the equations of motion, because of its minimum amount of computer memory and CPU time. The selection of a time step is also significant and the desirable time step is one with the order of scale less than the timescale of the shortest motion. Generally, the MD methods are sorted as two types, classical MD (CMD) and *ab initio* MD (AIMD).[305] AIMD is based on the quantum Schrödinger equation, does not use any empirical knowledge, but can be exceptionally time consuming. On the other hand, CMD involves the electronic motion in deriving the force acting on the atoms and calculations are much faster to treat millions of atoms.

Later, Car–Parrinello molecular dynamics (CPMD) reformulated AIMD as a two-component classical dynamical system.[306] The simulations in which the location, orientation, and geometry of a molecule or collection of molecules are chosen according to a statistical distribution are termed as Monte Carlo simulations.[307]

1.2.7 Hybrid QM/MM Methods

Hybrid quantum-mechanics/molecular-mechanics (QM/MM) simulations are the traditional tools for the simulation of extended atomistic systems, where the atoms in a core region of interest are treated with a QM calculator and the surrounding atoms are treated with an empirical potential.[308] The main applications of these methods include the clarification of the structures and energetics of stationary points on the potential energy surfaces and the prediction of free energy differences. Hybrid QM/MM methods are computationally effective, but anyhow their approximate nature limits the precision. The ONIOM (our own n-layered integrated molecular orbital and molecular mechanics) approach put forward by Morokuma *et al*. is one of the best approaches of this category and is highly preferential for reproducing benchmark calculations and experimental results.[309] The format can be extended to two-layer ONIOM (QM1: QM2), three-layer ONIOM (QM1: QM2: MM), and, in principle, any n-layer n-level-of-theory methods.

1.2.8 Potential Energy Surface (PES)

A potential energy surface can be defined as a mathematical function which can interpret the energy of a molecule as a function of geometry. The energy surface is particularly pronounced for the systems in which the bonding remains unchanged and sometimes applicable in systems for which bond breaking and bond formation happens. Regarding the molecular modeling, the minimum points on the energy surface make sense, as they correspond to the stable states and any distortion from the minimum will result in a configuration with higher energy. There can be a number of minima on the energy surface, and the most significant one is the global energy minimum with the lowest energy. A minimization algorithm is employed to spot the geometries of the system having minimum points. It is also important to know how the system changed from one lowest energy configuration to another and how the relative positions of atoms change

during the course of the reaction. The saddle point matches with the arrangement of atoms in the transition state, which can be marked as the higher point on the pathway between two minima. Both the minima and saddle points are stationary points on the energy surface, where the first derivative of the energy function vanishes with respect to all the coordinates. A schematic representation of the PES is given in Figure 1.14, which can be related to a geographical contour with long and narrow valley as minimum and mountain passes as saddle points.

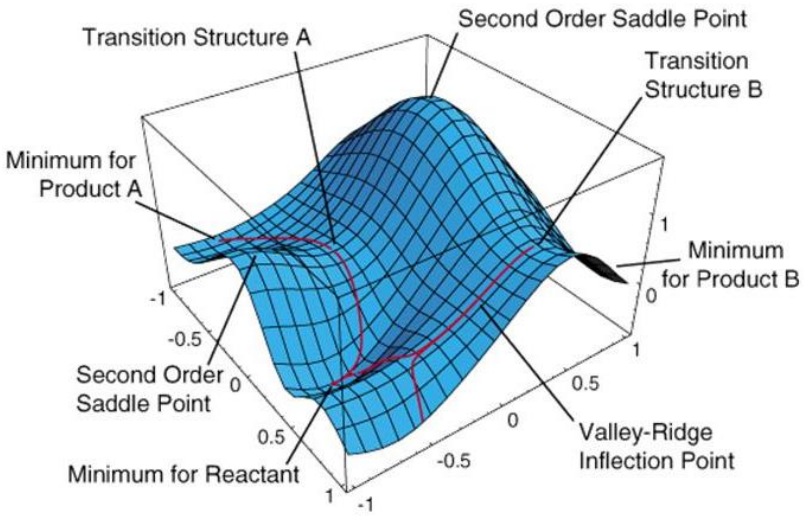

Figure 1.14 The representation of potential energy surface.

1.2.9 Solvation Models

Most of the laboratory chemistry is done in solution as the interaction between the species of interest and the solvent is not negligible. The simulation of molecules in solution can be sorted out in two ways, one is a list of effects that are not defined for a single molecule, and the second and most important one is a solvation effect, in which a change in the molecular behavior is caused by a solvent. The diverse models for solvation can be broadly divided into two categories, explicit and implicit models. In the explicit solvation, the solvent molecules will be inserted explicitly and then run molecular dynamics or Monte Carlo calculations to give the desirable property, which makes it the most accurate model.[310] But the primary disadvantage with the explicit solvent model is the expensive computer resources.

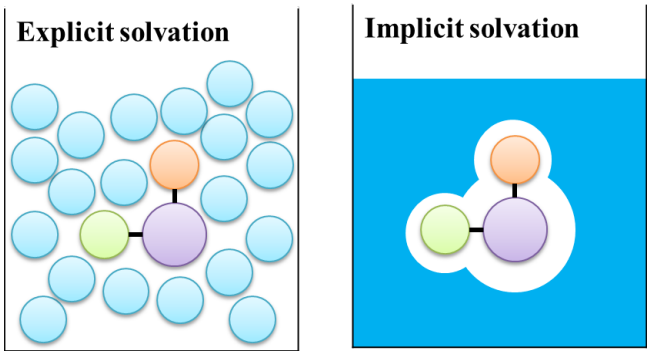

Figure 1.15 A schematic representation for explicit and implicit solvation.

An implicit or continuum model can be defined as a model in which a number of the degrees of freedom of the constituent particles are described in a continuous way, using a distribution function and are more effective owing to their reduced computational cost.[311, 312] The electrostatic interaction of a solute with the solvent depends delicately upon the charge distribution and polarizability of the solute. These are the most efficient techniques employed to include condensed-phase effects into quantum mechanical calculations. The reaction field is typically accomplished for treating solute polarization in solution and the method of iterating that reaction field to self-consistency is called self-consistent reaction field (SCRF). Most of the presently used continuum solvation models calculate the electrostatic component of the solvation free energy by solving the Poisson equation.[313] In short, SCRF approach that links a grid-based numerical solution of the Poisson equation to the quantum mechanical SCF procedure forms the basis of a continuum model.

The polarized continuum model (PCM), developed by Tomasi et al. is one of the most popular models used so far.[314] PCM cast the quantum mechanical SCRF equations into a boundary element problem with apparent surface charges (ASCs) on the solute cavity surface. Various PCM formulations include the integral-equation-formalism protocol (IEF-PCM), and the dielectric PCM (D-PCM).[315] The conductor-like screening model (COSMO) assumes that the surrounding medium is well modeled as a conductor, which simplifies the electrostatics computations.[316] The solvation model based on density (SMD) coined by Tomasi *et al.*[317] is an implicit solvation model based on density, in which interaction between the solute and solvent is calculated from the charge density

of the former and the electric polarization field of the latter.[318] SMD can be called as a universal solvation model, and "universal" stands for its applicability to any charged or uncharged solute in any solvent or liquid medium. SMD model distinguishes the solvation free energy into two key parts, the first being the bulk electrostatic contribution arising from a SCRF calculation that occupies the solution of the Poisson equation for electrostatics in terms of the IEF-PCM model and the second is the cavity-dispersion-solvent-structure term and arising from the contribution of short-range interactions between the solute and solvent in the first solvation shell. It was proven that SMD can predict the solvation energies with greater accuracy.

1.3 Conclusions

The importance of experimentally and computationally derived ligand electronic parameters has been summarized in part-A of Chapter 1. The experimental descriptors such as Hammett constants, Tolman Electronic Parameter (TEP), Lever Electronic Parameter (LEP), NMR chemical Shifts, and parameter for quantitative analysis of ligand effects (QALE) are discussed. Also reviewed are the prominent computationally derived descriptors such as computed electronic parameter (CEP), average local ionization energy and molecular electrostatic potential (MESP). All the ligand electronic parameters discussed here are beneficial in their specific modes to clarify the stereoelectronic profile of a range of ligands and consequently tuning the efficiency and reactivity of transition metal complexes.

The theories and principles behind various computational chemistry techniques, such as *ab initio* methods, semiempirical methods, density functional theory, molecular mechanics, molecular dynamics and hybrid QM/MM methods are briefly explained in part-B of Chapter 1. The explanations are made convenient with proper sub divisions. An overview regarding the concepts like basis sets, potential energy surface, and solvation models are also furnished. The better understanding of the computational concepts is inevitable in interpreting the outcome of a molecular modeling operation, which in turn leads to advancements in implementations for predicting the chemical properties with reasonable to high accuracy.

1.4 References

1. F. A. Cotton and G. Wilkinson, *JohnWiley: New York* **1988**.
2. C. Elschenbroich and A. Salzer, *VCH Publishers:New York* **1989**.
3. G. Frenking and N. Fröhlich, *Chem. Rev.* **2000**, *100*, 717-774.
4. C. K. Jørgensen, *Modern Aspects of Ligand Field Theory, New York, Elsevier* **1971.**
5. C. L. Ballhausen, *Introduction to Ligand Field Theory, McGraw-Hill: New York* **1962**.
6. M. J. S. Dewar, *Bull. Soc. Chim. Fr.* **1951**, *18*, C79.
7. J. Chatt and L. A. Duncanson, *J. Chem. Soc.* **1953**, *0*, 2939-2947
8. F. P. Pruchnik, P. Smoleński and K. J. Wajda-Hermanowicz, *Organomet. Chem.* **1998**, *570*, 63–69.
9. R. Gómez Arrayás, J. Adrio and J. C. Carretero, *Angew. Chem. Int. Ed.* **2006**, *45*, 7674-7715.
10. N. Fey, M. F. Haddow, J. N. Harvey, C. L. McMullin and A. G. Orpen, *Dalton Trans.* **2009**, 8183-8196.
11. H. von Schenck, B. Åkermark and M. Svensson, *Organometallics* **2002**, *21*, 2248-2253.
12. G. Mann, Q. Shelby, A. H. Roy and J. F. Hartwig, *Organometallics* **2003**, *22*, 2775-2789.
13. D. Weickmann, W. Frey and B. Plietker, *Chem. Eur. J.* **2013**, *19*, 2741-2748.
14. B. J. Coe and S. J. Glenwright, *Coord. Chem. Rev.* **2000**, *203*, 5-80.
15. P. C. J. Kamer, P. W. N. M. van Leeuwen and J. N. H. Reek, *Acc. Chem. Res.* **2001**, *34*, 895-904.
16. J. G. de Vries and L. Lefort, *Chem. Eur. J.* **2006**, *12*, 4722-4734.
17. J. Jover and N. Fey, *Chem. Asian J.* **2014**, *9*, 1714-1723.
18. D. R. Palo and C. Erkey, *Organometallics* **2000**, *19*, 81-86.
19. U. Christmann and R. Vilar, *Angew. Chem. Int. Ed.* **2005**, *44*, 366-374.
20. J.-P. Corbet and G. Mignani, *Chem. Rev.* **2006**, *106*, 2651-2710.
21. B. C. Hamann and J. F. Hartwig, *J. Am. Chem. Soc.* **1998**, *120*, 3694-3703.
22. L. Cavallo, A. Correa, C. Costabile and H. Jacobsen, *J. Organomet. Chem.* **2005**, *690*, 5407-5413.

23. R. H. Crabtree, *J. Organomet. Chem.* **2005**, *690*, 5451-5457.
24. D.-P. Song, X.-C. Shi, Y.-X. Wang, J.-X. Yang and Y.-S. Li, *Organometallics* **2012**, *31*, 966-975.
25. N. Fey, A. G. Orpen and J. N. Harvey, *Coord. Chem. Rev.* **2009**, *253*, 704-722.
26. N. Fey, J. N. Harvey, G. C. Lloyd-Jones, P. Murray, A. G. Orpen, R. Osborne and M. Purdie, *Organometallics* **2008**, *27*, 1372-1383.
27. C. A. Tolman, *J. Am. Chem. Soc.* **1970**, *92*, 2953-2956.
28. C. A. Tolman, *Chem. Rev.* **1977**, *77*, 313-348.
29. A. Fernandez, C. Reyes, T. YingLee, A. Prock, W. P. Giering, C. M. Haar and S. P. Nolan, *J. Chem.Soc., Perkin Trans. 2* **2000**, 1349-1357.
30. A. Fernandez, C. Reyes, M. R. Wilson, D. C. Woska, A. Prock and W. P. Giering, *Organometallics* **1997**, *16*, 342-348.
31. L. Perrin, E. Clot, O. Eisenstein, J. Loch and R. H. Crabtree, *Inorg. Chem.* **2001**, *40*, 5806-5811.
32. N. Fey, *Dalton Trans.* **2010**, *39*, 296-310.
33. D. G. Gusev, *Organometallics* **2009**, *28*, 6458-6461.
34. D. G. Gusev, *Organometallics* **2009**, *28*, 763-770.
35. R. Kalescky, E. Kraka and D. Cremer, *Inorg. Chem.* **2014**, *53*, 478-495.
36. D. Setiawan, R. Kalescky, E. Kraka and D. Cremer, *Inorg. Chem.* **2016**, *55*, 2332-2344.
37. J. Jover, N. Fey, J. N. Harvey, G. C. Lloyd-Jones, A. G. Orpen, G. J. J. Owen-Smith, P. Murray, D. R. J. Hose, R. Osborne and M. Purdie, *Organometallics* **2012**, *31*, 5302-5306.
38. R. B. DeVasher, J. M. Spruell, D. A. Dixon, G. A. Broker, S. T. Griffin, R. D. Rogers and K. H. Shaughnessy, *Organometallics* **2005**, *24*, 962-971.
39. L. P. Hammett, *Chem. Rev.* **1935**, *17*, 125-136.
40. L. P. Hammett, *J. Am. Chem. Soc.* **1937**, *59*, 96-103.
41. H. H. Jaffe and H. L. Jones, in *Adv. Heterocycl. Chem.*, ed. A. R. Katritzky, Academic Press **1964**, vol. 3, pp. 209-261.
42. D. H. McDaniel and H. C. Brown, *J. Org. Chem.* **1958**, *23*, 420-427.

43. M. Ciaccia, S. Pilati, R. Cacciapaglia, L. Mandolini and S. Di Stefano, *Org. Biomol. Chem.* **2014**, *12*, 3282-3287.
44. C. D. Johnson, *The Hammett equation*, CUP Archive **1973**.
45. C. Hansch, A. Leo and R. W. Taft, *Chem. Rev.* **1991**, *91*, 165-195.
46. M. Charton, *J. Org. Chem.* **1965**, *30*, 969-973.
47. R. W. Taft, *J. Am. Chem. Soc.* **1952**, *74*, 2729-2732.
48. R. W. Taft, *J. Am. Chem. Soc.* **1953**, *75*, 4538-4539.
49. L. R. Domingo, P. Pérez and R. Contreras, *J. Org. Chem.* **2003**, *68*, 6060-6062.
50. L. Meneses, A. Araya, F. Pilaquinga and P. Fuentealba, *Chem. Phys. Lett.* **2008**, *460*, 27-30.
51. G. Di Modica, E. Barni and A. Gasco, *J. Heterocycl. Chem.* **1965**, *2*, 457-458.
52. H. Mayr, O. Kuhn, M. F. Gotta and M. Patz, *J. Phys. Org. Chem.* **1998**, *11*, 642-654.
53. M. R. Crawley, K. J. Kadassery, A. N. Oldacre, A. E. Friedman, D. C. Lacy and T. R. Cook, *Organometallics* **2019**, *38*, 1664-1676.
54. S. E. Tignor, H.-Y. Kuo, T. S. Lee, G. D. Scholes and A. B. Bocarsly, *Organometallics* **2019**, *38*, 1292-1299.
55. J. N. McPherson, R. W. Hogue, F. S. Akogun, L. Bondì, E. T. Luis, J. R. Price, A. L. Garden, S. Brooker and S. B. Colbran, *Inorg. Chem.* **2019**, *58*, 2218-2228.
56. T. L. Brown and K. J. Lee, *Coord. Chem. Rev.* **1993**, *128*, 89-116.
57. G. Bistoni, S. Rampino, N. Scafuri, G. Ciancaleoni, D. Zuccaccia, L. Belpassi and F. Tarantelli, *Chem. Sci.* **2016**, *7*, 1174-1184.
58. A. B. P. Lever, *Inorg. Chem.* **1990**, *29*, 1271-1285.
59. A. B. P. Lever, *Inorg. Chem.* **1991**, *30*, 1980-1985.
60. S. S. Fielder, M. C. Osborne, A. B. P. Lever and W. J. Pietro, *J. Am. Chem. Soc.* **1995**, *117*, 6990-6993.
61. G. M. Bodner, M. P. May and L. E. McKinney, *Inorg. Chem.* **1980**, *19*, 1951-1958.
62. T. L. Brown, *Inorg. Chem.* **1992**, *31*, 1286-1294.
63. H. V. Huynh, Y. Han, R. Jothibasu and J. A. Yang, *Organometallics* **2009**, *28*, 5395-5404.
64. Q. Teng and H. V. Huynh, *Inorg. Chem.* **2014**, *53*, 10964-10973.
65. S. Guo, H. Sivaram, D. Yuan and H. V. Huynh, *Organometallics* **2013**, *32*, 3685-3696.

66. Q. Teng and H. V. Huynh, *Dalton Trans.* **2017**, *46*, 614-627.
67. A. Fabrello, C. Dinoi, L. Perrin, P. Kalck, L. Maron, M. Urrutigoity and O. Dechy-Cabaret, *Mag. Res. Chem.* **2010**, *48*, 848-856.
68. R. M. Mampa, M. A. Fernandes and L. Carlton, *Organometallics* **2014**, *33*, 3283-3299.
69. S. V. C. Vummaleti, D. J. Nelson, A. Poater, A. Gómez-Suárez, D. B. Cordes, A. M. Z. Slawin, S. P. Nolan and L. Cavallo, *Chem. Sci.* **2015**, *6*, 1895-1904.
70. O. Back, M. Henry-Ellinger, C. D. Martin, D. Martin and G. Bertrand, *Angew. Chem., Int. Ed.* **2013**, *52*, 2939-2943.
71. A. Liske, K. Verlinden, H. Buhl, K. Schaper and C. Ganter, *Organometallics* **2013**, *32*, 5269-5272.
72. M. R. Wilson, D. C. Woska, A. Prock and W. P. Giering, *Organometallics* **1993**, *12*, 1742-1752.
73. A. A. Tracey, K. Eriks, A. Prock and W. P. Giering, *Organometallics* **1990**, *9*, 1399-1405.
74. J. S. Panek, A. Prock, K. Eriks and W. P. Giering, *Organometallics* **1990**, *9*, 2175-2176.
75. M. R. Wilson, H. Liu, A. Prock and W. P. Giering, *Organometallics* **1993**, *12*, 2044-2050.
76. B. A. Lorsbach, A. Prock and W. P. Giering, *Organometallics* **1995**, *14*, 1694-1699.
77. B. A. Lorsbach, D. M. Bennett, A. Prock and W. P. Giering, *Organometallics* **1995**, *14*, 869-874.
78. A. L. Fernandez, A. Prock and W. P. Giering, *Organometallics* **1994**, *13*, 2767-2772.
79. A. J. Poe, D. H. Farrar and Y. Zheng, *J. Am. Chem. Soc.* **1992**, *114*, 5146-5152.
80. R. Romeo and G. Alibrandi, *Inorg. Chem.* **1997**, *36*, 4822-4830.
81. D. H. Farrar, J. Hao, A. J. Poë and T. A. Stromnova, *Organometallics* **1997**, *16*, 2827-2832.
82. X.-L. Luo, G. J. Kubas, C. J. Burns, J. C. Bryan and C. J. Unkefer, *J. Am. Chem. Soc.* **1995**, *117*, 1159-1160.
83. R. Romeo, G. Arena and L. Monsu Scolaro, *Inorg. Chem.* **1992**, *31*, 4879-4884.
84. H. Y. Liu, K. Eriks, A. Prock and W. P. Giering, *Organometallics* **1990**, *9*, 1758-1766.

85. C. Babij, H. Chen, L. Chen and A. J. Poë, *Dalton Trans.* **2003**, 3184-3191.
86. A. L. Fernandez, C. Reyes, A. Prock and W. P. Giering, *J. Chem. Soc., Perkin Trans. 2* **2000**, 1033-1041.
87. A.L. Fernandez, A. Prock and W.P. Giering, *The QALE Web Site*.
88. N. Koga and K. Morokuma, *Chem. Rev.* **1991**, *91*, 823-842.
89. S. Niu and M. B. Hall, *Chem. Rev.* **2000**, *100*, 353-406.
90. T. Ziegler, *Chem. Rev.* **1991**, *91*, 651-667.
91. S. Yoshida, S. Sakaki and H. Kobayashi, *Electronic Processes in Catalyst; VCH: New York* **1992**.
92. O. Kühl, *Coord. Chem. Rev.* **2005**, *249*, 693-704.
93. D. J. Durand and N. Fey, *Chem. Rev.* **2019**, *119*, 6561-6594.
94. R. Tonner and G. Frenking, *Organometallics* **2009**, *28*, 3901-3905.
95. F. Zobi, *Inorg. Chem.* **2009**, *48*, 10845-10855.
96. J. Mathew and C. H. Suresh, *Inorg. Chem.* **2010**, *49*, 4665-4669.
97. A. P. Gillespie, K.; Cundari, T.; White, D, *Internet Electron. J. Mol. Des.* **2002**, *1*, 242–251.
98. K. D. Cooney, T. R. Cundari, N. W. Hoffman, K. A. Pittard, M. D. Temple and Y. Zhao, *J. Am. Chem. Soc.* **2003**, *125*, 4318-4324.
99. C. Makedonas and C. A. Mitsopoulou, *Eur. J. Inorg. Chem.* **2007**, *2007*, 4176-4189.
100. Y. Canac and C. Lepetit, *Inorg. Chem.* **2017**, *56*, 667-675.
101. D. Cremer and E. Kraka, *Dalton Trans.* **2017**, *46*, 8323-8338.
102. P. Politzer, J. S. Murray and F. A. Bulat, *J. Mol. Model.* **2010**, *16*, 1731.
103. J. Murray;, T. Brinck; and P. Politzer, *J. Mol. Struct.(THEOCHEM)* **1992**, *255*, 271-281.
104. D. S. Coll, A. B. Vidal, J. A. Rodríguez, E. Ocando-Mavárez, R. Añez and A. Sierraalta, *Inorganica Chim. Acta* **2015**, *436*, 163-168.
105. P. Sjoberg, J. S. Murray, T. Brinck and P. Politzer, *Can. J. Chem.* **1990**, *68*, 1440.
106. R. G. Pearson, *J. Am. Chem. Soc.* **1963**, *85*, 3533-3539.
107. R. G. Pearson, *J. Am. Chem. Soc.* **1967**, *89*, 1827-1836.
108. R. F. Stewart, *Chem. Phys. Lett.* **1979**, *65*, 335-342.
109. K. Kato and H. Tanaka, *Adv. Phys.* **2016**, *1*, 55-80.

110. M. Drissi, N. Benhalima, Y. Megrouss, R. Rachida, A. Chouaih and F. Hamzaoui, *Molecules* **2015**, *20*, 4042-4054.
111. P. Politzer and D. G. Truhlar, *Chemical Applications of Atomic and Molecular Electrostatic Potentials; Plenum: New York* **1981**.
112. P. Politzer and J. S. Murray, *Theor. Chem. Acc .* **2002**, *108*, 134-142.
113. R. F. W. Bader, *J. Chem. Phys.* **1989**, *91*, 6989-7001.
114. S. R. Gadre, S. A. Kulkarni and I. H. Shrivastava, *J. Chem. Phys.* **1992**, *96*, 5253-5260.
115. S. R. Gadre, C. Koelmel and I. H. Shrivastava, *Inorg. Chem.* **1992**, *31*, 2279-2281.
116. R. K. Pathak and S. R. Gadre, *J. Chem. Phys.* **1990**, *93*, 1770-1773.
117. C. H. Suresh and N. Koga, *J. Am. Chem. Soc.* **2002** *124*, 1790.
118. E. Scrocco and J. Tomasi, *Top. Curr. Chem.* **1973**, *42*, 95
119. R. Bonaccorsi, R. Cimiraglia, E. Scrocco and J. Tomasi, *Theor. Chim. Acta* **1974**, *33*, 97.
120. A. Agresti, R. Bonaccorsi and J. Tomasi, *Theor. Chim. Acta* **1979**, *53*, 215-220.
121. P. Politzer, J. S. Murray and P. Lane, *J. Comput. Chem.* **2003**, *24*, 505.
122. J. Murray and P. Politzer, *Chem. Phys. Lett.* **1988**, *152*, 364–370.
123. P. Politzer, G. Kirschenheuter and J. Alster, *J. Am. Chem. Soc.* **1987**, *109*, 1033.
124. S. R. Gadre and S. S. Pundlik, *J. Phys. Chem. B* **1997**, *101*, 3298-3303.
125. P. Politzer, P. R. Laurence and K. Jayasuriya, *Environ. Health Perspect.* **1985**, *61*, 191.
126. C. S. Calero, J. Farwer, E. J. Gardiner, C. A. Hunter, M. Mackey, S. Scuderi, S. Thompsona and J. G. Vinterb, *Phys. Chem. Chem. Phys.* **2013**, *15*, 18262-18273.
127. P. Sjoberg and P. Politzer, *J. Phys. Chem.* **1990**, *94*, 3959-3961.
128. P. K. Weiner, R. Langridge, J. M. Blaney, R. Schaefer and P. A. Kollman, *Proc. Natl. Acad. Sci.* **1982**, *79*, 3754.
129. G. Merino, A. Vela and T. Heine, *Chem. Rev.* **2005**, *105*, 3812–3841.
130. A. S. Mahadevi, A. P. Rahalkar, S. R. Gadre and G. N. Sastry, *J. Chem. Phys.* **2010**, *133*, 164308.
131. P. Balanarayan, R. Kavathekar and S. R. Gadre, *J. Phys. Chem. A* **2007**, *111*, 2733-2738.
132. K. V. J. Jose and S. R. Gadre, *Int. J. Quantum Chem.* **2009**, *109*, 2238-2247.

133. D. S. Patel, P. Daga, P. V. Bharatam, R. K. Dongare and S. R. Gadre, *Indian J. Chem.* **2006**, *45A*, 13.
134. K. Babu and S. R. Gadre, *J. Comput. Chem.* **2003**, *24*, 484-495.
135. M. M. Deshmukh, L. J. Bartolotti and S. R. Gadre, *J. Phys. Chem. A* **2008**, *112*, 312-321.
136. S. R. Gadre and A. D. Kulkarni, *Indian J. Chem.* **2000**, *39A*, 50-59.
137. M. M. Deshmukh, S. R. Gadre, R. Tonner and G. Frenking, *Phys. Chem. Chem. Phys.* **2008**, *10*, 2298-2301.
138. S. R. Gadre and P. K. Bhadane, *J. Phys. Chem. A* **1999**, *103*, 3512-3517.
139. S. S. Pingale, S. R. Gadre and L. J. Bartolotti, *J. Phys. Chem. A* **1998**, *102*, 9987.
140. C. H. Suresh and N. Koga, *J. Am. Chem. Soc.* **2002**, *124*, 1790-1797.
141. S. R. Gadre and R. N. Shirsat, *Electrostatics of atoms and molecules (Hyderabad, India: Universities Press)* **2000**
142. S. R. Gadre and C. H. Suresh, *J. Org. Chem.* **1997**, *62*, 2625-2627.
143. C. H. Suresh and S. R. Gadre, *J. Am. Chem. Soc.* **1998**, *120*, 7049-7055.
144. C. H. Suresh and S. R. Gadre, *J. Phys. Chem. A* **2007**, *111*, 710-714.
145. C. H. Suresh and S. R. Gadre, *J. Org. Chem.* **1999**, *64*, 2505-2512.
146. R. Rakhi and C. H. Suresh, *J. Comput. Chem.* **2017**, *38*, 2232-2240.
147. R. Rakhi and C. H. Suresh, *Phys. Chem. Chem. Phys.* **2016**, *18*, 24631-24641.
148. F. B. Sayyed and C. H. Suresh, *New J. Chem.* **2009**, *33*, 2465-2471.
149. F. B. Sayyed, C. H. Suresh and S. R. Gadre, *J. Phys. Chem. A* **2010**, *114*, 12330-12333.
150. F. B. Sayyed and C. H. Suresh, *J. Phys. Chem. A* **2011**, *115*, 5660-5664.
151. F. B. Sayyed and C. H. Suresh, *J. Phys. Chem. A* **2011**, *115*, 9300-9307.
152. F. B. Sayyed and C. H. Suresh, *J. Phys. Chem. A* **2012**, *116*, 5723-5732.
153. Y. Ma and P. Politzer, *J. Chem. Phys.* **2004**, *120*, 8955-8959.
154. D. A. Dougherty, *J. Nutr.* **2007**, *137* 1504-1508.
155. D. A. Dougherty, *Acc.Chem. Res.* **2013**, *46*, 885-893.
156. S. E. Wheeler and J. W. G. Bloom, *J. Phys. Chem. A .* **2014**, *118*, 6133-6147.
157. S. E. Wheeler and J. W. G. Bloom, *Chem. Commun.* **2014**, *50*, 11118-11121.
158. S. E. Wheeler, *J. Am. Chem. Soc.* **2011**, *133*, 10262.
159. S. E. Wheeler and K. N. Houk, *J. Chem. Theory Comput.* **2009**, *5*, 2301-2312.

160. S. E. Wheeler and K. N. Houk, *J. Am. Chem. Soc.* **2009**, *131*, 3126-3127.
161. S. E. Wheeler and K. N. Houk, *J. Am. Chem. Soc.* **2008**, *130*, 10854-10855.
162. S. E. Wheeler, *Acc. Chem. Res.* **2013**, *46*,, 1029.
163. S. E. Wheeler and K. N. Houk, *J. Phys. Chem. A.* **2010**, *114*, 8658-8664.
164. P. Politzer, J. S. Murray and Z. peralta-Inga, *Int. J. Quantum Chem.* **2001**, *85*, 676–684.
165. J. S. Murray, P. Lane, T. Brinck, P. Politzer and P. Sjoberg, *J. Phys. Chem.* **1991**, *95*, 844–848.
166. P. Sjoberg and P. Politzer, *J. Phys. Chem.* **1990**, *94*, 3959.
167. T. Clark, M. Hennemann, J. S. Murray and P. Politzer, *J. Mol. Model.* **2007**, *13*, 291-296.
168. T. Clark, *WIREs Comput. Mol. Sci.* **2012**, *3*, 13-20.
169. P. Politzer, J. S. Murray and T. Clark, *Phys. Chem. Chem. Phys.* **2010**, *12*, 7748.
170. P. Politzer, J. S. Murray and P. Lane, *Int. J. Quantum Chem.* **2007**, *107*, 3047.
171. M. Hennemann, J. S. Murray, P. Politzer, K. E. Riley and T. Clark, *J. Mol. Model.* **2012**, *18*, 2461-2469.
172. A. Kumar, S. R. Gadre, N. M. and and C. H. Suresh, *J. Phys. Chem. A* **2014**, *118*, 526-532.
173. P. V. Bijina, C. H. Suresh and S. R. Gadre, *J. Comput. Chem.* **2018**, *39*, 488-499.
174. N. Mohan and C. H. Suresh, *J. Phys. Chem. A* **2014**, *118*, 4315-4324.
175. N. Mohan, C. H. Suresh, A. Kumar and S. R. Gadre, *Phys. Chem. Chem. Phys.* **2013**, *15*, 18401.
176. K. Remya and C. H. Suresh, *Phys. Chem. Chem.Phys.* **2015**, *17*, 27035-27044.
177. N. Mohan and C. H. Suresh, *J. Phys. Chem. A.* **2014**, *118*, 1697–1705.
178. P. V. Bijina and C. H. Suresh, *J. Chem..Sci.* **2016**, *128*, 1677-1686.
179. T. D. Della and C. H. Suresh, *ACS Omega* **2017**, *2*, 4505-4513.
180. T. D. Della and C. H. Suresh, *Phys. Chem. Chem. Phys.* **2018**, *20*, 6227-6235.
181. T. Davis Della and C. H. Suresh, *Phys. Chem. Chem. Phys.* **2018**, *20*, 24885-24893.
182. E. D. Jemmis, G. Subramanian, G. N. Sastry, G. Mehta, R. N. Shirsat and S. R. Gadre, *J. Chem. Soc., Perkin Trans. 2* **1996**, 2343-2346.

183. D.-L. Wang, H.-T. Shen, H.-M. Gu and Y.-C. Zhai, *J. Mol. Struct: THEOCHEM* **2006**, *776*, 47-51.
184. H. Ueno, K. Kokubo, Y. Nakamura, K. Ohkubo, N. Ikuma, H. Moriyama, S. Fukuzumi and T. Oshima, *Chem. Commun.* **2013**, *49*, 7376-7378.
185. C. H. Suresh, N. Koga and S. R. Gadre, *Organometallics* **2000**, *19*, 3008-3015.
186. A. D. Hunter, L. Shilliday, W. S. Furey and M. J. Zaworotko, *Organometallics* **1992**, *11*, 1550-1560.
187. L. Cavallo and M. Solà, *J. Am. Chem. Soc.* **2001**, *123*, 12294-12302.
188. N. Fey, A. C. Tsipis, S. E. Harris, J. N. Harvey, A. G. Orpen and R. A. Mansson, *Chem. Eur. J.* **2006**, *12*, 291 - 302.
189. R. A. Baber, M. F. Haddow, A. J. Middleton, A. G. Orpen, P. G. Pringle, A. Haynes, G. L. Williams and R. Papp, *Organometallics* **2007**, *26*, 713-725.
190. P. B. Dias, M. E. M. de Piedade and J. A. M. Simões, *Coord. Chem. Rev.* **1994**, *135-136*, 737-807.
191. P. Schwab, R. H. Grubbs and J. W. Ziller, *J. Am. Chem. Soc.* **1996**, *118*, 100-110.
192. G. C. Vougioukalakis and R. H. Grubbs, *Chem. Rev.* **2010**, *110*, 1746-1787.
193. C. H. Suresh and N. Koga, *Inorg. Chem.* **2002**, *41*, 1573.
194. C. H. Suresh, *Inorg. Chem.* **2006**, *45*, 4982-4986.
195. J. Mathew, T. Thomas and C. H. Suresh, *Inorg. Chem.* **2007**, *46*, 10800-10809.
196. J. Mathew and C. H. Suresh, *Organometallics* **2011**, *30*, 1438-1444.
197. M. Scholl, S. Ding, C. W. Lee and R. H. Grubbs, *Org. Lett.* **1999**, *1*, 953-956.
198. J. Mathew and C. H. Suresh, *Organometallics* **2011**, *30*, 3106-3112.
199. M. N. Hopkinson, C. Richter, M. Schedler and F. Glorius, *Nature* **2014**, *510*, 485-496.
200. H. V. Huynh, *Chem. Rev.* **2018**, *118* 9457-9492.
201. W. A. Herrmann, M. Elison, J. Fischer, C. Köcher and G. R. J. Artus, *Angew. Chem. Int. Ed.* **1995**, *34*, 2371-2374.
202. J. Mathew and C. H. Suresh, *Inorg. Chem.* **2010**, *49*, 4665-4669.
203. M. J. Ajitha and C. H. Suresh, *J. Org. Chem.* **2012**, *77*, 1087-1094.
204. A. Pidcock, R. E. Richards and L. M. Venanzi, *J. Chem. Soc. A* **1966**, 1707-1710.
205. R. Mason and A. D. C. Towl, *J. Chem Soc. A.* **1970**, 1601-1613.

206. J. E. Huheey, E. A. Keiter and R. L. Keiter, *Inorganic chemisty: principles of structure and reactivity Harper Collins College Publishers 4th ed.: New York* **1993**.
207. P. K. Sajith and C. H. Suresh, *Inorg. Chem.* **2011**, *50*, 8085-8093.
208. P. K. Sajith and C. H. Suresh, *Inorg. Chem.* **2012**, *51*, 967-977.
209. P. K. Sajith and C. H. Suresh, *Inorg. Chem.* **2013**, *52*, 6046-6054.
210. K. S. Sandhya and C. H. Suresh, *J. Phys. Chem. A* **2017**, *121*, 2814-2819.
211. K. S. Sandhya and C. H. Suresh, *Dalton Trans.* **2014**, *43*, 12279.
212. B. A. Anjali, F. B. Sayyed and C. H. Suresh, *J. Phys. Chem. A* **2016**, *120*, 1112-1119.
213. B. A. Anjali and C. H. Suresh, *ACS Omega* **2017**, *2*, 4196–4206.
214. B. A. Anjali and C. H. Suresh, *New J. Chem.* **2018**, *42*, 18217-18224.
215. E. Schrödinger, *Ann. Phys.* **1926**, *384*, 361-376.
216. R. A. Friesner, *Proc. Natl. Acad. Sci.* **2005**, *102*, 6648-6653.
217. M. Born and R. Oppenheimer, *Ann. Phys.* **1927**, *389*, 457-484.
218. C. J. Cramer, *Essentials of Computational Chemistry: Theories and Models*, Wiley **2013**.
219. A. Szabó and N. S. Ostlund, *Modern Quantum Chemistry: Introduction to Advanced Electronic Structure Theory* **1982**.
220. D. C. Young, *Computational Chemistry: A Practical Guide for Applying Techniques to Real-World Problem*, Wiley-Interscience, New York **2001**.
221. C. C. J. Roothaan, *Rev. Mod. Phys.* **1951**, *23*, 69-89.
222. G. G. Hall, *Proc. Royal Soc. A* **1951**, *205*, 541-552.
223. R. J. Bartlett and J. F. Stanton, *Reviews in Computational Chemistry* **1994**, pp. 65-169.
224. L. Visscher, *Theor. Comput. Chem.*, ed. P. Schwerdtfeger, Elsevier **2002**, vol. 11, pp. 291-331.
225. V. Magnasco, *Methods of Molecular Quantum Mechanics* **2009**, pp. 133-139.
226. C. Møller and M. S. Plesset, *Phys. Rev.* **1934**, *46*, 618-622.
227. J. A. Pople, J. S. Binkley and R. Seeger, *Int. J. Quant. Chem.* **1976**, *10*, 1-19.
228. O. Christiansen, *J. Chem. Phys.* **2003**, *119*, 5773-5781.
229. K. Hirao, *Chem. Phys. Lett.* **1992**, *190*, 374-380.
230. J. Gauss and D. Cremer, *Chem. Phys. Lett.* **1987**, *138*, 131-140.

231. C. David Sherrill and H. F. Schaefer, in *Adv. Quant. Chem.*, eds. P.-O. Löwdin, J. R. Sabin, M. C. Zerner and E. Brändas, Academic Press **1999**, vol. 34, pp. 143-269.
232. D. Casanova, Y. M. Rhee and M. Head-Gordon, *J. Chem. Phys.* **2008**, *128*, 164106.
233. J. D. Watts, I. Cernusak, J. Noga, R. J. Bartlett, C. W. B. Jr., T. J. Lee, A. P. Rendell and P. R. Taylor, *J. Chem. Phys.* **1990**, *93*, 8875-8880.
234. G. Das, *J. Chem. Phys.* **1973**, *58*, 5104-5110.
235. M. J. Watkins, K. Müller-Dethlefs and M. C. R. Cockett, *Phys. Chem. Chem. Phys.* **2000**, *2*, 5528-5537.
236. H. J. Werner and P. J. Knowles, *J. Chem. Phys.* **1988**, *89*, 5803-5814.
237. J. Čížek, *J. Chem. Phys.* **1966**, *45*, 4256-4266.
238. H. J. Monkhorst, *Int. J. Quant. Chem.* **1977**, *12*, 421-432.
239. K. Raghavachari, G. W. Trucks, J. A. Pople and M. Head-Gordon, *Chem. Phys. Lett.* **1989**, *157*, 479-483.
240. J.A.Pople and O.L.Beveridge, *Approximate Molecular Orbltal Theory", Academic Press, New York* **1970**.
241. G.A.Segal, *ed.I, "Modern Theoretlcal Chemistry". Plenum, New York, vol 7-8* **1977**.
242. W. Thiel, *Tetrahedron* **1988**, *44*, 7393-7408.
243. E. Hückel, *Zeitschrift für Physik* **1930**, *60*, 423-456.
244. J. A. Pople, D. P. Santry and G. A. Segal, *J. Chem. Phys.* **1965**, *43*, S129-S135.
245. M. J. S. Dewar and W. Thiel, *J. Am. Chem. Soc.* **1977**, *99*, 4899-4907.
246. M. A. Abdulsattar and K. H. Al-Bayati, *Phys. Rev. B* **2007**, *75*, 245201.
247. G. Náaray-Szabó, G. Tóth, G. G. Ferenczy and G. Csonka, *Int. J. Quant. Chem.* **1994**, *52*, 227-236.
248. M. J. S. Dewar, E. G. Zoebisch, E. F. Healy and J. J. P. Stewart, *J. Am. Chem. Soc.* **1985**, *107*, 3902-3909.
249. J. J. P. Stewart, *J. Comput. Chem.* **1989**, *10*, 209-220.
250. A. D. Becke, *J. Chem. Phys.* **2014**, *140*, 18A301.
251. W. Kohn, A. D. Becke and R. G. Parr, *J. Phys. Chem.* **1996**, *100*, 12974-12980.
252. W. Kohn, *Rev. Mod. Phys.* **1999**, *71*, 1253-1266.
253. M. Orio, D. A. Pantazis and F. Neese, *Photosynth. Res.* **2009**, *102*, 443-453.
254. L. H. Thomas, *Proc. Cambridge Philos. Soc.* **1927**, *23*.

255. E. Fermi, *Atti Accad. Naz. Lincei* **1927**, *6*, 602.
256. E. Fermi, *Z. Phys.* **1928**, *48*, 73 -79.
257. P. A. M. Dirac, *Proc. Cambridge Phil. Soc.* **1930**, *26*, 376-385.
258. P. Hohenberg and W. Kohn, *Phys. Rev.* **1964**, *136*, B864-B871.
259. W. Kohn and L. J. Sham, *Phys. Rev.* **1965**, *140*, A1133-A1138.
260. D. M. Ceperley and B. J. Alder, *Phys. Rev. Lett.* **1980**, *45*, 566-569.
261. S. H. Vosko, L. Wilk and M. Nusair, *Can. J. Phys.* **1980**, *58*, 1200-1211.
262. A. D. Becke, *Phys. Rev. A* **1988**, *38*, 3098-3100.
263. C. Lee, W. Yang and R. G. Parr, *Phys. Rev. B* **1988**, *37*, 785-789.
264. J. P. Perdew, *Phys. Rev. B* **1986**, *33*, 8822-8824.
265. J. P. Perdew, J. A. Chevary, S. H. Vosko, K. A. Jackson, M. R. Pederson, D. J. Singh and C. Fiolhais, *Phys. Rev. B* **1992**, *46*, 6671-6687.
266. J. P. Perdew, K. Burke and M. Ernzerhof, *Phys. Rev. Lett.* **1996**, *77*, 3865-3868.
267. F. Furche and J. P. Perdew, *J. Chem. Phys.* **2006**, *124*, 044103.
268. A. D. Becke, *J. Chem. Phys.* **1993**, *98*, 1372-1377.
269. L. A. Constantin, E. Fabiano and F. Della Sala, *J. Chem. Theory Comput.* **2013**, *9*, 2256-2263.
270. A. D. Becke, *J. Chem. Phys.* **1993**, *98*, 5648-5652.
271. Y. Zhao and D. G. Truhlar, *J. Chem. Phys.* **2006**, *125*, 194101.
272. S. Grimme, *J. Comput. Chem.* **2006**, *27*, 1787-1799.
273. J. P. Perdew and K. Schmidt, *AIP Conf. Proc.* **2001**, *577*, 1-20.
274. J. P. Perdew, A. Ruzsinszky, J. Tao, V. N. Staroverov, G. E. Scuseria and G. I. Csonka, *J. Chem. Phys.* **2005**, *123*, 062201.
275. S. Grimme, *J. Comput. Chem.* **2006**, *27*, 1787-1799.
276. S. Grimme, J. Antony, S. Ehrlich and H. Krieg, *J. Chem. Phys.* **2010**, *132*, 154104.
277. E. R. Johnson and A. D. Becke, *J. Chem. Phys.* **2005**, *123*, 024101.
278. A. Tkatchenko and M. Scheffler, *Phys. Rev. Lett.* **2009**, *102*, 073005.
279. Y. Zhao and D. G. Truhlar, *J. Chem. Theory Comput.* **2008**, *4*, 1849-1868.
280. S. Grimme, *J. Comput. Chem.* **2004**, *25*, 1463-1473.
281. J. C. Slater, *Phys. Rev.* **1930**, *35*, 210-211.
282. F. Jensen, *Introduction to Computational Chemistry*, John Wiley & Sons **2017**.

283. S. F. Boys and C. Egerton Alfred, *Proc. Royal Soc.* **1950**, *200*, 542-554.
284. D. E. Woon and T. H. Dunning, *J. Chem. Phys.* **1995**, *103*, 4572-4585.
285. W. J. Hehre, R. F. Stewart and J. A. Pople, *J. Chem. Phys.* **1969**, *51*, 2657-2664.
286. T. H. Dunning, *J. Chem. Phys.* **1989**, *90*, 1007-1023.
287. M. M. Francl, W. J. Pietro, W. J. Hehre, J. S. Binkley, M. S. Gordon, D. J. DeFrees and J. A. Pople, *J. Chem. Phys.* **1982**, *77*, 3654-3665.
288. M. J. Frisch, J. A. Pople and J. S. Binkley, *J. Chem. Phys.* **1984**, *80*, 3265-3269.
289. F. Weigend, F. Furche and R. Ahlrichs, *J. Chem. Phys.* **2003**, *119*, 12753-12762.
290. P. J. Hay and W. R. Wadt, *J. Chem. Phys.* **1985**, *82*, 270-283.
291. T. R. Cundari and W. J. Stevens, *J. Chem. Phys.* **1993**, *98*, 5555-5565.
292. M. Dolg, in *Theor. Comput. Chem.*, ed. P. Schwerdtfeger, Elsevier , vol. 11, pp. 793-862.
293. C. E. Check, T. O. Faust, J. M. Bailey, B. J. Wright, T. M. Gilbert and L. S. Sunderlin, *J. Phys. Chem. A* **2001**, *105*, 8111-8116.
294. E. M. Engler, J. D. Andose and P. V. R. Schleyer, *J. Am. Chem. Soc.* **1973**, *95*, 8005-8025.
295. Y. Duan, C. Wu, S. Chowdhury, M. C. Lee, G. Xiong, W. Zhang, R. Yang, P. Cieplak, R. Luo, T. Lee, J. Caldwell, J. Wang and P. Kollman, *J. Comput. Chem.* **2003**, *24*, 1999-2012.
296. P. K. Weiner and P. A. Kollman, *J. Comput. Chem.* **1981**, *2*, 287-303.
297. K. Vanommeslaeghe, E. Hatcher, C. Acharya, S. Kundu, S. Zhong, J. Shim, E. Darian, O. Guvench, P. Lopes, I. Vorobyov and A. D. Mackerell Jr., *J. Comput. Chem.* **2010**, *31*, 671-690.
298. C. Oostenbrink, A. Villa, A. E. Mark and W. F. Van Gunsteren, *J. Comput. Chem.* **2004**, *25*, 1656-1676.
299. N. L. Allinger, Y. H. Yuh and J. H. Lii, *J. Am. Chem. Soc.* **1989**, *111*, 8551-8566.
300. L.-G. Hammarström, T. Liljefors and J. Gasteiger, *J. Comput. Chem.* **1988**, *9*, 424-440.
301. N. Nevins, K. Chen and N. L. Allinger, *J. Comput. Chem.* **1996**, *17*, 669-694.
302. A. Hospital, J. R. Goñi, M. Orozco and J. L. Gelpí, *Adv. Appl. Bioinform. Chem.* **2015**, *8*, 37-47.

303. F. H. Stillinger and A. Rahman, *J. Chem. Phys.* **1974**, *60*, 1545-1557.
304. J. A. McCammon, B. R. Gelin and M. Karplus, *Nature* **1977**, *267*, 585-590.
305. M. Hawlitzky, J. Horbach, S. Ispas, M. Krack and K. Binder, *J. Phy- Condens. Matt.* **2008**, *20*, 285106.
306. J. Hutter, *WIREs Comput. Mol. Sci.* **2012**, *2*, 604-612.
307. W. M. C. Foulkes, L. Mitas, R. J. Needs and G. Rajagopal, *Rev. Mod. Phys.* **2001**, *73*, 33-83.
308. Y.-J. Zhang, A. Khorshidi, G. Kastlunger and A. A. Peterson, *J. Chem. Phys.* **2018**, *148*, 241740.
309. M. Svensson, S. Humbel, R. D. J. Froese, T. Matsubara, S. Sieber and K. Morokuma, *J. Phys. Chem.* **1996**, *100*, 19357-19363.
310. D. C. Young, *Computational Chemistry: A Practical Guide for Applying Techniques to Real-World Problems*, Wiley-Interscience, New York **2001**.
311. J. Tomasi, B. Mennucci and R. Cammi, *Chem. Rev.* **2005**, *105*, 2999-3094.
312. R. E. Skyner, J. L. McDonagh, C. R. Groom, T. van Mourik and J. B. O. Mitchell, *Phys. Chem. Chem. Phys.* **2015**, *17*, 6174-6191.
313. C. J. Cramer and D. G. Truhlar, *Chem. Rev.* **1999**, *99*, 2161-2200.
314. S. Miertuš, E. Scrocco and J. Tomasi, *Chem. Phys.* **1981**, *55*, 117-129.
315. B. Mennucci, E. Cancès and J. Tomasi, *J. Phys. Chem. B* **1997**, *101*, 10506-10517.
316. J. Andzelm, C. Kölmel and A. Klamt, *J. Chem. Phys.* **1995**, *103*, 9312-9320.
317. A. V. Marenich, C. J. Cramer and D. G. Truhlar, *J. Phys. Chem. B* **2009**, *113*, 6378-6396.
318. E. S. H. Gwee, Z. L. Seeger, D. R. T. Appadoo, B. R. Wood and E. I. Izgorodina, *ACS Omega* **2019**, *4*, 5254-5269.

Chapter 2

Quantification and Classification of Substituent Effects in Organic Chemistry

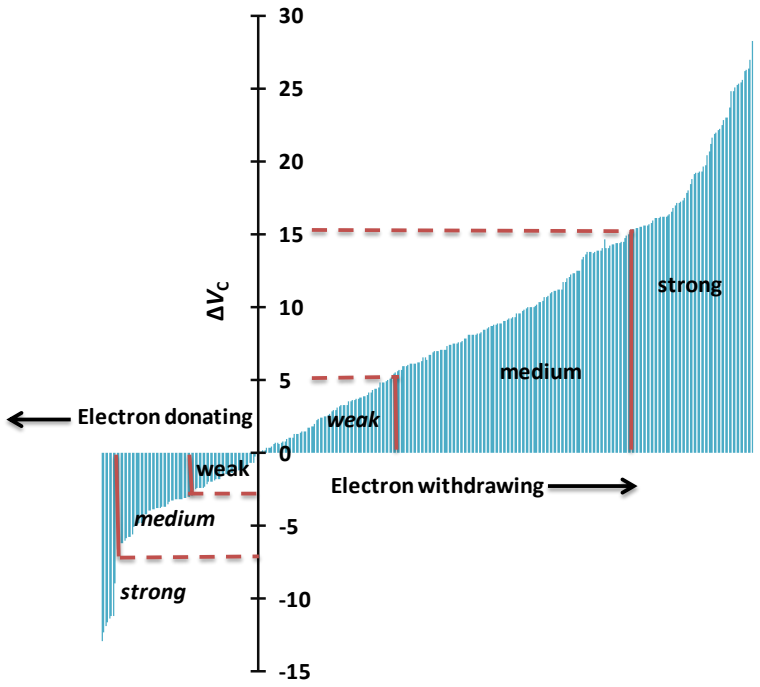

Quantification and Classification of Substituent Effects in Organic Chemistry

2.1 Abstract

Substituent effects in organic chemistry are generally described in terms of experimentally derived Hammett parameters whereas a convenient theoretical tool to study this effect in π-conjugated molecular systems is molecular electrostatic potential (MESP) analysis. The present study shows that the difference between MESP at the nucleus of the para carbon of substituted benzene and a carbon atom in benzene, designated as ΔV_C is very useful to quantify and classify substituent effects. On the basis of positive and negative ΔV_C values, a broad classification of around 381 substituents in electron withdrawing and donating categories is made. Each category is again sorted based on the magnitude of ΔV_C in subcategories such as very strong, strong, medium, and weak electron donating/ withdrawing. Further, the data is used to show the transferability and additivity of substituent effects in π-conjugated organic molecules such as condensed aromatics, olefinic, acetylenic, and heterocyclic systems. The transferability property holds good for ΔV_C in all these molecular systems. The additive property of substituent effect is strongly reflected on ΔV_C and the predictive power of the data to assign the total substituent effect of multiply substituted systems is verified. The ΔV_C data and the present classification of substituents are very useful to design π-conjugated organic molecular systems with desired electron rich/poor character.

2.2 Introduction

Many relationships have been recognized for correlating substituent effects in organic chemistry to various chemical properties.[1] Among them, Hammett equation is the most widely used structure-property correlations to explain the reaction rates and equilibria of a large variety of molecular systems.[2] The substituent constants σ_m and σ_p derived by Hammett are widely used as measures of the total electronic effect of a substituent in the *meta*- and *para*-substituted benzoic acids, respectively. These parameters correlate

well with a huge spectrum of thermo chemical properties.[3-8] Hammett constants reflect the extent to which the electronic environment of a substituted aromatic ring is tailored[9] with respect to the unsubstituted (substituent is H) system. The celebrated *Chem. Rev.* article on Hammett constants by Hansch and Leo lists a huge array of substituents including cationic and anionic substituents.[1]

Exner and Böhm have theoretically examined the validity of Hammett equation and studied quite a few *para* and *meta* substituted benzoic acids, which are the key compounds in elucidating Hammett equation.[10] Further, substituent effect was quantified with the aid of *meta* and *para* derivatives of benzene[11-13] and some representative heterocycles.[14-17] A large variety of mono and disubstituted benzenes were studied to relate several thermo chemical properties[18,19] to substituent effects. The acidity and basicity of substituted benzoic acids, benzonitriles and ethynyl benzenes were also evaluated for finding structure property correlations.[20,21] Exner interpreted inductive substituent effect[22] in terms of dipole-dipole interactions and energy of isodesmic reactions.[23] Exner and Böhm developed a scale of inductive effect and established the influence of polar groups on inductive[24-26] and resonance effects.[12] They have also showed that conjugative resonance interaction is strongly stabilizing for the combination acceptor–donor groups and destabilizing for two donors and weak for two acceptors.[27] Studies on straight chain and branched alkyl groups verified their weak[28] σ-bond influence compared to dipolar groups showing π-inductive effect.[29] The electrostatic theory was also applied for calculating substituent effect in model systems like bicyclo octanes.[30,31]

Krygowski *et al*. reported several noteworthy studies on the quantification of substituent effects, aromaticity, solvent effects and hydrogen bonds in physical organic chemistry.[32,33] They have portrayed substituent effect as a key structural aspect and argued that it controls every characteristic of a chemical species. The interpretation of Hammett constants has been made realistic by systematic studies on apposite substituents.[34] Hydrogen bonding is emerged as a key concept, which can manipulate the electron attracting and donating capacity of substituents. The effect of a substituent may be improved by the presence of hydrogen bonding, particularly in *ortho*

substituted systems.[35] Both intermolecular and intramolecular hydrogen bonding is incorporated to distinguish the reactivity of aniline derivatives and substituted phenols. A brief commentary on various aspects concerned with substituent effects and π-electron delocalization is found in the reviews by Krygowski *et al*.[36,37] The interconnection between substituent effect and aromaticity is well documented. The evaluations of the well-known aromaticity indices such as nucleus independent chemical shift (NICS),[38] harmonic oscillator model of aromaticity (HOMA),[39] substituent effect stabilization energy (SESE)[40] and aromatic stabilization energy (ASE)[41] for monosubstituted benzenes have shown that the systems get stabilized by electron accepting substituents and destabilized by electron donating substituents. Studies using monosubstituted benzenes established a strong correlation between the para delocalization index (PDI) and substituent constants.[42] In the case of *para*-di-homo substituted benzenes, the effect of substituents is stronger than the corresponding *meta* ones.[4]

As substituted benzoic acids are indispensable for concluding Hammett relationships, the theoretical studies conducted by Wiberg[43,44] shed some light on the origin of substituent effects on the acidity of benzoic acids. The electron donating groups stabilized benzoic acids and destabilized benzoate anions while the influence of electron withdrawing groups was the opposite. The *meta* substituted acids were more acidic compared to *para* substituted acids. A direct π-interaction is observed between the substituent and phenoxide ion, in the case of phenols.[45] Quantum chemical theoretical studies have shown that theoretically derived structural, electronic and energetic properties of molecules can be employed as quantitative measures of substituent effects as many of them show strong linear correlation with Hammett constants.[37,46] MESP analysis is one of the best quantifiers for the substituent effect.[47] The MESP analysis can portray significant changes in the molecular region and becomes more suitable for studying substituent effects, especially in organic chemistry.[48,49] However, these correlation studies were limited only to a handful of substituents and so far no attempt has been made to validate the findings to a vast variety of substituents.

We have selected an outsized range of substituents (total 381) listed by Hansch and Leo in their review for a systematic study of substituent effects.

2.3 Computational Methodology

The present study mainly deals with benzene and its several mono- and multiplies-substituted derivatives. Also for selected substituents, mono- and multiply substituted derivatives of pyridine, 1, 3-butadiene, 1, 3-butadiyne, and pyrene have been considered. All the structures involved in this study are optimized using the B3LYP level with 6-311+G(d,p) basis set. They are verified as energy minima by frequency calculation. The B3LYP/6-311+G(d,p) wave function is used for calculating V_{min} and V_C values of MESP. All the computational calculations and MESP analysis have been performed with density functional theory (DFT) using Gaussian 09 suite of programmes.[50]

2.4 Results and Discussion

2.4.1 Classification of Substituent Effects

The elucidation of Hammett constants for a choice of substituents is supported by experimental observations and is not based on one molecular system or a single reaction condition. But the significance of our classification is that it is based on a single molecular system, namely X-substituted benzene derivative wherein the reference molecule is benzene. The quantity ΔV_C calculated as the difference between MESP at the nucleus of *para* carbon of the X-substituted benzene and that of benzene is proposed as a standard parameter to categorize the various substituents. Negative ΔV_C values show the characteristic electron donating feature of substituents while positive ΔV_C values depict their electron withdrawing effect. A large positive value indicates a highly electron withdrawing substituent whereas a large negative value suggests a highly electron donating substituent.

From the earlier studies, it is instantly recognized that MESP parameters can be used as a descriptor of the electron attracting and withdrawing power of substituents.[48]

In the MESP topography of benzene, a π-face of the ring is characterized by the presence of six degenerate MESP minimum (V_{min}) which are ~1.73 Å away from the nearest ring carbon atom. This unique MESP topography of benzene is previously discussed by Suresh and Gadre.[51] They have also showed that in the case of X-substituted benzenes, the number of MESP V_{min} points decreases and in general, such points appear close to the π-region of *para* and *ortho* carbon atoms for electron donating groups or they appear close to *meta* carbon atoms for electron withdrawing groups.[52]

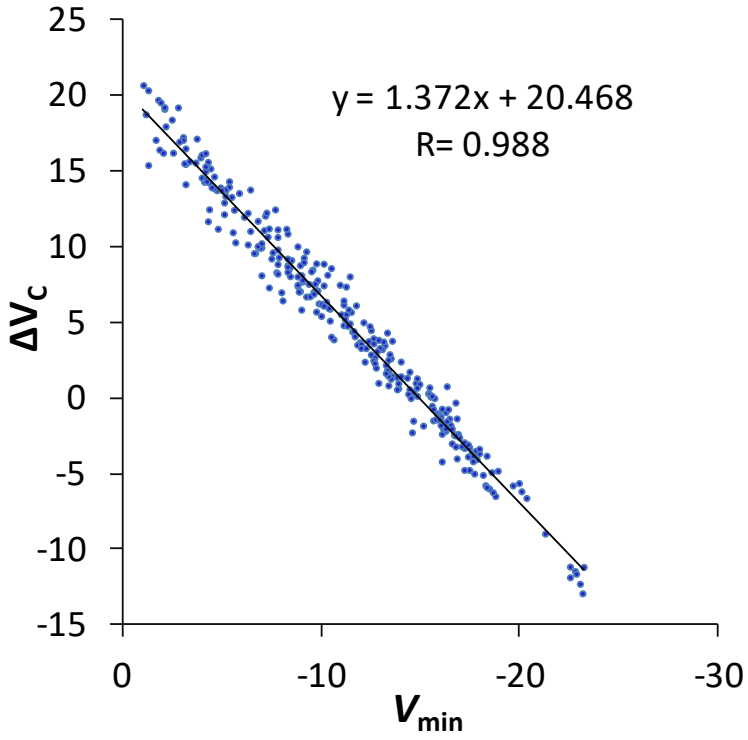

Figure 2.1 Correlation between ΔV_C and V_{min} values (kcal/mol).

In the present work, we report both the quantities ΔV_C and V_{min}. These quantities give almost identical assessment of the substituent effect as they show a strong linear correlation between them (Figure 2.1). The V_C of a system is directly obtained from the output of a MESP calculation using a standard quantum chemical program while a program to do the MESP topographical analysis is required to characterize V_{min}. The program developed by Gadre *et al.* is useful for such MESP analysis.[53] For any practical application focusing only on the value of V_{min}, a numerical approach dealing with

computation of MESP on a fine 3D grid is sufficient. The approach using V_{min} has a limitation when dealing with the quantification of a positively charged substituent. In general, cationic species do not show V_{min}. Such scenarios can also arise when the ring is substituted with multiple highly electron withdrawing groups. Hence, from a classification point of view of substituent effect dealing with a large variety of substituents (cationic, anionic and neutral) and ease of application and quick assessment, ΔV_C is more attractive than V_{min}. Hence, we do the present classification based on the values of ΔV_C. Since MESP is experimentally derivable from X-ray diffraction data, the experimental verification of the current approach is also possible.

The substituents with positive ΔV_C values are treated broadly as electron withdrawing substituents. We propose the use of a notation *S* with one or more '<' superscripts to indicate the very strong ($S^{<<<<}$), strong ($S^{<<<}$), medium ($S^{<<}$) and weak ($S^{<}$) electron withdrawing substituents. The cationic substituents show the largest range of positive values for ΔV_C (58.4 - 127.5 kcal/mol) and are considered in the very strong $S^{<<<<}$ category. Among the neutral substituents, substituents with ΔV_C above 0.0 up to 5.0 kcal/mol, above 5.0 up to 15.0 kcal/mol, and all above 15.0 kcal/mol are classified as weak ($S^{<}$), medium ($S^{<<}$), and strong ($S^{<<<}$) electron withdrawing category, respectively (Table 2.1).

Figure 2.2 schematically represents the classification of electron withdrawing neutral substituents. In this classification, the big gap between the most withdrawing neutral substituent (28.3 kcal/mol) to the least withdrawing cationic substituent (58.4 kcal/mol) cannot be filled with the present set of substituents. A meaningful assessment is to consider all cationic substituents in the $S^{<<<<}$ category as 58.4 kcal/mol cannot be taken as a strict boundary. The substituents with negative ΔV_C values are treated as electron donating (Table 2.2). Anions show the largest range of negative magnitudes for ΔV_C (-57.6 to-113.4 kcal/mol) and are classified under the very strong category ($S^{>>>>}$). Figure 2.3 schematically represents the classification of all other electron donating neutral substituents into the strong ($S^{>>>}$), medium ($S^{>>}$) and weak ($S^{>}$) categories.

Table 2.1 Classification of electron withdrawing substituents with positive ΔV_C values (kcal/mol).

Substituent	ΔV_C		Substituent	ΔV_C		Substituent	ΔV_C	
$N{=}N^+$	127.5	$S^{<<<<}$	$CF{=}CFCF_3$	14.6	$S^{<<}$	CH_2CONH_2	6.7	$S^{<<}$
NH_3^+	97.7	$S^{<<<<}$	SSO_2Me	14.0	$S^{<<}$	CH_2CN	6.7	$S^{<<}$
S^+Me_2	94.4	$S^{<<<<}$	$C(Me)(CN)_2$	13.9	$S^{<<}$	CONHMe	6.4	$S^{<<}$
$N^+(Me)_3$	87.9	$S^{<<<<}$	SCF_2CF_3	13.9	$S^{<<}$	$PS(C_6H_4\text{-}4Me)_2$	6.5	$S^{<<}$
P^+Me_3	87.7	$S^{<<<<}$	CH=CHCN	13.9	$S^{<<}$	$PO(isopropyl)_2$	6.5	$S^{<<}$
$CH_2NH_3^+$	84.9	$S^{<<<<}$	$N{=}NPO(OEt)_2$	13.8	$S^{<<}$	OSO_2Me	6.3	$S^{<<}$
$P(Et)_3^+$	84.1	$S^{<<<<}$	CF_3	13.7	$S^{<<}$	$NHSO_2Me$	6.2	$S^{<<}$
$CH_2NHMe_2^+$	79.8	$S^{<<<<}$	$CF(CF_3)_2$	13.8	$S^{<<}$	SCH_2F	6.2	$S^{<<}$
$P^+(Me)C_6H_5\text{-}C_6H_4\text{-}4Me$	78.3	$S^{<<<<}$	CHO	13.8	$S^{<<}$	$SN(Me)_2$	6.1	$S^{<<}$
$CH_2N(Me)_3^+$	78.0	$S^{<<<<}$	$S(O){=}NHCF_3$	13.8	$S^{<<}$	$PO(C_6H_5)C_6H_4\text{-}4Me$	6.1	$S^{<<}$
$CH_2CH_2NH_3^+$	78.0	$S^{<<<<}$	$SiBr_3$	13.6	$S^{<<}$	$N{=}NC_6H_5$	6.1	$S^{<<}$
$P^+(Me)(C_6H_4\text{-}4Me)_2$	76.9	$S^{<<<<}$	ONO_2	13.4	$S^{<<}$	$P(Cl)NMe_2$	6.1	$S^{<<}$
$CH_2CH_2NHMe_2^+$	74.0	$S^{<<<<}$	$CClF_2$	13.3	$S^{<<}$	SeCH=CHCl	6.0	$S^{<<}$
$CH_2CH_2NMe_3^+$	68.0	$S^{<<<<}$	$CH_2SO_2CF_3$	12.5	$S^{<<}$	$N{=}CCl_2$	5.9	$S^{<<}$
$(CH_2)_3N(Me)_3^+$	58.4	$S^{<<<<}$	$CH{=}NCOC_6H_5$	12.5	$S^{<<}$	SC_6H_5	5.9	$S^{<<}$
SO_2CN	28.3	$S^{<<<}$	$N{=}C(CF_3)_2$	12.5	$S^{<<}$	NHCN	5.9	$S^{<<}$
$C(CN){=}C(CN)_2$	27.0	$S^{<<<}$	$CF_2CF_2C_6H_4\text{-}4F$	12.3	$S^{<<}$	CH_2CF_3	5.7	$S^{<<}$
$SO_2C(CF_3)_3$	26.4	$S^{<<<}$	SCOMe	12.3	$S^{<<}$	C=CH	5.7	$S^{<<}$
$N(O){=}NCN$	26.3	$S^{<<<}$	$OCOCF_3$	12.2	$S^{<<}$	$PO(N(Me)_2)_2$	5.6	$S^{<<}$
SeO_2CF_3	26.2	$S^{<<<}$	BF_2	12.1	$S^{<<}$	$PO(CMe_3)_2$	5.5	$S^{<<}$
$SO_2CF_2CF_2CF_3$	25.6	$S^{<<<}$	OCF_2CF_3	12.0	$S^{<<}$	N_3	5.4	$S^{<<}$
$N{=}NCN$	25.4	$S^{<<<}$	CCl_3	11.7	$S^{<<}$	$PO(C_6H_4\text{-}4Me)_2$	5.2	$S^{<<}$
$SO_2CF(CF_3)_2$	25.3	$S^{<<<}$	$N(Me)NO_2$	11.7	$S^{<<}$	F	5.1	$S^{<<}$
SO_2Cl	25.2	$S^{<<<}$	CBr_3	11.2	$S^{<<}$	$SeCH_2CH{=}CH_2$	5.0	$S^{<}$

$C(NO_2)_3$	25.1	*S*<<<	$N(Me)SO_2CF_3$	11.2	*S*<<	CH=CHCOOEt	4.9	*S*<
SO_2CF_3	24.8	*S*<<<	CH_2SOCF_3	11.2	*S*<<	$SiClMe_2$	4.8	*S*<
$SO_2CF_2CF_3$	24.8	*S*<<<	$PO(OH)_2$	11.1	*S*<<	$NHSO_2C_6H_5$	4.8	*S*<
$CH=NSO_2CF_3$	23.7	*S*<<<	$OCCl_3$	11.1	*S*<<	$SCH_2CH=CH_2$	4.8	*S*<
SO_2CHF_2	23.0	*S*<<<	$NHNO_2$	11.0	*S*<<	SeMe	4.5	*S*<
$C(CN)_3$	23.0	*S*<<<	COOH	10.9	*S*<<	$OSO_2C_6H_5$	4.4	*S*<
$CH=C(CN)_2$	22.8	*S*<<<	$N(SO_2Me)_2$	10.8	*S*<<	CH_2OCOMe	4.4	*S*<
SF_3	22.5	*S*<<<	SCF_2CHF_2	10.7	*S*<<	$CH=NNHCOC_6H_5$	4.3	*S*<
POF_2	22.2	*S*<<<	S(O)OMe	10.7	*S*<<	$SCH=CH_2$	4.1	*S*<
PF_4	22.1	*S*<<<	CHF_2	10.4	*S*<<	$SCHMe_2$	4.1	*S*<
GeF_3	22.0	*S*<<<	$NHSO_2CF_3$	10.3	*S*<<	PH_2	4.0	*S*<
$P(CN)_2$	21.9	*S*<<<	$CH=NNHCSNH_2$	10.3	*S*<<	$N(Me)SO_2Me$	3.9	*S*<
SF_5	21.6	*S*<<<	C_6H_4-4NO_2	10.2	*S*<<	$C=CC_6H_5$	3.9	*S*<
NO_2	21.2	*S*<<<	OCF_2CHF_2	10.1	*S*<<	$CH=NNHCONHNH_2$	3.8	*S*<
$P(O)Cl_2$	20.7	*S*<<<	$CHCl_2$	10.0	*S*<<	SCH=CHCl	3.8	*S*<
$COCF_2CF_2CF_3$	20.4	*S*<<<	$COOC_6H_5$	10.0	*S*<<	CH=NOMe	3.7	*S*<
$P(S)Cl_2$	19.7	*S*<<<	N=C=S	10.0	*S*<<	C_6H_4-3Br	3.7	*S*<
$COCF_3$	19.6	*S*<<<	OCF_2CHFCl	10.0	*S*<<	$SeCH=CH_2$	3.6	*S*<
$CH=CHSO_2CF_3$	19.3	*S*<<<	$CHBr_2$	9.9	*S*<<	C_6H_4-3Cl	3.6	*S*<
$N=NCF_3$	19.3	*S*<<<	C_6F_5	9.8	*S*<<	SiH_3	3.5	*S*<
NO	19.2	*S*<<<	COMe	9.7	*S*<<	C_6H_4-4Br	3.5	*S*<
$N(SO_2CF_3)_2$	19.2	*S*<<<	$SiMeCl_2$	9.6	*S*<<	$N=NC_6H_3$-5Me,2-OH	3.3	*S*<
COCl	19.1	*S*<<<	SOMe	9.6	*S*<<	C_6H_4-4Cl	3.3	*S*<
SOF	18.8	*S*<<<	CH_2SCN	9.6	*S*<<	S(SMe)	3.3	*S*<
COF	18.4	*S*<<<	$CONHC_6H_5$	9.3	*S*<<	C_6H_4-3F	3.3	*S*<
CN	18.0	*S*<<<	$C(OH)(CF_3)_2$	9.3	*S*<<	S(OMe)	3.2	*S*<
$CH=CHNO_2$	17.8	*S*<<<	$P(S)Et_2$	9.2	*S*<<	NHCSMe	3.1	*S*<

SO_2NH_2	17.5	*S*<<<	$CSNH_2$	9.2	*S*<<	$SiFMe_2$	2.9	*S*<
$GeCl_3$	17.3	*S*<<<	$SCHF_2$	9.1	*S*<<	CH_2Br	2.9	*S*<
$P(CF_3)_2$	17.2	*S*<<<	$CH{=}NC_6H_5$	9.0	*S*<<	$OS(=O)CH_3$	2.8	*S*<
$SOCF_3$	17.1	*S*<<<	$N(COMe)_2$	9.0	*S*<<	CH_2Cl	2.7	*S*<
SCN	17.1	*S*<<<	COEt	8.9	*S*<<	GeH_3	2.6	*S*<
$CH(CN)_2$	17.0	*S*<<<	$COCHMe_2$	8.9	*S*<<	$CH_2NHCOMe$	2.5	*S*<
SO_2Me	16.8	*S*<<<	$SiMeF_2$	8.9	*S*<<	C_6H_4-4F	2.5	*S*<
$C(Me)(NO_2)_2$	16.5	*S*<<<	$PO(OMe)_2$	8.8	*S*<<	$SiMe(OMe)_2$	2.4	*S*<
SeCN	16.4	*S*<<<	CH=CHCOMe	8.8	*S*<<	$Si(OMe)_3$	2.4	*S*<
SC_6H_4-4NO_2	16.3	*S*<<<	$PO(OC_4H_9)_2$	8.7	*S*<<	$OCOC_6H_5$	2.3	*S*<
$NO{=}NCONH_2$	16.2	*S*<<<	$SCH{=}NSO_2C_6H_4$-4-Me	8.7	*S*<<	OCH_2Cl	2.2	*S*<
SOC_6H_4-4NO_2	16.2	*S*<<<	$PO(OPr)_2$	8.6	*S*<<	$NHCOCH_2Cl$	2	*S*<
$SOCHF_2$	16.2	*S*<<<	SOC_6H_5	8.5	*S*<<	P(isopropyl)$_2$	1.8	*S*<
C_6H_2-2,4,6$(NO_2)_3$	16.2	*S*<<<	$CH{=}CHCOC_6H_5$	8.4	*S*<<	CH_2F	1.8	*S*<
SiF_3	16.1	*S*<<<	COC_6H_5	8.4	*S*<<	$P(C_6H_5)_2$	1.7	*S*<
cyclo-C_4F_7	16.1	*S*<<<	OCF_3	8.3	*S*<<	$CH_2OC_6H_5$	1.7	*S*<
SO_2Et	16.1	*S*<<<	$NHCOCF_3$	8.2	*S*<<	OCOMe	1.5	*S*<
SCl	15.9	*S*<<<	COOMe	8.2	*S*<<	SH	1.5	*S*<
$SO_2NHC_6H_5$	15.8	*S*<<<	$CONH_2$	8.1	*S*<<	$P(CMe_3)_2$	1.5	*S*<
$SC(CF_3)_3$	15.7	*S*<<<	$PS(C_6H_5)_2$	8.1	*S*<<	OCH_2F	1.4	*S*<
$GeBr_3$	15.6	*S*<<<	C_6H_4-3NO_2	8.1	*S*<<	$P(Et)_2$	1.3	*S*<
$C{\equiv}CF_3$	15.6	*S*<<<	CH=CHCHO	8.1	*S*<<	NHCHO	1.3	*S*<
PCl_2	15.6	*S*<<<	CH_2SCF_3	8.1	*S*<<	C=CMe	1.3	*S*<
$SeC(CF_3)_3$	15.5	*S*<<<	$PO(OEt)_2$	7.8	*S*<<	$NHCSNH_2$	1.0	*S*<
$SCOCF_3$	15.5	*S*<<<	$P(O)Me_2$	7.8	*S*<<	$CH{=}CH_2$	1.0	*S*<
$C(Et)(NO_2)_2$	15.4	*S*<<<	$B(OH)_2$	7.7	*S*<<	CH(OH)Me	1.0	*S*<
$NO{=}NSO_2C_6H_5$	15.4	*S*<<<	$COC(Me)_3$	7.6	*S*<<	$Si(Me)_2OMe$	0.9	*S*<

$(CF_2)_3CF_3$	15.3	$S^{<<<}$	Br	7.6	$S^{<<}$	OC_6H_4-4F	0.8	$S^{<}$
$CF_2CF_2CF_3$	15.3	$S^{<<<}$	$OCHF_2$	7.5	$S^{<<}$	$Si(OEt)_3$	0.8	$S^{<}$
$N(CF_3)_2$	15.2	$S^{<<<}$	COOEt	7.5	$S^{<<}$	PMe_2	0.7	$S^{<}$
SOOH	15.0	$S^{<<}$	$SCH=CH_2$	7.5	$S^{<<}$	$Si(NMe_2)_3$	0.6	$S^{<}$
PF_2	14.9	$S^{<<}$	$OCHCl_2$	7.4	$S^{<<}$	$CH=CHC_6H_5$	0.7	$S^{<}$
CF_2CF_3	14.7	$S^{<<}$	C_6Cl_5	7.4	$S^{<<}$	$OCH=CH_2$	0.7	$S^{<}$
SO_2NMe_2	14.5	$S^{<<}$	$PS(C_6H_5)C_6H_4$-4Me	7.3	$S^{<<}$	CH_2OMe	0.6	$S^{<}$
$SCF_2CF_2CF_3$	14.5	$S^{<<}$	$PO(Et)_2$	7.1	$S^{<<}$	$Si(C_6H_5)_3$	0.4	$S^{<}$
$CH=CHCOC_6H_4$-4NO_2	14.4	$S^{<<}$	$PO(C_3H_7)_2$	7.1	$S^{<<}$	$SiH(Me)_2$	0.3	$S^{<}$
$SiCl_3$	14.4	$S^{<<}$	N=C=O	7.1	$S^{<<}$	$C(OMe)_3$	0.3	$S^{<}$
$SO_2C_6H_5$	14.4	$S^{<<}$	$PO(C_4H_9)_2$	7.1	$S^{<<}$	$CH_2CH(OH)Me$	0.3	$S^{<}$
NC	14.3	$S^{<<}$	Cl	7.0	$S^{<<}$	$SiMe(C_6H_5)_2$	0.2	$S^{<}$
$SCF(CF_3)_2$	14.3	$S^{<<}$	$C(NO_2)Me_2$	7.0	$S^{<<}$	C_6H_5	0.2	$S^{<}$
OCN	14.2	$S^{<<}$	CSNHMe	7.0	$S^{<<}$	$P(N(Pr)_2C_6H_4$-3F	0.1	$S^{<}$
$C(CF_3)_3$	14.0	$S^{<<}$	$PO(C_6H_5)_2$	6.9	$S^{<<}$	$Si(Me)_2OSiMe_3$	0.1	$S^{<}$
OSO_2CF_3	14.0	$S^{<<}$						

It may be noted that electron donating neutral substituents are largely derived from alkyl, amino and alkoxy groups whereas electron withdrawing groups can be selected from a large variety of functional groups. For the neutral electron withdrawing substituents, ΔV_C is in the range 0.0 and 30.0 kcal/mol while that of the electron donating groups is -15.0 to 0.0 kcal/mol. This suggests that the effect of the most donating group is nearly half of the most withdrawing group. Therefore, for the classification purpose, we consider ΔV_C values in the range below 0.0 up to -2.5 kcal/mol, below -2.5 up to -7.5 kcal/mol and all below -7.5 kcal/mol are considered as weak($S^{>}$), medium ($S^{>>}$), and strong ($S^{>>>}$) electron donating substituents, respectively (Figure 2.3). It may be noted that the most donating neutral substituent has ΔV_C -12.9 kcal/mol while the least donating anionic substituent has ΔV_C -57.6 kcal/mol.

Table 2.2 Classification of electron donating substituents with negative ΔV_C values (kcal/mol).

Substituent	ΔV_C		Substituent	ΔV_C		Substituent	ΔV_C	
C(Me)=CH_2	-0.5	$S^{>}$	$CH_2PO(C_6H_5)_2$	-2.5	$S^{>}$	NHOH	-5.1	$S^{>>}$
CH_2CH_2COOH	-0.3	$S^{>}$	CH_2NMe_2	-2.6	$S^{>>}$	N=$NNMe_2$	-5.6	$S^{>>}$
$Si(Me)(OSiMe_3)_2$	-0.7	$S^{>}$	$CH_2C(Me)_3$	-2.9	$S^{>>}$	OCH_2CH_3	-5.8	$S^{>>}$
$OPO(C_3H_7)_2$	-0.7	$S^{>}$	NHCOOEt	-3.0	$S^{>>}$	NHCONHEt	-5.8	$S^{>>}$
$Si(C_6H_5)Me_2$	-0.7	$S^{>}$	$CH_2CH(Me)_2$	-3.0	$S^{>>}$	$O(CH_2)_3CH_3$	-5.9	$S^{>>}$
$SiMe_3$	-0.9	$S^{>}$	$CH_2CH_2C_6H_5$	-3.1	$S^{>>}$	$OCH_2CH_2CH_3$	-6.0	$S^{>>}$
$CH(OH)C_6H_5$	-1.0	$S^{>}$	$CH_2CH_2CH_3$	-3.1	$S^{>>}$	$NHPO(C_3H7)_2$	-6.2	$S^{>>}$
C_6H_4-4Et	-1.1	$S^{>}$	$(CH_2)_3CH_3$	-3.2	$S^{>>}$	$O(CH_2)_4CH_3$	-6.2	$S^{>>}$
C_6H_4-4$CHMe_2$	-1.2	$S^{>}$	CH(Me)(Et)	-3.2	$S^{>>}$	$OCHMe_2$	-6.5	$S^{>>}$
C_6H_4-4Me	-1.2	$S^{>}$	$NHCOO(CH_2)_3CH_3$	-3.2	$S^{>>}$	N=$C(Me)NHC_6H_5$	-6.6	$S^{>>}$
C_6H_4-4CMe_3	-1.2	$S^{>}$	$(CH_2)_4CH_3$	-3.2	$S^{>>}$	NH_2	-9.0	$S^{>>>}$
N=CHC_6H_5	-1.3	$S^{>}$	$(CH_2)_6CH_3$	-3.2	$S^{>>}$	NHMe	-11.2	$S^{>>>}$
$GeMe_3$	-1.4	$S^{>}$	Me	-3.3	$S^{>>}$	$NHNH_2$	-11.2	$S^{>>>}$
NHCOMe	-1.4	$S^{>}$	isopropyl	-3.3	$S^{>>}$	NHEt	-11.4	$S^{>>>}$
$CH(C_6H_5)_2$	-1.4	$S^{>}$	$NHCOC_6H_4$-4OMe	-3.4	$S^{>>}$	$NH(CH_2)_3CH_3$	-11.6	$S^{>>>}$
SMe	-1.5	$S^{>}$	CH_2NH_2	-3.5	$S^{>>}$	$N(Et)_2$	-11.9	$S^{>>>}$
NMeCOMe	-1.5	$S^{>}$	$NHCONH_2$	-3.7	$S^{>>}$	$N(Me)_2$	-12.3	$S^{>>>}$
$NHCOC_6H_5$	-1.5	$S^{>}$	cyclopentyl	-3.7	$S^{>>}$	$N(C_3H_7)_2$	-12.9	$S^{>>>}$
$CH_2CH=CH_2$	-1.6	$S^{>}$	$CH_2C(OH)(Me)_2$	-3.7	$S^{>>}$	$CF_2OCF_2^-$	-57.6	$S^{>>>>}$
$Ge(Et)_3$	-1.6	$S^{>}$	N=CHC_6H_4-4-OMe	-3.8	$S^{>>}$	$OCH_2CH_2CH_2O^-$	-63.2	$S^{>>>>}$
$CH_2C_6H_5$	-1.8	$S^{>}$	cyclohexyl	-3.8	$S^{>>}$	$OCH_2CH_2O^-$	-66.8	$S^{>>>>}$
$NHCOCH(Me)_2$	-1.8	$S^{>}$	CH_2OH	-3.8	$S^{>>}$	SO_3^-	-67.2	$S^{>>>>}$
NHCSNHEt	-1.8	$S^{>}$	$C(Me)_3$	-3.9	$S^{>>}$	PO_3H^-	-70.4	$S^{>>>>}$
$P(N(Me)_2)_2$	-1.9	$S^{>}$	cyclobutyl	-3.9	$S^{>>}$	SO_2^-	-73.2	$S^{>>>>}$

OH	-2.0	$S^{>}$	$C(Et)_3$	-4.0	$S^{>>}$	$CH_2CO_2^-$	-74.5	$S^{>>>>}$
C_6H_4-4OMe	-2.0	$S^{>}$	Et	-4.0	$S^{>>}$	CO_2^-	-77.5	$S^{>>>>}$
$CH_2PO(OEt)_2$	-2.0	$S^{>}$	$C(Et)(Me)_2$	-4.2	$S^{>>}$	OPO_3H^-	-77.8	$S^{>>>>}$
SEt	-2.2	$S^{>}$	$OSiMe_3$	-4.2	$S^{>>}$	$CH_2CH_2CH_2^-$	-83.2	$S^{>>>>}$
$N(C_6H_5)_2$	-2.3	$S^{>}$	$OCH_2CH=CH_2$	-4.8	$S^{>>}$	NNO_2^-	-83.7	$S^{>>>>}$
NHCOOMe	-2.4	$S^{>}$	NHC_6H_5	-4.8	$S^{>>}$	$B(OH)_3^-$	-88.9	$S^{>>>>}$
cyclopropyl	-2.4	$S^{>}$	$CH_2OSi(CH_3)_3$	-4.8	$S^{>>}$	S^-	-95.8	$S^{>>>>}$
$(CH_2)_4NMe_2$	-2.4	$S^{>}$	$CH_2Si(Me)_3$	-4.9	$S^{>>}$	OCH_2O^-	-102.6	$S^{>>>>}$
$CH_2CH_2Si(Me)_3$	-2.4	$S^{>}$	OMe	-5.0	$S^{>>}$	O^-	-113.4	$S^{>>>>}$

The observed big jump in the magnitude of the values cannot be accounted by the present set of substituents. It is very likely that a neutral substituent showing ΔV_C value close to an anionic substituent may not exist in nature. So the $S^{>>>>}$ classification could be exclusively used for anions. Figure 2.4 shows the correlation between Hammett constant (σ_p) and ΔV_C for the neutral substituents. The limitation in using Hammett substituent constants uniformly for a huge database of substituents is evident from the figure. The significant scattering shown by some of the groups suggests major disagreement with Hammett constants. This is not surprising because the universality of Hammett constants is not tested rigorously for a large variety of functional groups as organic chemistry is centered mainly on a limited set of functional groups.

In fact, the strong linear trend in the correlation between ΔV_C and σ_p is evident in the case of representative set of substituents frequently encountered in correlation studies (the points marked in red squares in Figure 2.4 has a correlation coefficient 0.9821). The substituents and the corresponding σ_p values are given in Table 2.3. In the review by Hansch and Leo, the complications in deriving substituent constants for a large database are described in depth. In some cases, parameters such as Swain-Lupton constant[54], Taft-Topsom value[55] *etc*. have to be considered for a proper description of the substituent effect.

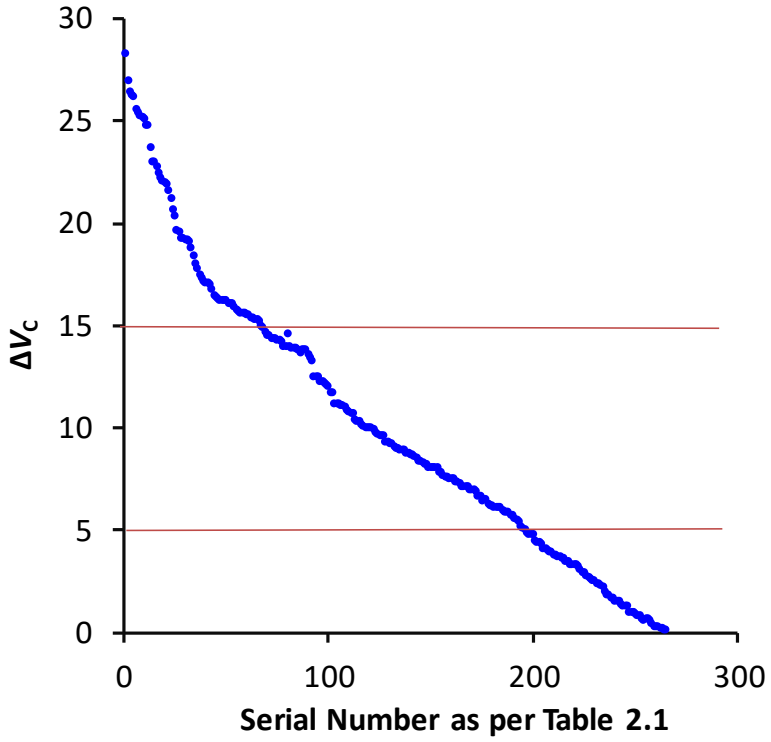

Figure 2.2 Classification of neutral substituents with positive ΔV_C values (kcal/mol).

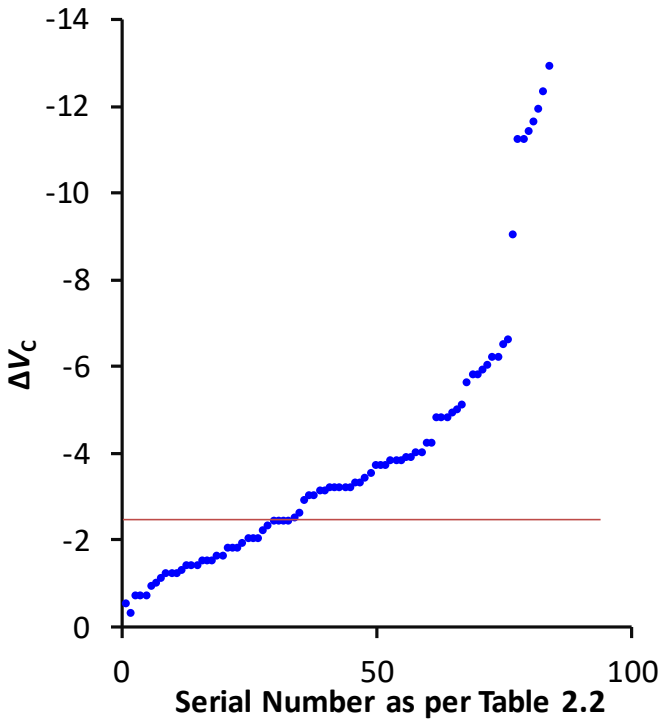

Figure 2.3 Classification of neutral substituents with negative ΔV_C values (kcal/mol).

It is noticeable that compared to the theoretical MESP data, the experimental data for the Hammett constant is not uniform as the former is derived from isolated gas phase molecule while the latter approach may vary case by case. Thus, the MESP data reflects on the inherent nature of substituent effect on the unperturbed gas phase molecule. Even though a lot of studies have been carried out by various research groups on substituent effects and aromaticity of several cyclic π electron systems, the results were summarized by twenty-five substituents only. The relevance of the present study is that a large number of substituents are taken to explore their effect and a brand new classification of all of them is possible using a single theoretically computed parameter. The MESP based study is effective as it gives a foremost idea about a large number of substituted aromatic systems.

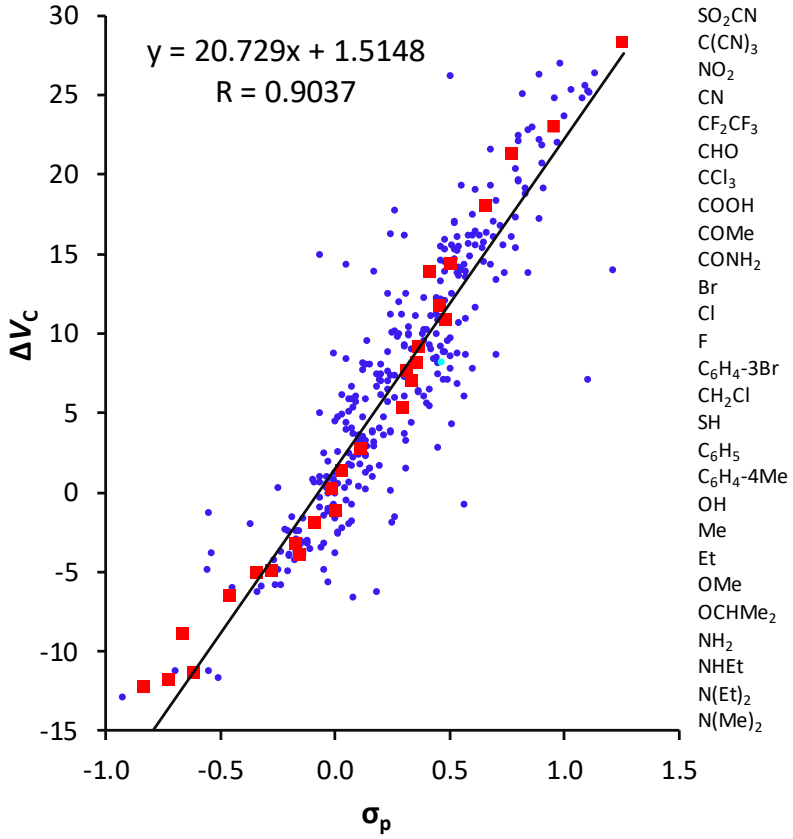

Figure 2.4 Correlation between σ_p and ΔV_C (kcal/mol). The red points are for the substituents listed in the right side.

Table 2.3 Substituents with the corresponding σ_P values

substituent	σ_p	substituent	σ_p	substituent	σ_p
SO_2CN	1.26	$CHCl_2$	0.32	$NHCOCH_2Cl$	-0.03
$C(CN)=C(CN)_2$	0.98	$COOC_6H_5$	0.44	$P(isopropyl)_2$	0.06
$SO_2C(CF_3)_3$	1.13	N=C=S	0.38	CH_2F	0.11
N(O)=NCN	0.89	OCF_2CHFCl	0.28	$P(C_6H_5)_2$	0.19
SeO_2CF_3	0.50	$CHBr_2$	0.32	$CH_2OC_6H_5$	0.07
$SO_2CF_2CF_2CF_3$	1.09	C_6F_5	0.27	OCOMe	0.31
N=NCN	1.03	COMe	0.50	SH	0.15
$SO_2CF(CF_3)_2$	1.10	$SiMeCl_2$	0.39	$P(CMe_3)_2$	0.15
SO_2Cl	1.11	SOMe	0.49	OCH_2F	0.02
$C(NO_2)_3$	0.82	CH_2SCN	0.14	$P(Et)_2$	0.13
SO_2CF_3	0.96	$CONHC_6H_5$	0.41	NHCHO	0.00
$SO2CF_2CF_3$	1.08	$C(OH)(CF_3)_2$	0.30	C=CMe	0.03
$CH=NSO_2CF_3$	1.00	$P(S)Et_2$	0.46	$NHCSNH_2$	0.16
SO_2CHF_2	0.86	$CSNH_2$	0.30	$CH=CH_2$	-0.04
$C(CN)_3$	0.96	$SCHF_2$	0.37	CH(OH)Me	-0.07
$CH=C(CN)_2$	0.84	$CH=NC_6H_5$	0.42	$Si(Me)_2OMe$	-0.02
SF_3	0.80	$N(COMe)_2$	0.33	OC_6H_4-4F	-0.10
POF_2	0.89	COEt	0.48	$Si(OEt)_3$	-0.01
PF_4	0.80	$COCHMe_2$	0.47	PMe_2	0.06
GeF_3	0.97	$SiMeF_2$	0.23	$Si(NMe_2)_3$	-0.04
$P(CN)_2$	0.90	$PO(OMe)_2$	0.53	$CH=CHC_6H_5$	-0.07
SF_5	0.68	CH=CHCOMe	-0.01	$OCH=CH_2$	-0.09
NO_2	0.78	$PO(OC_4H_9)_2$	0.57	CH_2OMe	0.01
$P(O)Cl_2$	0.90	$SCH=NSO_2C_6H_4$-4-Me	0.70	$Si(C_6H_5)_3$	0.10
$COCF_2CF_2CF_3$	0.79	$PO(OPr)_2$	0.50	$SiH(Me)_2$	0.04
$P(S)Cl_2$	0.80	SOC_6H_5	0.44	$C(OMe)_3$	-0.04
$COCF_3$	0.80	$CH=CHCOC_6H_5$	0.05	$CH_2CH(OH)Me$	-0.25
$CH=CHSO_2CF_3$	0.55	COC_6H_5	0.43	$SiMe(C_6H_5)_2$	0.13

$N{=}NCF_3$	0.68	OCF_3	0.35	C_6H_5	-0.01
NO	0.91	$NHCOCF_3$	0.12	$P(N(Pr)_2C_6H_4\text{-}3F$	0.24
$N(SO_2CF_3)_2$	0.83	COOMe	0.45	$Si(Me)_2OSiMe_3$	-0.01
COCl	0.61	$CONH_2$	0.36	OC_6H_5	-0.03
SOF	0.83	$PS(C_6H_5)_2$	0.47	H	0.00
COF	0.70	$C_6H_4\text{-}3NO_2$	0.20	$C(Me){=}CH_2$	0.05
CN	0.66	CH=CHCHO	0.13	CH_2CH_2COOH	-0.07
$CH{=}CHNO_2$	0.26	CH_2SCF_3	0.15	$Si(Me)(OSiMe_3)_2$	-0.01
SO_2NH_2	0.60	$PO(OEt)_2$	0.60	$OPO(C_3H_7)_2$	0.56
$GeCl_3$	0.79	$P(O)Me_2$	0.50	$Si(C_6H_5)Me_2$	0.07
$P(CF_3)_2$	0.89	$B(OH)_2$	0.12	$SiMe_3$	-0.07
$SOCF_3$	0.69	$COC(Me)_3$	0.32	$CH(OH)C_6H_5$	-0.03
SCN	0.52	Br	0.23	$C_6H_4\text{-}4Et$	-0.02
$CH(CN)_2$	0.52	$OCHF_2$	0.18	$C_6H_4\text{-}4CHMe_2$	0.01
SO_2Me	0.72	COOEt	0.45	$C_6H_4\text{-}4Me$	-0.03
$C(Me)(NO_2)_2$	0.61	$SCH{=}CH_2$	0.20	$C_6H_4\text{-}4CMe_3$	0.01
SeCN	0.66	$OCHCl_2$	0.26	$N{=}CHC_6H_5$	-0.55
$SC_6H_4\text{-}4NO_2$	0.24	C_6Cl_5	0.24	$GeMe_3$	0.00
$NO{=}NCONH_2$	0.63	$PS(C_6H_5)C_6H_4\text{-}4Me$	0.30	NHCOMe	0.00
$SOC_6H_4\text{-}4NO_2$	0.60	$PO(Et)_2$	0.47	$CH(C_6H_5)_2$	-0.05
$SOCHF_2$	0.58	$PO(C_3H_7)_2$	1.10	SMe	0.00
$C_6H_2\text{-}2,4,6(NO_2)_3$	0.30	N=C=O	0.19	NMeCOMe	0.26
SiF_3	0.69	$PO(C_4H_9)_2$	0.49	$NHCOC_6H_5$	-0.19
cyclo-C_4F_7	0.53	Cl	0.23	$CH_2CH{=}CH_2$	-0.14
SO_2Et	0.77	$C(NO_2)Me_2$	0.20	$Ge(Et)_3$	0.00
SCl	0.48	CSNHMe	0.34	$CH_2C_6H_5$	-0.09
$SO_2NHC_6H_5$	0.65	$PO(C_6H_5)_2$	0.53	$NHCOCH(Me)_2$	-0.10
$SC(CF_3)_3$	0.58	CH_2CONH_2	0.07	NHCSNHEt	0.07
$GeBr_3$	0.73	CH_2CN	0.18	$P(N(Me)_2)_2$	0.25
$C{=}CCF_3$	0.51	CONHMe	0.36	OH	-0.37

PCl_2	0.61	$PS(C_6H_4\text{-}4Me)_2$	0.23	$C_6H_4\text{-}4OMe$	-0.08
$SeC(CF_3)_3$	0.54	$PO(isopropyl)_2$	0.41	$CH_2PO(OEt)_2$	0.06
$SCOCF_3$	0.46	OSO_2Me	0.36	SEt	0.03
$C(Et)(NO_2)_2$	0.64	$NHSO_2Me$	0.03	$N(C_6H_5)_2$	-0.22
$NO{=}NSO_2C_6H_5$	0.79	SCH_2F	0.20	NHCOOMe	-0.17
$(CF_2)_3CF_3$	0.52	$SN(Me)_2$	0.09	cyclopropyl	-0.21
$CF_2CF_2CF_3$	0.48	$PO(C_6H_5)C_6H_4\text{-}4Me$	0.30	$(CH_2)_4NMe_2$	-0.16
$N(CF_3)_2$	0.53	$N{=}NC_6H_5$	0.39	$CH_2CH_2Si(Me)_3$	-0.17
SOOH	-0.07	$P(Cl)NMe_2$	0.56	$CH_2PO(C_6H_5)_2$	0.01
PF_2	0.59	SeCH=CHCl	0.26	CH_2NMe_2	0.01
CF_2CF_3	0.52	$N{=}CCl_2$	0.13	$CH_2C(Me)_3$	-0.17
SO_2NMe_2	0.65	SC_6H_5	0.07	NHCOOEt	-0.15
$SCF_2CF_2CF_3$	0.48	NHCN	0.06	$CH_2CH(Me)_2$	-0.12
$CH{=}CHCOC_6H_4\text{-}4NO_2$	0.05	CH_2CF_3	0.09	$CH_2CH_2C_6H_5$	-0.12
$SiCl_3$	0.56	C=CH	0.23	$CH_2CH_2CH_3$	-0.13
$SO_2C_6H_5$	0.68	$PO(N(Me)_2)_2$	0.40	$(CH_2)_3CH_3$	-0.16
NC	0.49	$PO(CMe_3)_2$	0.41	CH(Me)(Et)	-0.12
$SCF(CF_3)_2$	0.51	N_3	0.08	$NHCO_2(CH_2)_3CH_3$	-0.05
OCN	0.54	$PO(C_6H_4\text{-}4Me)_2$	0.30	$(CH_2)_4CH_3$	-0.15
$C(CF_3)_3$	0.55	F	0.06	$(CH_2)_6CH_3$	-0.16
OSO_2CF_3	1.21	$SeCH_2CH{=}CH_2$	-0.07	Me	-0.17
$CF{=}CFCF_3$	0.46	CH=CHCOOEt	0.03	isopropyl	-0.15
SSO_2Me	0.54	$SiClMe_2$	0.21	$NHCOC_6H_4\text{-}4OMe$	-0.06
$C(Me)(CN)_2$	0.57	$NHSO_2C_6H_5$	0.01	CH_2NH_2	-0.11
SCF_2CF_3	0.48	$SCH_2CH{=}CH_2$	0.12	$NHCONH_2$	-0.24
CH=CHCN	0.17	SeMe	0.00	cyclopentyl	-0.14
$N{=}NPO(OEt)_2$	0.74	$OSO_2C_6H_5$	0.33	$CH_2C(OH)(Me)_2$	-0.17
CF_3	0.54	CH_2OCOMe	0.05	$N{=}CHC_6H_4\text{-}4\text{-}OMe$	-0.54
$CF(CF_3)_2$	0.53	$CH{=}NNHCOC_6H_5$	0.51	cyclohexyl	-0.15
CHO	0.42	SCH $=CH_2$	0.19	CH_2OH	0.00

$S(O)=NHCF_3$	0.84	$SCHMe_2$	0.07	$C(Me)_3$	-0.20
$SiBr_3$	0.57	PH_2	0.05	cyclobutyl	-0.14
ONO_2	0.70	$N(Me)SO_2Me$	0.24	$C(Et)_3$	-0.20
$CClF_2$	0.46	$C=CC_6H_5$	0.16	Et	-0.15
$CH_2SO_2CF_3$	0.31	$CH=NNHCONHNH_2$	0.16	$C(Et)(Me)_2$	-0.18
$CH=NCOC_6H_5$	0.51	SCH=CHCl	0.24	$OSiMe_3$	-0.27
$N=C(CF_3)_2$	0.23	CH=NOMe	0.30	$OCH_2CH=CH_2$	-0.25
$CF_2CF_2C_6H_4$-4F	0.39	C_6H_4-3Br	0.08	NHC_6H_5	-0.56
SCOMe	0.44	$SeCH=CH_2$	0.21	$CH_2OSi(CH_3)_3$	-0.05
$OCOCF_3$	0.46	C_6H_4-3Cl	0.10	$CH_2Si(Me)_3$	-0.21
BF_2	0.48	SiH_3	0.10	OMe	-0.27
OCF_2CF_3	0.28	C_6H_4-4Br	0.12	NHOH	-0.34
CCl_3	0.46	$N=NC_6H_3$-5Me,2-OH	0.31	$N=NNMe_2$	-0.03
$N(Me)NO_2$	0.61	C_6H_4-4Cl	0.12	OCH_2CH_3	-0.24
CBr_3	0.29	S(SMe)	0.13	NHCONHEt	-0.26
$N(Me)SO_2CF_3$	0.44	C_6H_4-3F	0.10	$O(CH_2)_3CH_3$	-0.32
CH_2SOCF_3	0.24	S(OMe)	0.17	$OCH_2CH_2CH_3$	-0.45
$PO(OH)_2$	0.42	NHCSMe	0.12	$NHPO(C_3H_7)_2$	0.18
$OCCl_3$	0.35	$SiFMe_2$	0.17	$O(CH_2)_4CH_3$	-0.34
$NHNO_2$	0.57	CH_2Br	0.14	$OCHMe_2$	-0.45
COOH	0.45	$OS(=O)CH_3$	0.45	$N=C(Me)NHC_6H_5$	0.08
$N(SO_2Me)_2$	0.49	CH_2Cl	0.12	NH_2	-0.66
SCF_2CHF_2	0.47	GeH_3	0.01	NHMe	-0.70
S(O)OMe	0.54	$CH_2NHCOMe$	-0.05	$NHNH_2$	-0.55
CHF_2	0.32	C_6H_4-4F	0.06	NHEt	-0.61
$NHSO_2CF_3$	0.39	$SiMe(OMe)_2$	0.10	$NH(CH_2)_3CH_3$	-0.51
$CH=NNHCSNH_2$	0.40	$Si(OMe)_3$	0.13	$N(Et)_2$	-0.72
C_6H_4-4NO_2	0.26	$OCOC_6H_5$	0.13	$N(Me)_2$	-0.83
OCF_2CHF_2	0.25	OCH_2Cl	0.08	$N(C_3H_7)_2$	-0.93

2.4.2 Transferability of Substituent Effect

The transferability property of substituent effect is firmly established in chemistry from the numerous successful applications of Hammett constants in structure activity correlation studies of a large variety of molecular systems. This means that the substituent effect quantified using a benzene derivative can be directly used on another conjugated molecular system to describe its chemical reactivity. In order to prove this concept of transferability, the data presented in Tables 2.1 and 2.2 derived from benzene derivatives have to be directly used on other molecular systems to describe their substituent effect. We do this by analyzing the MESP of four different systems, *viz*. pyridine, 1, 3-butadiene, 1, 3-butadiyne, and pyrene. The molecules represent a heterocyclic aromatic molecule, an open chain π-conjugated double bonded system, an open chain π -conjugated triple bonded system and a polycyclic aromatic hydrocarbon respectively (Figure 2.5).

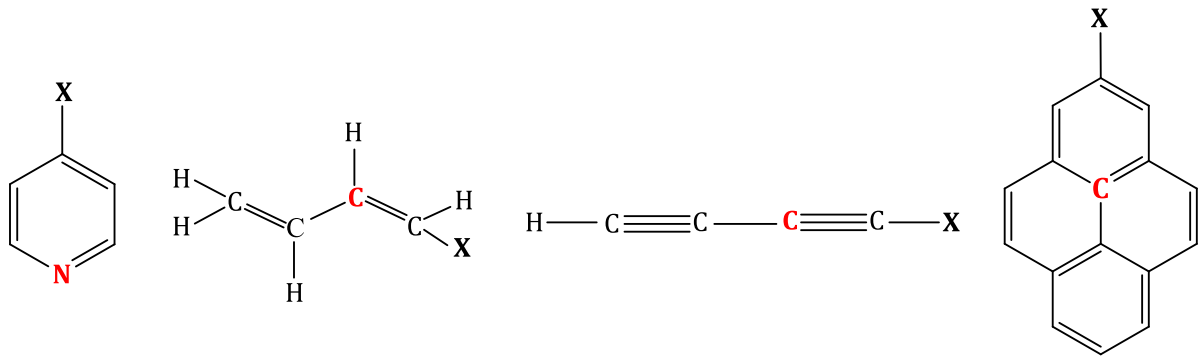

(a) (b) (c) (d)

Figure 2.5 Representative structures (a) pyridine, (b) 1, 3-butadiene, (c) 1, 3-butadiyne and (d) pyrene for studying transferability. Analysis of MESP is made on the atom colored in red.

For pyridine, MESP value at the N atom (V_N) is monitored while for pyrene, MESP at the carbon *para* to the substituent is analyzed. In the case of 1, 3-butadiene and 1, 3-butadiyne, MESP at the carbon atom nearest to the substituted carbon is investigated (Figure 2.5). ΔV_C and ΔV_N values are taken for each case with reference to the

corresponding unsubstituted systems (Table 2.4). The ΔV_C of benzene is found to be strongly correlated with ΔV_N of pyridine, ΔV_C of pyrene, ΔV_C of butadiene and ΔV_C of butadiyne, with correlation coefficients 0.996, 0.987, 0.990, 0.976, respectively.

Table 2.4 MESP ΔV_C values (ΔV_N for pyridine) for various systems (kcal/mol)

substituent	nature	benzene	pyrene	pyridine	butadiene	butadiyne
SO_2CN	$S^{<<<}$	28.3	20.5	26.7	40.4	42.6
$C(CN)_3$	$S^{<<<}$	23.0	16.7	22.5	32.2	33.5
NO_2	$S^{<<<}$	21.2	14.5	19.9	31.8	35.2
CN	$S^{<<<}$	18.0	13.0	16.9	25.0	29.2
$N(CF_3)_2$	$S^{<<<}$	15.2	10.9	13.0	19.4	12.5
CHO	$S^{<<}$	13.8	9.6	11.8	17.6	17.5
$NHNO_2$	$S^{<<}$	11.0	8.3	7.8	13.4	13.4
COMe	$S^{<<}$	9.7	6.4	7.9	13.1	11.6
OCF_3	$S^{<<}$	8.3	8.5	7.5	11.3	10.0
Cl	$S^{<<}$	7.0	5.3	6.5	8.7	4.9
NHCN	$S^{<<}$	5.9	4.9	7.1	8.0	9.4
SiH_3	$S^{<}$	3.5	2.1	2.2	5.9	-1.0
CH_2F	$S^{<}$	1.8	1.2	1.4	1.8	4.0
$CH=CH_2$	$S^{<}$	1.0	0.4	-1.1	0.0	-4.2
C_6H_5	$S^{<}$	0.2	-0.3	-1.8	-0.8	-6.1
H	S^{0}	0.0	0.0	0.0	0.0	0.0
$SiMe_3$	$S^{>}$	-0.9	-1.3	-2.5	-0.3	-9.3
SMe	$S^{>}$	-1.5	-1.0	-3.1	-1.9	-4.5
OH	$S^{>}$	-2.0	-1.3	-3.4	-9.2	-5.5
CH_2NMe_2	$S^{>>}$	-2.6	-2.3	-4.0	-3.6	-8.6
CH_3	$S^{>>}$	-3.3	-2.5	-3.7	-6.3	-11.2
CH_2OH	$S^{>>}$	-3.8	2.4	-4.4	0.4	-1.3
OCH_3	$S^{>>}$	-5.0	-3.1	-6.1	-6.3	-9.0
NH_2	$S^{>>>}$	-9.0	-5.9	-11.1	-15.3	-13.8
$N(C_3H_7)_2$	$S^{>>>}$	-12.9	-9.3	-16.0	-17.0	-19.5

Slight deviations are observed for some weak category substituents, which are at the brink of electron donating/withdrawing ones. These correlation plots (Figure 2.6) strongly suggest that the ΔV_C parameters derived using benzene derivatives can be applied to other conjugated systems. Thus the transferability property of substituent effect is clearly conveyed and also the proposed classification is more general and applicable to systems such as olefins, alkynes, condensed aromatics, and heterocyclic aromatics.

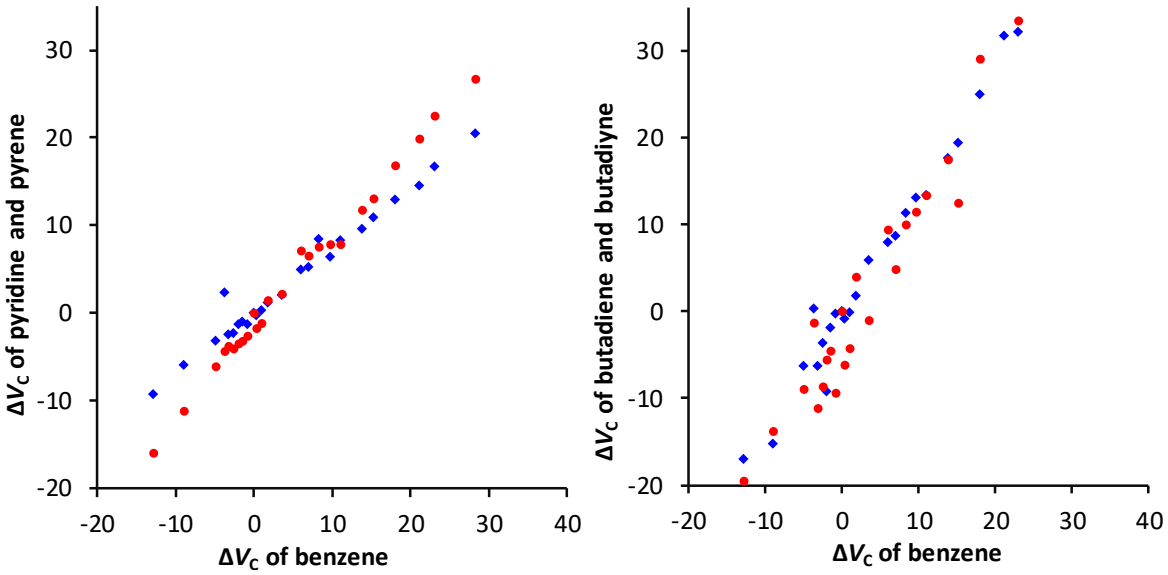

(a) (b)

Figure 2.6 Correlation between ΔV_C values of benzene against those of (a) pyridine (red dots) and pyrene (blue diamonds) and (b) 1, 3-butadiene (red dots) and 1, 3-butadiyne (blue diamonds). All values in kcal/mol.

2.4.3 Additivity of Substituent Effect

Substituent effect is said to be additive if the total effect of all the substituents in a molecular system can be reproduced almost entirely from the contributions of corresponding monosubstituted derivatives. Earlier studies from Suresh and Sayyed have shown that the additive nature of substituent effect is almost 86% in substituted benzoic acids.[56] Herein we consider multi substituted derivatives of five different

conjugated molecular systems, *viz*. benzene, pyridine, 1, 3-butadiene, 1, 3-butadiyne and pyrene (Figure 2.7) for assessing the additivity effect using the MESP parameters.

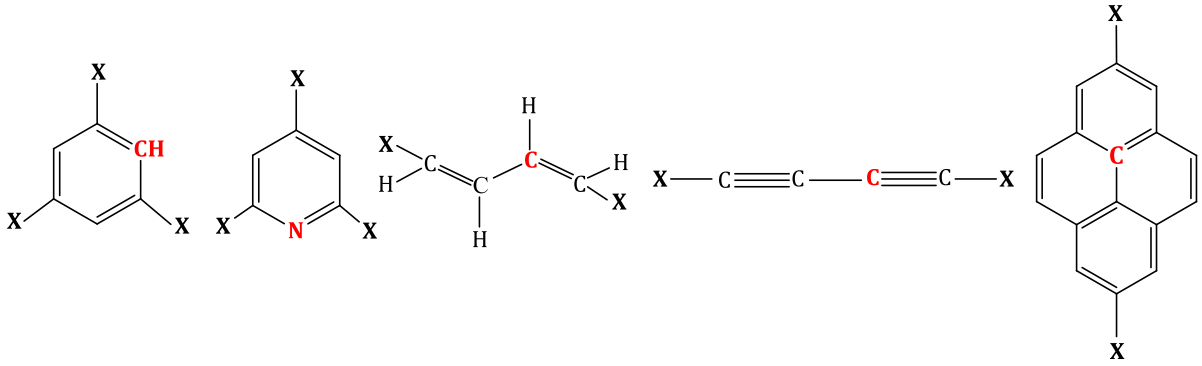

(a) (b) (c) (d) (e)

Figure 2.7 Representative structures (a) benzene, (b) pyridine, (c) 1, 3-butadiene, (d) 1, 3-butadiyne and (e) pyrene for studying additivity. Analysis of MESP is made on the atom colored in red.

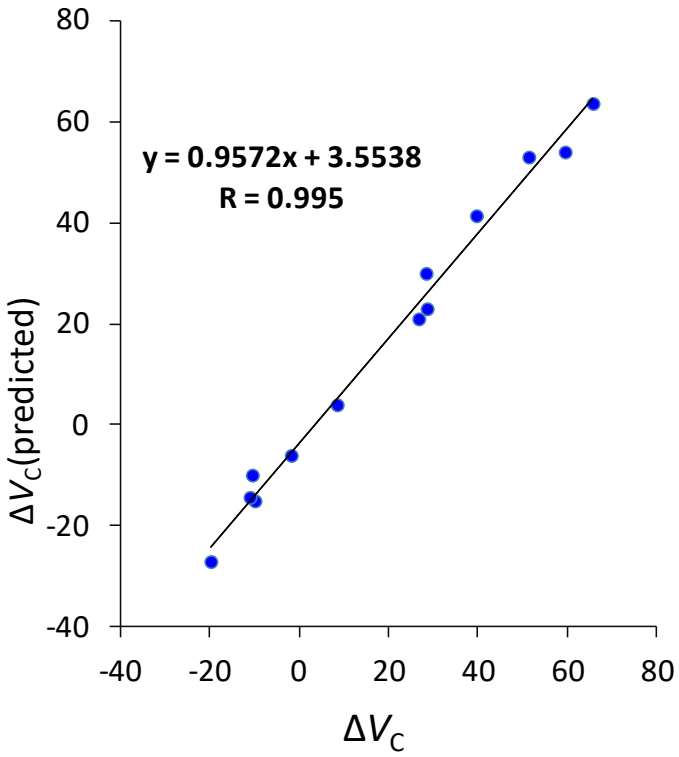

Figure 2.8 Correlation between calculated and predicted ΔV_C values for trisubstituted benzenes. Values in kcal/mol.

Table 2.5 Calculated and predicted ΔV_C (benzene) and ΔV_N (pyridine) values for tri substituted systems (kcal/mol).

Substituent		benzene		pyridine	
Combination	Nature	ΔV_c(pred)	ΔV_c	ΔV_N (pred)	ΔV_N
NO_2, NO_2, NO_2	$S^{<<<}$, $S^{<<<}$, $S^{<<<}$	63.6	65.7	59.7	63.7
CN, CN, CN	$S^{<<<}$, $S^{<<<}$, $S^{<<<}$	54.0	59.5	50.6	57.5
CHO, CHO, CHO	$S^{<<}$, $S^{<<}$, $S^{<<}$	41.4	39.6	35.5	35.8
Cl, Cl, Cl	$S^{<<}$, $S^{<<}$, $S^{<<}$	21.0	26.7	19.6	25.1
OH, OH, OH	$S^{>}$, $S^{>}$, $S^{>}$	-6.0	-1.9	-10.3	-4.6
Me, Me, Me	$S^{>>}$, $S^{>>}$, $S^{>>}$	-9.9	-10.6	-11.2	-12.3
OMe, OMe, OMe	$S^{>>}$, $S^{>>}$, $S^{>>}$	-15.0	-10.0	-18.3	-13.4
NH_2, NH_2, NH_2	$S^{>>>}$, $S^{>>>}$, $S^{>>>}$	-27.0	-19.9	-33.4	-25.5
NO_2, CN, CHO	$S^{<<<}$, $S^{<<<}$, $S^{<<}$	53.0	51.3	48.6	53.9
NO_2, CHO, OMe	$S^{<<<}$, $S^{<<}$, $S^{>>}$	30.0	28.3	25.6	28.4
CN, OMe, NH_2	$S^{<<<}$, $S^{>>}$, $S^{>>>}$	4.0	8.4	-0.4	7.0
CN, Cl, OH	$S^{<<<}$, $S^{<<}$, $S^{>}$	23.0	28.6	20.0	28.3
OH, Me, NH_2	$S^{>}$, $S^{>>}$, $S^{>>>}$	-14.3	-11.1	-18.3	-9.5

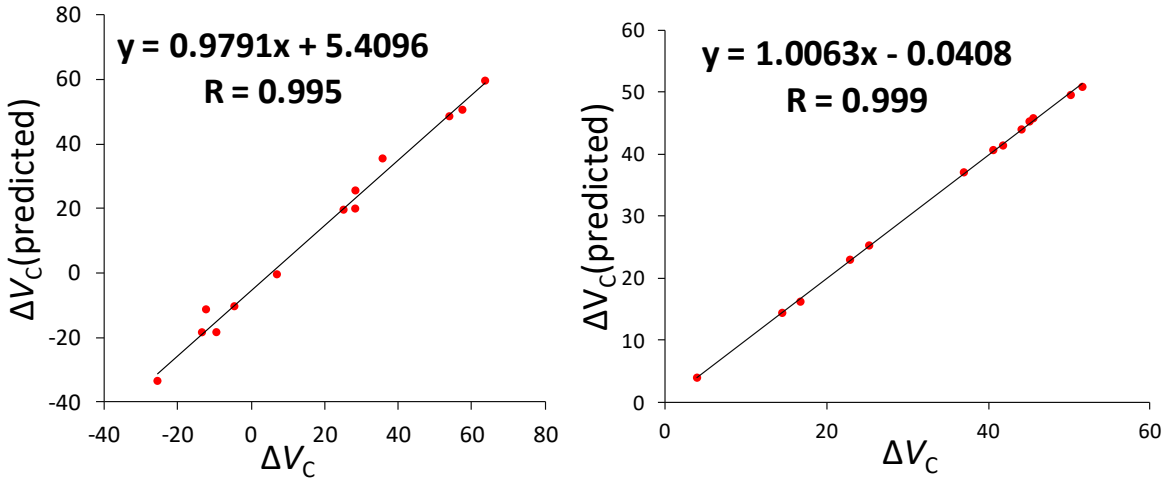

(a) (b)

Figure 2.9 Correlation between calculated potential and predicted potential for additivity in (a) pyridine (b) pyrene

Table 2.6 Calculated and predicted ΔV_C values for disubstituted systems (kcal/mol).

Substituent		pyrene		1, 3-butadiene		1, 3-butadiyne	
Combination	Nature	ΔV_c (pred)	ΔV_c	ΔV_c (pred)	ΔV_c	ΔV_c (pred)	ΔV_c
NO_2,NO_2	$S^{<<<}$, $S^{<<<}$	50.8	51.7	58.6	62.4	61.7	65.2
CN,CN	$S^{<<<}$, $S^{<<<}$	41.4	41.8	44.2	46.1	47.9	49.7
CHO,CHO	$S^{<<}$, $S^{<<}$	16.2	16.7	20.2	18	18.1	19.5
Cl, Cl	$S^{<<}$, $S^{<<}$	44.0	44.1	40.2	40.7	27.6	27.5
OH,OH	$S^{>}$, $S^{>}$	40.6	40.6	25.6	25.6	20.7	20.3
Me, Me	$S^{>>}$, $S^{>>}$	3.9	3.9	-5.2	-5.6	-16.4	-17.2
OMe, OMe	$S^{>>}$, $S^{>>}$	37.0	37.0	28.6	27.6	13.5	11.9
NH_2,NH_2	$S^{>>>}$, $S^{>>>}$	23.0	22.9	9.2	7.8	-5.5	-6.0
NO_2,CN	$S^{<<<}$, $S^{<<<}$	49.5	50.2	54.3	63.5	58.6	62.6
Cl, OH	$S^{<<}$, $S^{>}$	45.2	45.1	26.8	33.4	18.1	17.6
Me,NH_2	$S^{>>}$, $S^{>>>}$	25.3	25.2	13.9	21.2	-22.5	-23.9
CN,Me	$S^{<<<}$, $S^{>>}$	14.4	14.5	14.8	21.2	16.5	17.0
CHO, OMe	$S^{<<}$, $S^{>>}$	45.8	45.6	51.0	52.1	-7.9	-8.0

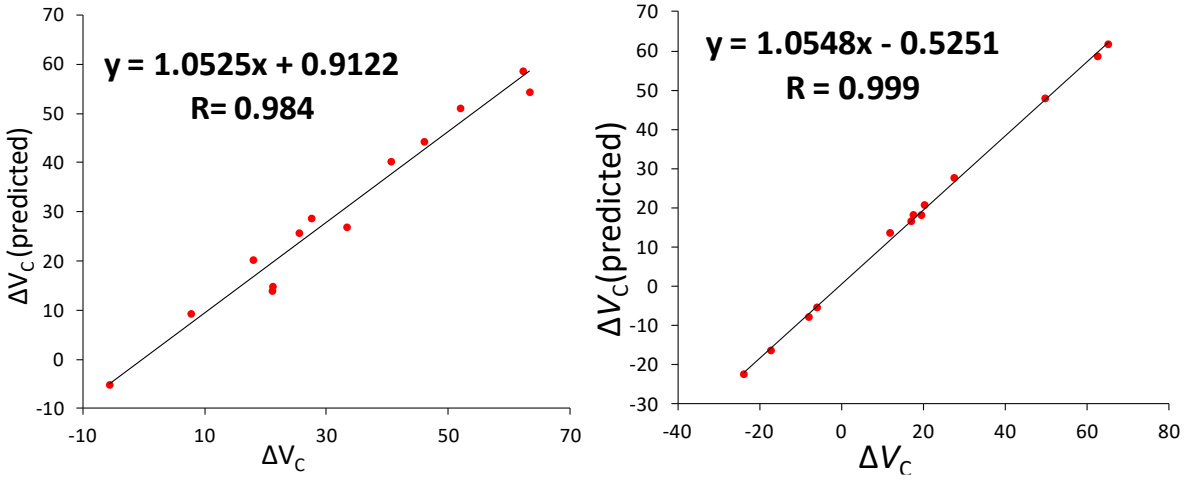

(a) (b)

Figure 2.10 Correlation between calculated potential and predicted potential for additivity in (a) 1, 3-butadiene and (b) 1, 3-butadiyne.

The selected substituents and their classification from Tables 2.1 and 2.2 are NO_2 ($S^{<<<}$), CN ($S^{<<<}$), CHO ($S^{<<}$), Cl ($S^{<<}$), OH ($S^{>}$), Me ($S^{>}$), OMe ($S^{>>}$), and NH_2 ($S^{>>>}$). Using these substituents, various multi substitutions have been considered on each molecular system. Good correlations are obtained for calculated ΔV_C and predicted ΔV_C. The combinations of substituents, the observed MESP and predicted MESP values obtained from monosubstituted ones are listed in Tables 2.5 and 2.6. A representative correlation plot for trisubstituted benzenes is depicted in Figure 2.8. The correlation plots for other systems (pyridine, pyrene, 1, 3-butadiene and 1, 3-butadiyne) are given in Figures 2.9 and 2.10. The strong linear correlation plots obtained in all the cases confirm the additive nature of substituent effect for these molecular systems.

2.5 Conclusions

MESP analysis has been widely used to characterize electron rich and electron deficient regions of molecular systems, to derive critical features useful for understanding molecular reactivity, to describe a number of chemical phenomena and even to build up new concepts like σ-hole interactions. Previous studies have shown that substituent effect is extremely reflected in MESP based parameters while the present study dealing with a large set of substituents popular in organic chemistry confirms that MESP based analysis has the potential to quantify and classify substituent effects in a systematic and comprehensive way. The ΔV_C parameter emerges as a convenient and powerful theoretical tool to assess the electron withdrawing/donating character of a substituent. The immediate outcome of this is a broad classification of substituents into very strong/strong/medium/weak electron donating/withdrawing categories. The variations observed in ΔV_C can be directly associated with the substituent effect as its derivation uniformly applicable to all the systems and based on standard gas phase DFT calculations. The accuracy of the results solely depends on the accuracy of the methodology used in deriving the wave function or the electron density distribution. Thus the theoretical quantity is more advantageous to study the inherent electron donating/withdrawing nature of a substituent than the experimentally derived

Hammett constant as the latter is not derived using a single set of reaction conditions or evaluated using the same kind of experimental techniques for all the substituents.

The very strong electron withdrawing substituents in $S^{<<<<}$ category is the cationic substituents while those in $S^{>>>>}$ category is the very strongly donating anionic substituents. The data presented in this work clearly suggest that compared to electron withdrawing neutral substituents, the number of electron donating substituents are very less in organic chemistry. In fact, the search for the most electron donating neutral substituent stops at N, N-dilakyl amino group. It is thus apparent that the development of new type of neutral substituents more donating than amino group is necessary for further advancement in improving molecular design strategies. Among the wide variety of electron withdrawing substituents, SO_2CN emerged as the most electron withdrawing in the $S^{<<<}$ category. There are at least 22 substituents more withdrawing than NO_2, one of the strongest electron withdrawing substituents frequently encountered in organic chemistry.

Even though monosubstituted benzenes are the key compounds for the classification criteria, the transferability is verified for other organic systems like condensed aromatics, heterocyclic aromatics and open chain conjugated systems. The uniformity of the classification in various systems is a significant aspect which would be helpful in the design of new systems as we can clearly predict the nature of miscellaneous substituents commonly used in organic synthesis. Even the substituent effect of a newly synthesized system can be easily predicted from MESP parameter. The additive effect of substituents on various organic systems is also proven from studies on multi substituted structures. In summary, the data presented in this work is supportive to assign electron richness and electron deficiency for any conjugated organic molecular system and can be viewed as a valuable tool for target oriented molecular design strategies for highly tuned electronic properties.

2.6 References

1. C. Hansch, A. Leo and R. W. Taft, *Chem. Rev.* **1991**, *91*, 165-195.

2. L. P. Hammett, *Chem. Rev.* **1935**, *17*, 125-136.
3. I. Fernandez and G. Frenking, *J. Org. Chem.* **2006**, *71*, 2251-2256.
4. T. M. Krygowski, M. A. Dobrowolski, K. Zborowski and M. K. Cyranski, *J. Phys. Org. Chem.* **2006**, *19*, 889-895.
5. O. Exner, P. Fiedler and M. Budesınsky, *J. Org. Chem.* **1999**, *64*, 3513-3518.
6. S. Böhm and O. Exner, *New J. Chem.* **2005**, *29*, 336-342.
7. T. M. Krygowski, B. T. Stepien and M. K. Cyrański, *Int. J. Mol. Sci.* **2005**, *6*, 45-51.
8. M. J. Ajitha and C. H. Suresh, *J. Org. Chem.* **2012**, *77*, 1087-1094.
9. H. H. Jaffe, *Chem. Rev.* **1953**, *53*, 191-261.
10. O. Exner and S. Böhm, *J. Org. Chem.* **2002**, *67*, 6320–6327.
11. M. Ludwig, S. Wold, O. Exner, E. Sletten, A. Z.-Q. Khan, J. Sandstrom and P. Krogsgaard-Larsen, *Acta Chem. Scand.* **1992**, *46*, 549-554.
12. S. Böhm and O. Exner, *J. Mol. Struc. Theochem.* **2002**, *578*, 103-109.
13. O. Exner, M. J. Cook and T. J. Howe, *J. Mol. Struc.* **1990**, *240*, 11-18.
14. R. Fruttero, D. Boschi, E. Fornatto, A. Serafino, A. Gasco and O. Exner, *J. Chem. Res.* **1998**, *495*, 2545-2562.
15. K. Waisser and O. Exner, *J. Phys. Org. Chem.* **2000**, *13*, 127-132.
16. K. Waisser, K. Palat and O. Exner, *Collect. Czech. Chem. Commun.* **1999**, *64*, 1295-1306.
17. O. Exner, M. Ingr and P. Carsky, *J. Mol. Struc. Theochem.* **1997**, *397*, 231-238.
18. S. Böhm and O. Exner, *New J. Chem.* **2001**, *25*, 250-254.
19. S. Böhm and O. Exner, *J. Comput. Chem.* **2005**, *27*, 571-577.
20. O. Exner and S. Böhm, *Org. Biomol. Chem.* **2005**, *3*, 1838-1843.
21. O. Exner and S. Böhm, *J. Chem. Soc. Perkin Trans.* **1997**, *2*, 1235-1240.
22. O. Exner, *J. Phys. Org. Chem.* **1999**, *12*, 265-274.
23. O. Exner and P. Naus, *J. Phys. Org. Chem.* **2000**, *13*, 693-698.
24. O. Exner and S. Böhm, *Chem. Eur. J.* **2002**, *8*, 5147-5152.
25. O. Exner and S. Böhm, *J. Phys. Org. Chem.* **2004**, *17*, 124-130.
26. O. Exner and S. Bohm, *J. Comput. Chem.* **2004**, *25*, 1979-1986.
27. O. Exner and S. Böhm, *J. Phys. Org. Chem.* **2006**, *19*, 1-9.
28. O. Exner and S. Böhm, *Eur. J. Org. Chem.* **2007**, 2870-2876.

29. S. Böhm and O. Exner, *J. Mol. Struct. Theochem.* **2004**, *682*, 171-177.
30. R. Ponec and S. V. Damme, *J. Phys. Org. Chem.* **2007**, *20*, 662-670.
31. O. Exner and S. Böhm, *Chem. Eur. J.* **2003**, *9*, 4718-4723.
32. S. Irle, T. M. Krygowski, J. E. Niu and W. H. E. Schwarz, *J. Org. Chem.* **1996**, *60*, 6744–6755.
33. M. K. Cyranski, T. M. Krygowski, A. R. Katritzky and P. v. R. Schleyer, *J. Org. Chem.* **2002**, *67*, 1333-1338.
34. T. M. Krygowski and N. Sadlej-Sosnowska, *Struct. Chem.* **2011**, *22*, 17-22.
35. T. M. Krygowski, J. E. Zachara-Horeglad and M. Palusiak, *J. Org. Chem.* **2010**, *75*, 4944–4949.
36. L. Sobczyk, S. J. Grabowski and T. M. Krygowski, *Chem. Rev.* **2005**, *105*, 3513-3560.
37. T. M. Krygowski and B. T. Stepien, *Chem. Rev.* **2005**, *105*, 3482−3512.
38. Z. Chen, C. S. Wannere, C. Corminboeuf, R. Puchta and P. v. R. Schleyer, *Chem. Rev.* **2005**, *105*, 3842-3888.
39. T. M. Krygowski and M. K. Cyranski, *Chem. Rev.* **2001**, *101*, 1385-1419.
40. T. M. Krygowski, B. T. Stepien, M. K. Cyranski and K. Ejsmont, *J. Phys. Org. Chem.* **2005**, *18*, 886-891.
41. M. K. Cyranski, *Chem. Rev.* **2005**, *105*, 3773-3811.
42. T. M. Krygowski, K. Ejsmont, B. T. Stepien, M. K. Cyranski, J. Poater and M. Sola, *J. Org. Chem.* **2004**, *69*, 6634-6640.
43. K. B. Wiberg, *J. Org. Chem.* **2002**, *67*, 1613-1617.
44. K. B. Wiberg, *J. Org. Chem.* **2002**, *67*, 4787-4794.
45. K. B. Wiberg, *J. Org. Chem.* **2003**, *68*, 875-882.
46. B. Galabov, S. Ilieva, B. Hadjieva, Y. Atanasov and H. F. Schaefer, *J. Phys. Chem. A* **2008**, *112*, 6700-6707.
47. M. M. Deshmukh, S. R. Gadre and L. J. Bartolotti, *J. Phys. Chem. A* **2006**, *110*, 12519-12523.
48. C. H. Suresh and S. R. Gadre, *J. Phys. Chem. A* **2007**, *111*, 710-714.
49. C. H. Suresh and S. R. Gadre, *J. Am. Chem. Soc.* **1998**, *120*, 7049-7055.

50. M. J. Frisch, G. W. Trucks, H. B. Schlegel, G. E. Scuseria, M. A. Robb, J. R. Cheeseman, G. Scalmani, V. Barone, B. Mennucci, G. A. Petersson, H. Nakatsuji, M. Caricato, X. Li, H. P. Hratchian, A. F. Izmaylov, J. Bloino, G. Zheng, J. L. Sonnenberg, M. Hada, M. Ehara, K. Toyota, R. Fukuda, J. Hasegawa, M. Ishida, T. Nakajima, Y. Honda, O. Kitao, H. Nakai, T. Vreven, J. A. Montgomery, J. E. P. Jr., F. Ogliaro, M. Bearpark, J. J. Heyd, E. Brothers, K. N. Kudin, V. N. Staroverov, R. Kobayashi, J. Normand, K. Raghavachari, A. Rendell, J. C. Burant, S. S. Iyengar, J. Tomasi, M. Cossi, N. Rega, J. M. Millam, M. Klene, J. E. Knox, J. B. Cross, V. Bakken, C. Adamo, J. Jaramillo, R. Gomperts, R. E. Stratmann, O. Yazyev, A. J. Austin, R. Cammi, C. Pomelli, J. W. Ochterski, R. L. Martin, K. Morokuma, V. G. Zakrzewski, G. A. Voth, P. Salvador, J. J. Dannenberg, S. Dapprich, A. D. Daniels, O. Farkas, J. B. Foresman, J. V. Ortiz, J. Cioslowski and D. J. Fox, *Gaussian09*, *Revision D. 01,* **2013**, *Gaussian, Inc., Wallingford CT.*
51. C. H. Suresh and S. R. Gadre, *J. Org. Chem.* **1999**, *64*, 2505-2512.
52. S. R. Gadre and C. H. Suresh, *J. Org. Chem.* **1997**, *62*, 2625-2627.
53. R. N. Shirsat, S. V. Bapat and S. R. Gadre, *Chem. Phys. Lett.* **1992**, *200*, 373-378.
54. C. G. Swain and E. C. Lupton, *J. Am. Chem. Soc.* **1968**, *90*, 4328-4337.
55. R. W. Taft and R. D. Topsom, *Prog. Phys. Org. Chem.* **1987**, *16*, 1-83.
56. F. B. Sayyed and C. H. Suresh, *New J. Chem.* **2009**, *33*, 2465-2471.

Chapter 3

Part A

Assessment of Electron Donor Properties of Substituted Phenanthroline Ligands in Molybdenum Carbonyl Complexes

Part B

Substituent Effect Parameters: Extending the Applications to Organometallic Chemistry

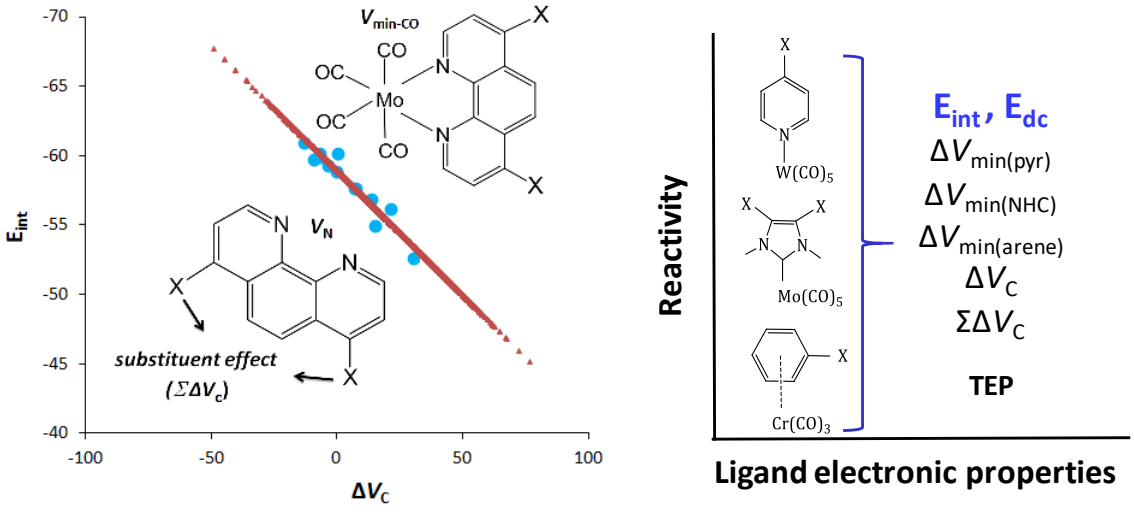

Part A. Assessment of Electron Donor Properties of Substituted Phenanthroline Ligands in Molybdenum Carbonyl Complexes

3.1 Abstract

The relevance of substituents effects in the design and development novel molecules has considerable interest in many industrial and synthetic reactions in organic chemistry. Molecular electrostatic potential (MESP) parameters are found to be excellent descriptors for characterizing the substituent and ligand effects in chemistry. Here we use MESP parameters derived for substituted benzenes as a measure of substituent effect to assess the coordination ability of substituted 1, 10-phenanthrolines with $Mo(CO)_4$. The MESP approach to substituent effect provides an easy way to predict ligand effects before any theoretical calculations or experimental verification and it is endowed with the most accessible guidelines for the quantification of electron donating power of aromatic N-heterocyclic ligands.

3.2 Introduction

Substituent chemistry has grown to become an attention-grabbing subject in the field of organic synthesis while quantification of substituent effect is considered as very crucial in deducing the structure-activity relationships.[1-4] Generally, Hammett constants[5,6] were used to convey the ability of a substituent to attract or lose electrons, which are derived based on the ionization of substituted benzoic acids. Quantum mechanically derived substituent parameters are trending now, instead of the experimentally observed and classical mechanics based parameters.[7-10] Among such parameters, molecular electrostatic potential (MESP) has materialized as a remarkable descriptor of the electronic properties of molecules.[11-13] Our previous studies have shown that MESP parameters behave very similarly like Hammett constants to describe the substituent effects in chemistry.[14,15] In a recent study, 381 substituents were classified into different

categories, such as very strong, strong, weak, and very weak based on their electron donating/withdrawing ability measured using the change in MESP value at the para carbon (ΔV_C) of a substituted benzene with respect to benzene.[16] The entire database of V_C deduced for benzene is found to be transferable to π-conjugated systems such as butadiene, butadiyne, pyridine and pyrene. The aim of the present study is to show that ΔV_C database is useful for finding structure activity relationships in molecular complexes. Here we try to deduce such a relationship for selected substituted 1,10-phenanthrolines (phen*) which is a key class of bidentate chelating ligands in inorganic chemistry.[17-25] The phenanthrolines refer to diazaphenanthrenes that contain one nitrogen atom in a peripheral position in each of the two outer rings of phenanthrene.[26,27] The ligand is said to be highly versatile due to the planar structure, aromaticity and strong chelating ability.[28-30] Very recently, the donor-acceptor properties of a large set of substituted 1,10-phenanthrolines have been experimentally and theoretically determined by Brenna *et al*.[31] and reported significant amount of data in terms of energetic contributions to describe the bonding between molybdenum tetra carbonyl, $Mo(CO)_4$ and 1,10-phenanthrolines. The present study uses the data reported by Brenna *et al.* to verify the MESP based approach to assess substituent effects in 1,10-phenanthrolines. To be aware of the coordination behaviour of metal complexes, it is indispensable to gain knowledge about the ligand design and metal-ligand interactions.[32-34] MESP minimum (V_{min}) at the lone pair bearing nitrogen atom of the phen* ligand and MESP at the nitrogen nucleus (V_N) have been used here to predict the interactive behaviour of phen* with $Mo(CO)_4$ to form [$Mo(CO)_4$(phen*)].

3.3 Computational Methodology

All the computational calculations have been performed with density functional theory (DFT) using Gaussian 09 suite of programmes.[35] The 1,10-phenanthroline ligands are optimized using the B3LYP level with 6-311+G(d, p) basis set. For optimizing the molybdenum complexes, QZVP basis set is used for Mo. All the structures are verified as energy minima by frequency calculation. The B3LYP/6-311+G(d, p) wave function is used for calculating V_{min} and V_C values of MESP. The descriptors obtained from molecular

electrostatic potential (MESP) through the topographical analysis are advantageous for the design of new QSAR models.[36,37]

3.4 Results and Discussion

3.4.1 Design strategies

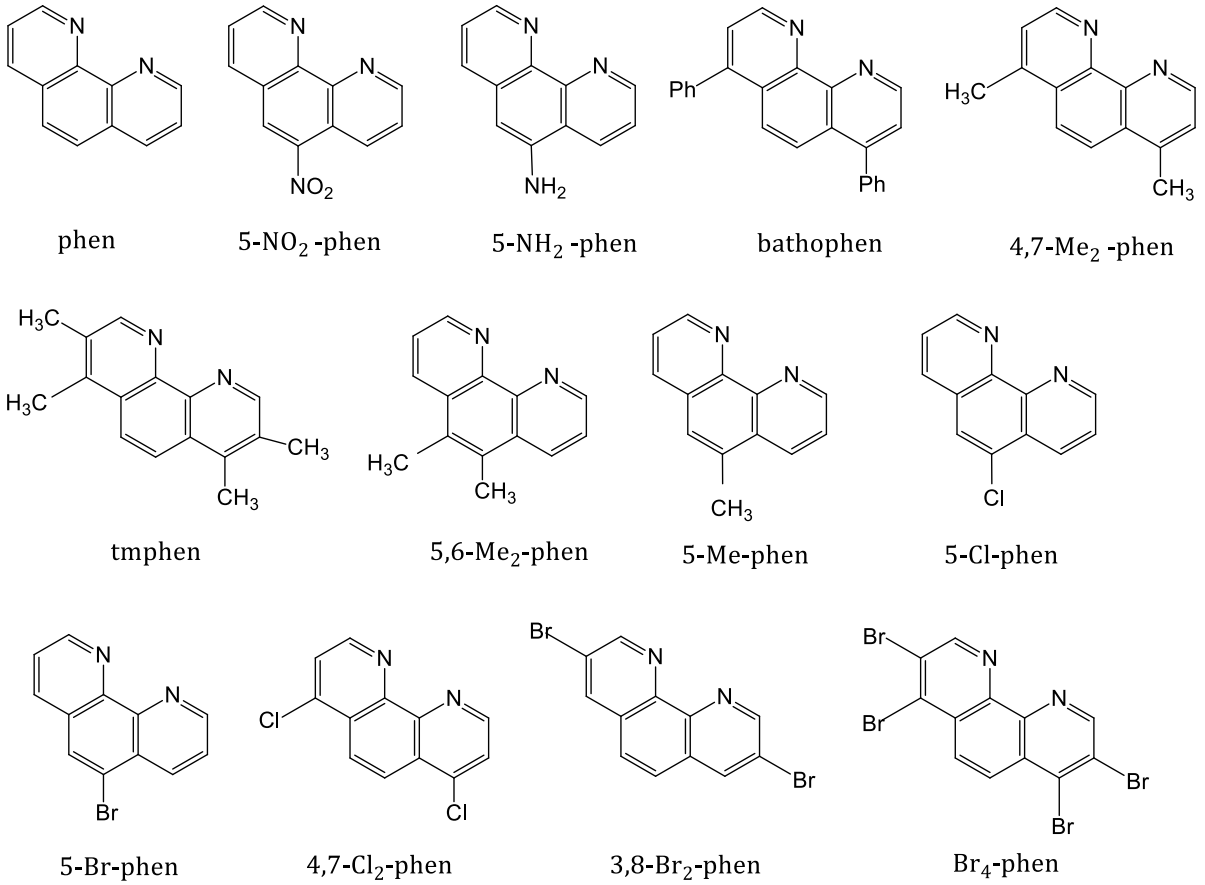

Figure 3.1 Experimentally known substituted 1, 10-phenanthroline ligands

The thirteen 1, 10-phenanthroline derivatives (phen* ligands) selected for this study used for forming [Mo(CO)$_4$(phen*)] complexes are depicted in Figure 3.1. Synthesis of all these ligands is recently reported by Brenna *et al*.[31] The phen* ligands can be distinguished on the basis of the nature of substituents and their positions on the phenanthroline framework. All the ligands are named according to the naming scheme given by Brenna *et al*. We use these systems as a test set to analyze the MESP features to

find correlation with experimental data. The ΔV_C parameter reported in the previous study, derived from substituted benzenes will also be tested for finding the transferability of the MESP property to describe the substituent effect in 1,10-phenanthrolines and their Mo complexes. The experimental IR stretching frequency A_{1ax} of the CO groups in $[Mo(CO)_4(phen^*)]$, reported by Brenna *et al*.[31] is selected as the experimental electronic parameter to find correlation with MESP features. Further, interaction energy (E_{int}) due to the coordination of 1, 10-phenantrolines to $Mo(CO)_4$ is calculated and correlated with the substituent effect parameters. The correlations found in the test set will be applied to a test set containing 108 phenanthroline derivatives to make predictions on their E_{int}. Moreover, the predictions will be verified by calculating E_{int} of many representative cases. Finally, a randomization procedure on substitution pattern will be adopted to predict the substituent effect of 5000 multiply substituted 1,10-phenanthrolines.

3.4.2 MESP Analysis of Substituted 1,10-phenanthroline Ligands

The MESP parameters ΔV_N and ΔV_{min} are used for interpreting the interaction energy of $[Mo(CO)_4(phen^*)]$ complexes are defined in Eq. 3.1 and Eq. 3.2, respectively. ΔV_N accounts for the difference between the V_N of $phen^*$ and phen ligands while ΔV_{min} describes the difference between the corresponding V_{min} values. MESP minimum for the carbonyl oxygen ($V_{min\text{-}CO}$) in the complex $[Mo(CO)_4(phen^*)]$ is also analyzed. The interaction energy (E_{int}) of the $[Mo(CO)_4(phen^*)]$ complex is calculated by subtracting the energy of $[Mo(CO)_4(phen^*)]$ from the sum of the energies of the fragments $Mo(CO)_4$ and $phen^*$ (Eq. 3.3).

$$\Delta V_N = V_N(phen^*) - V_N(phen) \quad \text{(Eq. 3.1)}$$

$$\Delta V_{min} = V_{min}(phen^*) - V_{min}(phen) \quad \text{(Eq. 3.2)}$$

$$E_{int} = E[Mo(CO)_4(phen^*)] - \{E[Mo(CO)_4] + E[phen^*]\} \quad \text{(Eq. 3.3)}$$

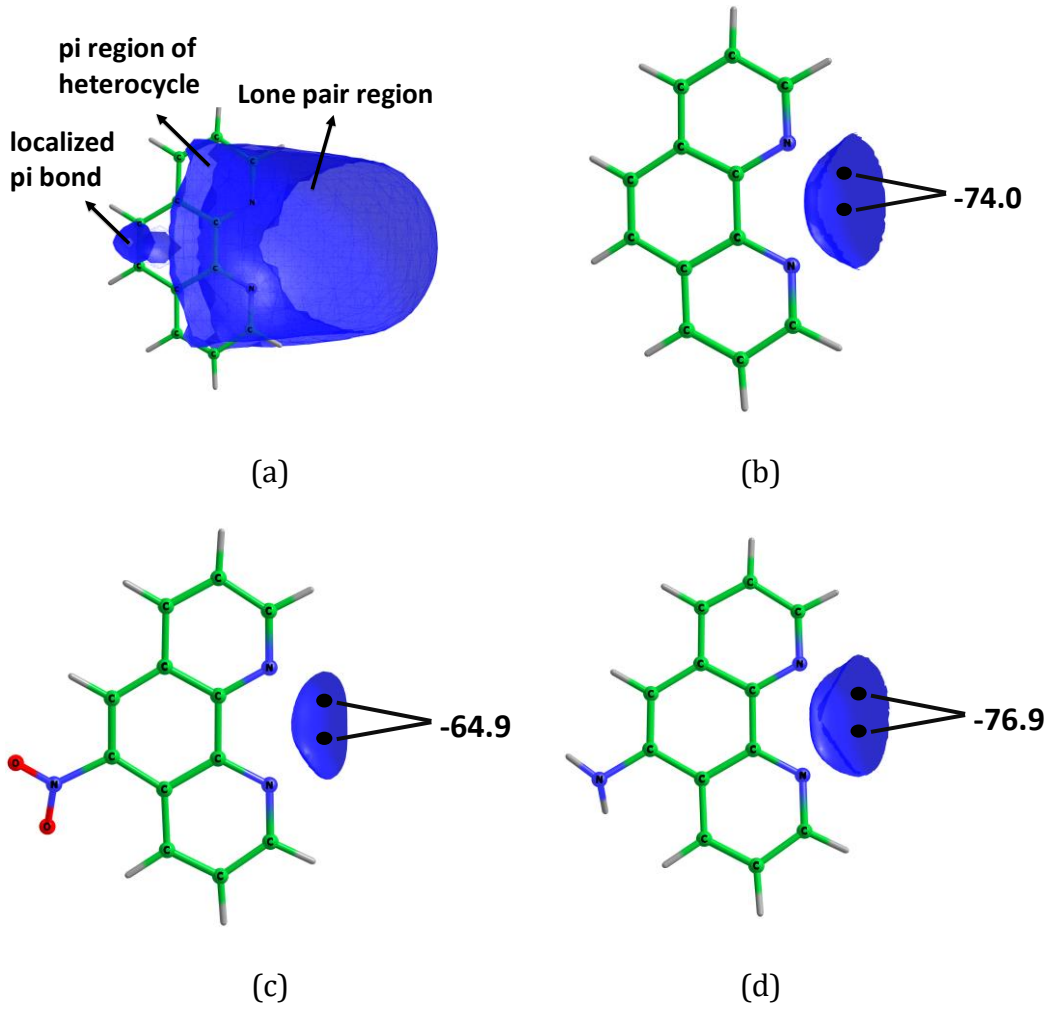

Figure 3.2 MESP plots of phen ligand are shown with (a) 6 kcal/mol isosurface of phen ligand (b) MESP plots of phen ligand with 44 kcal/mol isosurface and V_{min} points, (c) MESP plots of NO_2-phen ligand with 44 kcal/mol isosurface and V_{min} points and (d) MESP distribution of NH_2-phen ligand with 44 kcal/mol isosurface and V_{min} points.

The MESP features of the phen* ligands are presented in Figure 3.2 using suitable isosurfaces. The 6.0 kcal/mol valued isosurface (Figure 3.2a) shows the π-electron region of the aromatic rings and lone pair site of the nitrogen centers. Also localization of a double bond for the central arene ring is visible in MESP while a lower MESP value shows electron rich nitrogen centers and the lowest point (V_{min}) indicates the lone pair centers of the nitrogen atoms (Figure 3.2b). V_{min} represents a (3, +3) critical point (CP) in the MESP topography. The three positive eigenvalues of V_{min} indicate how sharply the function is increasing in all the three directions at the CP while the corresponding

eigenvector represents the axis of the curvature. As per the criteria suggested by Suresh, Gadre and co-workers to characterize a lone pair,[38] the largest eigenvalue and the corresponding eigenvector of the Hessian matrix at V_{min} is found to be in the direction of N-centers.

The topographical features of Figures 3.2c and 3.2d represent MESP V_{min} features of 5-NO_2-phen and 5-NH_2-phen ligands, respectively. Compared to phen, the change in V_{min} (ΔV_{min}) observed for 5-NO_2-phen is 9.04 kcal/mol and that for 5-NH_2-phen is -2.95 kcal/mol indicating the strong electron withdrawing effect of NO_2 and electron donating influence of NH_2 substituents, respectively. We also computed MESP at both N nuclei (V_N) as it shows significant change with respect to the nature of the substituent on aryl ring. For instance, V_N of phen ligand (-18.4095 au) is changed by 10.72 kcal/mol for 5-NO_2-phen and -2.51 kcal/mol for 5-NH_2-phen. The quantities ΔV_{min} and ΔV_N (change in MESP at N nucleus) are used as a measure of substituent effect.[39]

3.4.3 MESP Analysis and Interaction Energy of [Mo(CO)$_4$(phen*)] Complexes

The MESP isosurface plots given in Figure 3.3a for $Mo(CO)_4$ show the lone pair regions of carbonyl groups. The two trans disposed carbonyl groups show significantly higher MESP minimum value -13.2 kcal/mol ($V_{min\text{-}CO}$) than the other two carbonyl groups, -24.0 kcal/mol due to trans influence.[40] As shown in Figure 3.3b, coordination of phen* ligand to Mo describes the donation of two lone pairs from the nitrogen centers. This donation increases the electron rich character of the carbonyl groups in [$Mo(CO)_4$(phen)] compared to those in $Mo(CO)_4$ and accordingly $V_{min\text{-}CO}$ of [$Mo(CO)_4$(phen)] becomes more negative by 14.8 kcal/mol for the trans disposed carbonyl groups and by 13.4 kcal/mol for the other two carbonyl groups. Compared to [$Mo(CO)_4$(phen)], $V_{min\text{-}CO}$ of [$Mo(CO)_4$(5-NO_2-phen)] becomes less negative by 4.7 kcal/mol for the trans carbonyl groups and by 4.9 kcal/mol for the other two carbonyls whereas in case of [$Mo(CO)_4$(5-NH_2-phen)], $V_{min\text{-}CO}$ becomes more negative by 1.0 kcal/mol for the trans carbonyl groups and by 1.4 kcal/mol for the other two carbonyls. The $V_{min\text{-}CO}$ data is in accordance with the electron withdrawing nature of NO_2 substituent and electron donating nature of NH_2 substituent.

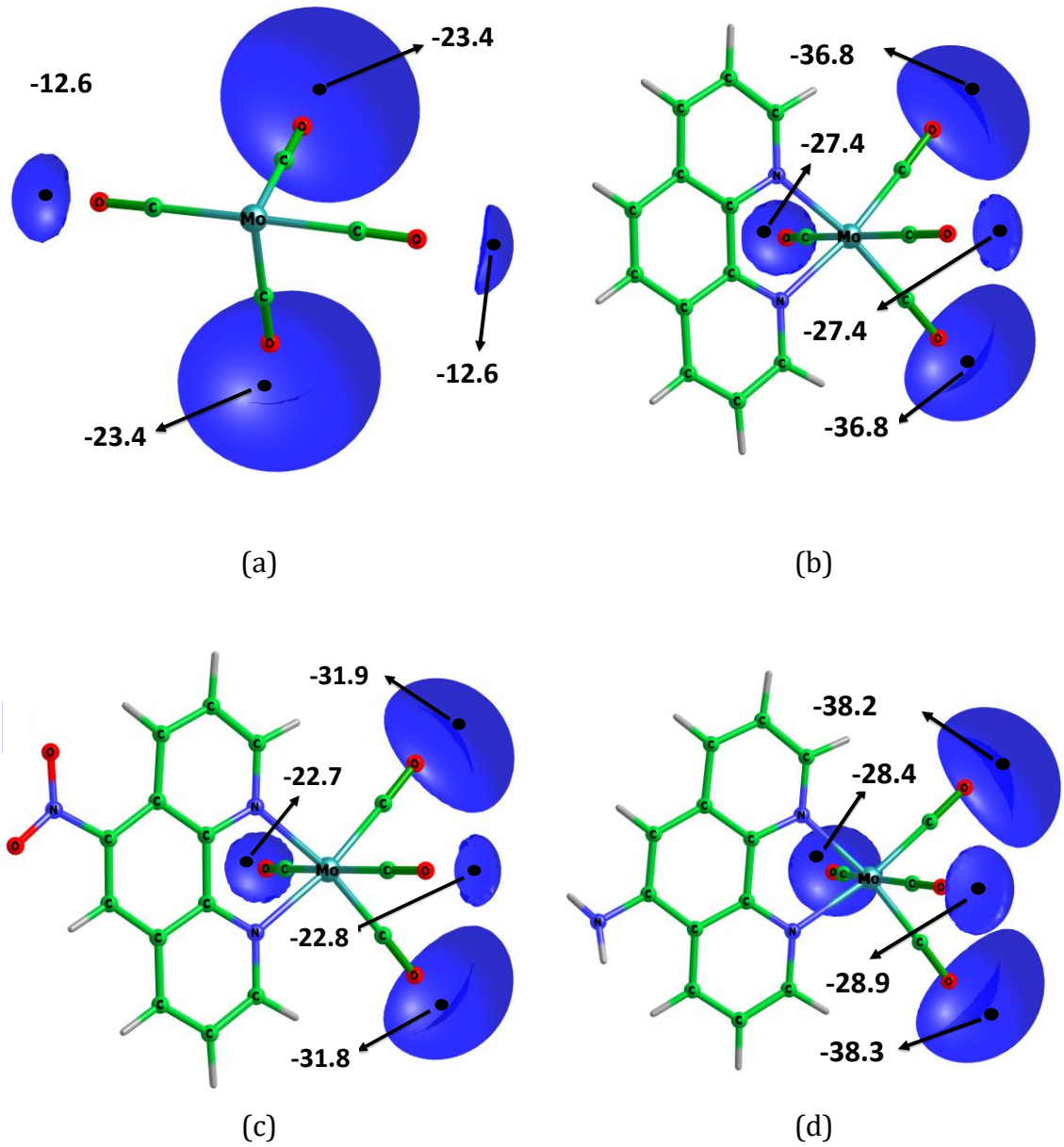

Figure 3.3 MESP plots of V_{min} on carbonyls is shown with (a) 11 kcal/mol isosurfaces, of $Mo(CO)_4$ (b) 26 kcal/mol isosurfaces, of $[Mo(CO)_4(phen)]$, (c) 22 kcal/mol isosurfaces, of $[Mo(CO)_4(5\text{-}NO_2\text{-}phen)]$, and (d) 26 kcal/mol isosurfaces, of $[Mo(CO)_4(5\text{-}NH_2\text{-}phen)]$. V_{min} values are given in kcal/mol.

Table 3.1 MESP properties ΔV_N, ΔV_{min} and $V_{min\text{-}CO}$, A_{1ax} values and calculated E_{int} values. MESP values and E_{int} in kcal/mol and A_{1ax} in cm^{-1}.

Name	ΔV_N	ΔV_{min}	$V_{min\text{-}CO}$	A_{1ax}	E_{int}
phen	0.0	0.0	-36.8	2015.1	-58.9
5-NO_2- phen	10.7	9.0	-31.9	2017.4	-56.2
5-NH_2 -phen	-2.5	-2.9	-38.3	2014.1	-59.7
bathophen	-2.9	-2.5	-38.8	2013.9	-60.2
4,7-Me_2 -phen	-4.8	-3.8	-39.1	2013.7	-60.2
tmphen	-7.8	-5.5	-40.3	2013.1	-61.0
5,6-Me_2 -phen	-3.1	-3.0	-38.2	2014.2	-59.9
5-Me- phen	-1.4	-1.0	-37.5	2014.7	-59.3
5-Cl- phen	4.4	3.8	-35.1	2016.3	-57.7
5-Br phen	4.5	4.1	-35.1	2016.2	-57.7
4,7-Cl_2- phen	7.8	6.7	-33.6	2017.0	-56.9
3,8-Br_2- phen	12.1	11.3	-33.8	2018.0	-55.0
Br_4-phen	15.9	14.4	-32.3	2019.0	-52.6

In Table 3.1, ΔV_{min} and ΔV_N of all phen* ligands and $\Delta V_{min\text{-}CO}$ of all $[Mo(CO)_4(phen^*)]$ complexes are presented along with the experimental CO stretching frequency A_{1ax} and the calculated interaction energy (E_{int}) for the complex formation (Eq. 3.3) between phen* ligand and $Mo(CO)_4$. The calculated interaction energy is found to agree very well with the interaction energy reported by Brenna *et al*. using ETS-NOCV[41-44] approach at PBE0 level (mean absolute deviation is 0.85 kcal/mol). All the three MESP parameters, *viz*. ΔV_{min}, ΔV_N and $\Delta V_{min\text{-}CO}$ show strong linear correlation with A_{1ax} with correlation coefficient (R) 0.995, 0.996 and 0.967 respectively. A representative plot is given in Figure 3.4a. Similarly, ΔV_{min}, ΔV_N and $\Delta V_{min\text{-}CO}$ exhibit linear correlation with E_{int} and the corresponding r values are 0.986, 0.981 (Eq. 3.4 and Figure 3.4b) and 0.918. These correlations indicate that the electron rich character of N centers measured in terms of MESP parameter V_{min} or V_N has the power to predict the strength of a phen* ligand to coordinate with a metal center decorated by other ligands. Further, the outcome of the

coordination can also be measured in terms of the change in MESP observed at sensitive ligands in the complex. Here carbonyl groups show significant change in MESP value due to electron donation from the phen* ligand to metal and that change is also proportional to the Tolman electronic parameter, the CO stretching frequency.[45-47]

$$E_{int} = 0.3251\ (\Delta V_N) - 58.92 \qquad \text{(Eq. 3.4)}$$

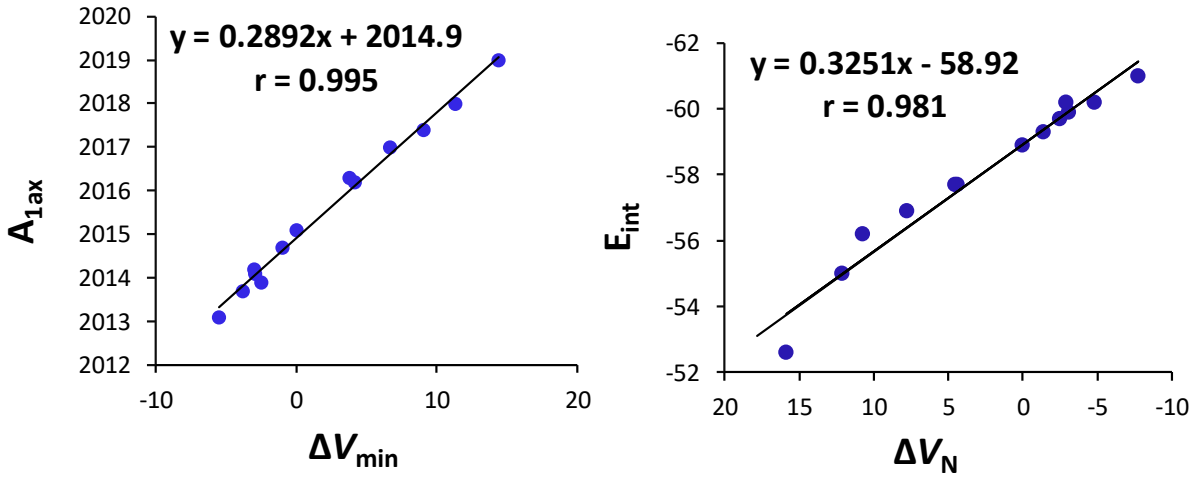

(a) (b)

Figure 3.4 Correlation of (a) ΔV_{min} against A_{1ax} frequency and (b) ΔV_N against E_{int} values. A_{1ax} in cm^{-1} and other values in kcal/mol.

3.4.4 Correlation between Interaction Energy and MESP parameter of Benzene Derivatives

Previously, change in MESP value at the para carbon of a monosubstituted benzene relative to benzene (ΔV_C) has been proposed as an electronic descriptor to quantify the substituent effect which showed strong correlation with the well-known Hammett σ_p constant.[16] Further, on the basis of the magnitude of ΔV_C, a large variety of 381 substituents have been classified into various categories, *viz.* very strong ($S^{>>>>}$) strong ($S^{>>>}$), medium ($S^{>>}$) and weak ($S^{>}$) electron donating and very strong ($S^{<<<<}$), strong ($S^{<<<}$), medium ($S^{<<}$) and weak ($S^{<}$) electron withdrawing. If phenanthroline systems obey the transferability property of substituent effect, strong similarity in ΔV_C and ΔV_N

parameters can arise which is true as strong linear correlation exists between them (Figure 3.5a). As per the correlation plot in Figure 3.5a for the 13 substituents,

$$\Delta V_N = 0.5519\ (\Delta V_C) \qquad \text{(Eq. 3.5)}$$

Substituting ΔV_N in Eq. 3.4 leads to

$$E_{int} = 0.1794\ (\Delta V_C) - 58.92 \qquad \text{(Eq. 3.6)}$$

ΔV_N is approximately 0.5519 times ΔV_C which indicates that without doing any calculation on phenanthroline derivatives, the knowledge of ΔV_C derived from simple benzene derivatives alone can be utilized for predicting the strength of the complex formation between phen* and $Mo(CO)_4$ *via* Eq. 3.6. In order to test this hypothesis, representative sets of substituents from various categories, *viz*. $S^{>>>>}$, $S^{>>>}$, $S^{>>}$, $S^{>}$, $S^{<<<<}$, $S^{<<<}$, $S^{<<}$ and $S^{<}$ are selected and populated them at different positions of the phenanthroline ligand to create 108 substituted phenanthroline ligands which contain mono-, di- and tetra-substitutions.

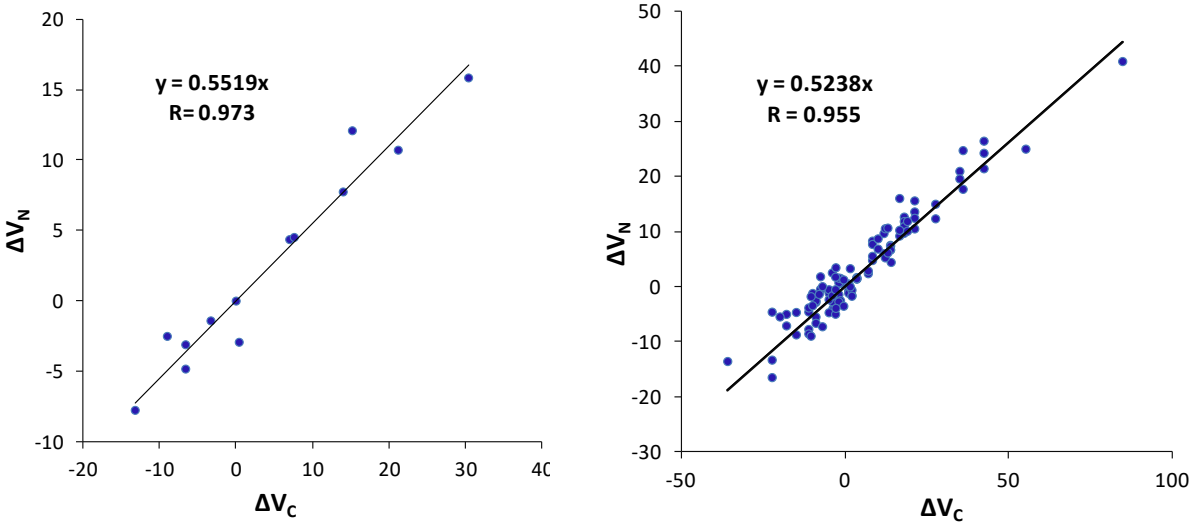

(a) (b)

Figure 3.5 Correlation between ΔV_C and ΔV_N values for (a) the thirteen phenanthrolines and (b) the 108 ligands given in Table 3.2. All values in kcal/mol.

Table 3.2 The actual ΔV_N values and predicted E_{int} using Eq. 3.4 and Eq. 3.6 for the 108 systems. Values in kcal/mol.

ligand	ΔV_N	$E_{int\text{-Eq. 3.4}}$	$E_{int\text{-Eq. 3.6}}$	ligand	ΔV_N	$E_{int\text{-Eq. 3.4}}$	$E_{int\text{-Eq. 3.6}}$
2-NO_2	15.7	-53.8	-55.1	4,7-$(NO_2)_2$	24.3	-51.0	-51.3
2-CN	12.7	-54.8	-55.7	4,7-$(OCF_3)_2$	9.3	-55.9	-55.9
2-CHO	6.7	-56.7	-56.4	4,7-$(CH=CH_2)_2$	-1.5	-59.4	-58.6
2-OCF_3	8.4	-56.2	-57.4	4,7-$(SMe)_2$	-4.9	-60.5	-59.5
2-$CH=CH_2$	-0.7	-59.1	-58.7	4,7-$(CH_2OH)_2$	-0.6	-59.1	-60.3
2-SiH_3	1.7	-58.4	-58.3	4,7-$(NHMe)_2$	-16.4	-64.3	-62.9
2-SMe	0.9	-58.6	-59.2	3,8-$(NO_2)_2$	26.5	-50.3	-51.3
2-OH	-1.4	-59.4	-59.3	3,8-$(CHO)_2$	15.1	-54.0	-54.0
2-CH_2OH	-3.9	-60.2	-59.6	3,8-$(SiH_3)_2$	2.9	-58.0	-57.7
2-OMe	-1.1	-59.3	-59.8	3,8-$(OH)_2$	2.6	-58.1	-59.6
2-NH_2	-5.4	-60.7	-60.5	3,8-$(OMe)_2$	-1.1	-59.3	-60.7
2-NHMe	-7.7	-61.4	-60.9	3,8-$(NH_2)_2$	-4.9	-60.5	-62.1
3-NO_2	13.7	-54.5	-55.1	5,6-$(CN)_2$	17.8	-53.1	-52.5
3-CN	11.9	-55.0	-55.7	5,6-$(OCF_3)_2$	10.3	-55.6	-55.9
3-CHO	7.6	-56.5	-56.4	5,6-$(CH=CH_2)_2$	-0.6	-59.1	-58.6
3-OCF_3	7.8	-56.4	-57.4	5,6-$(SMe)_2$	1.8	-58.3	-59.5
3-$CH=CH_2$	0.6	-58.7	-58.7	5,6-$(CH2OH)_2$	-0.4	-59.0	-60.3
3-SiH_3	1.6	-58.4	-58.3	5,6-$(NHMe)_2$	-4.5	-60.4	-62.9
3-SMe	0.7	-58.7	-59.2	3,4-7,8-$(NO_2)_4$	41.0	-45.6	-43.7
3-OH	0.8	-58.7	-59.3	3,4-7,8-$(CHO)_4$	25.1	-50.8	-49.0
3-CH_2OH	-2.7	-59.8	-59.6	3,4-7,8-$(SiH_3)_4$	4.5	-57.5	-56.4
3-OMe	-0.5	-59.1	-59.8	3,4-7,8-$(OH)_4$	-1.3	-59.3	-60.4
3-NH_2	-2.8	-59.8	-60.5	3,4-7,8-$(OMe)_4$	-5.4	-60.7	-62.5
3-NHMe	-4.5	-60.4	-60.9	3,4-7,8-$(NH_2)_4$	-13.5	-63.3	-65.4
4-NO_2	12.5	-54.9	-55.1	2,9-$(CN)_2$	24.8	-50.9	-52.5
4-CN	11.0	-55.3	-55.7	2,9-$(OCF3)_2$	16.1	-53.7	-55.9
4-CHO	7.4	-56.5	-56.4	2,9-$(CH=CH2)_2$	-1.6	-59.5	-58.6

4-OCF_3	4.8	-57.3	-57.4	2,9-$(SMe)_2$	-0.5	-59.1	-59.5
4-$CH=CH_2$	-1.1	-59.3	-58.7	2,9-$(CH_2OH)_2$	1.9	-58.3	-60.3
4-SiH3	1.5	-58.4	-58.3	2,9-$(NHMe)_2$	-13.2	-63.2	-62.9
4-SMe	-2.5	-59.7	-59.2	4,7-NO_2,CHO	21.0	-52.1	-52.6
4-OH	-2.7	-59.8	-59.3	4,7-CN,$CH=CH_2$	11.9	-55.0	-55.5
4-CH_2OH	-4.1	-60.3	-59.6	4,7-OCF_3,SiH_3	9.7	-55.8	-56.8
4-Ome	-4.6	-60.4	-59.8	4,7-OH,OMe	0.1	-58.9	-60.2
4-NH_2	-6.6	-61.1	-60.5	4,7-SMe,NH_2	-1.7	-59.5	-60.8
4-NHMe	-8.5	-61.7	-60.9	4,7-CH_2OH,NHMe	-4.6	-60.4	-61.6
5-NO_2	10.6	-55.5	-55.1	4,7-NO_2,NH_2	10.6	-55.5	-56.7
5-CN	9.8	-55.7	-55.7	4,7-CN,OMe	10.7	-55.4	-56.6
5-CHO	6.8	-56.7	-56.4	4,7-CHO,CH_2OH	8.8	-56.1	-57.1
5-OCF3	5.6	-57.1	-57.4	4,7-SiH_3,OH	3.4	-57.8	-58.7
5-$CH=CH_2$	0.5	-58.8	-58.7	4,7-$CH=CH_2$,SMe	1.3	-58.5	-59.0
5-SiH_3	1.5	-58.4	-58.3	4,7-OCF_3,NHMe	3.5	-57.8	-59.4
5-SMe	1.6	-58.4	-59.2	3,8-NO_2,CHO	19.7	-52.5	-52.6
5-OH	1.6	-58.4	-59.3	3,8-CN,$CH=CH_2$	10.2	-55.6	-55.5
5-CH_2OH	-1.6	-59.4	-59.6	3,8-OCF_3,SiH_3	6.1	-56.9	-56.8
5-OMe	-2.3	-59.7	-59.8	3,8-OH,OMe	-7.2	-61.3	-60.2
5-NH_2	-2.5	-59.7	-60.5	3,8-SMe,NH_2	-8.9	-61.8	-60.8
5-NHMe	-3.8	-60.1	-60.9	3,8-CH_2OH,NHMe	-8.7	-61.7	-61.6
3,4-$(NO_2)_2$	21.5	-51.9	-51.3	3,8-NO_2,NH_2	5.3	-57.2	-56.7
3,4-$(CHO)_2$	12.4	-54.9	-54.0	3,8-CN,OMe	6.2	-56.9	-56.6
3,4-$(SiH_3)_2$	2.4	-58.1	-57.7	3,8-CHO,CH_2OH	6.9	-56.7	-57.1
3,4-$(OH)_2$	-1.6	-59.4	-59.6	3,8-SiH_3,OH	0.1	-58.9	-58.7
3,4-$(OMe)_2$	-3.4	-60.0	-60.7	3,8-$CH=CH_2$,SMe	-3.5	-60.0	-59.0
3,4-$(NH_2)_2$	-7.0	-61.2	-62.1	3,8-OCF_3,NHMe	-3.8	-60.2	-59.4

For di- and tetra-substituted systems, ΔV_C values were added twice and four times, respectively, assuming the additive nature of substituent effect.[16] The predicted E_{int} using Eq. 3.4 and Eq. 3.6, and actual ΔV_N, values of 108 combinations are presented in Table 3.2. The transferability property deduced for the 108 selected systems are given in Figure 3.5b. The mean absolute deviation between actual ΔV_N and Eq. 3.5 is 2.23 kcal/mol while that between Eq. 3.4 and Eq. 3.6 is 0.72 kcal/mol indicating that the quantification of substituent effect empowers us to make strong prediction on the binding affinity of a large variety of substituted phenanthroline derivatives to $Mo(CO)_4$. The additivity and transferability properties of the substituent effects are also well evident in the good agreement seen in the ΔV_N and ΔV_C based predictions on interaction energy.

3.4.5 Direct Prediction of Interaction Energy Solely by Substituent Effect Parameter

The MESP based analysis of interaction energy clearly suggests that the coordination behavior of a phenanthroline ligand to a metal complex is very much predictable provided the substituent effect is known for them. The MESP based parameter ΔV_C and ΔV_N emerge as effective measures of the substituent effect. Using the ΔV_C values from the database, a-priori prediction on the coordination behavior of phenanthroline ligands to metal complexes can be achieved without doing a calculation on the ligand or the complex whereas more precise predictions can be obtained by calculating ΔV_N for each ligand. In order to rigorously test these hypotheses, a set of 50 substituents are considered along with their ΔV_C values from our substituent database.[16] The E_{int} is predicted for mono-, di- and tetra-substituted systems using Eq. 3.7, which is a generalized version of Eq. 3.6 for a multiply substituted phen*.

$$E_{int} = 0.1794\ (\Sigma(\Delta V_C)) - 58.92 \qquad \text{(Eq. 3.7)}$$

Here, assuming additivity[48] of substituent effects, $\Sigma(\Delta V_C)$ represents the total ΔV_C values due to all the substituents. Table 3.3 gives the multiple effect of the same substituent on 50 phen* ligands.

Table 3.3 ΔV_C values and $E_{int\text{-Eq. 3.7}}$ values for mono, di and tetra combinations of 50selected substituted phen* ligands. All values in kcal/mol.

ligand	ΔV_C	E_{int}(mono)	E_{int}(di)	E_{int}(tetra)
COCl	19.1	-55.5	-52.1	-45.2
CN	18.0	-55.7	-52.5	-46.0
SO_2Me	16.8	-55.9	-52.9	-46.9
cyclo-C_4F_7	16.1	-56.0	-53.1	-47.4
$C(Et)(NO_2)_2$	15.4	-56.2	-53.4	-47.9
CF_2CF_3	14.7	-56.3	-53.6	-48.4
OCN	14.2	-56.4	-53.8	-48.7
CHO	13.8	-56.4	-54.0	-49.0
ONO_2	13.4	-56.5	-54.1	-49.3
$OCOCF_3$	12.2	-56.7	-54.5	-50.2
$N(Me)NO_2$	11.7	-56.8	-54.7	-50.5
COOH	10.9	-57.0	-55.0	-51.1
$COOC_6H_5$	10.0	-57.1	-55.3	-51.7
COMe	9.7	-57.2	-55.4	-52.0
$CONHC_6H_5$	9.3	-57.3	-55.6	-52.2
COEt	8.9	-57.3	-55.7	-52.5
COOMe	8.2	-57.4	-56.0	-53.0
Br	7.6	-57.6	-56.2	-53.5
$C(NO_2)Me_2$	7.0	-57.7	-56.4	-53.9
CONHMe	6.4	-57.8	-56.6	-54.3
C≡CH	5.7	-57.9	-56.9	-54.8
$SiClMe_2$	4.8	-58.1	-57.2	-55.5
$SCH=CH_2$	4.1	-58.2	-57.4	-56
C_6H_4-3Cl	3.6	-58.3	-57.6	-56.3
NHCSMe	3.1	-58.4	-57.8	-56.7
$CH_2NHCOMe$	2.5	-58.5	-58.0	-57.1

OCOMe	1.5	-58.7	-58.4	-57.8
$CH=CH_2$	1.0	-58.7	-58.6	-58.2
$OCH=CH_2$	0.7	-58.8	-58.7	-58.4
C_6H_5	0.2	-58.9	-58.8	-58.8
$C(Me)=CH_2$	-0.5	-59.0	-59.1	-59.3
$SiMe_3$	-0.9	-59.1	-59.2	-59.6
C_6H_4-4Me	-1.2	-59.1	-59.4	-59.8
NHCOMe	-1.4	-59.2	-59.4	-59.9
$CH_2C_6H_5$	-1.8	-59.2	-59.6	-60.2
OH	-2.0	-59.3	-59.6	-60.4
cyclopropyl	-2.4	-59.4	-59.8	-60.6
CH_2NMe_2	-2.6	-59.4	-59.9	-60.8
$CH_2CH_2CH_3$	-3.1	-59.5	-60.0	-61.1
Me	-3.3	-59.5	-60.1	-61.3
$NHCONH_2$	-3.7	-59.6	-60.2	-61.6
cyclohexyl	-3.8	-59.6	-60.3	-61.6
Et	-4.0	-59.6	-60.4	-61.8
NHC_6H_5	-4.8	-59.8	-60.6	-62.4
OMe	-5.0	-59.8	-60.7	-62.5
$O(CH_2)_3CH_3$	-5.9	-60.0	-61.0	-63.2
$OCHMe_2$	-6.5	-60.1	-61.3	-63.6
NH_2	-9.0	-60.5	-62.1	-65.4
$NHNH_2$	-11.2	-60.9	-62.9	-67
NMe_2	-12.3	-61.1	-63.3	-67.7

In order to analyze the multiple effect of different substituents, we have generated 5000 tetra-substituted phen* ligands by populating randomly four different substituents from catogeries at various positions on the aromatic ring. Figure 3.6 shows the relationship between ΔV_C and E_{int} for all the 5000 randomly generated ligands. The predicted E_{int} of a representative set of 50 tetra substituted derivatives are provided in Table 3.4. The depiction of the E_{int} of the 13 experimentally known systems along the prediction line (Figure 3.6) clearly reflects the use of ΔV_C as an effective parameter to quantify substituent effect. It may be noted that ΔV_C based prediction of E_{int} for a multiply substituted system does not take into account the influence of the position of the substituent in the phenanthroline ligand as the model is based on the additive nature of substituent effect. Definitely there is influence from changes in position of the substituent upon the reactivity patterns of the selected metal complexes. Fortunately, such changes are not very noteworthy unless there occur sterically bulkier close positions of substituents.

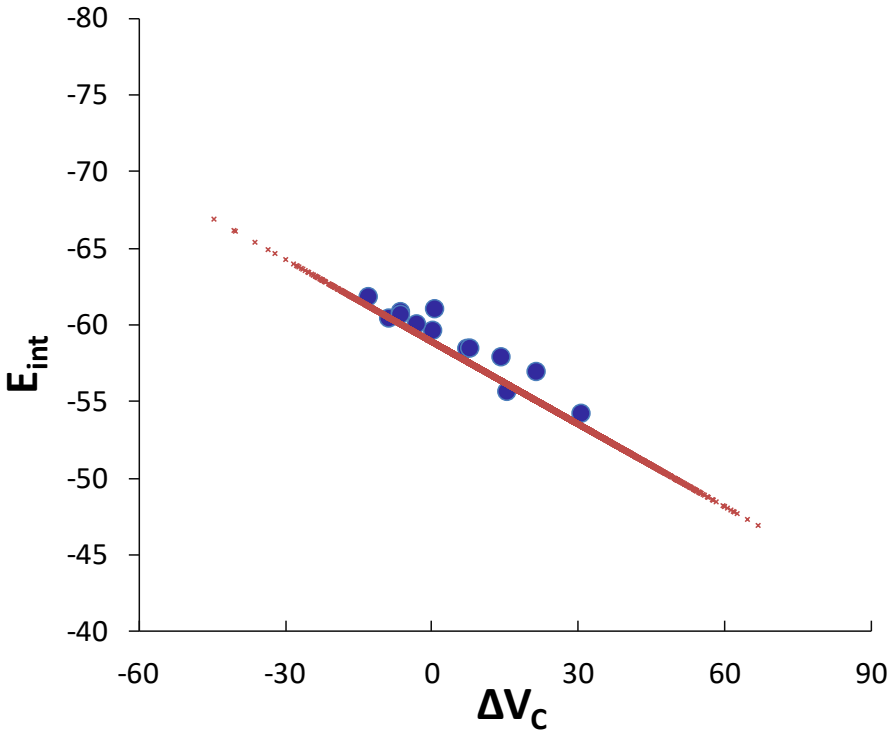

Figure 3.6 Correlation between ΔV_C and E_{int} for 5000 random generated combinations. The blue dots stand for the experimentally known systems. Values in kcal/mol.

Table 3.4 Prediction of $E_{int\text{-}Eq.\ 3.7}$ values for randomly generated substituent combinations.

ΔV_C	Randomly generated no.s				Randomly generated ΔV_C				$\Sigma\Delta V_C$	$E_{int\text{-}Eq.\ 3.7}$
19.1	15	28	11	30	9.3	1.0	11.7	0.2	22.2	-54.9
18.0	8	41	24	32	13.8	-3.7	3.6	-0.9	12.8	-56.6
16.8	34	13	36	26	-1.4	10.0	-2.0	2.5	9.1	-57.3
16.1	20	31	8	38	6.4	-0.5	13.8	-2.6	17.1	-55.9
15.4	9	12	1	43	13.4	10.9	19.1	-4.0	39.4	-51.9
14.7	33	20	18	46	-1.2	6.4	7.6	-5.9	6.9	-57.7
14.2	8	5	6	29	13.8	15.4	14.7	0.7	44.6	-50.9
13.8	2	11	2	35	18.0	11.7	18.0	-1.8	45.9	-50.7
13.4	18	33	44	19	7.6	-1.2	-4.8	7.0	8.6	-57.4
12.2	2	27	18	17	18.0	1.5	7.6	8.2	35.3	-52.6
11.7	32	32	11	8	-0.9	-0.9	11.7	13.8	23.7	-54.7
10.9	32	3	38	32	-0.9	16.8	-2.6	-0.9	12.4	-56.7
10.0	29	10	49	29	0.7	12.2	-11.2	0.7	2.4	-58.5
9.7	47	11	20	22	-6.5	11.7	6.4	4.8	16.4	-56.0
9.3	16	4	38	18	8.9	16.1	-2.6	7.6	30.0	-53.5
8.9	16	19	12	2	8.9	7.0	10.9	18.0	44.8	-50.9
8.2	34	41	26	7	-1.4	-3.7	2.5	14.2	11.6	-56.8
7.6	20	49	46	8	6.4	-11.2	-5.9	13.8	3.1	-58.4
7.0	4	13	16	46	16.1	10.0	8.9	-5.9	29.1	-53.7
6.4	30	47	10	41	0.2	-6.5	12.2	-3.7	2.2	-58.5
5.7	45	24	38	39	-5.0	3.6	-2.6	-3.1	-7.1	-60.2
4.8	16	40	43	29	8.9	-3.3	-4.0	0.7	2.3	-58.5
4.1	37	26	31	20	-2.4	2.5	-0.5	6.4	6.0	-57.8
3.6	17	39	17	7	8.2	-3.1	8.2	14.2	27.5	-54.0
3.1	50	34	41	42	-12.3	-1.4	-3.7	-3.8	-21.2	-62.7

2.5	32	21	3	47	-0.9	5.7	16.8	-6.5	15.1	-56.2
1.5	10	25	3	8	12.2	3.1	16.8	13.8	45.9	-50.7
1.0	28	1	15	34	1.0	19.1	9.3	-1.4	28.0	-53.9
0.7	14	3	10	12	9.7	16.8	12.2	10.9	49.6	-50.0
0.2	34	39	13	34	-1.4	-3.1	10.0	-1.4	4.1	-58.2
-0.5	25	8	28	24	3.1	13.8	1.0	3.6	21.5	-55.1
-0.9	6	35	5	44	14.7	-1.8	15.4	-4.8	23.5	-54.7
-1.2	28	45	29	15	1.0	-5.0	0.7	9.3	6.0	-57.8
-1.4	6	22	10	19	14.7	4.8	12.2	7.0	38.7	-52.0
-1.8	49	43	37	45	-11.2	-4.0	-2.4	-5.0	-22.6	-63.0
-2.0	22	12	28	27	4.8	10.9	1.0	1.5	18.2	-55.7
-2.4	41	42	34	25	-3.7	-3.8	-1.4	3.1	-5.8	-60.0
-2.6	40	5	43	41	-3.3	15.4	-4.0	-3.7	4.4	-58.1
-3.1	3	38	28	5	16.8	-2.6	1.0	15.4	30.6	-53.4
-3.3	17	36	26	48	8.2	-2.0	2.5	-9.0	-0.3	-59.0
-3.7	48	8	17	41	-9.0	13.8	8.2	-3.7	9.3	-57.3
-3.8	15	4	33	25	9.3	16.1	-1.2	3.1	27.3	-54.0
-4.0	14	15	17	3	9.7	9.3	8.2	16.8	44.0	-51.0
-4.8	35	8	48	44	-1.8	13.8	-9.0	-4.8	-1.8	-59.2
-5.0	41	7	30	24	-3.7	14.2	0.2	3.6	14.3	-56.4
-5.9	24	20	11	40	3.6	6.4	11.7	-3.3	18.4	-55.6
-6.5	40	6	40	36	-3.3	14.7	-3.3	-2.0	6.1	-57.8
-9.0	23	15	46	21	4.1	9.3	-5.9	5.7	13.2	-56.6
-11.2	17	8	49	17	8.2	13.8	-11.2	8.2	19.0	-55.5
-12.3	42	43	37	20	-3.8	-4.0	-2.4	6.4	-3.8	-59.6

For instance, the prediction of interaction energies may deviate from the actual if the electronic effects exerted by the substituent at different positions are significantly different or significant steric influence arises due to the occupancy of substituents at adjacent positions. To verify this feature, E_{int} values of 12 phenanthroline derivatives given in Figure 3.7 have been calculated and compared with the predicted E_{int} using $E_{int\text{-}Eq.\ 3.4}$ and $E_{int\text{-}Eq.\ 3.6}$ and the data are depicted in Table 3.5. In general, majority of the systems obey the additivity rule to a great extend while significant deviation occurs for systems showing the steric effect such as 3, 4-7, 8-$(OMe)_4$-phen) and 3, 4-$(OMe)_2$-phen).

Table 3.5 Calculated E_{int} values of 12 representative phenanthroline derivatives along with the E_{int} values predicted using Eq. 3.4 and Eq. 3.6 Values in kcal/mol.

Complexes	E_{int}	$E_{int\text{-}Eq.\ 3.4}$	$E_{int\text{-}Eq.\ 3.6}$
[Mo $(CO)_4$(3-CHO-phen)]	-56.4	-56.4	-56.5
[Mo $(CO)_4$(4-OH-phen)]	-59.2	-59.3	-59.8
[Mo $(CO)_4$(5-CH=CH_2-phen)]	-61.0	-58.7	-58.8
[Mo $(CO)_4$(2-NH_2-phen)]	-59.1	-60.5	-60.7
[Mo $(CO)_4$(4-CN-phen)]	-57.3	-55.7	-55.3
[Mo $(CO)_4$(5,6-$(CN)_2$-phen)]	-54.5	-52.5	-53.1
[Mo $(CO)_4$(4,7-NO_2,NH_2-phen)]	-55.3	-56.7	-55.5
[Mo $(CO)_4$(3,8-CN,OMe-phen)]	-54.4	-56.6	-56.9
[Mo $(CO)_4$(3,8-$(NH_2)_2$-phen)]	-60.5	-62.1	-60.5
[Mo $(CO)_4$(3,4-7,8-$(OMe)_4$-phen)]	-55.1	-62.5	-60.7
[Mo $(CO)_4$(2,9-$(NH_2)_2$-phen)]	-58.0	-62.2	-62.3
[Mo $(CO)_4$(3,4-$(OMe)_2$-phen)]	-54.1	-60.7	-60.0

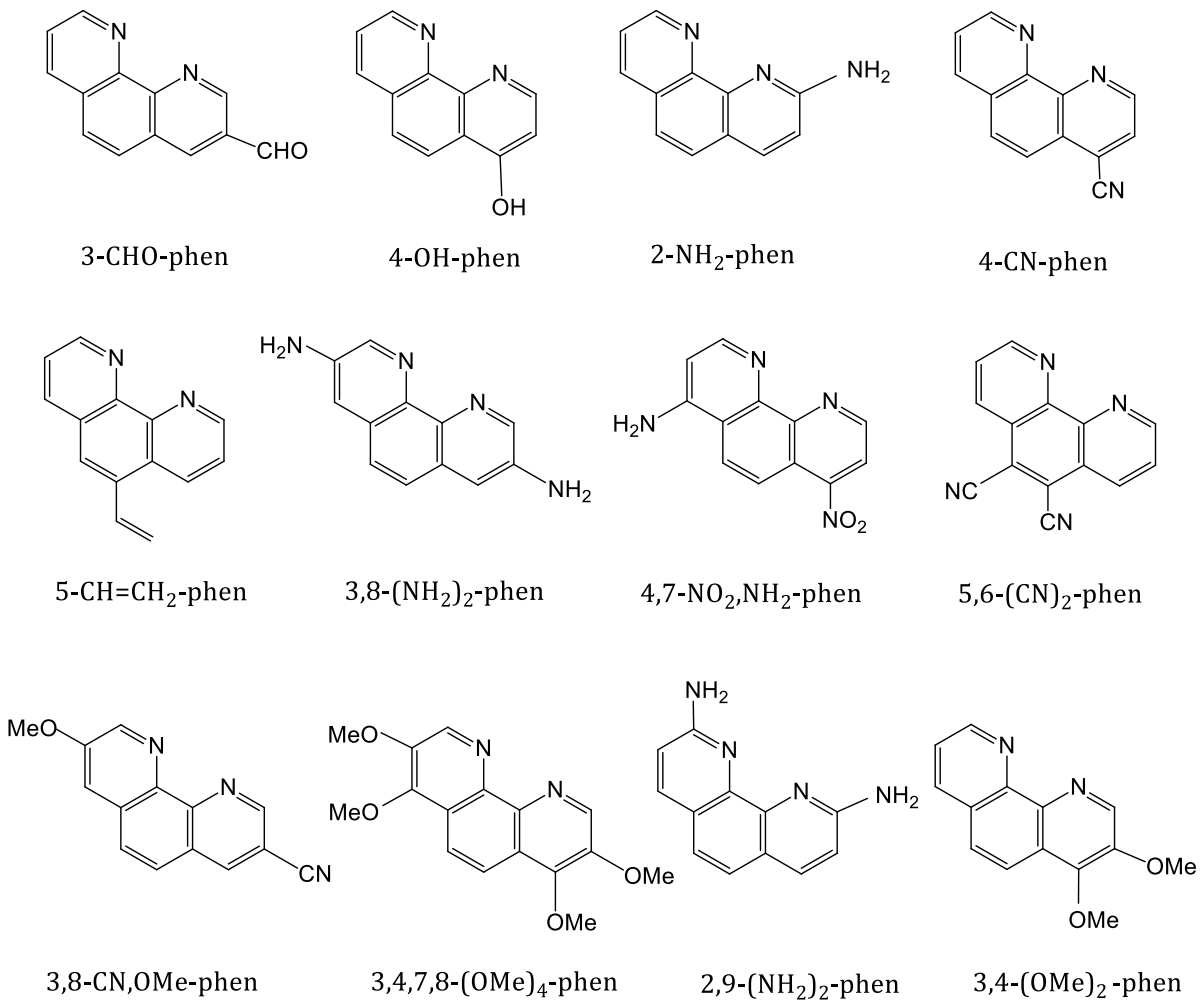

Figure 3.7 Twelve phenanthroline derivatives for comparing the predicted E_{int} with calculated E_{int} values.

3.5 Conclusions

Quantum-chemical methods and molecular modelling techniques enable the accurate description of a large number of molecular properties and effective utilization of them leads to the understanding of primitive patterns of molecular reactivity.[49,50] Here MESP, an electronic property of the molecular system is utilized to follow the electron rich/deficient character of the lone pair bearing nitrogen centers in substituted 1,10-phenanthroline systems. The primitive pattern of molecular reactivity is evident in MESP as it identifies a more electron rich nitrogen center from an electron deficient one and interpret the higher binding affinity of the former with $Mo(CO)_4$ solely based on the MESP

parameter V_N. The electron donation from the phenanthroline ligands to metal center can be correlated to the increase in negative character of MESP observed at CO ligands or to the decrease in CO stretching frequency. The MESP based quantification and classification of substituent effects deduced for simple benzene systems are found to be applicable for the 1,10-phenantrholine ligands which indicates that substituent effects obey the transferability property. The binding energy between the ligand and $Mo(CO)_4$ is highly predictable from the knowledge of total substituent effect experienced by the ligands which supports the additivity property of substituent effects. The MESP analysis is also shown as a general approach to fine tune the electronic properties of 1,10-phenanthroline ligands to achieve the highest coordination power of the ligand towards a transition metal center.

Part B. Substituent Effect Parameters: Extending the Applications to Organometallic Chemistry

3.6 Abstract

Typically metal complexes are constituted of an acceptor metal ion and one or more ligands containing the donor atoms. Accordingly, the properties of a metal complex are equally dependent on the nature of the metal ion and the ligands. Minute structural variations in the ligand will result in linear changes in the respective energetic parameters and such linear relationships have paramount importance in organometallic chemistry. The variation in ligands is virtually limitless and substantial because of the extent of organic chemistry available for the modelling of desirable ligands, apart from the variation in metal ions. Anyhow, there is still a need of new parameters for the design and quantification of new ligands which in turn leads to synthesis of metal complexes with possibly predictable chemical properties. Previous studies have demonstrated that quantum chemically derived MESP parameters can be listed as one of the superior quantifiers in this regard, which can act as an effective ligand electronic parameters. The interaction between the ligand part and metal containing part will be crucial in assessing the reactivity of organometallic complexes. Here, we are applying MESP based substituent constants derived from substituted benzenes to forecast the interaction energies in three different set of metal carbonyls, such as (pyr*)$W(CO)_5$, (NHC*)$Mo(CO)_5$ and (η^6-arene*)$Cr(CO)_3$. Ligands and metal ions are varied in each case for better understanding and transparency.

3.7 Introduction

Transition metal carbonyl complexes are considered as the foundation stones of modern coordination chemistry and organometallic chemistry and are employed as typical models for studying metal-ligand interactions.[51-54] They have widespread roles in the field of catalysis and synthesis, as carbon monoxide activation and reduction by transition-metal atoms are critical aspects.[55-57] Carbon monoxide is a π-acceptor ligand,

which makes it capable to stabilize the zero oxidation state of metals in carbonyl complexes.[58,59] The reactivities and characterization of metal carbonyls are well explored[60-62] after the first report of $Ni(CO)_4$ in 1890.[63] Quantum chemically derived models, especially DFT methods have expanded over the years in successfully updating the bonding models in transition-metal complexes with high accuracy.[64-66] Dewar-Chatt-Duncanson model is the typical model that elucidates the ligand to metal σ-donation and metal to ligand π-back-donation in transition-metal complexes.[67,68] Later, it has been shown that, in transition-metal carbonyl complexes, metal to CO π-back-donation is more significant than CO to metal σ-donation for assessing the binding energies.[69] Usually, transition-metal carbonyls have CO stretching frequencies less than 2143 cm^{-1} (value for free CO) and this can be explained by the metal to CO π-back donation.[70]

Here, our prime interest is to look at the interaction between different functionalities of conventional ligands in literature with the metal carbonyls like $W(CO)_5$, $Mo(CO)_5$, and $Cr(CO)_3$. The ligands selected are pyridine, N-heterocyclic carbenes (NHC) and η^6-arene. The electron donating/withdrawing profile of the axial ligands may act as a determining factor in predicting the reactivity of organometallic complexes.[71,72] The efficiency of ligands is attributed to the variation in electronic and steric properties and the bonding interactions between the ligands and metal carbonyls are well interpreted in terms of ligand electronic parameters.[73] IR spectroscopy is widely used for the characterization of metal carbonyls.[74] MESP parameters can also give an insight about the stereoelectronic properties of various ligands in assorted organometallic systems.[75,76]

Pyridine is a versatile heterocycle, and its nitrogen lone pair in the aromatic environment provides two-electron donor character for forming coordination bonds with transition metals. This and associated ligands are widely used in the development of homogeneous catalysts as the reactivity of the metal within the complex can be controlled by the nature of the coordination bond.[77,78] Earlier, there were attempts to estimate the metal-ligand electron transfer for a series of square-planar Rh and Ir complexes containing pyridine ligands using Hammett constants and ^{13}C NMR values.[79]

The distinct reactivity of pyridine containing ligands contributed well in the architecture of various organo-transition metal complexes, such as pincer systems.[80,81]

The chemistry of NHCs[82] has recorded a tremendous growth in the last two decades due to the versatile nature of this ligands in developing robust organometallic systems for catalytic applications.[83,84] The NHC ligands were utilized as better replacement for phosphine ligands in many of the organometallic reactions as they form stronger bonds with low and high valent transition metals, and lanthanides.[85,86] The ease of preparation and the robust metal- ligand bonds made the chemistry of transition metal-NHC complexes momentous.[87,88] Various ligand electronic parameters were described for NHC ligands, such as Lever electronic parameter (LEP),[89] Tolman electronic parameter(TEP),[90] Local TEP (LTEP),[91] MESP[92] *etc*. The stereoelectronic properties and reactivity of NHC ligands have been extensively evaluated by Huynh and co-workers by proposing a choice of experimental methodologies.[93] Huynh group introduced an electronic descriptor called Huynh electronic parameter (HEP) collectively for a group of bidentate ligands including NHCs, based on ^{13}C NMR spectroscopy.[94-96] The electron-donating power associated with N-heterocyclic carbenes is also assessed with MESP topological features such as MESP at the carbene nucleus, V_C and MESP minimum at the carbene lone pair region, $V_{min.}$[24]

The arene – chromium tricarbonyl complexes were first reported in 1958,[97] and their specific reactivity towards nucleophiles is featured by the electron density transfer from the aromatic ring to the metal fragment.[98,99] The arene complexes of transition metals can act as efficient catalysts, reagents, and intermediates in organic synthesis.[100,101] Previously, Suresh *et al*. verified the structure and reactivity of substituted arenes in (η^6-arene)$Cr(CO)_3$ complexes using MESP analysis.[102] The present study aiming at quantifying the reactivity patterns of different metal carbonyl systems using MESP and TEP. The findings can serve as a connecting factor between substituent organic chemistry and transition metal chemistry.

3.8 Computational Methodology

All the computational calculations have been performed with density functional theory (DFT) using Gaussian 16 suite of programmes.[103] All the ligands and complexes are optimized using the DFT method B3LYP/BS1 wherein BS1 stands for a mixed basis set, *viz*. QZVP for Cr, Mo and W and 6-311+G(d, p) for the rest. Previous studies have shown that B3LYP method is reliable to evaluate substituent effects and structure activity relationships.[16,104] Stretching frequencies of CO ligand in the carbene-metal complexes are obtained from the frequency calculations.

3.9 Results and Discussion

3.9.1 Substituent Effects

Table 3.6 The selected substituents and the corresponding ΔV_C values

substituent	category	ΔV_C	substituent	category	ΔV_C
NO_2	$S^{<<<}$	21.2	$OCH{=}CH_2$	$S^{<}$	0.7
CN	$S^{<<<}$	18.0	$SiMe_3$	$S^{>}$	-0.9
SiF_3	$S^{<<<}$	16.1	$CH_2\text{-}CH{=}CH_2$	$S^{>}$	-1.6
NC	$S^{<<}$	14.3	OH	$S^{>}$	-2.0
CF_3	$S^{<<}$	13.7	CH_2NMe_2	$S^{>}$	-2.6
$NHNO_2$	$S^{<<}$	11.0	Me	$S^{>>}$	-3.3
COOH	$S^{<<}$	10.9	Et	$S^{>>}$	-4.0
OCF_3	$S^{<<}$	8.3	OMe	$S^{>>}$	-5.0
$CONH_2$	$S^{<<}$	8.1	$OCHMe_2$	$S^{>>}$	-6.5
NHCN	$S^{<<}$	5.9	NH_2	$S^{>>>}$	-9.0
SiH_3	$S^{<}$	3.5	NHMe	$S^{>>>}$	11.2
PH_2	$S^{<}$	4.0	NMe_2	$S^{>>>}$	12.3
CH_2F	$S^{<}$	1.8			

Previously, it was shown that the substituent effect data deduced for substituted benzenes is transferable for predicting the binding patterns of substituted 1, 10-phenanthroline ligands in molybdenum carbonyl complexes.[104] For the present study, twenty five substituents from the substituent database given in our previous study are selected.[16] The substituents, the sub-categories and the corresponding ΔV_C values are given in Table 3.6. The wide applicability of the organic substituent effects in the field of transition metal chemistry may furnish a priori prediction on the chemical reactivity of the complexes. The organometallic systems selected are (pyr*)$W(CO)_5$, (NHC*)$Mo(CO)_5$ and (η^6-arene*)$Cr(CO)_3$ and this selection will allow us to study the binding patterns of ligands given in Scheme 3.1 such as pyridine, NHC and η^6-benzene with the third, second and first row transition metal carbonyls. The reactivity of these specific complexes is also evaluated by studying their decarbonylation reaction. For the reaction given in Eq. 3.8, the interaction energy (E_{int}) of the metal carbonyl with the ligand is calculated as per Eq. 3.9.

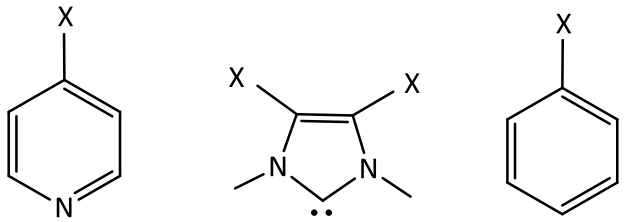

(a) (b) (c)

Scheme 3.1 Modification of ligands, where X denotes the substituent. Substituted arene ligands are used for η^6 coordination.

$$L^* + M(CO)_n \longrightarrow L^*M(CO)_n \qquad \text{(Eq. 3.8)}$$

$$E_{int} = E_3 - (E_1 + E_2) \qquad \text{(Eq. 3.9)}$$

where E_1, E_2, and E_3 correspond to the total energies of ligand, metal carbonyl fragment and metal carbonyl complex, respectively. In the same manner, for the reaction given in Eq. 3.10, the decarbonylation energies are calculated using Eq. 3.11.

$$L^*M(CO)_n \longrightarrow L^*M(CO)_{n-1} + CO \qquad \text{(Eq. 3.10)}$$

$$E_{dc} = (E_4 + E_5) - E_3 \quad \text{(Eq. 3.11)}$$

where E_4 and E_5 are the total energies of $L^*M(CO)_{n-1}$ and CO ligand, respectively.

3.9.2 (pyr*)W(CO)$_5$ Complexes

The electron richness over the substituted pyridine ligands is assessed with the help of MESP critical values observed at the nitrogen lone pair region. For pyridine, MESP V_{min} value is -61.9 kcal/mol and with substitution, V_{min} shows a wide range of values from -47.7 to -71.7 kcal/mol. The MESP plots for the representative para substituted pyridine ligands *viz*. pyr-NO_2, and pyr-NMe_2 are given in Figure 3.8 which clearly shows the strongly withdrawing character of NO_2 and strongly donating character of NMe_2. The ΔV_{min} values are proposed to depict the change in MESP with respect to unsubstituted pyridine ligand as per Eq. 3.12.

$$\Delta V_{min(pyr)} = V_{min}(pyr^*) - V_{min}(pyr) \quad \text{(Eq. 3.12)}$$

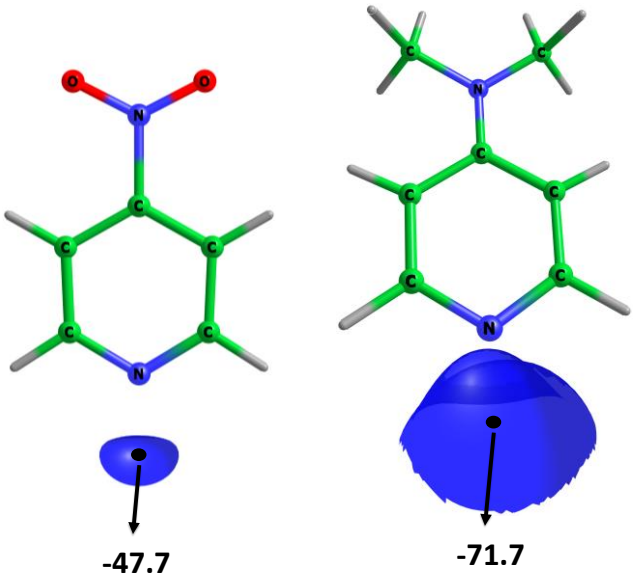

pyr-NO_2 pyr-NMe_2

Figure 3.8 MESP plots of V_{min} (black dots on the surface) on nitrogen centers shown with 31.0 kcal/mol isosurfaces of pyr-NO_2 and pyr-NMe_2.

Table 3.7 The MESP $\Delta V_{min(pyr)}$, E_{int}, E_{dc} and TEP values of (pyr*)$W(CO)_5$ complexes. TEP in cm^{-1} and all other values in kcal/mol.

substituent	$\Delta V_{min(pyr)}$	E_{int}	E_{dc}	TEP
NO_2	14.2	-27.6	37.6	2131.0
CN	12.9	-27.9	37.7	2131.4
SiF_3	11.4	-28.4	37.7	2131.7
NC	10.5	-28.3	37.7	2131.3
CF_3	10.2	-28.3	37.9	2132.1
$NHNO_2$	7.2	-29.3	37.3	2130.7
COOH	6.6	-29.4	37.5	2130.7
OCF_3	6.8	-29.0	37.4	2131.7
$CONH_2$	5.3	-29.7	37.4	2130.6
NHCN	5.0	-29.6	37.0	2130.9
SiH_3	1.9	-30.5	37.4	2130.2
PH_2	1.0	-30.7	37.1	2130.0
CH_2F	1.7	-30.4	37.3	2130.7
$OCH=CH_2$	0.1	-30.8	36.7	2130.1
$SiMe_3$	-1.7	-31.5	37.1	2129.4
CH_2-$CH=CH_2$	-1.5	-31.3	37.0	2129.8
OH	-1.3	-31.0	36.6	2130.3
CH_2NMe_2	-2.7	-31.6	37.0	2129.6
Me	-2.3	-31.4	37.0	2129.9
Et	-2.9	-31.6	36.9	2129.7
OMe	-3.5	-31.7	36.3	2129.6
$OCHMe_2$	-4.8	-32.2	36.1	2129.2
NH_2	-6.8	-32.9	35.5	2128.6
NHMe	-9.2	-33.7	35.2	2128.0
NMe_2	-9.8	-34.0	35.1	2127.6

The $\Delta V_{min(pyr)}$, E_{int} for the complexation between pyr* and $W(CO)_5$, E_{dc} and Tolman electronic parameter (TEP) for (pyr*)$W(CO)_5$ are depicted in Table 3.7. Though all pyridine ligands are two electron donors, the value of $\Delta V_{min(pyr)}$ give a direct assessment of the influence of substituent on their donating power. The $\Delta V_{min(pyr)}$ shows a strong linear correlation with E_{int} (Figure 3.9a) which indicates that the strength of the coordination bond formed by $W(CO)_5$ with pyridine ligands can be directly assessed from the V_{min} of nitrogen lone pair. In Tolman analysis, the focus is on understanding the variation in CO stretching frequency of the full complex (pyr*)$W(CO)_5$ due to change in ligand environment. A more electron-donating pyr* can lower the frequency due to the π-back-donation from the filled metal d orbitals into the low-lying antibonding π* CO orbital. The TEP is observed in a narrow range 2131 to 2127 cm^{-1} and can be considered as a less sensitive property than MESP to estimate the ligand effects. Obviously $\Delta V_{min(pyr)}$ – a measure of the ligand's donating power – is directly proportional to TEP. TEP is not a property of the pyr* ligand as it measures indirectly the influence of that ligand on other ligands in the complex.

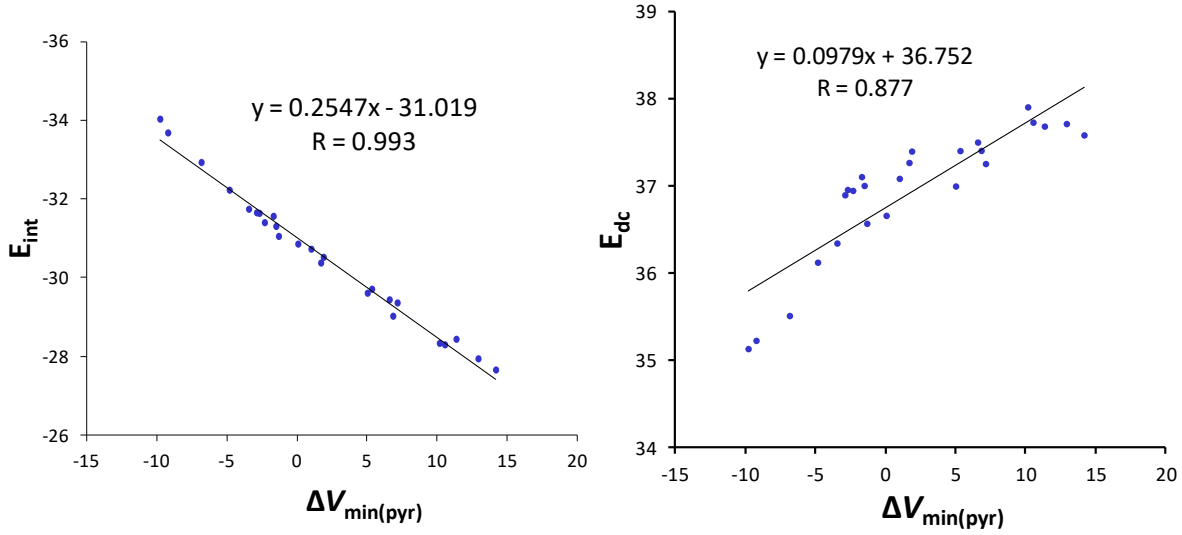

(a) (b)

Figure 3.9 Correlation of $\Delta V_{min(pyr)}$ against (a) E_{int} and (b) E_{dc} for (pyr*)$W(CO)_5$ complexes. Values in kcal/mol.

The $\Delta V_{min(pyr)}$ characterizes a pyr* ligand and empowers us with a powerful prediction on the interactive behavior of it with $W(CO)_5$. Even the change in TEP can be justified from an analysis of this property. The MESP analysis predicts the ligand effects before the complex formation while TEP predicts these effects after the complex formation. In order to further check the validity of $\Delta V_{min(pyr)}$ parameter in deducing the reactivity of metal carbonyls, the energy of decarbonylation reaction as per Eq. 3.10 and Eq. 3.11 is taken as the reactivity descriptor (E_{dc}). The E_{dc} values fall in a narrow range 37.6 to 35.1 kcal/mol for pyridine ligands and $\Delta V_{min(pyr)}$ correlates well with E_{dc}. This correlation strongly suggests the sensitive character of MESP to even distinguish the subtle variation in the chemical reactivity due to a remote substituent effect on a pyridine ligand (Figure 3.10b).

3.9.3 (NHC*)Mo(CO)$_5$ Complexes

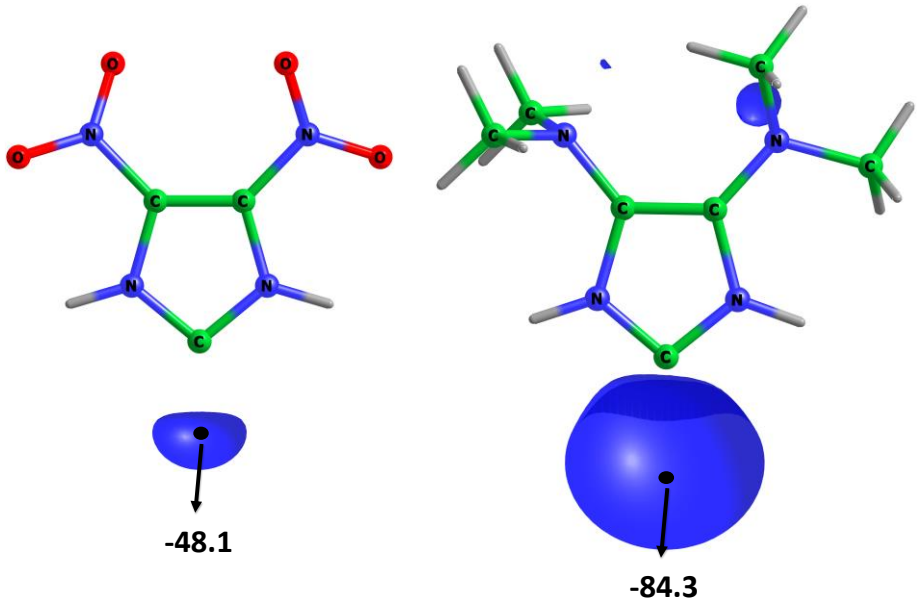

NHC-NO_2 NHC-NMe_2

Figure 3.10 MESP isosurface plot of value -31.0 kcal/mol, embedded with V_{min} (black dot in the surface) for N-heterocyclic carbenes.

The MESP properties of representative substituted NHC ligands NHC-NO_2 and NHC-NMe_2 are given in Figure 3.10. The NHC ligands are found to be more electron rich compared to the corresponding pyridine derivatives.

Table 3.8 The MESP properties of the ligands, E_{int} and TEP values of $(NHC^*)Mo(CO)_5$ complexes. TEP in cm^{-1} and other values in kcal/mol.

substituent	$\Delta V_{min(NHC)}$	E_{int}	E_{dc}	TEP
NO_2	31.0	-39.6	35.7	2135.7
CN	28.3	-39.7	35.6	2134.2
SiF_3	22.5	-41.4	35.6	2132.2
NC	24.0	-40.7	35.4	2132.3
CF_3	20.5	-41.3	35.5	2132.7
$NHNO_2$	17.6	-42.2	35.1	2131.0
COOH	12.7	-43.1	35.6	2130.5
OCF_3	16.4	-42.3	35.3	2130.9
$CONH_2$	10.9	-43.8	35.0	2129.7
NHCN	15.9	-42.1	35.0	2130.5
SiH_3	4.8	-45.4	35.1	2126.0
PH_2	4.2	-45.3	35.1	2126.4
CH_2F	7.3	-44.5	35.0	2128.5
$OCH=CH_2$	4.9	-45.1	34.8	2126.6
$SiMe_3$	-2.0	-47.5	34.9	2123.1
CH_2-CH=CH_2	-3.0	-47.3	34.8	2124.0
OH	1.3	-45.8	34.6	2126.2
CH_2NMe_2	-3.5	-47.6	34.9	2123.5
Me	-4.3	-47.6	34.8	2124.1
Et	-4.5	-47.8	34.7	2123.7
OMe	-0.8	-46.6	34.8	2125.0
$OCHMe_2$	-2.8	-47.3	34.6	2123.8
NH_2	-4.8	-47.5	34.6	2124.2
NHMe	-5.1	-47.8	34.7	2123.6
NMe_2	-5.2	-48.2	34.2	2122.4

$$\Delta V_{min(NHC)} = V_{min}(NHC^*) - V_{min}(NHC) \qquad \text{(Eq. 3.13)}$$

It may be attributed to the advantages of the NHC functionality and also due to doubling the substitution effect. For the unsubstituted NHC ligand, the MESP V_{min} value is -79.1 kcal/mol and on substitution, the values cover a range -48.1 to -84.3 kcal/mol. The ΔV_{min} accounts for the change in MESP with respect to the unsubstituted NHC moiety (Eq. 3.13). The MESP $\Delta V_{min(NHC)}$, E_{int}, E_{dc} and Tolman parameter of the complexes are depicted in Table 3.8. The $\Delta V_{min(NHC)}$ correlates strongly with E_{int} of NHC ligands (Figure 3.11a). The difference between the highest and lowest E_{dc} is only 1.5 kcal/mol and even for this narrow range, $\Delta V_{min(NHC)}$ shows a significant correlation with E_{dc} (Figure 3.11b). The correlation plots hold good for the whole range of substituents ranging from $S^{<<<}$ (strong electron withdrawing) to $S^{>>>}$ (strong electron donating) category. The TEP for the CO stretching is observed in the range 2122 to 2135 cm^{-1}. Compared the pyridine complexes, increasing trend in CO stretching is more pronounced in NHC complexes which can be attributed to the inherent higher electron donating power of the NHC ligands. The TEP increases with increase in $|E_{int}|$.

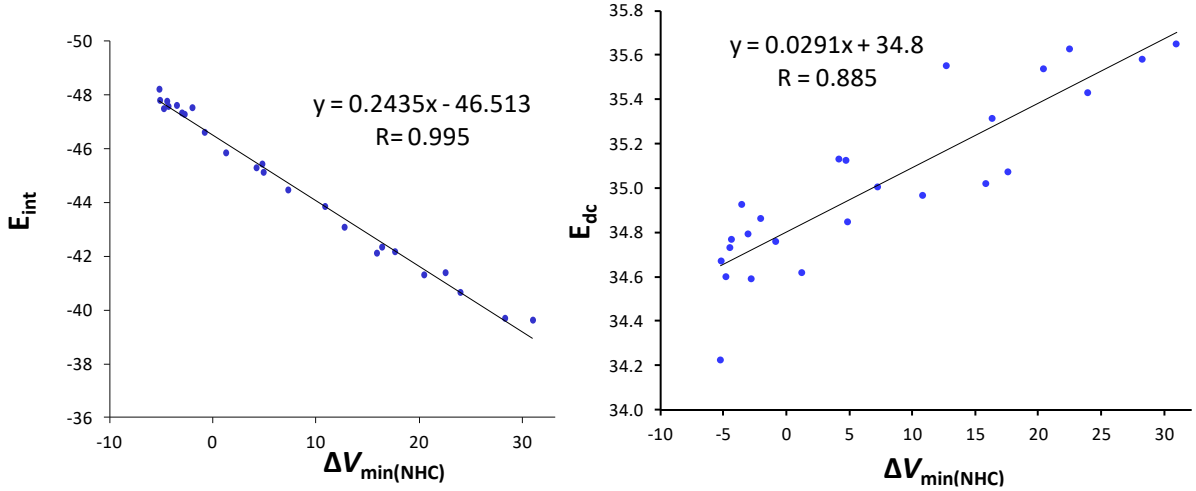

(a) (b)

Figure 3. 11 Correlation of (a) $\Delta V_{min(NHC)}$ against E_{int} and (b) E_{dc} for $(NHC^*)Mo(CO)_5$ complexes. Values in kcal/mol.

3.9.4 (η^6-arene*)$Cr(CO)_3$ Complexes

In the previous sections, the binding patterns between a specific ligand center and a metal fragment is discussed and quantified. It would be interesting if the binding and decarbonylation energies can be predicted for a different type of coordination, such as η^6. Here, the MESP V_{min} of benzene and a substituted benzene ($\Delta V_{min(arene)}$) can be compared (Eq. 3.14) to understand the substituent effect.

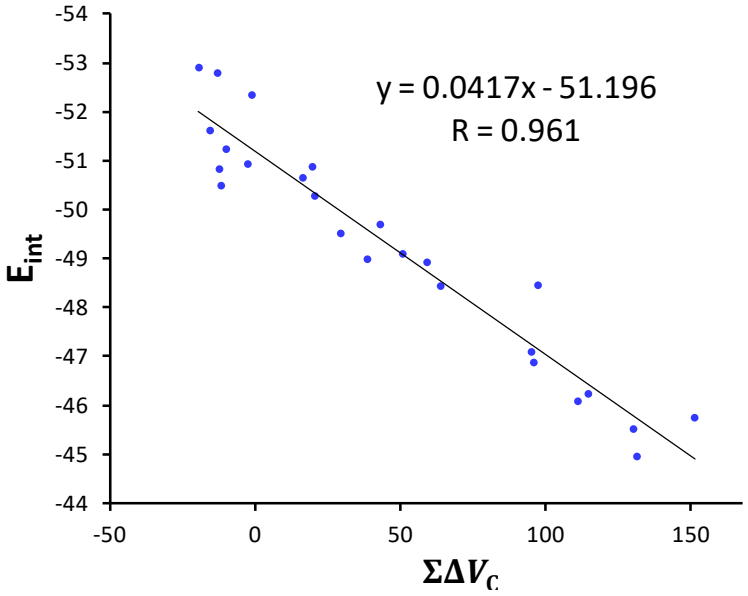

Fig. 3.12 Correlation between $\Sigma\Delta V_C$ and E_{int} for (η^6-arene*)$Cr(CO)_3$ complexes . Values in kcal/mol.

$$\Delta V_{min(arene)} = V_{min}(arene^*) - V_{min}(arene) \qquad \text{(Eq. 3.14)}$$

Since all the carbon atoms are directly involved in the coordination, the change in MESP at the nucleus of the six carbon atoms of the substituted benzene with respect to the six carbon atoms of reference benzene ($\Sigma\Delta V_C$) can also be taken as a response parameter to understand the variation in interaction energies. The $\Delta V_{min(arene)}$, $\Sigma\Delta V_C$, E_{int}, E_{dc} and TEP values of the (η^6-arene*)$Cr(CO)_3$ complexes are given in Table 3.9. Compared to $\Delta V_{min(arene)}$, $\Sigma\Delta V_C$ shows a stronger correlation with E_{int} (Figure 3.12) indicating that the influence of substituent on all the carbon atoms can be accurately represented by $\Sigma\Delta V_C$ for describing the η^6 coordination behavior of substituted arenes.

Table 3.9 The MESP $\Delta V_{min(arene)}$, $\Sigma\Delta V_C$, E_{int}, E_{dc} and TEP values of (η^6-arene*)$Cr(CO)_3$ complexes. TEP in cm^{-1} and all other values in kcal/mol.

substituent	$\Delta V_{min(arene)}$	$\Sigma\Delta V_C$	E_{int}	E_{dc}	TEP
NO_2	-	151.2	-45.8	43.6	2071.3
CN	13.6	130.2	-45.5	44.0	2065.5
SiF_3	11.7	97.3	-48.5	43.2	2066.0
NC	11.6	131.4	-45.0	44.3	2060.9
CF_3	10.2	95.8	-46.9	44.2	2064.4
$NHNO_2$	10.2	111.0	-46.1	45.3	2054.4
COOH	7.4	63.7	-48.4	44.8	2061.5
OCF_3	7.9	114.6	-46.2	44.0	2058.5
$CONH_2$	6.7	50.7	-49.1	44.7	2053.7
NHCN	6.7	95.0	-47.1	45.2	2052.1
SiH_3	2.5	16.3	-50.7	45.3	2050.2
PH_2	3.0	29.3	-49.5	45.8	2046.4
CH_2F	2.3	38.5	-49.0	45.8	2050.2
$OCH=CH_2$	1.8	59.1	-48.9	45.9	2047.6
$SiMe_3$	-0.6	-15.7	-51.6	45.9	2043.0
CH_2-$CH=CH_2$	-0.4	-2.7	-50.9	46.1	2044.8
OH	-0.4	42.9	-49.7	45.8	2048.1
CH_2NMe_2	-1.3	-12.5	-50.8	46.1	2043.8
Me	-1.7	-10.1	-51.2	46.3	2044.8
Et	-1.7	-11.9	-50.5	46.0	2043.1
OMe	-2.0	20.4	-50.3	46.1	2044.2
$OCHMe_2$	-3.1	19.6	-50.9	46.2	2041.3
NH_2	-5.6	-1.3	-52.4	46.1	2039.1
NHMe	-6.9	-13.1	-52.8	46.6	2035.7
NMe_2	-7.3	-19.5	-52.9	46.4	2032.5

The influence of substituent on E_{dc} parameter is very small as its range is 3.2 kcal/mol. The positive $\Delta V_{min(arene)}$ and $\Sigma\Delta V_C$ show the electron withdrawing effect of the substituents, while their negative values indicate the donating effect of the substituents. In general, when the electron donating substituent effect increases, the interactive behavior of the arene ring with Cr center increases. In such cases, an increasing trend in E_{dc} occurs.

3.9.5 Comparison of Ligand Effect in Group VI Metal Carbonyls

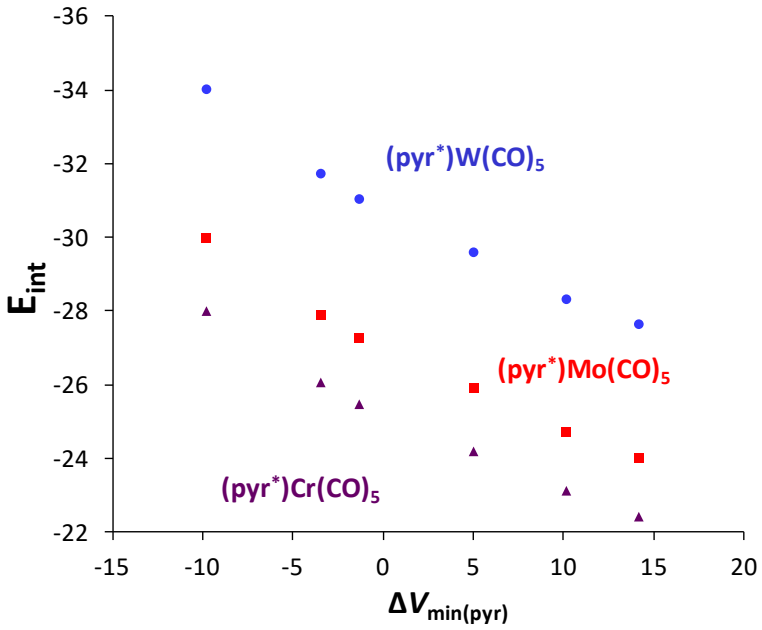

Figure 3.13 Correlation of $\Delta V_{min(pyr)}$ against E_{int} (kcal/mol) for (pyr*)$W(CO)_5$, (pyr*)$Mo(CO)_5$ and (pyr*)$Cr(CO)_5$ complexes.

The trend in reactivity when the metal center is changed for a specific ligand is analyzed using the MESP approach. The analysis is done by comparing the E_{int} of a selected set of (pyr*)$W(CO)_5$ complexes with the corresponding group VI metal carbonyls, *viz.* (pyr*)$Mo(CO)_5$ and (pyr*)$Cr(CO)_5$. Figure 3.13 shows the change in E_{int} with respect to the change in ΔV_{min}. The three series of complexes show similar increasing trend in $|E_{int}|$ with increase in the electron donation effect of the ligand. The ligand is significantly more interacting with W compared to Mo and Cr. In other words, the electron accepting power of the metal centers can be interpreted as W >> Mo > Cr. For the same pyr* ligand, the

interaction energy varies ~4 kcal/mol between W and Mo complexes and ~2.0 kcal/mol between Mo and Cr complexes. Although a pyr* ligand has a certain in-built power to acts as a two electron donor to a metal center, the strength of electron donation from the ligand to the metal or the strength of the resulting coordination bond also depends on the electron accepting power of the metal center. A periodic increasing trend is the characteristic of such interaction along Cr, Mo and W complexes.

3.9.6 Transferability Property of Substituent Effect

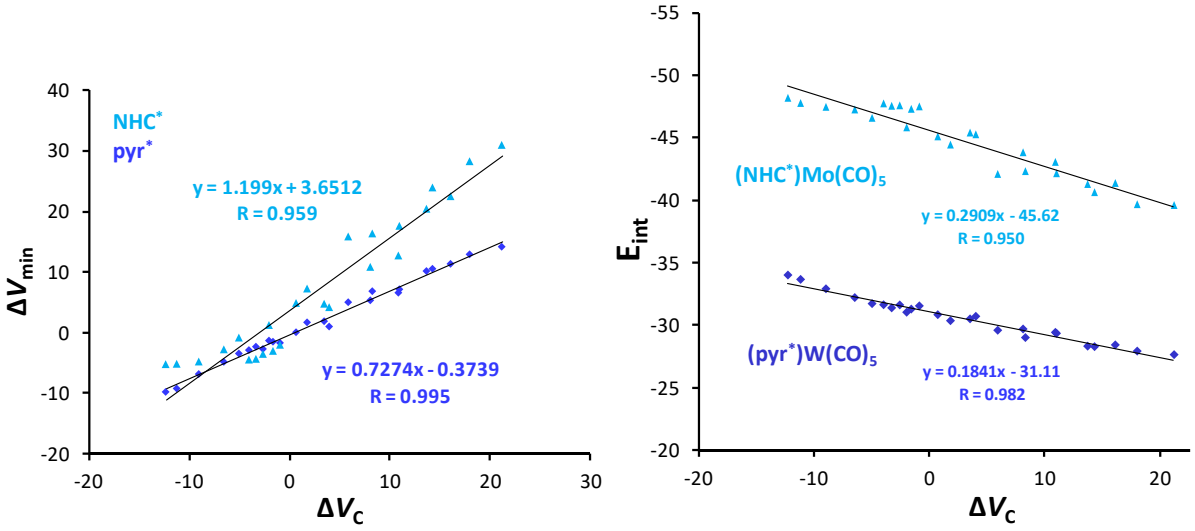

(a) (b)

Figure 3.14 Correlation of ΔV_C values against (a) ΔV_{min} values of pyr* and NHC* ligands and (b) E_{int} for $(pyr^*)W(CO)_5$ and $(NHC^*)Mo(CO)_5$ complexes. Values in kcal/mol.

Previous studies have shown that the substituent effect parameter deduced using benzene derivatives (ΔV_C) can be used for interpreting and quantifying such an effect in many other π-conjugated systems.[16] The transferability property of the substituent effect is revealed in that study. Invoking this property, one may argue that ΔV_C is sufficient enough to describe the electron donating property of pyridine and NHC ligands. The correlation plots of ΔV_C versus ΔV_{min} of pyr* and NHC* ligands given in Figure 3.14a clearly suggests the influence of substituent is similar in all. The slope 1.199 observed for NHC* indicates that the substituent effect is more expressed on the NHC framework than benzene while the slope 0.7274 obtained for pyr* suggests that the influence is higher on

a pyridine framework than benzene. Thus, a priori prediction on the reactivity patterns of metal carbonyl complexes with various substituted ligands can be achieved by interpreting the substituent effect in terms of ΔV_C parameter (Figure 3.14b).

3.10 Conclusions

The MESP based substituent constants proposed instead of Hammett constants in organic chemistry have been successfully applied in understanding the reactivity patterns of various metal carbonyls. Ligands such as pyridine, NHC and η^6-arene are used to interpret their binding with the first, second and third row transition metal carbonyl fragments. For $(pyr^*)W(CO)_5$ and $(NHC^*)Mo(CO)_5$, the interpretation of E_{int} is possible by knowing the electron donation ability of pyr^* and NHC^* ligands, which can be easily monitored by the MESP V_{min} at the electron rich centers. In an analogous approach, the E_{dc} values are also gauged using $\Delta V_{min(pyr)}$ and $\Delta V_{min(NHC)}$. For the $(\eta^6\text{-arene}^*)Cr(CO)_3$ complexes, a response parameter, $\Sigma\Delta V_C$, which specifies the effect of all the six carbon atoms participating in η^6-coordination is taken for interpreting the reactivity patterns. The TEP parameters are also used along with the MESP features, since it can monitor the change in ligand environment with respect to the variation in CO stretching frequency of the $(L^*)M(CO)_n$ complexes. In order to test the periodic trend in reactivity for a single ligand, the E_{int} values of representative $(pyr^*)W(CO)_5$, $(pyr^*)Mo(CO)_5$ and $(pyr^*)Cr(CO)_5$ complexes are compared. The interaction energies show a parallel trend with respect to MESP $\Delta V_{min(pyr)}$ based on the electron accepting power of W, Mo and Cr centers. The transferability property of substituent effect parameter, ΔV_C is also discussed in a wider outlook for the studied ligands. Since the MESP V_{min} values of the pyr^* and NHC^* ligands are comparable with ΔV_C, the latter can directly be used for the better understanding of reactivity in the corresponding metal carbonyls. Since metal carbonyls may be considered as the model systems for interpreting ligand-metal binding, this strategy can be extended to study the reactivity patterns of an array of transition metal complexes. The study also suggests that the substituent effect observed in organic chemistry can be directly applied on organometallic chemistry of transition metal complexes.

3.11 References

1. G. A. Olah, *Acc. Chem. Res.* **1971**, *4*, 240-248.
2. C. Hansch, A. Leo, S. H. Unger, K. H. Kim, D. Nikaitani and E. J. Lien, *J. Med. Chem.* **1973**, *16*, 1207-1216.
3. P. K. Chattaraj, N. González-Rivas, M. H. Matus and M. Galván, *J. Phys. Chem. A* **2005**, *109*, 5602-5607.
4. H. Kubinyi, in *QSAR: Hansch Analysis and Related Approaches* **2008**, pp. 57-89.
5. L. P. Hammett, *J. Am. Chem. Soc.* **1937**, *59*, 96-103.
6. C. Hansch, A. Leo and R. W. Taft, *Chem. Rev.* **1991**, *91*, 165-195.
7. L. R. Domingo, P. Perez and R. Contreras, *J. Org. Chem.* **2003**, *68*, 6060–6062.
8. T. Siodła, W. P. Oziminski, M. Hoffmann, H. Koroniak and T. M. Krygowski, *J. Org. Chem.* **2014**, *79*, 7321–7331.
9. W. L. Jorgensen, *Science* **2004**, *303*, 1813-1818.
10. A. R. Katritzky, V. S. Lobanov and M. Karelson, *Chem. Soc. Rev.* **1995**, *24*, 279-287
11. A. Agresti, R. Bonaccorsi and J. Tomasi, *Theor. Chim. Acta* **1979**, *53*, 215-220.
12. B. Galabov, S. Ilieva and H. F. Schaefer, *J. Org. Chem.* **2006**, *71*, 6382–6387.
13. P. Politzer, J. S. Murray and Z. peralta-Inga, *Int. J. Quantum Chem.* **2001**, *85*, 676–684.
14. C. H. Suresh and S. R. Gadre, *J. Org. Chem.* **1999**, *64*, 2505-2512.
15. S. R. Gadre and C. H. Suresh, *J. Org. Chem.* **1997**, *62*, 2625-2627.
16. G. S. Remya and C. H. Suresh, *Phys. Chem. Chem. Phys.* **2016**, *18*, 20615-20626.
17. P. G. Sammes and G. Yahioglu, *Chem. Soc. Rev.* **1994**, *23*, 327-334.
18. A. Bencini and V. Lippolis, *Coord. Chem. Rev.* **2010**, *254*, 2096-2180.
19. W. R. McWhinnie and J. D. Miller, in *Adv. Inorg. Chem. Radiochem.*, eds. H. J. Emeléus and A. G. Sharpe, Academic Press **1970**, pp. 135-215.
20. S. Bodige and F. M. MacDonnell, *Tetrahedron Lett.* **1997**, *38*, 8159-8160.
21. B. Bosnich and F. Dwyer, *Austr. J.Chem.* **1966**, *19*, 2229-2233.
22. W. W. Brandt, F. P. Dwyer and E. D. Gyarfas, *Chem.Rev.* **1954**, *54*, 959-1017.
23. W. Cabri, I. Candiani, A. Bedeschi and R. Santi, *J. Org. Chem.* **1993**, *58*, 7421-7426.
24. Y. Shen and B. P. Sullivan, *Inorg. Chem.* **1995**, *34*, 6235-6236.

25. G. F. Smith and W. H. McCurdy, *Analyt.Chem.* **1952**, *24*, 371-373.
26. L. A. Summers, in *Advances in Heterocyclic Chemistry*, eds. A. R. Katritzky and A. J. Boulton, Academic Press **1978**, pp. 1-69.
27. G. Chelucci, D. Addis and S. Baldino, *Tetrahedron Lett.* **2007**, *48*, 3359-3362.
28. G. Accorsi, A. Listorti, K. Yoosaf and N. Armaroli, *Chem. Soc. Rev.* **2009**, *38*, 1690-1700.
29. W. W. Brandt, F. P. Dwyer and E. D. Gyarfas, *Chem. Rev.* **1954**, *54*, 959-1017.
30. W. R. McWhinnie and J. D. Miller, in *Ad. Inorg. Chem. Radiochem.*, eds. H. J. Emeléus and A. G. Sharpe, Academic Press **1970**, pp. 135-215.
31. G. A. Ardizzoia, M. Bea, S. Brenna and B. Therrien, *Eur. J. Inorg. Chem.* **2016**, *2016*, 3829-3837.
32. D. S. C. Black and A. J. Hartshorn, *Coord. Chem. Rev.* **1973**, *9*, 219-274.
33. G. Frenking and N. Fro¨hlich, *Chem. Rev.* **2000**, *100*, 717−774.
34. P. L. Damon, C. J. Liss, R. A. Lewis, S. Morochnik, D. E. Szpunar, J. Telser and T. W. Hayton, *Inorg. Chem.* **2015**, *54*, 10081−10095.
35. M. J. Frisch, G. W. Trucks, H. B. Schlegel, G. E. Scuseria, M. A. Robb, J. R. Cheeseman, G. Scalmani, V. Barone, B. Mennucci, G. A. Petersson, H. Nakatsuji, M. Caricato, X. Li, H. P. Hratchian, A. F. Izmaylov, J. Bloino, G. Zheng, J. L. Sonnenberg, M. Hada, M. Ehara, K. Toyota, R. Fukuda, J. Hasegawa, M. Ishida, T. Nakajima, Y. Honda, O. Kitao, H. Nakai, T. Vreven, J. J. A. Montgomery, J. E. Peralta, F. Ogliaro, M. Bearpark, J. J. Heyd, E. Brothers, K. N. Kudin, V. N. Staroverov, T. Keith, R. Kobayashi, J. Normand, K. Raghavachari, A. Rendell, J. C. Burant, S. S. Iyengar, J. Tomasi, M. Cossi, N. Rega, J. M. Millam, M. Klene, J. E. Knox, J. B. Cross, V. Bakken, C. Adamo, J. Jaramillo, R. Gomperts, R. E. Stratmann, O. Yazyev, A. J. Austin, R. Cammi, C. Pomelli, J. W. Ochterski, R. L. Martin, K. Morokuma, V. G. Zakrzewski, G. A. Voth, P. Salvador, J. J. Dannenberg, S. Dapprich, A. D. Daniels, O. Farkas, J. B. Foresman, J. V. Ortiz, J. Cioslowski and and D. J. Fox, *Gaussian 09, Revision D.01,* **2013**, *Gaussian, Inc., Wallingford CT*.
36. T. A. Chohan, J.-J. Chen, H.-Y. Qian, Y.-L. Pana and J.-Z. Chen, *Mol. BioSyst.* **2016**, *12*, 1250-1268.
37. C. F. Matta, *J. Comput. Chem.* **2014**, *35*, 1165-1198.

38. A. Kumar, S. R. Gadre, N. Mohan and C. H. Suresh, *J. Phys. Chem. A* **2014**, *118*, 526-532.
39. C. H. Suresh and S. R. Gadre, *J. Am. Chem. Soc.* **1998**, *120*, 7049-7055.
40. P. K. Sajith and C. H. Suresh, *Inorg. Chem.* **2012**, *51*, 967-977.
41. M. Radoń, *Theor. Chem. Acc.* **2008**, *120*, 337-339.
42. M. P. Mitoraj and A. Michalak, *Inorg. Chem.* **2010**, *49*, 578-582.
43. G. F. Caramori, L. C. Garcia, D. M. Andrada and G. Frenking, *Dalton Trans.* **2014**, *43*, 14710-14719.
44. P. Umadevia and L. Senthilkumar, *RSC Adv.* **2016**, *6*, 38919-38930
45. R. K. Dani Setiawan, Elfi Kraka, and Dieter Cremer, *Inorg. Chem.* **2016**, *55*, 2332-2344.
46. G. A. Ardizzoia and S. Brenna, *Phys. Chem. Chem. Phys.* **2017**, *19*, 5971--5978.
47. C. A. Tolman, *Chem. Rev.* **1977**, *77*, 313-348
48. F. B. Sayyed and C. H. Suresh, *New J. Chem.* **2009**, *33*, 2465-2471.
49. F. Feixas, E. Matito, J. Poater and M. Solà, *Chem. Soc. Rev.* **2015**, *44*, 6434-6451.
50. H. Szatylowicz, T. Siodla, O. A. Stasyuka and T. M. Krygowski, *Phys. Chem. Chem. Phys.* **2016**, *18*, 11711-11721.
51. E. R. Davidson, K. L. Kunze, F. B. C. Machado and S. J. Chakravorty, *Acc. Chem. Res.* **1993**, *26*, 628-635.
52. L. J. Farrugia and C. Evans, *J. Phys. Chem. A* **2005**, *109*, 8834-8848.
53. R. B. King, *Acc. Chem. Res.* **1970**, *3*, 417-427.
54. W. A. Herrmann, *J. Organomet. Chem.* **1990**, *383*, 21-44.
55. L. Weber, *Angew. Chem. Int. Ed.* **1994**, *33*, 1077-1078.
56. M. Zhou, L. Andrews and C. W. Bauschlicher, *Chem. Rev.* **2001**, *101*, 1931-1962.
57. J. E. Ellis, *Organometallics* **2003**, *22*, 3322-3338.
58. V. Bhatt, *Essentials of Coordination Chemistry*, Academic Press **2016**, pp. 191-236.
59. G. Bistoni, S. Rampino, N. Scafuri, G. Ciancaleoni, D. Zuccaccia, L. Belpassi and F. Tarantelli, *Chem. Sci.* **2016**, *7*, 1174-1184.
60. A. Diefenbach, F. M. Bickelhaupt and G. Frenking, *J. Am. Chem.Soc.* **2000**, *122*, 6449-6458.
61. R. K. Hocking and T. W. Hambley, *Organometallics* **2007**, *26*, 2815-2823.

62. E. W. Abel and F. G. A. Stone, *Q. Rev. Chem. Soc.* **1969**, *23*, 325-371.
63. L. Mond, C. Langer and F. Quincke, *J. Chem. Soc,Trans.* **1890**, *57*, 749-753.
64. G. Frenking and N. Fröhlich, *Chem. Rev.* **2000**, *100*, 717-774.
65. T. Ziegler, *Chem. Rev.* **1991**, *91*, 651-667.
66. N. E. Schultz, Y. Zhao and D. G. Truhlar, *J. Phys. Chem. A* **2005**, *109*, 11127-11143.
67. J. Chatt and L. A. Duncanson, *J. Chem. Soc.* **1953**, 2939-2947.
68. A. W. Ehlers, S. Dapprich, S. F. Vyboishchikov and G. Frenking, *Organometallics* **1996**, *15*, 105-117.
69. R. K. Szilagyi and G. Frenking, *Organometallics* **1997**, *16*, 4807-4815.
70. P. K. Hurlburt, J. J. Rack, J. S. Luck, S. F. Dec, J. D. Webb, O. P. Anderson and S. H. Strauss, *J. Am. Chem. Soc.* **1994**, *116*, 10003-10014.
71. C. L. McMullin, N. Fey and J. N. Harvey, *Dalton Trans.* **2014**, *43*, 13545-13556.
72. R. H. Crabtree, *New J. Chem.* **2011**, *35*, 18-23.
73. Y. Canac and C. Lepetit, *Inorg. Chem.* **2017**, *56*, 667-675.
74. C. A. Tolman, *J. Am. Chem. Soc.* **1970**, *92*, 2953–2956.
75. J. Mathew, T. Thomas and C. H. Suresh, *Inorg. Chem.* **2007**, *46*, 10800-10809.
76. M. J. Ajitha and C. H. Suresh, *J. Org. Chem.* **2012**, *77*, 1087–1094.
77. W. Khodja, A. Leclair, J. Rull-Barrull, F. Zammattio, K. V. Kutonova, M. E. Trusova, F.-X. Felpin and M. Rodriguez-Zubiri, *New J. Chem.* **2016**, *40*, 8855-8862.
78. H.-L. Kwong, H.-L. Yeung, C.-T. Yeung, W.-S. Lee, C.-S. Lee and W.-L. Wong, *Coord. Chem. Rev.* **2007**, *251*, 2188-2222.
79. D. Sieh, M. Schlimm, L. Andernach, F. Angersbach, S. Nückel, J. Schöffel, N. Šušnjar and P. Burger, *Eur. J. Inorg. Chem.* **2012**, *2012*, 444-462.
80. J. Cámpora, A. Rodríguez-Delgado and P. Palma, *Pincer Compounds*, Elsevier **2018**, pp. 539-586.
81. E. Peris and R. H. Crabtree, *Chem. Soc. Rev.* **2018**, *47*, 1959-1968.
82. A. J. Arduengo III, R. L. Harlow and M. Kline, *J. Am. Chem. Soc.* **1991**, *113*, 361-363.
83. T. Dröge and F. Glorius, *Angew. Chem. Int. Ed.* **2010**, *49*, 6940-6952.
84. D. J. Nelson and S. P. Nolan, *Chem. Soc. Rev.* **2013**, *42*, 6723-6753.
85. M. N. Hopkinson, C. Richter, M. Schedler and F. Glorius, *Nature* **2014**, *510*, 485-496.

86. H. D. Velazquez and F. Verpoort, *Chem. Soc. Rev.* **2012**, *41*, 7032-7060.
87. H. V. Huynh, T. T. Lam and H. T. T. Luong, *RSC Adv.* **2018**, *8*, 34960-34966.
88. Q. Teng, W. Wu, H. A. Duong and H. V. Huynh, *Chem. Commun.* **2018**, *54*, 6044-6047.
89. A. B. P. Lever, *Inorg. Chem.* **1990**, *29*, 1271-1285.
90. D. G. Gusev, *Organometallics* **2009**, *28*, 6458-6461.
91. D. Setiawan, R. Kalescky, E. Kraka and D. Cremer, *Inorg. Chem.* **2016**, *55*, 2332-2344.
92. J. Mathew and C. H. Suresh, *Inorg.Chem.* **2010**, *49*, 4665-4669.
93. H. V. Huynh, *Chem. Rev.* **2018**, *118*, 9457-9492.
94. H. V. Huynh, Y. Han, R. Jothibasu and J. A. Yang, *Organometallics* **2009**, *28*, 5395-5404.
95. Q. Teng and H. V. Huynh, *Dalton Trans.* **2017**, *46*, 614-627.
96. Q. Teng, P. S. Ng, J. N. Leung and H. V. Huynh, *Chem. Eur. J.* **2019**, *25*, 13956-13963.
97. E.O.Fischer and K.Öfele, *Z. Naturforsch. B* **1958**, *13*, 458.
98. A. Pfletschinger, T. K. Dargel, J. W. Bats, H.-G. Schmalz and W. Koch, *Chem. Eur. J.* **1999**, *5*, 537-545.
99. K. Schellhaas, H.-G. Schmalz and J. W. Bats, *Chem. Eur. J.* **1998**, *4*, 57-66.
100. M. Otsuka, K. Endo and T. Shibata, *Chem. Commun.* **2010**, *46*, 336-338.
101. E. E. Karslyan, A. O. Borissova and D. S. Perekalin, *Angew. Chem. Int. Ed.* **2017**, *56*, 5584-5587.
102. C. H. Suresh, N. Koga and S. R. Gadre, *Organometallics* **2000**, *19*, 3008-3015.
103. M. J. Frisch, G. W. Trucks, H. B. Schlegel, G. E. Scuseria, M. A. Robb, J. R. Cheeseman, G. Scalmani, V. Barone, G. A. Petersson, H. Nakatsuji, X. Li, M. Caricato, A. V. Marenich, J. Bloino, B. G. Janesko, R. Gomperts, B. Mennucci, H. P. Hratchian, J. V. Ortiz, A. F. Izmaylov, J. L. Sonnenberg, D. Williams-Young, F. Ding, F. Lipparini, F. Egidi, J. Goings, B. Peng, A. Petrone, T. Henderson, D. Ranasinghe, V. G. Zakrzewski, J. Gao, N. Rega, G. Zheng, W. Liang, M. Hada, M. Ehara, K. Toyota, R. Fukuda, J. Hasegawa, M. Ishida, T. Nakajima, Y. Honda, O. Kitao, H. Nakai, T. Vreven, K. Throssell, J. J. A. Montgomery, J. E. Peralta, F. Ogliaro, M. J. Bearpark, J. J. Heyd, E. N. Brothers, K. N. Kudin, V. N. Staroverov, T. A. Keith, R. Kobayashi, J. Normand, K.

Raghavachari, A. P. Rendell, J. C. Burant, S. S. Iyengar, J. Tomasi, M. Cossi, J. M. Millam, M. Klene, C. Adamo, R. Cammi, J. W. Ochterski, R. L. Martin, K. Morokuma, O. Farkas, J. B. Foresman and and D. J. Fox, *Gaussian 16, Revision A.03,* **2016**, *Gaussian, Inc., Wallingford CT*.

104. G. S. Remya and C. H. Suresh, *New J. Chem.* **2018**, *42*, 3602-3608.

Chapter 4

Part A

Pincer Ligand Modifications to Tune the Activation Barrier for H_2 Elimination in Water Splitting Milstein Catalyst

Part B

Hydrogen Elimination Reactivity of Ruthenium Pincer Hydride Complexes

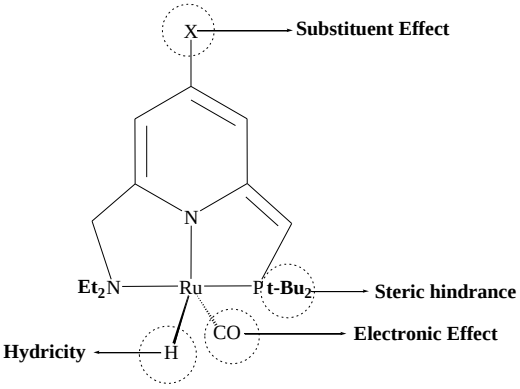

X = F, Cl, CHO, CN, NH_2, NMe_2, CH_3, OCH_3, COOH, OH and NO_2

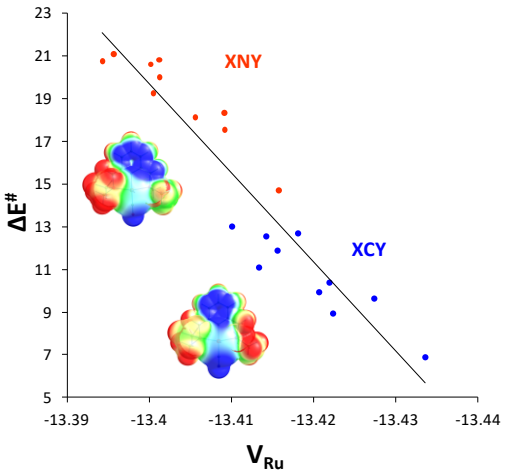

Part A. Pincer Ligand Modifications to Tune the Activation Barrier for H_2 Elimination in Water Splitting Milstein Catalyst

4.1 Abstract

Modifications on the ligand environment of Milstein Ruthenium (II) pincer hydride catalysts have been proposed to fine-tune the activation free energy, $\Delta G^{\#}$ for the key step of H_2 elimination in the water splitting reaction. This study conducted at B3LYP level of density functional theory including solvation effect reveals that changing the bulky t-butyl group at the P-arm of the pincer ligand by methyl or ethyl group can reduce the $\Delta G^{\#}$ by a substantial margin ~10 kcal/mol. The reduction in the steric effect of the pincer ligand causes exothermic association of water molecule to the metal center and leads to significant stabilization of all the subsequent reaction intermediates and transition states compared to the original Milstein catalyst that promotes endothermic association of the water molecule. Though electron donating groups on the pyridyl unit of the pincer ligand is advantageous for reducing the activation barrier in the gas phase, the effect is only 1 – 1.4 kcal/mol compared to an electron withdrawing group. The absolute minimum of the electrostatic potential at the hydride ligand and carbonyl stretching frequency of the catalyst are useful parameters to gauge the effect of ligand environment on the H_2 elimination step of the water splitting reaction.

4.2 Introduction

The recent developments in theoretical methodologies facilitated accurate assessment of mechanisms for catalytic processes and provided impetus to the theoretical computation-aided search for new generation catalysts.[1,2] Production of hydrogen through homogeneous catalytic water splitting reaction offers an attractive strategy to obtain sustainable clean energy[3-9] while molecular electrocatalyst assisted hydrogen production has attracted considerable attention, owing to high turnover with respect to

the catalyst.[10-15] Recently, Milstein *et al*. have reported the discovery of one of the most elegant water splitting reaction promoted by a pincer Ru(II) **PNN** complex (Milstein catalyst).[16] The reaction proceeded through consecutive water reduction under thermal condition and water oxidation under light driven condition. This complex has henceforth attracted great interest[17-19] due to the intriguing aromatization-dearomatization strategy[20] offered by the pincer tridentate **PNN** ligand ((2-(di-tert-butylphosphinomethyl)-6-diethylaminomethyl)pyridine) in the mechanistic pathway which led to large cooperativity between ligand and Ru metal for the activation of the OH bond of water. Milstein catalyst has also showed diverse catalytic activity in synthesizing organic compounds such as esters, alcohols, amides, polyamides and aldehydes.[21-27]

The versatile reactivity of Milstein catalyst is mainly attributed to its pincer ligand which upon a small modification leads to substantial change in the entire reactivity of the complex.[28,29] Exquisite mechanism of hydrogen elimination from Milstein catalyst has been theoretically elucidated by Yoshizawa *et al*. and Yang and Hall.[30,31] We have also proposed that the hydride ligand-assisted outer sphere mechanism of hydrogen elimination from water is possible for the Milstein catalyst.[32] In this mechanism, the reductive elimination of H_2 occurred in a concerted step without the aromatization-dearomatization activity of the pincer ligand (Scheme 4.1). This mechanism suggested a direct pathway for the elimination of H_2 from the pincer complex whereas the subsequent aromatization-deraomatization activity at the pincer ligand led to the formation of experimentally observed hydrido hydroxo pincer complex intermediate in the reaction.

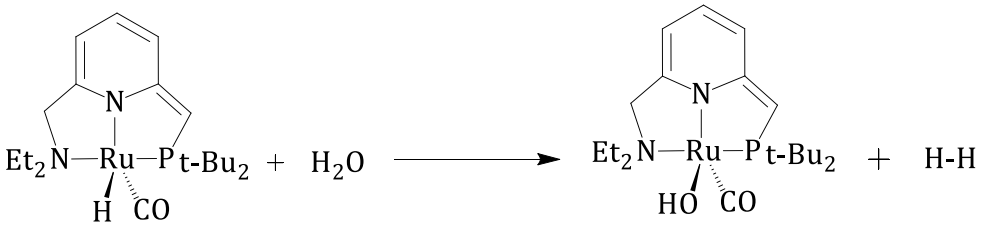

Milstein catalyst **Hydroxo Ru(II) pincer complex**

Scheme 4.1 Dihydrogen elimination of Milstein catalyst with water.

In the present study, our aim is to tune the rate determining activation free energy of the hydrogen elimination pathway given in Scheme 4.1 for the Milstein catalyst by applying modifications on the pincer ligand. Various types of electron withdrawing or donating groups at the para position of the pyridyl group of **PNN** ligand, *viz*. F, Cl, CHO, CN, NH_2, CH_3, OCH_3, COOH, OH, NMe_2 and NO_2 and different alkyl substituents (methyl, ethyl, and t-butyl) at the P- and N-arms of pincer ligand are considered for tuning the ligand environment of the Milstein catalyst which leads to large number of modified Milstein complexes. Figure 4.1 shows a schematic picture of the modified Milstein catalysts that are grouped into four categories.

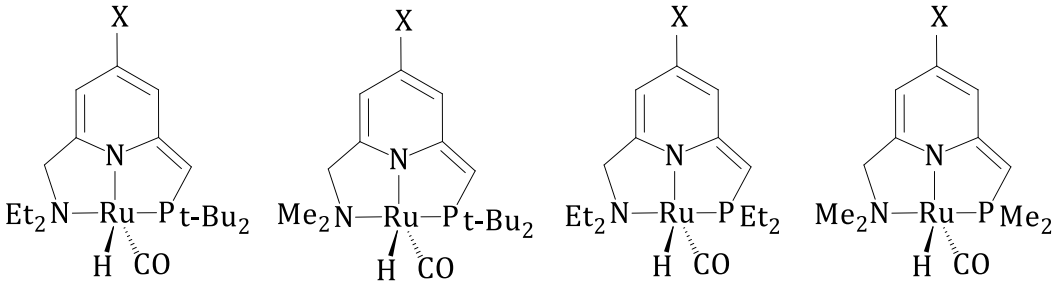

X = NO_2, CN, COOH, CHO, Cl, F, H, CH_3, OCH_3, OH, NH_2 and NMe_2

Figure 4.1 Various modifications on the Milstein catalyst. X represents the substituent.

The first category of complexes is named as **1-F, 1-Cl, 1-CHO, 1-CN, 1-H, 1-NH_2, 1-CH_3, 1-OCH_3, 1-COOH, 1-OH, 1-NMe_2,** and **1-NO_2**. Similarly, other categories are named by combining the numbers **2**, **3**, and **4** with the substituent notation. Also the general notations **1-X, 2-X, 3-X** and **4-X** are used for the different categories of the complexes. **1-H** is the original Milstein catalyst which is composed of Et substituents on N-arm and t-butyl substituent on P-arm. The pincer ligand of second category complexes comprises of Me substitution at the N-arm and t-butyl substitution at the P-arm. For the third class of models, both the arm positions are substituted with ethyl groups. For the fourth set of models, methyl groups are used as substituents for both N- and P-arms. These types of pincer backbones on Fe, Ni, Ir, Ru, Rh, and Pd centers are reported in the

literature.[33-39] Further, the meta-substitution on the pyridyl ring and the effect of bulky groups at N arm are also studied for some representative catalysts.

4.3 Computational Methodology

All the calculations have been carried out using Gaussian 09 suite of programs.[40] The Becke three-parameter hybrid functional combined with the Lee-Yang-Parr correlation functional and in conjunction with the BS1 basis set (B3LYP/BS1 method) is used for optimizing all the molecular geometries. For Ru, BS1 stands for double-ξ valence basis set (LANL2DZ) with additional f polarization functions (for valence electrons) and effective core potential (ECP) of Hay and Wadt for replacing the core electrons.[41] For all other atoms, BS1 indicates the use of 6-31G(d, p) basis set. All the minimum energy configuration of the geometries showed positive mode of vibration in the frequency calculations while the transition states (TSs) showed one imaginary frequency. The harmonic frequencies have been used for thermal and entropic correction to enthalpies and free energies at 298 K and 1 atm pressure. Implicit description of solvation effect on the catalyst, water-bound complex, transition state and the dihydrogen-coordinated product complex is incorporated in the calculation using Truhlar and co-workers SMD method[42] as implemented in Gaussian09 at B3LYP/BS2 level. Water is used as the solvent. In BS2, 6-311++G(d,p) basis set is used for all nonmetal atoms while the Ru basis set is same as BS1. As recommended in Gaussian09, the $\Delta G_{solvation}$ is calculated by taking the difference between the energies in gas phase and solvent phase. SMD is an implicit solvation model[43] based on density, in which interaction between the solute and solvent is calculated from the charge density of the former and the electric polarization field of the latter.[44] It was proven that SMD can predict the solvation energies with greater accuracy.[42] The Molecular electrostatic potential (MESP) of the complex on a three-dimensional grid is calculated at B3LYP/BS1 level using Gaussian09. The negative-valued MESP provide useful information on the electron rich character of the ligand that is expected to be the most negative at the hydride ligand.[45] The MESP at the hydride nucleus (V_H) is evaluated, obtained directly from the Gaussian09 output of a MESP calculation.

The substituent effect on pincer ligand is analyzed by correlating theoretically derived electronic/thermodynamic parameters.[46]

4.4 Results and Discussion

4.4.1 Energetics of H_2 Activation

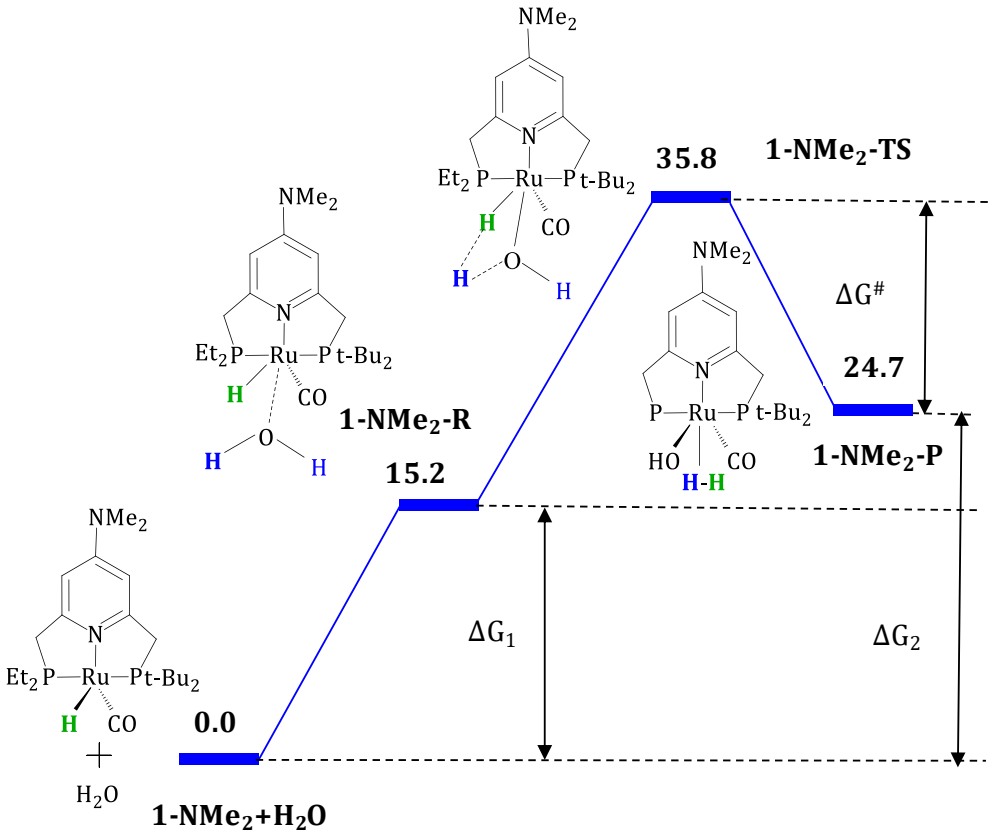

Figure 4.2 Mechanism of η^2-dihydrogen complex formation in the water splitting Milstein catalyst, **1-NMe2**. Values in kcal/mol at B3LYP/BS2 level with solvation effect.

A total of 192 catalysts have been studied for their H_2 elimination reaction with water. In order to simplify the results and discussion, we will focus solely on the rate-determining transition state, its connected reactant and the product. The energy profile of this reaction for a representative example **1-NMe2** is given in Figure 4.2. The reactant complex **1-NMe2-R** is formed by coordination of a water molecule with the catalyst through a dihydrogen bonded complex between hydride ligand and H of the water molecule.

Table 4.1 The ΔE_1, $\Delta E^{\#}$, ΔE_2, ΔG_1, $\Delta G^{\#}$ and ΔG_2 values for **1-X** and **2-X** type catalysts. Values in kcal/mol at B3LYP/BS2 level with solvation effect.

Catalysts	ΔE_1	ΔG_1	$\Delta E^{\#}$	$\Delta G^{\#}$	ΔE_2	ΔG_2
1-NO_2	6.1	13.7	22.3	23.0	28.4	36.7
1-CN	6.4	14.5	21.9	21.4	28.4	35.9
1-COOH	6.5	13.9	21.4	22.1	27.9	35.9
1-CHO	6.6	14.1	21.8	21.7	28.4	35.8
1-Cl	6.5	13.8	21.9	21.6	28.4	35.4
1-F	7.0	14.6	20.7	21.2	27.7	35.9
1-H	7.4	14.8	20.1	20.4	27.5	35.1
1-CH_3	7.2	14.8	20.1	20.5	27.2	35.3
1-OCH_3	7.3	13.7	20.6	22.0	27.9	35.7
1-OH	7.2	14.9	20.3	20.7	27.4	35.6
1-NH_2	7.4	15.1	19.8	20.2	27.2	35.3
1-NMe_2	7.1	15.2	20.3	20.6	27.4	35.8
2-NO_2	5.8	13.5	22.1	22.4	27.9	35.9
2-CN	5.7	13.3	22.0	22.1	27.6	35.3
2-COOH	6.0	13.7	21.5	21.8	27.5	35.5
2-CHO	5.7	13.3	21.8	21.7	27.6	34.9
2-Cl	5.7	13.8	21.9	21.7	27.6	35.5
2-F	6.0	13.5	21.8	21.7	27.9	35.2
2-H	5.9	13.0	21.3	21.5	27.2	34.5
2-CH_3	6.3	13.4	21.0	21.6	27.3	35.0
2-OCH_3	6.2	13.7	21.1	20.9	27.4	34.6
2-OH	6.2	13.5	21.4	21.5	27.7	35.0
2-NH_2	7.3	14.5	20.1	20.4	27.4	34.9
2-NMe_2	6.8	14.0	20.3	21.3	27.1	35.3

Since the water coordination leads to loss of entropy, the overall feasibility of the reaction can be judged by the relative energy and relative free energy of **1-NMe_2-R, 1-NMe_2-TS** and **1-NMe_2-P** with respect to the infinitely separated catalyst and water at 0.0

kcal/mol. For the discussion on energy parameters depicted in Figure 4.2, *viz.* ΔE_1, $\Delta E^{\#}$, ΔE_2, ΔG_1, $\Delta G^{\#}$, and ΔG_2. B3LYP/BS2 level values that incorporate the solvation effect are used throughout unless otherwise mentioned. The ΔE_1 is useful to assess the coordination ability of the catalyst for a water molecule while ΔG_1 gives a measure of the free energy loss associated with such an association reaction. The $\Delta E^{\#}$ is the activation energy for the H_2 elimination from the water complex while $\Delta G^{\#}$ is the corresponding activation free energy. The final analysis on the feasibility of H_2 elimination reaction is based on the infinitely separated catalyst and water which can be judged from the activation energy ΔE_2 and the activation free energy ΔG_2.

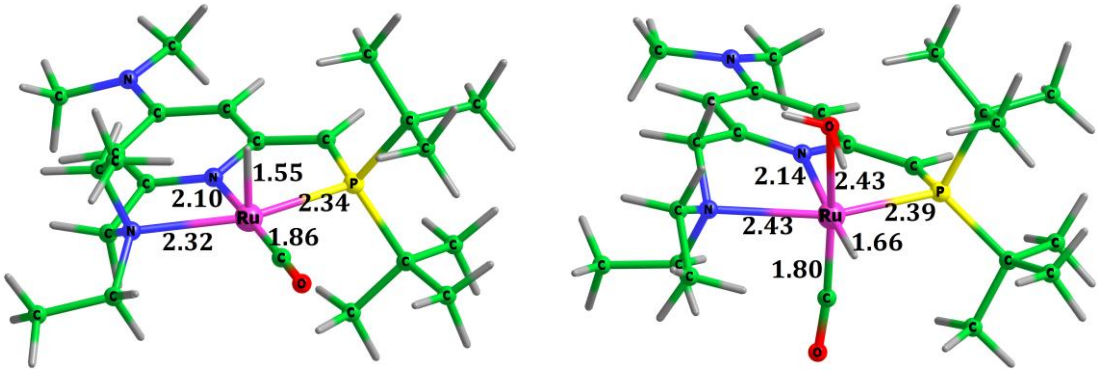

1-NMe$_2$ **1-NMe$_2$-R**

Figure 4.3 Optimized geometry of **1-NMe$_2$** and **1-NMe$_2$** complexed with a water molecule (**1-NMe$_2$-R**). Distances in Å at B3LYP/BS1 level.

Since our attention is on transition state, discussion on minor aspects related to the initial water coordination process to the catalyst is avoided. In Table 4.1, the values of ΔE_1, $\Delta E^{\#}$, ΔE_2, ΔG_1, $\Delta G^{\#}$ and ΔG_2 are depicted for **1-X** and **2-X** type catalysts. These data clearly suggest that the effect of para-substituent on the pincer ligand is negligible in tuning any of the energy parameters as the values observed for them all fall in a very narrow range. In the catalyst, the hydride and CO ligands respectively occupy *cis* and *trans* position with respect to the pyridyl N atom while the coordination of water forces the hydride ligand to move to a position trans and CO ligand *cis* with respect to the pyridyl N atom (Figure 4.3). As we can see from ΔE_1, the coordination of water is endothermic by

5.7 to 7.4 kcal/mol for the **1-X** and **2-X** type catalysts which in turn leads to higher values of ΔG_1 (13.0 – 15.2 kcal/mol).

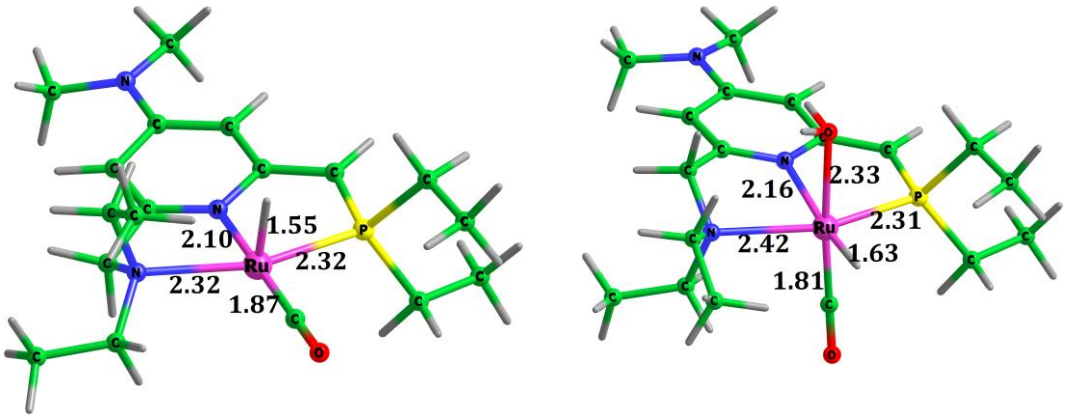

3-NMe$_2$ **3-NMe$_2$-R**

Figure 4.4 Optimized geometry of (a) Modified Milstein catalyst **3-NMe$_2$** and (b) **3-NMe$_2$** complexed with a water molecule (**3-NMe$_2$-R**). Distances in Å at B3LYP/BS1 level.

Comparison of the bond length data of **1-NMe$_2$** and **1-NMe$_2$-R** structures given in Figure 4.3 suggests that the coordination of water to Ru weakens the Ru-H, Ru-P, Ru-N (amino) and Ru-N (pyridyl) bonds while it strengthens the Ru-CO bond. Although the coordination of water to the metal gives stabilizing Ru-O bonding effect, the gain in energy due to this bond is not sufficient to overcome the energy loss due to the weakening of the pincer ligand bonds to the metal as well as the Ru-H bond. This causes endothermic association of water to the catalyst. Moreover, the coordination bond of water to Ru may not be very strong as the Ru-O distance is significantly larger (2.43 Å) than that of a typical Ru-O bond distance ~2.20 Å. The coordinated oxygen of water also shows two noncovalent CH interactions from the t-butyl substituent on the phosphorous (Figure 4.3) meaning that steric effects from this bulky group may prevent water from strongly coordinating to the metal. These observations noted for **1-NMe$_2$** complex and its water coordinated structures are applicable for the entire set of **1-X** and **2-X** systems as they all show Ru-O distance in the range 2.35 – 2.43 Å (Table 4.3) and Ru-O....HC noncovalent interactions in the water coordinated complex. It is noteworthy that trans influence of P-

arm increases the weakening of the Ru-N bond by ~0.1 Å for all six coordinated complexes compared to initial four coordinated catalysts.[47]

Table 4.2 The ΔE_1, $\Delta E^{\#}$, ΔE_2, ΔG_1, $\Delta G^{\#}$ and ΔG_2, values for **3-X** and **4-X** type catalysts. Values in kcal/mol at B3LYP/BS2 level with solvation effect.

Catalysts	ΔE_1	ΔG_1	$\Delta E^{\#}$	$\Delta G^{\#}$	ΔE_2	ΔG_2
3-NO_2	-2.6	4.2	22.6	22.6	20.0	26.7
3-CN	-2.9	4.1	22.5	22.4	19.7	26.5
3-COOH	-2.4	4.5	22.1	21.8	19.7	26.3
3-CHO	-4.7	3.5	22.3	21.4	17.5	24.8
3-Cl	-3.1	4.2	22.4	21.9	19.3	26.1
3-F	-2.5	4.8	21.8	21.4	19.3	26.2
3-H	-2.1	4.7	21.4	20.6	19.3	25.3
3-CH_3	-2.3	5.2	21.1	20.6	18.8	25.7
3-OCH_3	-1.1	5.7	21.6	21.1	20.5	26.8
3-OH	-2.6	5.0	21.4	20.9	18.8	25.9
3-NH_2	-2.1	5.5	21.0	20.4	18.9	25.9
3-NMe_2	-1.6	5.1	20.9	20.7	19.3	25.8
4-NO_2	-3.7	2.9	22.7	22.4	19.1	25.4
4-CN	-4.0	2.9	22.8	22.3	18.8	25.2
4-COOH	-3.4	3.5	22.2	21.6	18.8	25.1
4-CHO	-5.6	2.0	22.5	22.1	16.9	24.0
4-Cl	-3.7	3.2	22.5	22.0	18.8	25.1
4-F	-3.7	2.9	22.3	22.1	18.6	25.0
4-H	-3.3	3.3	21.8	21.6	18.4	24.9
4-CH_3	-3.3	2.9	21.8	21.9	18.5	24.8
4-OCH_3	-2.2	3.9	21.7	21.8	19.5	25.7
4-OH	-3.6	2.8	21.8	21.9	18.2	24.7
4-NH_2	-2.7	3.9	21.1	20.8	18.4	24.7
4-NMe_2	-2.6	4.5	20.9	20.4	18.3	24.8

From the water coordinated complex, the formation of the hydroxyl complex through the elimination of H_2 is easy to explain. In the water complex, the Ru-H bond (1.66 Å for **1-NMe$_2$**) is substantially activated compared to the catalyst (1.55 Å) which leads to an early transition state. For all the **1-X** and **2-X** cases, the activation barrier $\Delta E^{\#}$ in the range 19.8 – 22.3 kcal/mol as well as activation free energy $\Delta G^{\#}$ in the range 20.2 – 23.0 kcal/mol suggests a facile H_2 elimination process. On the basis of infinitely separated catalyst and water, the overall activation energy, ΔE_2 for **1-X** and **2-X** systems is 27.1 – 28.4 kcal/mol and the overall activation free energy ΔG_2 is 34.5 – 36.7 kcal/mol. Though these values remain almost a constant for all the systems irrespective of the substituent on the pyridyl unit of the pincer ligand, electron donating substituents can be grouped at the lower end of $\Delta E^{\#}$ values while electron withdrawing substituents can be grouped at the higher end.

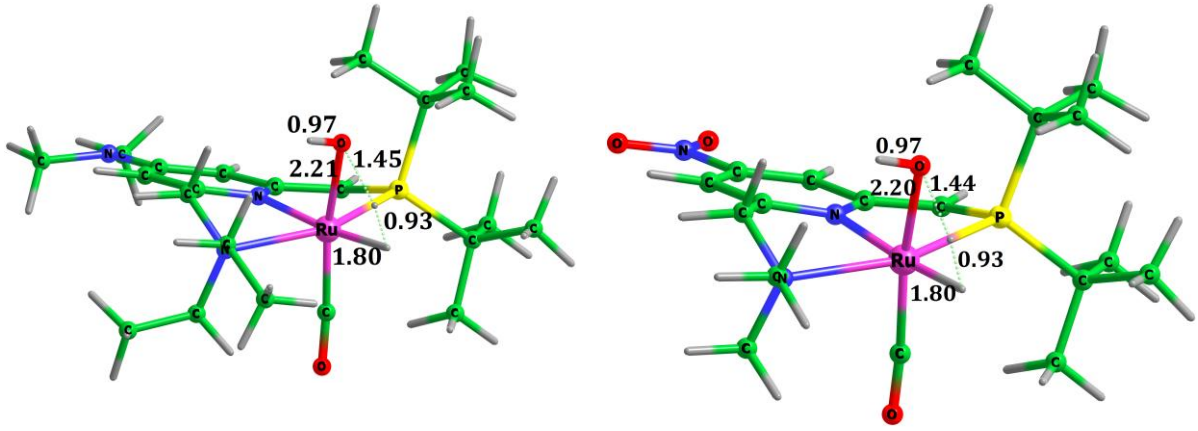

1-NMe$_2$-TS **2-NO$_2$-TS**

Figure 4.5 Transition states of representative structures **1- NMe$_2$ and 2-NO$_2$**. Distances in Å at B3LYP/BS1 level.

In Table 4.2, the values of ΔE_1, $\Delta E^{\#}$, ΔE_2, ΔG_1, $\Delta G^{\#}$ and ΔG_2 are depicted for **3-X** and **4-X** type catalysts. Similar to the data in Table 4.1, these data too clearly suggest that the effect of *para*-substituent on the pincer ligand is negligible in tuning any of the energy parameters. Comparison of the optimized structure of **3-NMe$_2$** with **1-NMe$_2$** suggests that changing the t-butyl substituent on the P-arm of the Milstein catalyst does not change significantly any of the metal-ligand bonding interactions. The only noticeable, though

minor, observation is the change in Ru-P bond length 2.34 Å in **1-NMe$_2$** to 2.32 Å in **3-NMe$_2$**, which could be explained on the basis of release of steric congestion from the t-butyl group. The release of steric effect is substantial in the water-coordinated complex which can be observed from the Ru-O and Ru-P distances (Tables 4.3 and 4.4). All the water-coordinated of **3-X** and **4-X** complexes show significantly shorter Ru-O and Ru-P bond distances than the **1-X** and **2-X** complexes. For instance, 3-**NMe$_2$-R** shows Ru-O distance 2.33 Å and Ru-P distance 2.31 Å which are respectively 0.10 and 0.09 Å shorter than those of **1-NMe$_2$-R**.

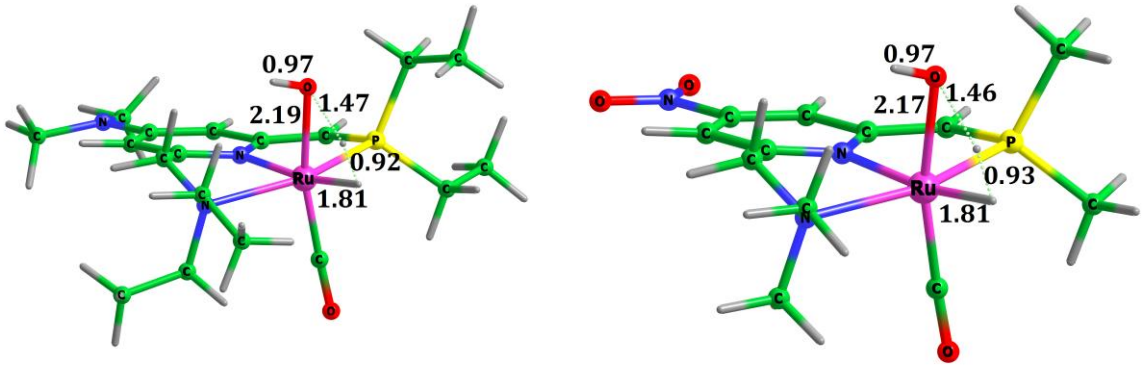

3-NMe$_2$-TS **4-NO$_2$-TS**

Figure 4.6 Transition states of representative structures **3-NMe$_2$** and **4-NO$_2$.** Distances in Å at B3LYP/BS1 level.

The substantial influence of steric effect in **1-X** and **2-X** systems is clearly seen if the energy parameters of these systems are compared against those of **3-X** and **4-X** systems. Unlike **1-X** and **2-X** systems, the water coordination process is exothermic by -1.1 to -5.6 kcal/mol in **3-X** and **4-X** systems. The exothermic character of the water coordination process could significantly improve the water splitting reaction catalyzed by **3-X** and **4-X** type systems as it offers substantial reduction in the overall energetics of H_2 elimination. In fact, ΔE_2 in the range 16.9 – 20.5 kcal/mol and ΔG_2 in the range 24.0 – 26.7 kcal/mol observed for **3-X** and **4-X** are ~10 kcal/mol smaller than those observed for **1-X** and **2-X** systems. The $\Delta E^{\#}$ and $\Delta G^{\#}$ values are nearly the same for all types of catalysts. However, the gas phase values of $\Delta E^{\#}$ and $\Delta G^{\#}$ for the precise step of H_2 elimination from the water coordinated complex is 18.1 – 19.0 kcal/mol and 16.5 – 18.0

kcal/mol, respectively which are ~4 kcal/mol higher than those observed for **1-X** and **2-X** type catalysts. These values suggest that the transition state corresponding to the H_2 elimination is slightly late in **3-X** and **4-X** type systems compared to **1-X** and **2-X** type systems (Figures 4.5, 4.6). For instance, the O...H distance for the proton transfer to the hydride ligand in the TS for **3-NMe2** is slightly larger than that of **1-NMe2** while the Ru-O distance in the TS of the former is slightly shorter compared to the latter.

It may be noted that the water splitting leading to dihydrogen formation is initiated by an outer sphere coordination of one water molecule to the catalyst via the hydride ligand through a dihydrogen interaction.[32] This mechanism also suggests that the solvated metal complex is susceptible for H-H bond formation reaction. Therefore, more than one water molecule may operate in the reaction mechanism.[48, 49] A recent metadynamics simulation study performed on a system of water molecules with Milstein catalyst has shown that the activation energy for H_2 elimination is 31.1 kcal/mol[50] which is very close to the value reported by us (35.1 kcal/mol) for the Milstein catalyst **1-H** with one water molecule.[32] This suggests that the catalytic reaction studied herein with one water molecule is reliable and the effect of more water molecules may reduce the barrier by a small amount. This argument is also supported by a recent study from our group on a molybdenum complex $MoH(NO)(CO)(PMe_3)_3$ wherein the involvement of a second molecule of water showed only 1 kcal/mol decrease in the activation free energy for H_2 elimination compared to the reaction modeled with one water moelcule.[51]

4.4.2 MESP and TEP Analyses

Previously, we have shown that the absolute minimum of the molecular electrostatic potential (MESP) at the hydride ligand (V_{min}) and MESP at the hydride nucleus (V_H) are sensitive electronic properties of octahedral group VI, VII and VIII metal hydride complexes.[52] Monitoring these properties is easy and they provide a way to fine-tune the ligand environment of the complex to achieve high hydricity for the hydride ligand. Tables 4.3 and 4.4 gives V_{min} and ΔV_{min} values of all the systems.

Table 4.3 MESP and TEP values for **1-X** and **2-X** complexes at B3LYP/BS1 level. MESP in kcal/mol and TEP in cm^{-1}. Ru-O and Ru-P distances (Å) in respective water complexes are given.

Catalysts	V_{min}	ΔV_{min}	TEP	$d_{(Ru-O)}$	$d_{(Ru-P)}$
1-NO_2	-11.2	8.4	2010.3	2.35	2.39
1-CN	-12.6	6.9	2009.8	2.35	2.39
1-COOH	-15.9	3.6	2005.3	2.37	2.39
1-CHO	-14.6	4.9	2006.6	2.35	2.4
1-Cl	-15.8	3.7	2006.2	2.35	2.39
1-F	-17.1	2.5	2004.7	2.38	2.39
1-H	-19.5	0.0	2002.9	2.38	2.39
1-CH_3	-19.9	-0.4	2001.5	2.39	2.39
1-OCH_3	-20.1	-0.6	2002.0	2.39	2.39
1-OH	-19.7	-0.2	2001.7	2.39	2.39
1-NH_2	-21.9	-2.4	1999.2	2.41	2.39
1-NMe_2	-23.5	-4.0	1997.4	2.43	2.39
2-NO_2	-11.7	7.7	2013.8	2.35	2.40
2-CN	-11.7	7.7	2013.4	2.36	2.40
2-COOH	-16.5	2.9	2009.3	2.37	2.40
2-CHO	-14.1	5.3	2010.9	2.36	2.40
2-Cl	-15.3	4.1	2009.3	2.37	2.40
2-F	-16.8	2.6	2008.5	2.36	2.40
2-H	-19.4	0.0	2006.2	2.38	2.40
2-CH_3	-20.0	-0.6	2005.3	2.37	2.40
2-OCH_3	-19.8	-0.4	2005.6	2.39	2.40
2-OH	-19.6	-0.3	2005.5	2.37	2.40
2-NH_2	-21.9	-2.5	2003.1	2.41	2.40
2-NMe_2	-23.2	-3.8	2001.9	2.44	2.40

Though V_{min} and V_H give almost parallel results, V_{min} is more suited for this study to monitor the ligand environment as this spatial property is more sensitive to steric influence of the substituents than the nuclear property V_H.[53] Another aim of the MESP analysis is to show that even a minor variation in the ligand environment is well reflected on V_{min} and by studying this property; more insight into the reactive behaviour of the complex for H_2 elimination reaction can be obtained. Figure 4.7 depicts V_{min} and MESP isosurface of some representative examples of ruthenium hydride complexes. The V_{min} is the most negative for **-NMe$_2$** substitution at the para position of the pyridyl unit while **–NO$_2$** substitution gives the least negative V_{min}. The relative increase in the negative character of V_{min} compared to **–H** substituted systems (ΔV_{min}) provides a measure of the substituent effect on the hydride ligand. From the depicted values of V_{min}, ΔV_{min} values -4.0, +8.4, -4.0 and +8.4 kcal/mol can be assigned for **1-NMe$_2$, 1- NO$_2$, 3-NMe$_2$** and **3-NO$_2$** systems, respectively.

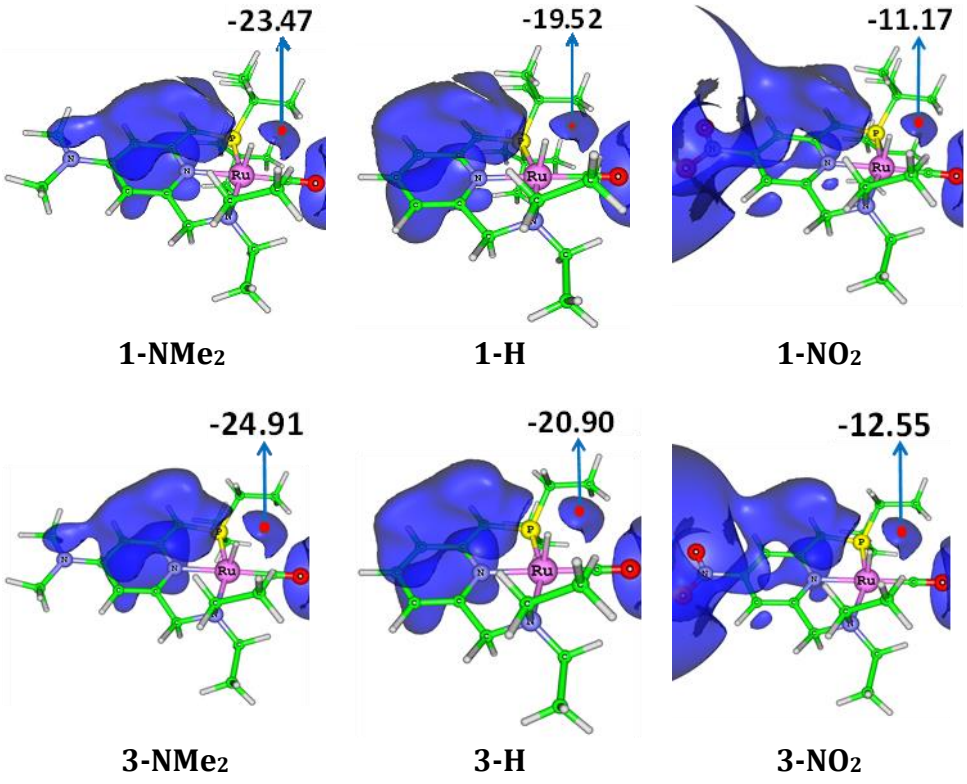

Figure 4.7 V_{min} of **1-NMe$_2$**, **1-H**, **1- NO$_2$**, **3-NMe$_2$**, **3-H**, and **3- NO$_2$** complexes. Isosurface values are shown in kcal/mol.

Table 4.4 MESP and TEP values for 3-X and 4-X complexes **at B3LYP/BS1 level**. MESP in kcal/mol and TEP in cm^{-1}. Ru-O and Ru-P distances (Å) in respective water complexes are given.

Catalysts	V_{min}	ΔV_{min}	TEP	$d_{(Ru-O)}$	$d_{(Ru-P)}$
3-NO_2	-12.6	8.4	2015.7	2.31	2.31
3-CN	-13.4	7.5	2014.9	2.31	2.31
3-COOH	-17.3	3.6	2010.9	2.31	2.31
3-CHO	-15.9	5.0	2012.2	2.31	2.31
3-Cl	-16.9	4.0	2012.0	2.31	2.31
3-F	-18.6	2.3	2010.4	2.32	2.31
3-H	-20.9	0.0	2008.0	2.32	2.31
3-CH_3	-21.4	-0.5	2006.9	2.33	2.32
3-OCH_3	-22.0	-1.1	2005.9	2.32	2.31
3-OH	-21.2	-0.3	2007.5	2.33	2.32
3-NH_2	-23.6	-2.7	2004.6	2.33	2.32
3-NMe_2	-24.9	-4.0	2003.2	2.33	2.31
4-NO_2	-12.6	8.5	2026.4	2.31	2.31
4-CN	-13.4	7.7	2025.5	2.31	2.31
4-COOH	-17.6	3.5	2021.0	2.31	2.31
4-CHO	-16.2	5.0	2022.0	2.31	2.31
4-Cl	-17.3	3.9	2023.0	2.31	2.31
4-F	-18.6	2.6	2020.0	2.31	2.31
4-H	-21.2	0.0	2018.0	2.32	2.31
4-CH_3	-22.0	-0.8	2016.0	2.32	2.31
4-OCH_3	-22.6	-1.4	2017.0	2.32	2.31
4-OH	-21.5	-0.3	2017.0	2.32	2.31
4-NH_2	-24.4	-3.2	2014.0	2.33	2.31
4-NMe_2	-25.5	-4.4	2013.0	2.33	2.31

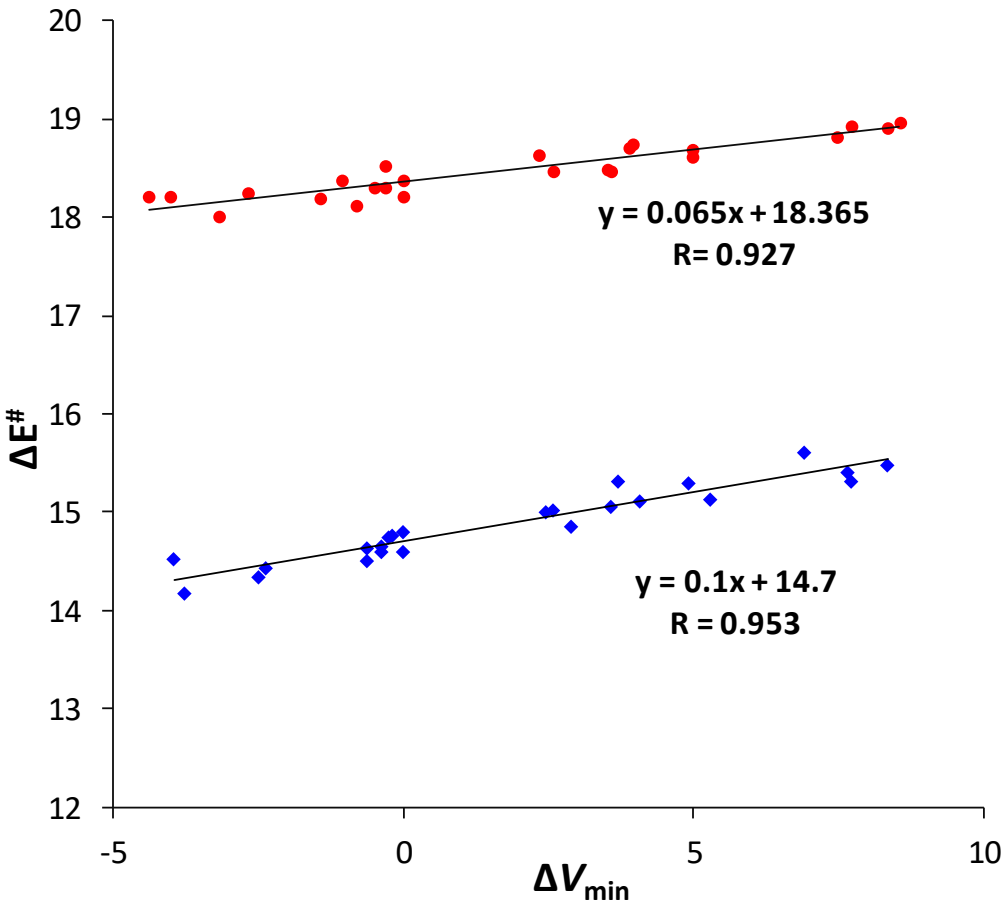

Figure 4.8 Correlation between electrostatic potential at the hydride ligand, ΔV_{min} and activation energy for H_2 elimination, $\Delta E^{\#}$ (blue diamonds for **1-X** and **2-X** complexes, red dots for **3-X** and **4-X** complexes). Values in kcal/mol at B3LYP/BS1 level.

In Figure 4.8, two linear correlation plots are given, one depicts the relationship between ΔV_{min} and $\Delta E^{\#}$ for **1-X** and **2-X** type systems in the gas phase, and the other portrays a similar relationship for **3-X** and **4-X** type systems. It is noteworthy that the difference between the highest and lowest $\Delta E^{\#}$ values is only 1.44 kcal/mol for **1-X** and **2-X** type systems while that for **3-X** and **4-X** systems is only 0.97 kcal/mol. The correlation coefficients 0.953 and 0.927 for the ΔV_{min} *vs* $\Delta E^{\#}$ plots clearly suggest that even the apparently negligible change in activation barrier for H_2 elimination can be well reflected in MESP in the form of a significant change in the value of the electronic property V_{min} at the hydride ligand. Previously we have shown that V_{min} can be used as a highly sensitive electronic parameter to tune activation barrier for water splitting reaction by octahedral

hydride complexes of tungsten, *viz*. $WH(PH_3)_n(CO)_{4-n}(NO)$ (n = 4, 3, 2) and $W(dpe)_2H(CH)$ (dpe=1,2-diphosphine-ethane).[52]

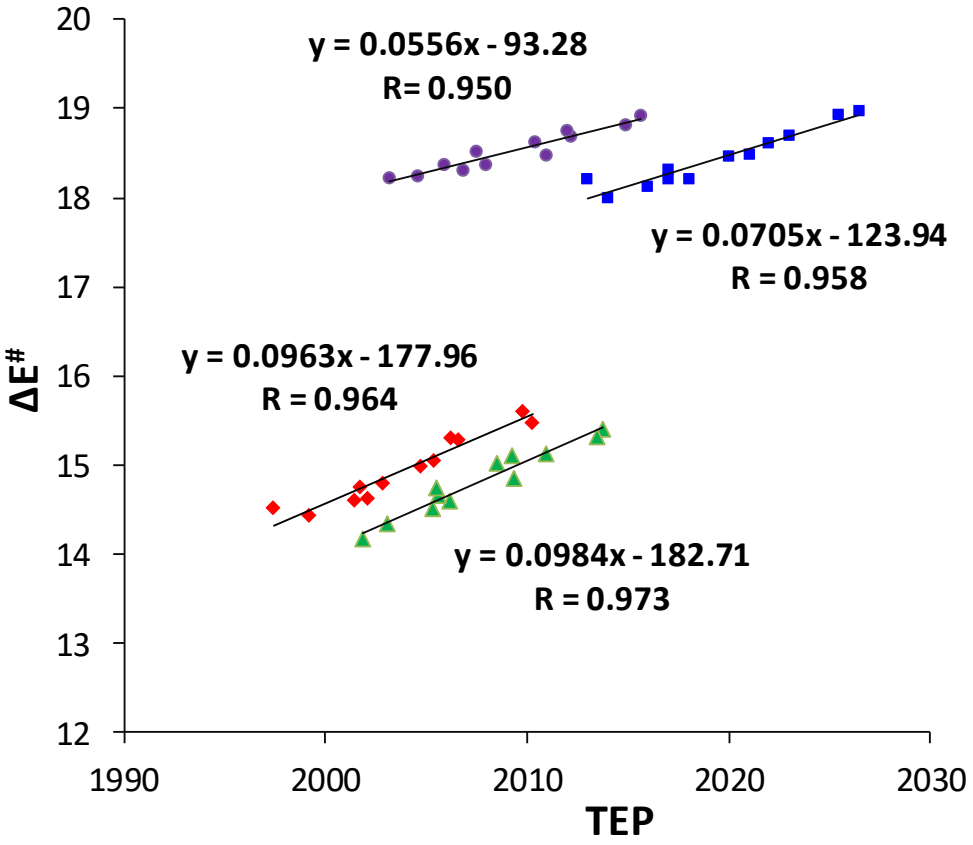

Figure 4.9 Correlation between TEP and $\Delta E^{\#}$ for H_2 elimination (red diamonds for **1-X**, green triangles for **2-X**, violet dots for **3-X** and blue squares for **4-X** complexes). Energy values in kcal/mol and TEP in cm^{-1} at B3LYP/BS1 level.

We have seen that para substituent on the pyridyl unit of the pincer ligand has only a minor influence on the activation barrier for the H_2 elimination reaction. What about the meta substitution on the pyridyl unit? To understand this, we have modeled the energy profile in Figure 4.2 for four more systems, *viz*. **5-OH, 5-NH_2, 5-CH_3** and **5-F**. These systems are derived from the **4-X** category by substituting –OH, -NH_2, -CH_3 or –F at the 3, and 5 positions of the pyridyl unit of the pincer ligand. The $\Delta E^{\#}$ for the H_2 elimination reaction in the gas phase is found to be 18.6, 18.1, 18.1 and 19.3 kcal/mol for **5-OH**, **5-NH_2**, **5-CH_3** and **5-F**, respectively whereas the corresponding $\Delta G^{\#}$ is 17.3, 16.2, 17.1 and 18.0 kcal/mol (Table 4.5). No significant change in $\Delta E^{\#}$ or $\Delta G^{\#}$ is observed for any of these

complexes compared to the those of the unsubstituted **4-H** system ($\Delta E^{\#}$ = 18.2 kcal/mol and $\Delta G^{\#}$ = 17.1 kcal/mol).

Table 4.5 The $\Delta E^{\#}$ and $\Delta G^{\#}$ values for **5-X** and **6-X** type catalysts. Values in kcal/mol at B3LYP/BS1 level.

catalyst	$\Delta E^{\#}$	$\Delta G^{\#}$	catalyst	$\Delta E^{\#}$	$\Delta G^{\#}$	catalyst	$\Delta E^{\#}$	$\Delta G^{\#}$
4-OH	18.3	17.4	**5-OH**	18.6	17.3	**6- OH**	22.9	21.0
4-NH_2	18.0	16.5	**5-NH_2**	18.1	16.2	**6- NH_2**	22.5	20.5
4-CH_3	18.1	17.2	**5-CH_3**	18.1	17.1	**6- CH_3**	22.6	20.6
4-F	18.5	17.5	**5-F**	19.3	18.0	**6-F**	23.1	21.5

We have also seen that reducing the steric bulkiness of the P-arm substitution has a significant effect in decreasing the activation barrier of the reaction whereas little attention is given to the steric influence of the substituents present in the N-arm. To understand the effect of a sterically bulky group on the N-arm, we have studied four more systems, *viz*. **6-OH, 6-NH_2, 6-CH_3** and **6-F**. These systems are derived from **4-X** category by substituting t-butyl group at the N-arm of the pincer complexes **4-OH**, **4-NH_2**, **4-CH_3** and **4-F**. The gas phase $\Delta E^{\#}$ and $\Delta G^{\#}$ values of these complexes increase by around 4 kcal/mol compared to **4-OH**, **4-NH_2**, **4-CH_3** and **4-F**. This means that bulky group at N-arm is not beneficial for the water splitting reaction.

4.5 Conclusions

To explore the outcome of pincer ligand modifications on water splitting Milstein catalysts, a total of 56 models, their transition states, water complexes, and hydroxy product complexes were studied using B3LYP method. Major ligand modifications were done on the P- and N-arms of the pincer ligand as well as on the para position of the pyridyl unit of the pincer ligand for tuning the activation barrier for H_2 elimination. When bulky t-butyl substituents at the P-arm are replaced with methyl or ethyl substituents, the efficiency of the catalyst is improved significantly by promoting the coordination for H_2O in an undemanding way for H_2 elimination. Molecular electrostatic potential and carbonyl stretching frequency are found to be excellent tools for the interpretation of

activation energy barrier. From the discussed examples, it is evident that the substitution at the P-arm is significant, whereas the substitution at the N-arm is somewhat insignificant while the substitution at the para or meta positions of the pyridyl unit imparts a minor effect on the activity of the catalyst.

Part B. Hydrogen Elimination Reactivity of Ruthenium Pincer Hydride Complexes

4.6 Abstract

The tridentate rigid coordination of a pincer ligand in meridional configuration is expected to enhance the catalytic reactivity of a pincer transition metal complex compared to a non-pincer complex composed of similar ligand environment. Here a DFT study is conducted on Ru(II) ***PNN*** *type Milstein catalyst and a large variety of trans-hydrido carbonyl Ru(II) pincer complexes having* ***XZY****-type pincer ligands ('pincer atoms' X and Y are selected from N, O, S, and P and Z is either C or N) to quantify the reactivity of the water splitting hydrogen elimination reaction. A homodesmotic reaction scheme in conjunction with molecular electrostatic potential (MESP) analysis is used to quantify and characterize the stabilizing/destabilizing effect of the pincer coordination in comparison with non-pincer coordination. The pincer type coordination always led to more electron-rich ruthenium center than the non-pincer coordination. The H_2 elimination mechanism revealed for the Ru(II) complexes showed a decreasing activation energy ($\Delta E^{\#}$) trend with increase in the electron rich character of the metal center which is quantified in terms of the MESP at Ru(II), V_{Ru}. Pincer complexes having pincer atom Z = N showed $\Delta E^{\#}$ 17.5 – 21.1 kcal/mol (****NNN*** *is an exception) for the rate determining H_2 elimination step while those having Z = C showed $\Delta E^{\#}$ 6.9 – 13.0 kcal/mol. These results suggest that benzene based* ***XCY*** *type pincer ligands can be more effective than pyridine based* ***XNY*** *type ligands for designing water splitting catalysts.*

4.7 Introduction

Transition metal centered chemical reactions are well explored in the field of organic synthesis and catalysis.[54-56] Theoretical reports in this area showed the usefulness of computational methods in elucidating the reactivity of transition metal complexes.[57-61] Development of complexes comprising pincer type ligands in its structure has accepted considerable attention in numerous disciplines of chemistry.[62-64] Transition metal

complexes containing pincer ligands have emerged as an attractive research area in organometallic chemistry, as a result of their potential applications as robust catalysts for hydrogen transfer reactions,[65] Kharasch additions,[66] Heck reactions,[67] Suzuki couplings,[68] dehydrogenation reactions,[69] aldol reactions,[70] Michael reactions,[71] and cyclopropanation reactions.[72] Their use can also be extended for a number of applications in polymer chemistry,[73] photochemistry,[74] and in the design of sensors,[75] and switches[76] . The versatility of pincer complex is mainly featured by the desirable ligand modifications, together with the selection of the metal center. Different research groups from all over the world, like Morales-Morales,[77,78] Milstein,[79,80] Szabo,[81] Kirchner,[82,83] Crabtree[84] and Koten[85] groups synthesized several Ru, Pd, Pt, Ni, Ir, Os and Fe pincer complexes containing different functionality of pincer ligands for various applications. Ruthenium pincer complexes have achieved a substantial consideration among the various pincers due to their diverse set of applications in organic synthesis and ability to activate strong chemical bonds.[86,87]

Pincer ligands form chelating complexes with transition metals due to the simultaneous coordination of three donor atoms from adjacent sites to the metal center.[88] The nomenclature of any pincer complexes is made by their particular coordination mode of tridentate ligand to metal centers.[89] For instance, if P, N and P atoms are present in the arm of the tridentate ligand then it is named as **PNP** ligand. Central N arm may be a part of aromatic pyridine, or an aliphatic moiety. In addition, the alkyl or the aryl group attached to the donor atom is included in the name as superscript for the donor atom, e.g., **PNP**$_{Me}$ and **PCP**$_{Et}$. The modifications of the ligands are imaginable in three ways; altering the metal center, the donor atoms and the side arms, and the central moiety.[90] Recently, Crabtree *et al*.[91] reviewed the design principles of pincer ligands. A small modification of the pincer ligand can often change the entire reactivity of the complex, which leads to variety of anticipated applications. Recently, Suresh *et al*. have reported the tuning of the activation free energy for the H_2 elimination pathway in the water splitting reaction catalysed by ruthenium(II) pincer hydride catalysts by modifying the pincer ligand environment.[92] In this work, the focus is on the quantification of mechanistic aspects of water splitting reaction using the energetic criteria and MESP

parameters. A large variety of Ru (II) pincer hydride complexes have been taken as suitable systems for studying the same.

4.8 Computational Methodology

All the computational calculations have been performed with density functional theory (DFT) using Gaussian 16 suite of programmes.[93] All the structures are optimized using BP86/BS1 level of DFT where BS1 stands for a mixed basis set. The BS1 contains LANL2DZ basis set with additional f polarization functions for Ru and 6-311++G (d, p) basis set for all other atoms. Also the core electrons of Ru are replaced with the Hay and Wadts effective core potential (ECP). All the minimum energy configuration of the geometries showed positive mode of vibration in the frequency calculations whereas the transition states showed one imaginary frequency. Moreover, BP86/BS1 level energetics is corrected for solvation effect using the self-consistent reaction field method SMD[42] and D3 dispersion[94] effect by single point calculations. Water is used as the solvent. The single point calculation is abbreviated as BP86-D3/SMD/BS1 and the energetics using this method is used for all the discussions unless otherwise mentioned. The solvent corrected free energy at 298 K and 1 atm is obtained by adding BP86-D3/SMD/BS1 level energy and BP86/BS1 level free energy correction. MESP at the hydride and carbonyl ligands as well as at the ruthenium metal center are calculated at BP86/BS1 level.

4.9 Results and Discussion

4.9.1 Design Strategy

Several ruthenium pincer complexes with different functionalities are known in the literature for various catalytic applications. Some of the most commonly used precursors are $RuHCl(CO)(PPh_3)_3$ and $RuCl_2(PPh_3)_3$ which on reaction with different pincer ligands yield ruthenium hydrido-chloro carbonyl and ruthenium phosphino-chloro derivatives, respectively. A few experimentally reported ruthenium pincer catalysts such as **PNN** (for conversion of alcohol to esters),[95] **PNP** (for synthesis of imines from alcohols and amines),[96] **PNS** (for dehydrogenative coupling of alcohols with amines),[97] **NNP** (for dehydrogenative homocoupling of primary alcohols to form esters and coupling of

amines to form imines),[98] **SNS** (for transfer hydrogenation of acetophenone),[99] **NCN**,[100] **PCP**,[101] and **NNN**[102] are depicted in Figure 4.10.

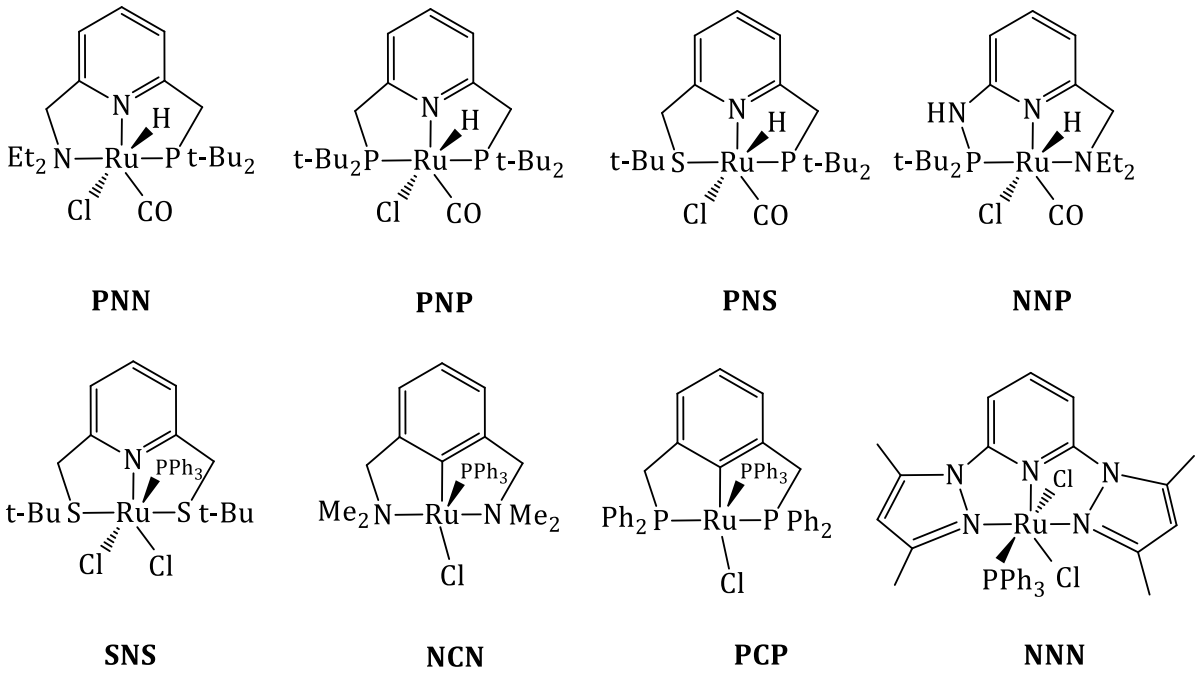

Figure 4.10 Experimentally known Ru pincer complexes

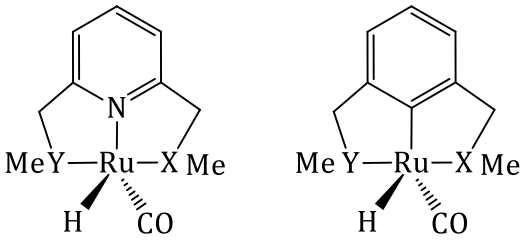

Scheme 4.2 Schematic representation for the modification of pyridine based and benzene based pincer ligands respectively. **X**, **Y** = **PR**, **NR**, **O**, **S**.

Since the first report of Milstein catalyst in 2009,[16] several mechanisms have been reported for the water reduction step of the reaction.[103] Mechanisms concerning metal ligand cooperation (MLC) and aromatization–dearomatization of ligands are vital in the case of H_2 elimination with pincer type catalysts.[104-107] This study focuses on the similar outer sphere mechanism reported by Suresh *et al.*[32] for several Ru pincer hydride complexes, distinguished by different donor atoms to understand the role of pincer

ligands in tuning the activation barrier. A scheme for the systematic modification of pincer ligands is depicted in Scheme 4.2 and the selected systems are depicted in Figure 4.11.

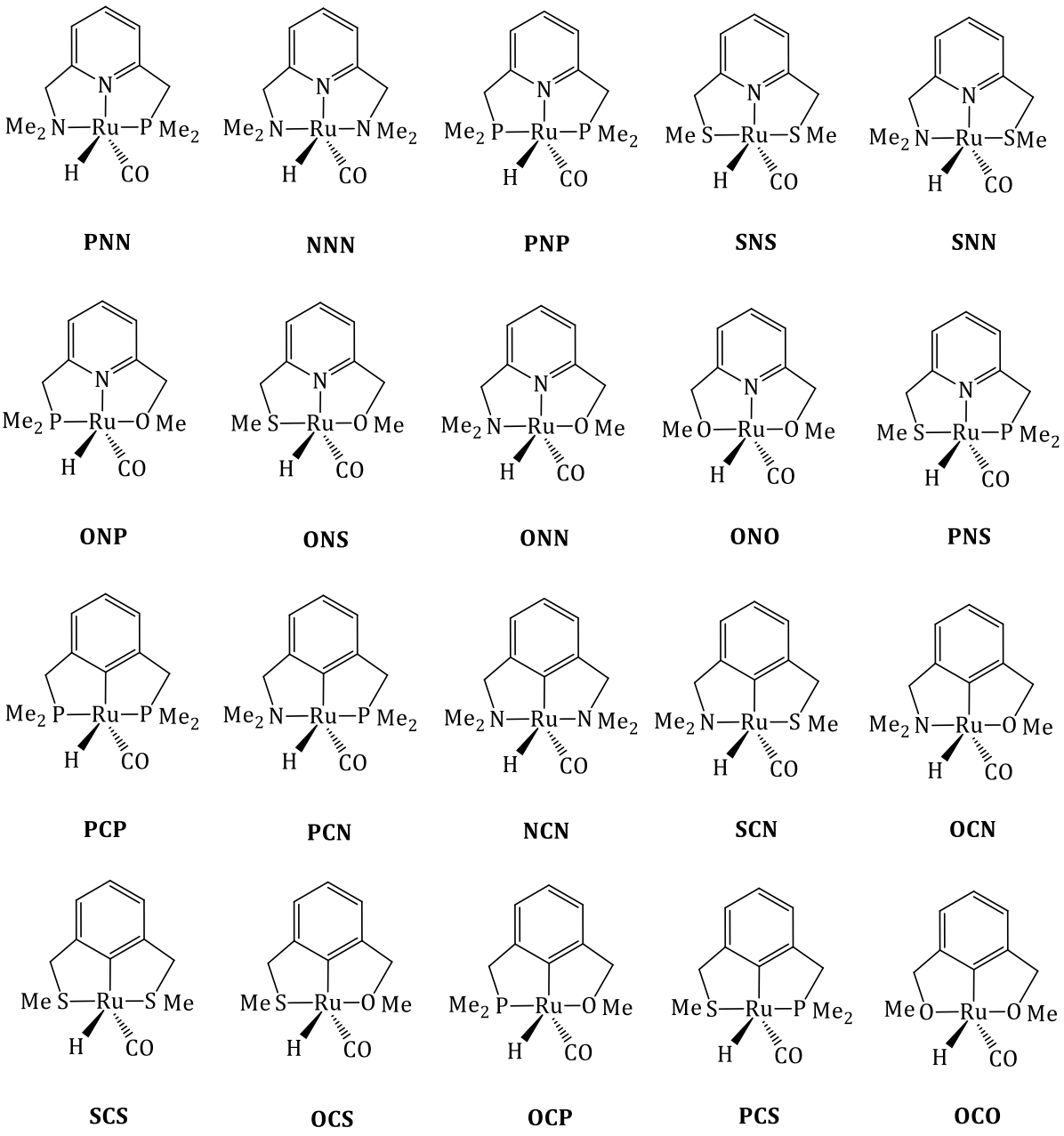

Figure 4.11 Different pincer complexes selected for the study. Complexes **1-10** in the first two rows are pyridine based and **11-20** in the last two rows are benzene based.

These 20 pincer complexes are selected using the possible combinations of the donor atoms, **P**, **N**, **S** and **O**. The donor sites may be similar, resulting in a symmetric

pincer (**XZX**) complex while dissimilar donor sites make unsymmetrical pincer (**XZY**) complex. The central moiety in complexes **1** - **10** is pyridine ring, whereas in complexes **11** -**20**, it is benzene. The side arm substituents are not mentioned in the nomenclature, since methyl groups are used in all the complexes.

4.9.2 Designing Homodesmotic Reaction

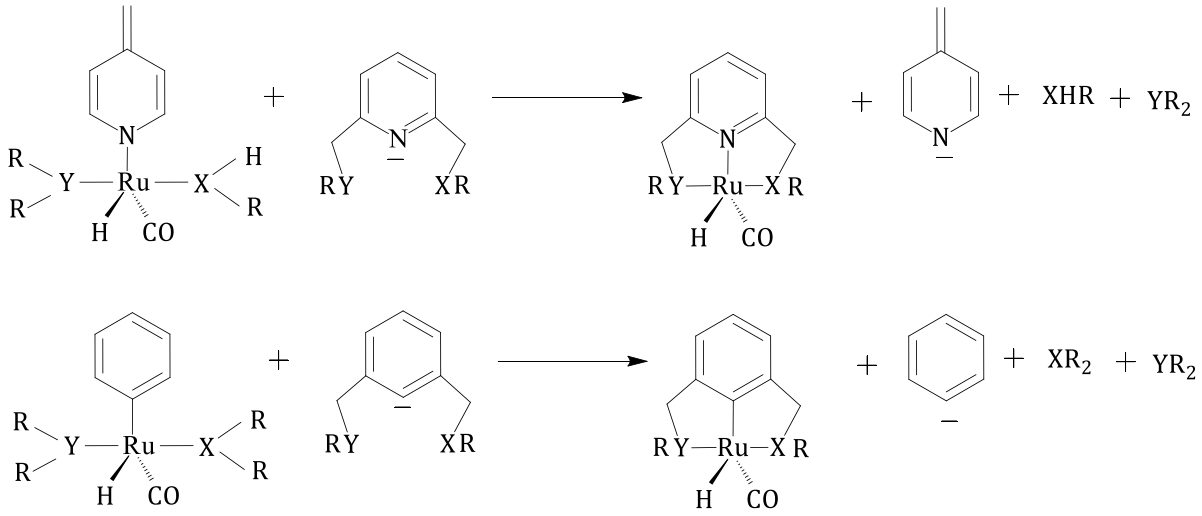

Figure 4.12 Designed homodesmotic reaction for pyridine based and benzene based pincer complexes.

A homodesmotic reaction is defined as a hypothetical chemical process in which hybridization and number of bond breaking and bond forming steps should be same on each side of the reaction. A schematic representation of a homodesmotic reaction for both the pyridine and benzene based pincer hydride complexes is given in Figure 4.12. The proposed homodesmotic reaction in our study involves the formation of pincer complexes from non-pincer Ru complexes and the pincer ligand. In order to balance the equation, substituents (**X** and **Y**) should be placed in the right side of the equation. The pyridine based ligands are dearomatized ones and such ligands were chosen to maintain the +2 oxidation state of ruthenium complexes. The quantity ΔE_{hdr} represents heat of homodesmotic reaction for pincer complexes (Table 4.6). The negative value of ΔE_{hdr} indicates the more stable character of the pincer complex than the non-pincer complex. Milstein catalyst (**PNN** complex) with ΔE_{hdr} -10.5 kcal/mol is the most stable among all

compared to the non-pincer systems. The simple HDR scheme presented here is not looking at the dissociation of the pincer ligand, but addressing the energetic advantage or disadvantage due to pincer mode of complexation compared to separate coordination from three ligands.

Table 4.6 Homodesmotic energies (kcal/mol) for the pincer complexes.

sl No.	pincer	ΔE_{hdr}	sl No.	pincer	ΔE_{hdr}
1	**PNN**	-10.5	11	**PCP**	6.3
2	**NNN**	-6.8	12	**PCN**	1.5
3	**PNP**	-5.5	13	**NCN**	-1.8
4	**SNS**	-8.2	14	**SCN**	1.1
5	**SNN**	-9.8	15	**OCN**	2.4
6	**ONP**	-3.2	16	**SCS**	6.7
7	**ONS**	-4.2	17	**OCS**	6.0
8	**ONN**	-4.5	18	**OCP**	3.2
9	**ONO**	-1.8	19	**PCS**	6.6
10	**PNS**	-5.5	20	**OCO**	7.5

4.9.3 MESP Analysis

Computationally derived ligand electronic parameters can act as convenient quantifiers for tuning the possible ligand modifications.[108,109] In a previous study dealing with the pincer ligand modifications in Ru(II) complexes, MESP minimum (V_{min}) at the hydride ligand and Tolman parameters were used to interpret the activation barriers for H_2 elimination.[92] Here MESP at Ru nucleus (V_{Ru}) and V_{min} at hydride and CO ligands are examined to understand the effect of pincer ligands in various catalysts. The MESP distribution given in Figure 4.13 illustrates the electron rich/deficient regions of the pyridine- and benzene-based pincer and non-pincer complexes. Here the side arms of the

pincer ligands are PR_3 type and the coordination bonds from these arms make them formally positively charged which can be identified by the red-colored MESP region (positive region) whereas the aromatic ring and the carbonyl ligand show electron rich features with the characteristic blue-colored region in MESP. Further, MESP distribution around the hydride ligand indicates accumulation of some amount of electron density over there. A visual inspection of the MESP pictures clearly indicates that pincer complexes show more negative MESP distribution than the non-pincer complexes meaning that pincer ligand configuration exerts more electron donating influence on the metal than a matching non-pincer configuration.

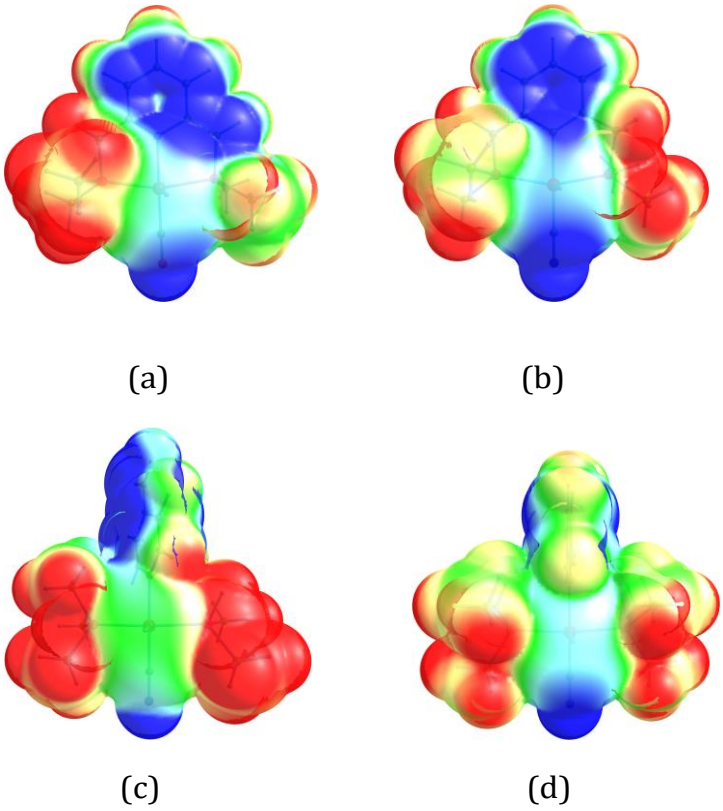

Figure 4.13 MESP mapped at 0.01 au isodensity surface for (a) **PNP** pincer and (b) **PCP** pincer (c) **PNP** non-pincer and (d) **PCP** non-pincer complexes. MESP ranging from −0.02 au (blue) to 0.02 au (red).

Table 4.7 MESP values(kcal/mol) of pincer and non-pincer complexes. V_{Ru} values in au.

		MESP(pincer)			MESP(non-pincer)			
Sl No.	pincer	V_{Ru}	$V_{min\text{-}H}$	$V_{min\text{-}CO}$	V_{Ru}	$V_{min\text{-}H}$	$V_{min\text{-}CO}$	ΔV_{Ru}
1	**PNN**	-13.4091	-17.5	-32.6	-13.3909	-6.3	-24.7	-11.4
2	**NNN**	-13.4158	-20.5	-35.2	-13.4005	-9.3	-27.5	-9.6
3	**PNP**	-13.4012	-16.4	-30.3	-13.3893	-10.1	-24.9	-7.5
4	**SNS**	-13.3943	-12.9	-30.4	-13.3840	-8.6	-23.4	-6.5
5	**SNN**	-13.4056	-16.9	-32.3	-13.3900	-6.5	-24.9	-9.8
6	**ONP**	-13.4013	-19.2	-31.6	-13.3893	-8.4	-24.8	-7.5
7	**ONS**	-13.3957	-16.7	-32.3	-13.3861	-10.1	-26.7	-6.0
8	**ONN**	-13.4092	-20.9	-34.8	-13.3958	-9.5	-27.2	-8.4
9	**ONO**	-13.4005	-17.9	-33.8	-13.3887	-11.0	-26.7	-7.4
10	**PNS**	-13.4002	-18.3	-29.4	-13.3866	-13.2	-25.7	-8.5
11	**PCP**	-13.4156	-23.0	-33.0	-13.4128	-20.3	-30.9	-1.8
12	**PCN**	-13.4224	-23.4	-34.5	-13.4181	-21.0	-31.6	-2.7
13	**NCN**	-13.4336	-26.8	-37.8	-13.4256	-24.2	-33.8	-5.0
14	**SCN**	-13.4207	-22.2	-33.3	-13.4159	-21.3	-30.9	-3.0
15	**OCN**	-13.4274	-25.7	-36.3	-13.4215	-22.5	-32.9	-3.7
16	**SCS**	-13.4101	-23.0	-30.4	-13.4094	-18.8	-28.7	-0.5
17	**OCS**	-13.4142	-24.8	-32.3	-13.4118	-18.4	-29.6	-1.5
18	**OCP**	-13.4181	-24.2	-33.1	-13.4148	-19.4	-30.6	-2.1
19	**PCS**	-13.4134	-21.0	-33.1	-13.4121	-19.6	-29.7	-0.8
20	**OCO**	-13.4219	-26.4	-35.2	-13.4185	-21.2	-31.9	-2.2

A quantification of the MESP features can be achieved by analyzing V_{Ru}, V_{min} at hydride ligand ($V_{min\text{-}H}$) and V_{min} at CO ligand ($V_{min\text{-}CO}$). An illustration of the same is given in Figure 4.14 for a representative pincer and the corresponding non-pincer complexes. Further, these MESP parameters for all the pincer and non-pincer complexes are depicted in Table 4.7. The MESP data show that V_{Ru}, $V_{min\text{-}H}$ and $V_{min\text{-}CO}$ are always more negative in pincer complexes. Moreover, benzene-based pincer ligands always show more negative character for MESP parameters than the pyridine-based pincer complexes. For example, V_{min} at the hydride ligand (-23.0 kcal/mol) and carbonyl ligand (-33.0 kcal/mol) are more negative for the **PCP** pincer complexes than the **PCP** non-pincer, **PNP** pincer and **PNP** non-pincer complexes. Apparently, the benzene-based pincer complexes show more electron donating features than the pyridine-based ones.

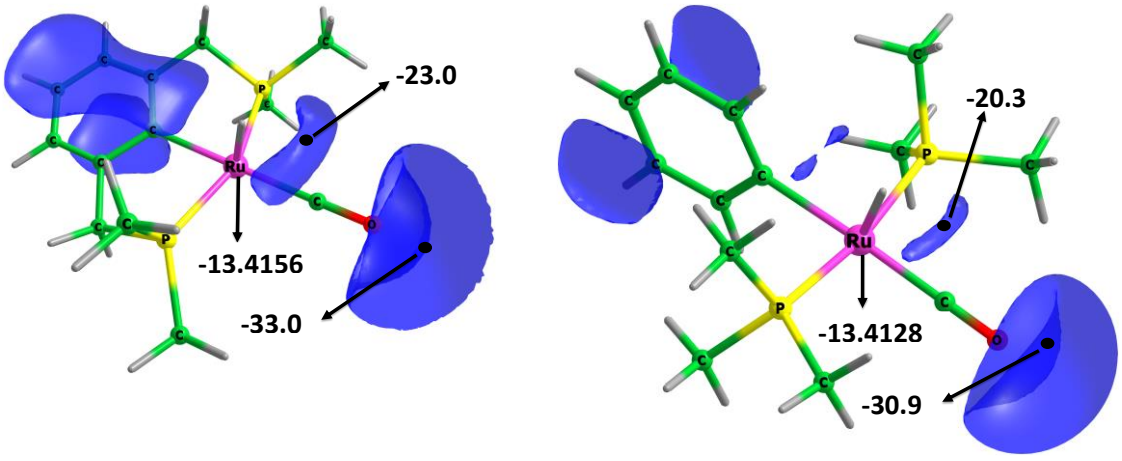

PCP **PCP-non**

Figure 4.14 MESP plots of V_{min} on hydride and carbonyl ligands shown with 18.8 kcal/mol isosurfaces of **PCP** pincer and **PCP** non-pincer complexes. V_{min} in kcal/mol.

The difference in MESP at the ruthenium centers of the pincer and the corresponding non-pincer complex (ΔV_{Ru}) can be regarded as a quantity to measure the electronic perturbations at Ru due to the ligand effects. This argument is valid considering the fact that ΔV_{Ru} shows a good linear correlation with the ΔE_{hdr} and also suggests that the electron donating effect has stabilizing influence on the complex and vice versa. The electron donating character of pincer lignads may play a role in increasing the catalytic

activity of the ruthenium complex towards hydrogen elimination reaction by splitting water. This can be understood by correlating the mechanistic energetic aspects of the reaction with the MESP based assessment of the ligand influence.

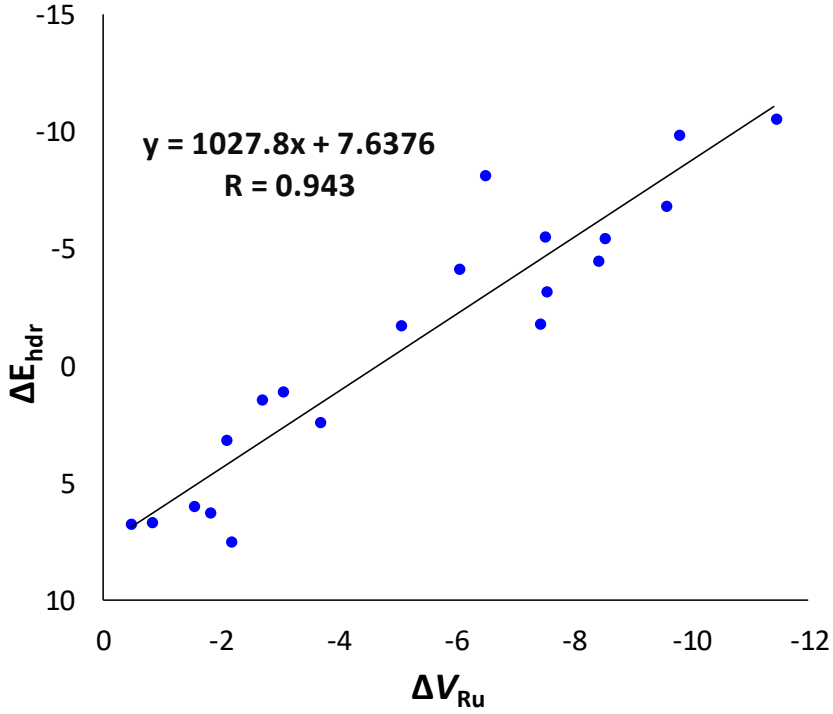

Figure 4.15 Correlation between ΔV_{Ru} and ΔE_{hdr} (kcal/mol) .

4.9.4 Activation Barrier for H_2 Elimination

The hydride ligand assisted outer sphere mechanism of H_2 elimination from water is previously established for the Milstein catalyst.[32] The effect of various ligands on the mechanism is assessed by computing the H_2 elimination mechanism for all the pincer complexes and representative energy profile diagrams are given for pyridine based (**PNP**) and benzene based (**PCP**) complexes (Figure 4.16). The reactants **PNP-R** and **PCP-R** symbolize the water coordinated structures of the corresponding **PNP** and **PCP** pincer catalysts. ΔE_1 indicates the interaction energy of water molecule with the catalyst and ΔG_1 is the corresponding free energy change. $\Delta E^{\#}$ is the activation energy for the H_2 elimination from the transition state structures (**PNP-TS** and **PCP-TS**) and $\Delta G^{\#}$ is the corresponding activation free energy. ΔE_2 and ΔG_2 are the overall activation energy and activation free energy with respect to the reactants (**PNP** + H_2O and **PCP** + H_2O) and the activated catalysts (**PNP-P** and **PCP-P**).

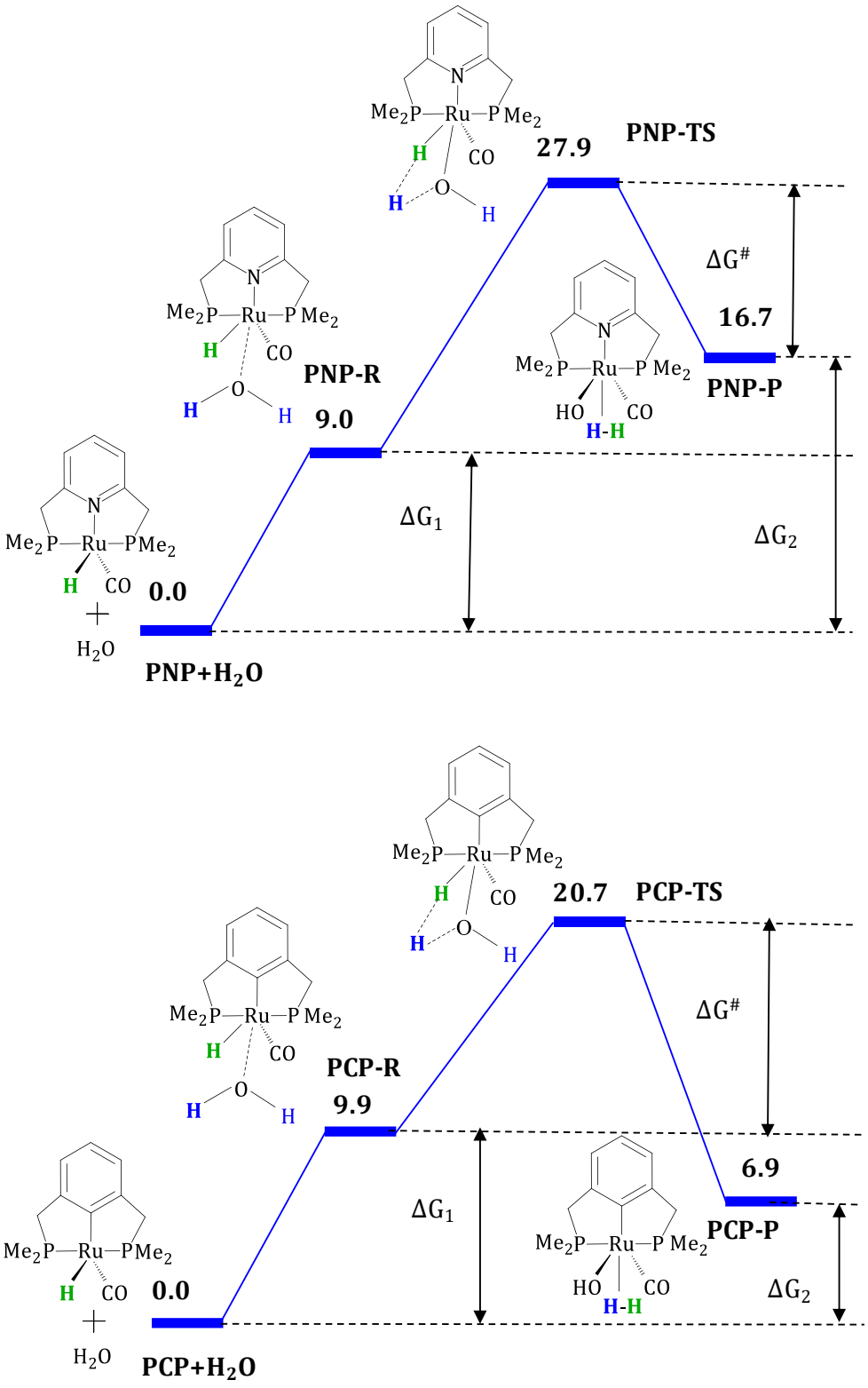

Figure 4.16 Free energy profile diagram for η²-dihydrogen complex formation in **PNP** and **PCP** pincer complexes at BP86-D3/SMD/BS1//BP86/BS1 level. Values in kcal/mol.

Table 4.8 The ΔE_1, ΔG_1, $\Delta E^{\#}$, $\Delta G^{\#}$, ΔE_2 and ΔG_2 values for the selected catalysts at BP86-D3/SMD/BS1//BP86/BS1 level. Values in kcal/mol.

Sl No.	pincer	ΔE_1	ΔG_1	$\Delta E^{\#}$	$\Delta G^{\#}$	ΔE_2	ΔG_2
1	**PNN**	-1.4	10.2	18.3	17.8	3.4	15.4
2	**NNN**	3.3	14.8	14.7	14.1	4.2	16.3
3	**PNP**	-3.1	9.0	20.8	18.9	5.4	16.7
4	**SNS**	-0.5	12.7	20.8	17.9	9.1	20.5
5	**SNN**	0.0	13.3	18.1	15.3	5.2	16.9
6	**ONP**	-1.1	12.2	20.0	16.9	7.8	18.7
7	**ONS**	0.8	13.7	21.1	18.0	9.4	20.6
8	**ONN**	0.8	13.7	17.5	15.2	5.5	17.1
9	**ONO**	-1.1	11.5	19.3	16.5	5.6	16.8
10	**PNS**	-3.1	9.0	20.6	19.3	4.8	16.6
11	**PCP**	-1.8	9.9	11.9	10.8	-4.8	6.9
12	**PCN**	-0.4	11.6	8.9	8.2	-7.4	5.0
13	**NCN**	0.5	12.5	6.9	5.8	-8.9	3.9
14	**SCN**	-1.3	10.2	9.9	9.5	-6.8	4.9
15	**OCN**	-1.6	9.5	9.6	8.8	-8.8	2.7
16	**SCS**	-3.8	7.8	13.0	12.2	-6.4	5.5
17	**OCS**	-4.2	7.6	12.5	11.3	-7.2	4.6
18	**OCP**	-2.6	9.2	12.7	11.3	-5.2	6.5
19	**PCS**	-0.9	10.3	11.1	10.5	-4.8	7.2
20	**OCO**	-2.7	9.4	10.4	9.0	-8.5	3.8

The energetic parameters at the BP86-D3/SMD/BS1//BP86/BS1 level of theory, viz. ΔE_1, ΔG_1, $\Delta E^{\#}$, $\Delta G^{\#}$, ΔE_2, and ΔG_2 are given in Table 4.8. The optimized structures of the **PNP** catalyst and its water coordinated complex **PNP-R** are given in Figure 4.17.

Coordination of water leads to significant elongation of Ru-H bond from 1.56 to 1.62 Å. The Ru-N (pyridyl) bond also elongates while the Ru-CO bond shows shortening due to water coordination. Similar observations in bond length are noted for the **PCP** catalyst and its water coordinated complex **PCP-R** (Figure 4.18). When comparing the bonding parameters of all the other pincer catalysts and their corresponding water complexes, it is clear that the coordination of water leads to significant activation of the Ru-H bond. Except **NNN** catalyst, the coordination is exothermic (ΔE_1) in the range -0.5 to -4.2 kcal/mol.

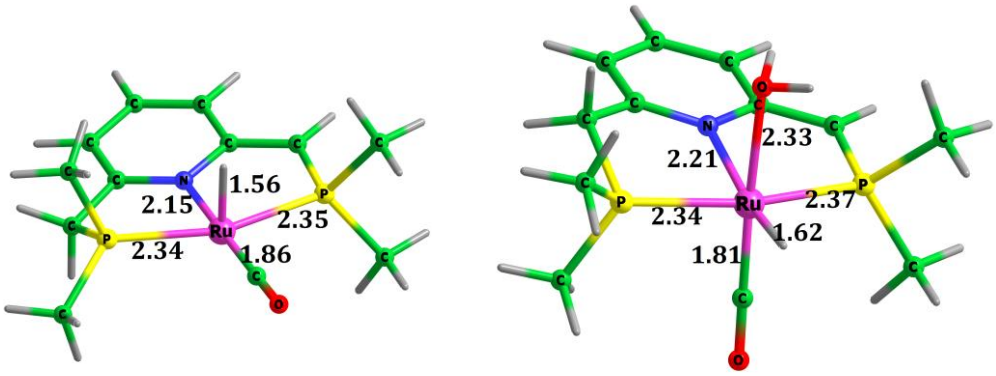

PNP **PNP-R**

Figure 4.17 Optimized structures of **PNP** Milstein catalyst and **PNP** complexed with a water molecule (**PNP-R**). Distances in Å.

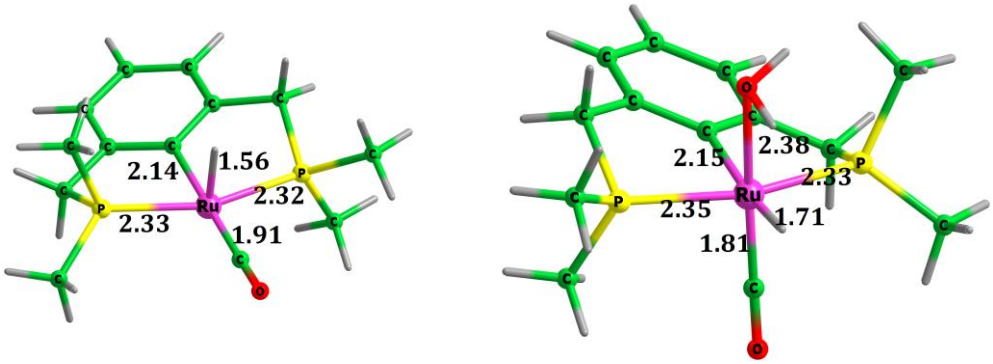

PCP **PCP-R**

Figure 4.18 Optimized structures of **PCP** Milstein catalyst and **PCP** complexed with a water molecule (**PCP-R**). Distances in Å.

The activated Ru-H bond suggests strong hydridic character for the hydrogen and that facilitates Ru-H…HOH dihydrogen interaction in the transition states **PNP-TS** and **PCP-TS** (Figure 4.19). The next parameters to be explored are the energetic parameters correspond to the H_2 elimination from the transition state structures. The values of $\Delta E^{\#}$ (in the range 6.9 to 13.0 kcal/mol) and $\Delta G^{\#}$ (in the range 5.8 to 12.2 kcal/mol) for the benzene based pincer complexes are approximately 7 kcal/mol lower than that of the pyridine based pincer complexes which are in the range 14.7 to 21.1 kcal/mol for $\Delta E^{\#}$ and 14.1 to 19.3 kcal/mol for $\Delta G^{\#}$. These suggest the early formation of TS in benzene based pincer systems which can be substantiated by the fact that the O-H bond distance 1.36 Å observed in **PCP-TS** is significantly shorter than that of **PNP-TS** (1.50 Å).

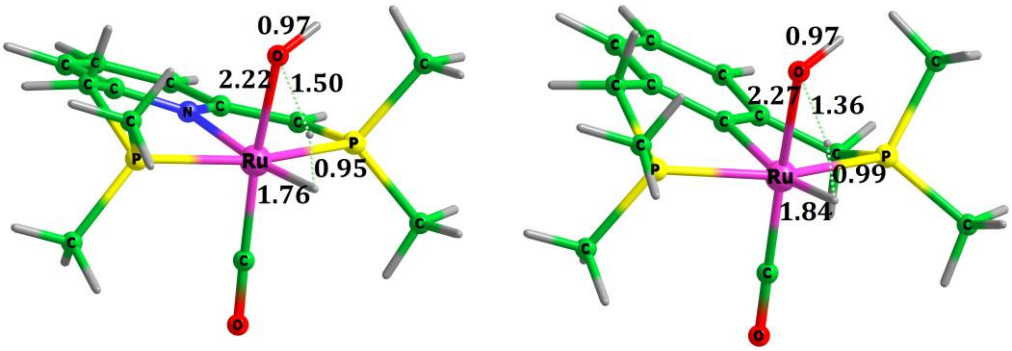

PNP-TS **PCP-TS**

Figure 4.19 Representative transition state structures for **PNP** and **PCP** pincer complexes.

The MESP parameter V_{Ru} is useful to measure the overall electron rich character of the metal center due to the electron donation from the ligand environment. It has already seen than a pincer ligand environment is more electron donating than a corresponding non-pincer environment. The correlation plot given in Figure 4.20 between V_{Ru} and $\Delta E^{\#}$ unambiguously suggest that by increasing the electron rich character of metal center, the activation barrier for H_2 elimination can be reduced. Definitely the benzene based pincer ligands are more effective as they are more electron donating than the pyridine based ones. Thus the MESP analysis gives a simple interpretation of the activation barriers of the reaction.

The general feasibility of the reaction can be judged by analysing the overall energy parameters ΔE_2 and ΔG_2. The ΔE_2 of benzene based pincer complexes support exothermic character by -4.8 to -8.9 kcal/mol while ΔG_2 is exergonic by 2.7 to 7.2 kcal/mol. For the pyridine based pincer complexes, ΔE_2 is in the range 3.4 to 9.4 kcal/mol and ΔG_2 is in the range 15.4 to 20.6 kcal/mol. These energetic features suggest the use of the benzene based pincer catalysts for the activation of the OH bond of water which may show higher efficiency than the pyridine based ones. It may be noted that the rigid structure of pincer ligands may facilitate favorable orientation for an incoming reactant to pass through a transition state. Our mechanistic studies were on the realistic pincer systems, and the non-pincer systems were only used to study the HDR energetics.

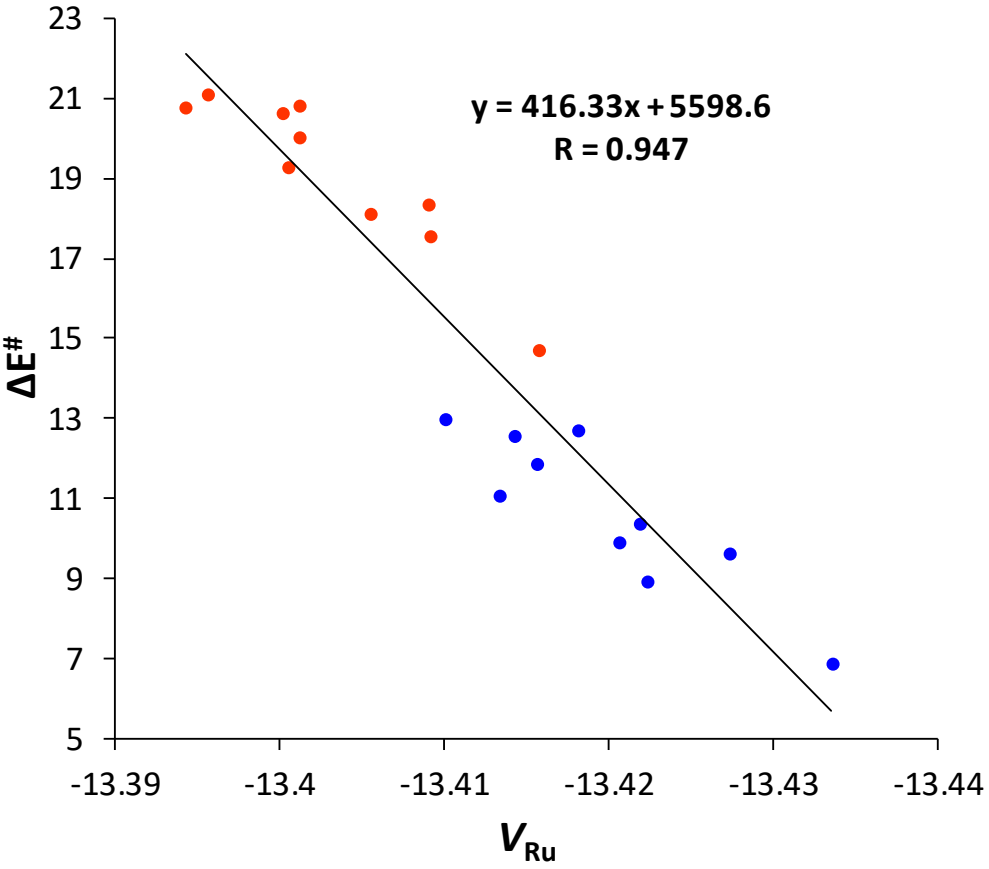

Figure 4.20 Correlation between V_{Ru} (au) and activation barriers $\Delta E^{\#}$ (kcal/mol).

4.9.5 Effect of Bulkier Arms on Reactivity

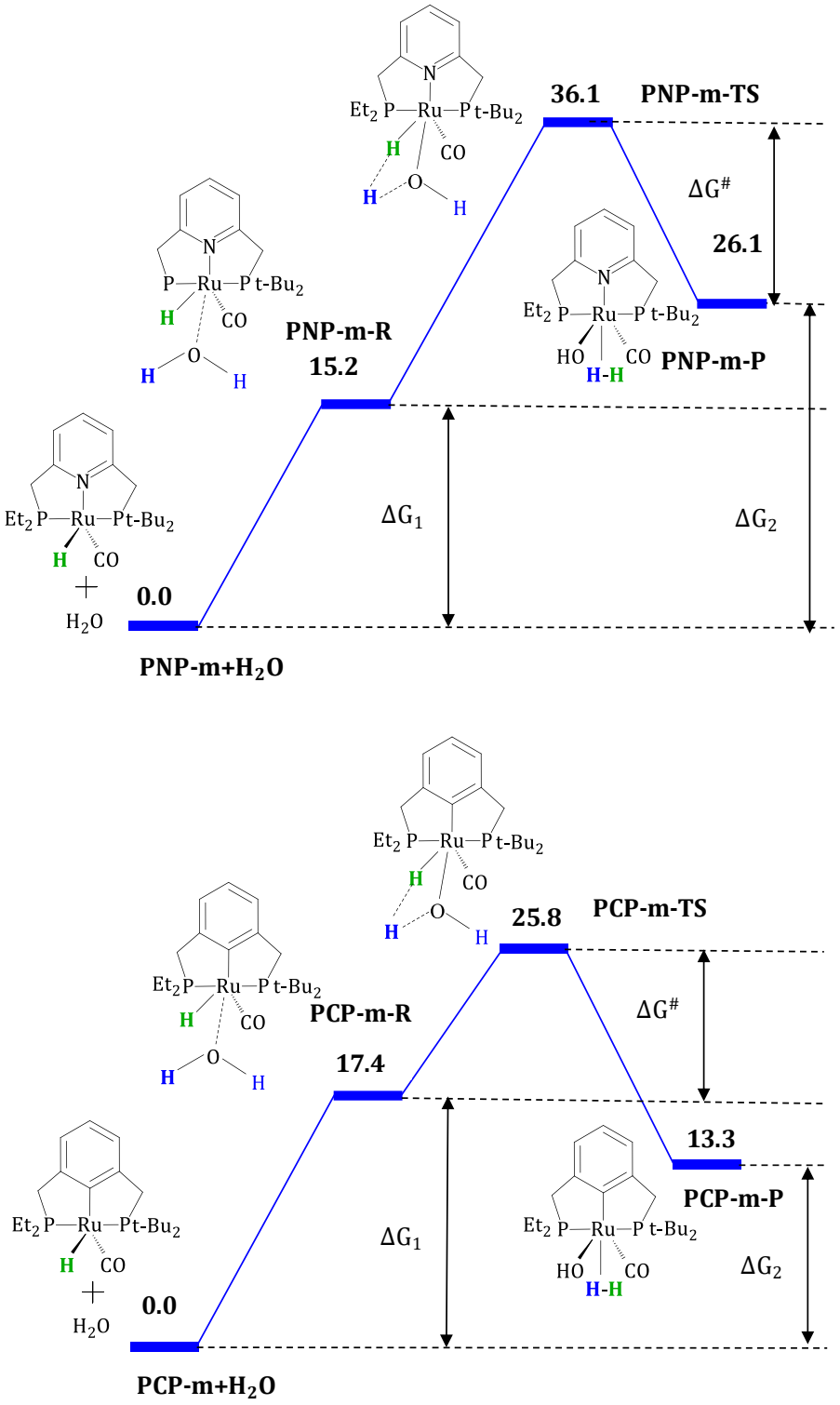

Figure 4.21 Free energy profile diagram for η^2-dihydrogen complex formation in **PNP-m** and **PCP-m** complexes at BP86-D3/SMD/BS1//BP86/BS1 level. Values in kcal/mol.

The Milstein catalyst has t-butyl and ethyl groups as the side arms on the **PNN** framework. The effect of using the Me_2 groups in this study, rather than the more basic tBu_2 groups, can be addressed by investigating the H_2 elimination reaction for representative **PNP** and **PCP** catalysts with t-butyl and ethyl groups as the side arms. The new catalysts are named as **PNP-m** and **PCP-m** and the mechanistic aspects are depicted in Figure 4.21. According to our previous report, reducing the steric bulkiness over the P and N arms of the modified Milstein catalysts improves the efficiency of the catalyst by promoting the coordination for H_2O in an undemanding way for H_2 elimination.[92] The comparison of the energetics of the newly studied catalysts with the previous systems supports this fact for pyridine and benzene based pincer complexes.

4.10 Conclusions

The Ru (II) Milstein catalyst, a **PNN** type pincer complex and nineteen other Ru (II) complexes designed with large variations in pincer type chelation have been studied to understand their H_2 elimination reaction pathway. The study also focused on quantifying the electron donating feature of the pincer ligands in terms of the MESP parameters. The proposed homodesmotic reaction scheme is useful to quantify the stabilizing/destabilizing effect of a pincer ligand compared to that of a non-pincer ligand. The ΔE_{hdr} directly accounts for the energetic effect of the pincer ligand. The MESP analysis at the metal center, hydride ligand and carbonyl ligand confirms that the pincer configuration is inherently more electron donating to the metal center than a non-pincer configuration. The **XCY** type benzene based pincer complexes are more electron rich than the **XNY** type pyridine based complexes for the same **X** and **Y** environments. The studies are further extended to the mechanistic aspects of the hydride ligand assisted outer sphere mechanism of H_2 elimination from water. A decreasing trend in the activation barrier is observed with increase in the electron rich character of the metal center. The more electron donating **XCY** type pincer complexes showed significantly lower barriers than the **XNY** type complexes. The benzene based pincer complexes are suggested as more efficient water reduction catalysts than the pyridine based ones.

4.11 References

1. S. Niu and M. B. Hall, *Chem. Rev.* **2000**, *100*, 353-406.
2. C. Bo, F. Maseras and N. López, *Nat. Cat.* **2018**, *1*, 809-810.
3. D. Das and T. N. Veziroglu, *Int. J. Energy Res.* **2001**, *26*, 13-28.
4. N. S. Lewis and D. G. Nocera, *Proc. Natl. Acad. Sci. U.S.A.* **2006**, *103*, 15729-15735.
5. W. Lubitz and W. Tumas, *Chem. Rev.* **2007**, *107*, 3900-3903.
6. C. Pan, Y. Fan and H. Hou, *Ind. Eng. Chem. Res.* **2008**, *47*, 5812-5818.
7. T. Lazarides, T. McCormick, P. Du, G. Luo, B. Lindley and R. Eisenberg, *J. Am. Chem. Soc.* **2009**, *131*, 9192-9194.
8. J. D. Holladay, J. Hu, D. L. King and Y. Wang, *Catal. Today* **2009**, *139*, 244-260.
9. K. Christopher and R. Dimitriosa, *Energy Environ. Sci.* **2012**, *5*, 6640-6651.
10. William R. McNamara, Zhiji Han, Paul J. Alperin, William W. Brennessel, a. Patrick L. Holland and R. Eisenberg, *J. Am. Chem. Soc.* **2011**, *133,* 15368-15371.
11. Bryan D. Stubbert, Jonas C. Peters and a. H. B. Gray, *J. Am. Chem. Soc.* **2011**, *133*, 18070–18073.
12. C. C. L. McCrory, C. Uyeda and J. C. Peters, *J. Am. Chem. Soc.* **2012**, *134*, 3164-3170.
13. C. S. Letko, J. A. Panetier, M. Head-Gordon and T. D. Tilley, *J. Am. Chem. Soc.* **2014**, *136*, 9364-9376.
14. P. L. Zhang, M. Wang, Y. Yang, T. Y. Yao and L. C. Sun, *Angew. Chem. Int. Ed.* **2014**, *53*, 13803-13807.
15. J. Willkomm, N. M. Muresan and E. Reisner, *Chem. Sci.* **2015**, *6*, 2727-2736.
16. S. W. Kohl, L. Weiner, L. Schwartsburd, L. Konstantinovski, L. J. W. Shimon, Y. Ben-David, M. A. Iron and D. Milstein, *Science* **2009**, *324*, 74-77.
17. L. Hammarström and S. Styring, *Nat. Chem.* **2009**, *1*, 185-186.
18. R. Eisenberg, *Science* **2009**, *324*, 44-45.
19. D. G. H. Hetterscheid, J. I. van der Vlugt, B. de Bruin and J. N. H. Reek, *Angew. Chem. Int. Ed.* **2009**, *48*, 8178-8181.
20. M. A. Iron, E. Ben-Ari, R. Cohen and D. Milstein, *Dalton Trans.* **2009**, 9433-9439.
21. E. Balaraman, B. Gnanaprakasam, L. J. W. Shimon and D. Milstein, *J. Am. Chem. Soc.* **2010**, *132*, 16756-16758.

22. B. Gnanaprakasam and D. Milstein, *J. Am. Chem. Soc.* **2011**, *133*, 1682-1685.
23. C. Gunanathan and D. Milstein, *Acc. Chem. Res.* **2011**, *44*, 588-602.
24. B. Gnanaprakasam, E. Balaraman, C. Gunanathan and D. Milstein, *J. Polym. Sci., Part A: Polym. Chem.* **2012**, *50*, 1755-1765.
25. D. Srimani, E. Balaraman, B. Gnanaprakasam, Y. Ben-David and D. Milstein, *Adv. Synth. Catal.* **2012**, *354*, 2403-2406.
26. E. Balaraman, E. Khaskin, G. Leitus and D. Milstein, *Nat. Chem.* **2013**, *5*, 122-125.
27. C. Gunanathan and D. Milstein, *Chem. Rev.* **2014**, *114*, 12024-12087.
28. H. X. Li, X. T. Wang, F. Huang, G. Lu, J. L. Jiang and Z. X. Wang, *Organometallics* **2011**, *30*, 5233-5247.
29. D. Milstein, *Phil. Trans. R. Soc. A* **2015**, *373*, 20140189.
30. X. Yang and M. B. Hall, *J. Am. Chem. Soc.* **2010**, *132*, 120-130.
31. J. Li, Y. Shiota and K. Yoshizawa, *J. Am. Chem. Soc.* **2009**, *131*, 13584-13585.
32. K. S. Sandhya and C. H. Suresh, *Organometallics* **2011**, *30*, 3888-3891.
33. L. C. Liang, W. Y. Lee, Y. T. Hung, Y. C. Hsiao, L. C. Cheng and W. C. Chen, *Dalton Trans.* **2012**, *41*, 1381-1388.
34. L. Canovese, F. Visentin, C. Levi, C. Santo and V. Bertolasi, *Inorg. Chim. Acta* **2012**, *390*, 105-118.
35. M. Feller, Y. Diskin-Posner, L. J. W. Shimon, E. Ben-Ari and D. Milstein, *Organometallics* **2012**, *31*, 4083-4101.
36. D. Gelman and S. Musa, *ACS Catal.* **2012**, *2*, 2456-2466.
37. R. Langer, M. A. Iron, L. Konstantinovski, Y. Diskin-Posner, G. Leitus, Y. Ben-David and D. Milstein, *Chem. Eur. J.* **2012**, *18*, 7196-7209.
38. M. Vogt, O. Rivada-Wheelaghan, M. A. Iron, G. Leitus, Y. Diskin-Posner, L. J. W. Shimon, Y. Ben-David and D. Milstein, *Organometallics* **2013**, *32*, 300-308.
39. M. Feller, E. Ben-Ari, Y. Diskin-Posner, R. Carmieli, L. Weiner and D. Milstein, *J. Am. Chem. Soc.* **2015**, *137*, 4634-4637.
40. M. J. Frisch, G. W. Trucks, H. B. Schlegel, G. E. Scuseria, M. A. Robb, J. R. Cheeseman, G. Scalmani, V. Barone, B. Mennucci, G. A. Petersson, H. Nakatsuji, M. Caricato, X. Li, H. P. Hratchian, A. F. Izmaylov, J. Bloino, G. Zheng, J. L. Sonnenberg, M. Hada, M. Ehara, K. Toyota, R. Fukuda, J. Hasegawa, M. Ishida, T. Nakajima, Y. Honda, O. Kitao,

H. Nakai, T. Vreven, J. J. A. Montgomery, J. E. Peralta, F. Ogliaro, M. Bearpark, J. J. Heyd, E. Brothers, K. N. Kudin, V. N. Staroverov, T. Keith, R. Kobayashi, J. Normand, K. Raghavachari, A. Rendell, J. C. Burant, S. S. Iyengar, J. Tomasi, M. Cossi, N. Rega, J. M. Millam, M. Klene, J. E. Knox, J. B. Cross, V. Bakken, C. Adamo, J. Jaramillo, R. Gomperts, R. E. Stratmann, O. Yazyev, A. J. Austin, R. Cammi, C. Pomelli, J. W. Ochterski, R. L. Martin, K. Morokuma, V. G. Zakrzewski, G. A. Voth, P. Salvador, J. J. Dannenberg, S. Dapprich, A. D. Daniels, O. Farkas, J. B. Foresman, J. V. Ortiz, J. Cioslowski and and D. J. Fox, *Gaussian 09, Revision D.01,* **2013**, *Gaussian, Inc., Wallingford CT*.

41. P. J. Hay and W. R. Wadt, *Chin. J. Chem. Phys.* **1985**, *82*, 270-283.
42. A. V. Marenich, C. J. Cramer and D. G. Truhlar, *J. Phys. Chem. B* **2009**, *113*, 6378-6396.
43. V. Barone and M. Cossi, *J. Phys. Chem. A* **1998**, *102*, 1995-2001.
44. E. S. H. Gwee, Z. L. Seeger, D. R. T. Appadoo, B. R. Wood and E. I. Izgorodina, *ACS Omega* **2019**, *4*, 5254-5269.
45. S. R. Gadre and S. S. Pundlik, *J. Phys. Chem. B* **1997**, *101*, 3298-3303.
46. L. P. Hammett, *J. Am. Chem. Soc* **1937**, *59*, 96-103.
47. P. K. Sajith and C. H. Suresh, *Inorg. Chem.* **2012**, *51*, 967-977.
48. J. X. Liang, B. J. Wang and Z. X. Cao, *J. Chem. Theory Comput.* **2013**, *12*.
49. Q. Wang, C. Wei, L. M. Pérez, W. J. Rogers, M. B. Hall and M. S. Mannan, *J. Phys. Chem. A* **2010**, *114*, 9262-9269.
50. C. Ma, S. Piccinin and S. Fabris, *ACS Catal.* **2012**, *2*, 1500-1506.
51. K. S. Sandhya and C. H. Suresh, *Dalton Trans.* **2012**, *41*, 11018-11025.
52. K. S. Sandhya and C. H. Suresh, *Dalton Trans.* **2014**, *43*, 12279-12287.
53. M. J. Ajitha and C. H. Suresh, *J. Org. Chem.* **2012**, *77*, 1087-1094.
54. F. A. Cotton and G. Wilkinson, *Advanced Inorganic Chemistry* **1988**, John Wiley: New York.
55. C. Elschenbroich and A. Salzer, *Organometallics* **1989**, VCH Publishers: New York.
56. R. H. Crabtree, *The Organometallic Chemistry of the Transition Metals, 2nd ed.* **1994**, Wiley: New York.

57. N. Koga and K. Morokuma, *Chem. Rev.* **1991**, *91*, 823-842
58. J. N. Harvey, *Annu. Rep. Prog. Chem. Sect. C* **2006**, *102*, 203-226.
59. M. Mitoraj and A. Michalak, *J. Mol. Model.* **2007**, *13*, 347-355.
60. D. Balcells, E. Clot and O. Eisenstein, *Chem. Rev.* **2010**, *110*, 749-823.
61. T. Sperger, I. A. Sanhueza, I. Kalvet and F. Schoenebeck, *Chem. Rev.* **2015**, *115*, 9532-9586.
62. C.J. Moulton and B. L. Shaw, *J. Chem. Soc. Dalton Trans.* **1976**, *0*, 1020-1024.
63. D. Morales-Morales, *Rev. Soc. Quím. Méx.* **2004**, *48*, 338-346.
64. M. A. W. Lawrence, K.-A. Green, P. N. Nelson and S. C. Lorraine, *Polyhedron* **2018**, *143*, 11-27.
65. Paulo Dani, Thomas Karlen, Robert A. Gossage, a. Serafino Gladiali and G. v. Koten, *Angew. Chem. Int. Ed.* **2000**, *39*, 743-745.
66. R. A. Gossage, L. A. v. d. Kuil and G. v. Koten, *Acc. Chem. Res.* **1998**, *31*, 423-431.
67. M. Ohff, A. Ohff, M. E. v. d. Boom and D. Milstein, *J. Am. Chem. Soc.* **1997**, *119*, 11687-11688.
68. R. B. Bedford, S. M. Draper, P. N. Scully and S. L. Welch, *New J. Chem.* **2000**, *24*, 745-747.
69. M. Gupta, C. Hagen, R. J. Flesher, W. C. Kaska and C. M. Jensen, *Chem. Commun.* **1996**, *0*, 2083-2084.
70. F. Gorla, A. Togni, L. M. Venanzi, A. Albinati and F. Lianza, *Organometallics* **1994**, *13,* 1607-1616.
71. M. A. Stark, G. Jones and C. J. Richards, *Organometallics* **2000**, *19,* 1282-1291.
72. H. Nishiyama, Y. Itoh, Y. Sugawara, H. Matsumoto, K. Aoki and K. Itoh, *Bull. Chem. Soc. Jpn* **1995**, *68*, 1247-1262.
73. L. Luconi, J. Klosin, A. J. Smith, S. Germain, E. Schulz, J. Hannedouche and G. Giambastiani, *Dalton Trans.* **2013**, *42*, 16056-16065
74. C. K. Prier, D. A. Rankic and D. W. C. MacMillan, *Chem. Rev.* **2013**, *113,* 5322-5363.
75. M. Albrecht, M. Schlupp, J. Bargon and G. v. Koten, *Chem. Commun.* **2001**, 1874-1875.
76. M. a.-C. Lagunas, R. A. Gossage, A. L. Spek and G. v. Koten, *Organometallics* **1998**, *17*, 731-741.

77. D. Morales-Morales, D. W. Lee, Z. Wang and C. M. Jensen, *Organometallics* **2001**, *20,* 1144-1147.
78. D. Morales-Morales, R. Redón, C. Yung and C. M. Jensen, *Chem. Commun.* **2000**, *0*, 1619-1620.
79. R.-g. M. Gauvin, H. Rozenberg, L. J. W. Shimon, Y. Ben-David and D. Milstein, *Chem. Eur. J.* **2007**, *13*, 1382 - 1393.
80. M. E. v. d. Boom and D. Milstein, *Chem. Rev.* **2003**, *103*, 1759–1792.
81. N. Selander and K. J. Szabó, *Chem. Rev.* **2011**, *111,* 2048-2076.
82. D. Benito-Garagorri, M. Puchberger, K. Mereiter and K. Kirchner, *Angew. Chem. Int. Ed.* **2008**, *47*, 9142 -9145.
83. D. Benito-Garagorri, V. Bocokic´, K. Mereiter and K. Kirchner, *Organometallics* **2006**, *25*, 3817-3823.
84. L. S. Sharninghausen, B. Q. Mercado, R. H. Crabtree and N. Hazari, *Chem. Commun.* **2015**, *51*, 16201-16204.
85. M. Albrecht and G. v. Koten, *Angew. Chem. Int. Ed.* **2001**, *40*, 3750 -3781.
86. C. Gunanathan and D. Milstein, *Chem. Rev.* **2014**, *114*, 12024−12087.
87. D. Benito-Garagorri and K. Kirchner, *Acc. Chem. Res.* **2008**, *41,* 201-213.
88. D. Morales-Morales and C. Jensen, *The Chemistry of Pincer Compounds* **2007**, Elsevier Science, Amsterdam.
89. H. A. Younus, N. Ahmada, W. Su and F. Verpoort, *Coord. Chem. Rev.* **2014**, *276*, 112-152.
90. H. A. Younus, W. Su, N. Ahmad, S. Chen and F. Verpoort, *Adv. Synth. Catal.* **2015**, *357*, 283 - 330.
91. E. Peris and R. H. Crabtree, *Chem. Soc. Rev.* **2018**, *47*, 1959-1968.
92. K. S. Sandhya, G. S. Remya and C. H. Suresh, *Inorg. Chem.* **2015**, *54,* 11150-11156.
93. M. J. Frisch, G. W. Trucks, H. B. Schlegel, G. E. Scuseria, M. A. Robb, J. R. Cheeseman, G. Scalmani, V. Barone, G. A. Petersson, H. Nakatsuji, X. Li, M. Caricato, A. V. Marenich, J. Bloino, B. G. Janesko, R. Gomperts, B. Mennucci, H. P. Hratchian, J. V. Ortiz, A. F. Izmaylov, J. L. Sonnenberg, D. Williams-Young, F. Ding, F. Lipparini, F. Egidi, J. Goings, B. Peng, A. Petrone, T. Henderson, D. Ranasinghe, V. G. Zakrzewski, J. Gao, N. Rega, G. Zheng, W. Liang, M. Hada, M. Ehara, K. Toyota, R. Fukuda, J.

Hasegawa, M. Ishida, T. Nakajima, Y. Honda, O. Kitao, H. Nakai, T. Vreven, K. Throssell, J. J. A. Montgomery, J. E. Peralta, F. Ogliaro, M. J. Bearpark, J. J. Heyd, E. N. Brothers, K. N. Kudin, V. N. Staroverov, T. A. Keith, R. Kobayashi, J. Normand, K. Raghavachari, A. P. Rendell, J. C. Burant, S. S. Iyengar, J. Tomasi, M. Cossi, J. M. Millam, M. Klene, C. Adamo, R. Cammi, J. W. Ochterski, R. L. Martin, K. Morokuma, O. Farkas, J. B. Foresman and a. D. J. Fox, *Gaussian 16, Revision A.03,* **2016**, *Gaussian, Inc., Wallingford CT*.

94. S. Grimme, J. G. Brandenburg, C. Bannwarth and A. Hansen, *J. Chem. Phys.* **2015**, *143*, 054107.
95. J. Zhang, G. Leitus, Y. Ben-David and D. Milstein, *J. Am. Chem. Soc.* **2005**, *127*, 10840-10841.
96. B. Gnanaprakasam, J. Zhang and D. Milstein, *Angew. Chem. Int. Ed.* **2010**, *49*, 1468-1471.
97. M. Gargir, Y. Ben-David, G. Leitus, Y. Diskin-Posner, L. J. W. Shimon and D. Milstein, *Organometallics* **2012**, *31*, 6207-6214.
98. L.-P. He, T. Chen, D. Gong, Z. Lai and K.-W. Huang, *Organometallics* **2012**, *31*, 5208-5211.
99. M. J. Page, J. Wagler and B. A. Messerle, *Organometallics* **2010**, *29*, 3790-3798.
100. J.-P. Sutter, S. L. James, P. Steenwinkel, T. Karlen, D. M. Grove, N. Veldman, W. J. J. Smeets, A. L. Spek and G. van Koten, *Organometallics* **1996**, *15*, 941-948.
101. T. Karlen, P. Dani, D. M. Grove, P. Steenwinkel and G. van Koten, *Organometallics* **1996**, *15*, 5687-5694.
102. C. A. Bessel, R. F. See, D. L. Jameson, M. R. Churchill and K. J. Takeuchi, *J. Chem. Soc. Dalton Trans.* **1993**, *0*, 1563-1576.
103. Y. S. Jun Li and K. Yoshizawa, *J. Am. Chem. Soc.* **2009**, *131*, 13584-13585.
104. S. Shu, M. Huang, J. Jiang, L.-B. Qu, Y. Liu and Z. Ke, *Catal. Sci. Technol.* **2019**, *9*, 2305-2314
105. C. Hou, J. Jiang, Y. Li, C. Zhao and Z. Ke, *ACS Catal.* **2017**, *7*, 786-795.
106. C. Gunanathan and D. Milstein, *Acc. Chem. Res.* **2011**, *44*, 588-602.

107. S. Qu, Y. Dang, C. Song, M. Wen, K.-W. Huang and Z.-X. Wang, *J. Am. Chem. Soc.* **2014**, *136*, 4974-4991.
108. K. S. Sandhya and C. H. Suresh, *J. Phys. Chem. A* **2017**, *121,* 2814-2819.
109. D. J. Durand and N. Fey, *Chem. Rev.* **2019**, *119*, 6561-6594.

List of Publications

(i) Publications related to thesis

1. Pincer ligand modifications to tune the activation barrier for H_2 elimination in water splitting Milstein catalyst, K S Sandhya, **G. S. Remya** and C. H. Suresh, *Inorg. Chem.,* **2015**, 54, 11150-11156
2. Quantification and classification of substituent effects in organic chemistry: a theoretical molecular electrostatic potential study, **G. S. Remya** and C. H. Suresh, *Phys. Chem. Chem. Phys*., **2016**, 18, 20615-20626
3. Assessment of the electron donor properties of substituted phenanthroline ligands in molybdenum carbonyl complexes using molecular electrostatic potentials: **G. S. Remya** and C. H. Suresh, *New J. Chem.*, **2018**, 42, 3602-3608
4. Hydrogen elimination reactivity of ruthenium pincer hydride complexes: a DFT study, **G. S. Remya** and C. H. Suresh, *New J. Chem.*, **2019**, 43, 14634-14642
5. Substituent effect parameters: extending the applications to organometallic chemistry, **G. S. Remya** and C. H. Suresh, *ChemPhysChem*, **2020**, 1028-1035
6. Molecular electrostatic potential theory: an approach to molecular reactivity, **G. S. Remya** and C. H. Suresh (to be submitted)

(ii) Publications out of thesis

7. Intermolecular dihydrogen bonding in VI, VII, and VIII group octahedral metal hydride complexes with water, K. S. Sandhya, **G. S. Remya** and C. H. Suresh, *J. Chem. Sci*., **2018**, 130, 98
8. Extending the library of boron bases: a contribution from theory, S. S. Rohman, B. Sarmah, B. Borthakur, **G. S. Remya**, C. H. Suresh and A. K. Phukan, *Organometallics,* **2019**, 38, 2770-2781
9. On the incompetence of iron(II) catalysis for olefin metathesis: role of triplet state and bond stretch isomerism, **G. S. Remya** and C. H. Suresh (to be submitted)

Contributions to academic conferences

1. Presented a poster entitled " Quantification and classification of substituent effects in organic chemistry: a theoretical molecular electrostatic potential study" at the 5th Modeling of Chemical and Biological (Re) Activity (MCBR), CSIR-Central Leather Research Institute, 18-21 February, 2017 (Best Poster)
2. Presented a poster entitled " Assessment of electron donor properties of substituted phenanthroline ligands in molybdenum carbonyl complexes using MESP" at the Theoretical Chemistry Symposium (TCS), BITS Pilani, Pilani, Rajasthan, 13-16 February, 2019.
3. Presented a poster entitled "Hydrogen elimination reactivity of ruthenium pincer hydride complexes", at the National Conference on New Frontiers in Chemistry - From Fundamentals to Applications (NFCFA2019) organized at BITS Pilani, K K Birla Goa Campus, Goa, 20-22 December, 2019.